AUTOMATED FREEFORM ASSEMBLY OF THREADED FASTENERS

By

KARTHICK DHARMARAJ

A Doctoral Thesis

Submitted in partial fulfilment of the requirements for the award of Doctor of Philosophy of Loughborough University

November 2015

ABSTRACT

Over the past two decades, a major part of the manufacturing and assembly market has been driven by its customer requirements. Increasing customer demand for personalised products create the demand for smaller batch sizes, shorter production times, lower costs, and the flexibility to produce families of products - or different parts - with the same sets of equipment. Consequently, manufacturing companies have deployed various automation systems and production strategies to improve their resource efficiency and move towards right-first-time production. However, many of these automated systems, which are involved with robot-based, repeatable assembly automation, require component- specific fixtures for accurate positioning and extensive robot programming, to achieve flexibility in their production.

Threaded fastening operations are widely used in assembly. In high-volume production, the fastening processes are commonly automated using jigs, fixtures, and semi-automated tools. This form of automation delivers reliable assembly results at the expense of flexibility and requires component variability to be adequately controlled. On the other hand, in low- volume, high- value manufacturing, fastening processes are typically carried out manually by skilled workers.

This research is aimed at addressing the aforementioned issues by developing a freeform automated threaded fastener assembly system that uses 3D visual guidance. The proof-of-concept system developed focuses on picking up fasteners from clutter, identifying a hole feature in an imprecisely positioned target component and carry out torque-controlled fastening. This approach has achieved flexibility and adaptability without the use of dedicated fixtures and robot programming.

This research also investigates and evaluates different 3D imaging technology to identify the suitable technology required for fastener assembly in a non-structured industrial environment. The proposed solution utilises the commercially available technologies to enhance the precision and speed of identification of components for assembly processes, thereby improving and

validating the possibility of reliably implementing this solution for industrial applications.

As a part of this research, a number of novel algorithms are developed to robustly identify assembly components located in a random environment by enhancing the existing methods and technologies within the domain of the fastening processes. A bolt identification algorithm was developed to identify bolts located in a random clutter by enhancing the existing surface-based matching algorithm. A novel hole feature identification algorithm was developed to detect threaded holes and identify its size and location in 3D.

The developed bolt and feature identification algorithms are robust and has sub-millimetre accuracy required to perform successful fastener assembly in industrial conditions. In addition, the processing time required for these identification algorithms - to identify and localise bolts and hole features - is less than a second, thereby increasing the speed of fastener assembly.

ACKNOWLEDGEMENT

I owe my deepest gratitude to my supervisors, Dr Radmehr P Monfared and Professor Michael R Jackson for their support and guidance throughout my research, without which I would not have succeeded.

I am thankful to EPSRC Centre for Innovative Manufacturing in Intelligent Automation and Loughborough University for giving me this wonderful opportunity.

I want to thank my colleagues for supporting me in my difficult times and also for creating a comfortable environment to work. At this juncture, I also want to acknowledge the assistance provided by the EPSRC centre administration and technicians during my research.

Finally, I am indebted to the most important people in my life - my family and friends for their care and immense faith in my ability. I also want to extend my gratitude to my wife for her understanding and patience, which really helped me to go through the final phase of my research.

I want to dedicate this thesis to my father, mother and to my late grandmother whom I dearly miss, as I was not able to be with her in her last moments.

LIST OF FIGURES

Figure 1-1 : Scope of the research 8
Figure 2-1: Academic review approach based on complete or partial assembly process 12
Figure 2-2 : Automated assembly review categorised based on guidance 16
Figure 2-3 : A reconfigurable fixture and laser seam finder used for aerospace skin panel assembly [30]..... 18
Figure 2-4 : Peg-in-hole assembly involved in automotive sub-assemblies..... 19
Figure 2-5 : Automotive sub-assembly in a semi-structured environment [35]. 20
Figure 2-6 : Contact forces for components a) Linear movements and b) Pure rotation Rz+ and Rz- [40]..... 22
Figure 2-7 : Tracking component markings for 3D alignment 24
Figure 2-8 : Categorising review on object pick up task..... 27
Figure 2-9 : Training patterns for different shapes a) radiused-square b) Circle c) Square [51] 29
Figure 2-10 : Monitoring and controlling of screw insertion process 34
Figure 2-11 : Contact points anlaysis of bolt and nut (CP1 and CP2) [66]..... 35
Figure 2-12 : Fastening tool identfication using IR cameras 38
Figure 2-13 : QA4 series Pneumatic Nut-runner [85]..... 41
Figure 2-14 : Thread protector assembly using machine vision [87]..... 42
Figure 2-15 : Rixan aerospace fastener sorting and pick up system [12] 43
Figure 2-16 : Kuka robot automatic drilling and inspection [13] 44
Figure 3-1 : Process involved in automated freeform assembly solution 49
Figure 3-2 : Different stages of research plan..... 50
Figure 4-1 : Automation Approach 53
Figure 4-2 : System hardware requirements..... 54
Figure 4-3 : Yasakawa Motoman SDA-20[88]..... 55
Figure 4-4 : Schunk PGN-Plus 80-1 Gripper[89]..... 56
Figure 4-5 : Gripping finger design with arc cut 57
Figure 4-6 : Finger design CAD model 58
Figure 4-7 : Bosch Rexroth tightening system[90] 59
Figure 4-8 : Tightening spindle exploded view[90]..... 59
Figure 4-9 : Visual sensors 60

Figure 4-10 : Cradle with different size bolts 61
Figure 4-11 : Fastening plate with different size holes mounted on a holder ... 62
Figure 4-12 : Communication setup for the fastener system..... 63
Figure 4-13 : HMS Anybus X-Gateway[94] 64
Figure 4-14 : Ethernet server communication outline 65
Figure 4-15 : HMS Anybus Communicator for DeviceNet [96]..... 69
Figure 4-16 : Communication between PC and tightening spindle controller... 70
Figure 4-17 : System setup for fastener assembly..... 71
Figure 4-18 : Maximum angle deviation of hex bolt head..... 72
Figure 4-19 : Accuracy test 73
Figure 4-20 : Average error and repeatability for all ranges..... 75
Figure 5-1 : Bolts in cradle 78
Figure 5-2 : Fastening plate mounted on a holder 78
Figure 5-3 : Field of view and Stand-off distance of the 2D camera 79
Figure 5-4 : Basler camera[91] with illumination 80
Figure 5-5 : System setup for 2D fastener assembly 81
Figure 5-6 : Bolt dimensional attributes..... 82
Figure 5-7 : Axis used in the experiment conditions 84
Figure 5-8 : 2D fastener assembly steps 86
Figure 5-9 : Imaging work area 87
Figure 5-10 : Fastening plate and bolt cradle imaging 88
Figure 5-11 : Assembling bolts into corresponding size threaded hole 89
Figure 5-12 : Bolt pick up process 90
Figure 5-13 : Steps invovled in fastening a bolt into a threaded hole..... 90
Figure 5-14 : Process involved in hole feature detection (2D) 92
Figure 5-15 : Image processing - hole feature detection..... 94
Figure 5-16 : Process involved in bolt head detection 95
Figure 5-17 : Image Processing - bolt head detection 96
Figure 5-18 : Camera calibration 97
Figure 5-19 : Experiment condition 98
Figure 5-20 : M10 bolts mean error and standard deviation - controlled lighting 102
Figure 5-21 : M10 holes mean error and standard deviation - controlled lighting 102

Figure 5-22 : M10 bolts mean error and standard deviation - ambient lighting 103
Figure 5-23 : M10 holes mean error and standard deviation - ambient lighting 103
Figure 6-1 : 3D sensors used for evaluation 106
Figure 6-2 : Ensenso N10 [100] 107
Figure 6-3 : Enseno technology 107
Figure 6-4 : PrimeSense Carmine 1.09[101] 108
Figure 6-5 : PrimeSense technology 108
Figure 6-6 : VC-Nano yr80[102] 109
Figure 6-7 : VC-Nano technology 110
Figure 6-8 : Micro-Epsilon scanControl 2900-25[92] 111
Figure 6-9 : Micro-Epsilon laser scanner technology 111
Figure 6-10 : Test Plate 113
Figure 6-11 : Bolt M12 114
Figure 6-12 : Fastening Plate 114
Figure 6-13 : Depth map of normal objects - Ensenso 115
Figure 6-14 : Depth map with ARDROX white spray - Ensenso 116
Figure 6-15 : Depth map of normal objects - PrimeSense 117
Figure 6-16 : Depth map with ARDROX white spray – PrimeSense 118
Figure 6-17 : PCD comparison of Bolt M10 with and without white spray 119
Figure 6-18 : Measurement Conditions for evaluating 3D sensors 120
Figure 6-19 : Test plate with physical size 121
Figure 6-20 : Slip gauge bar (20 mm) 121
Figure 6-21 : Test plate measurement error in ambient lighting 125
Figure 6-22 : Test plate measurement error in controlled lighting 126
Figure 6-23 : Z-axis accuracy measurement setup 128
Figure 6-24 : Actual increment vs. measured increment - PrimeSense 3D 130
Figure 6-25 : Actual increment vs. measured increment – Ensenso 3D 130
Figure 6-26 : Straight laser line reflection obtained through VC-Nano 131
Figure 6-27 : VC-Nano initial test 132
Figure 6-28 : Size measurement under ambient lighting 135
Figure 6-29 : Size measurement under controlled lighting 135
Figure 6-30 : Z-axis accuracy measurement results 137

Figure 7-1 : Bolts in clutter 141
Figure 7-2 : Hole on angled surface with chamfer and internal threads 141
Figure 7-3 : Scenario first stage - less complex assembly 142
Figure 7-4 : Scenario second stage – non-structured assembly 143
Figure 7-5 : Test rig developed for 3D fastener assembly 144
Figure 7-6 : Automated assembly step by step process 145
Figure 7-7 : Bolt manipulation 146
Figure 7-8 : Bolt assembly 147
Figure 7-9 : Scanning regions 148
Figure 7-10 : Process involved in hole feature detection (3D) 150
Figure 7-11 : Step by step process involved in hole feature detection 152
Figure 7-12 : Preparing reference surface model for matching 156
Figure 7-13 : Detecting bolt from the scene using surface matching 157
Figure 7-14 : Co-ordinates of robot tools, laser scanner and reference object 159
Figure 7-15 : Calibration artefact with stylus 160
Figure 7-16 : Transformation of co-ordinates 160
Figure 7-17 : Three different clutter forms of bolts used for evaluation 163
Figure 7-18 : Hole identification algorithm - accuracy measurement setup.... 164

LIST OF TABLES

Table 4-1 : Small angle range rotation 74
Table 4-2 : Medium angle range rotation 74
Table 4-3 : Large angle range rotation 74
Table 5-1 : Physical Measurement values 82
Table 5-2 : Socket alignment results 84
Table 5-3 : Measured values of bolt and threaded hole - controlled lighting 99
Table 5-4 : Measured values of bolt and threaded hole - ambient lighting 100
Table 5-5 : Mean and standard deviation of errors - controlled lighting 101
Table 5-6 : Mean error and standard deviation - ambient lighting 102
Table 6-1 : 3D sensors manufacturer specification 112
Table 6-2 : Test plate size measurement - Normal object 123
Table 6-3 : Test plate size measurement - object with spray 123
Table 6-4 : Test plate size measurement - Normal object 124
Table 6-5 : Test plate size measurement - object with spray 124
Table 6-6 : Z-increment measurement for PrimeSense 3D 128
Table 6-7 : Z-increment measurement for Ensenso 3D 129
Table 6-8 : Size measurements under ambient lighting condition – Micro-Epsilon 133
Table 6-9 : Size measurements under controlled lighting conditions – Micro-Epsilon 134
Table 6-10 : Z-axis increment measurement in ambient lighting condition 136
Table 6-11 : Z-axis increment measurement in controlled lighting condition .. 137
Table 6-12 : 3D imaging sensor comparison 138
Table 7-1 : Point Cloud Data (PCD) representation 149
Table 7-2 : Summary of fastening experiment 162
Table 7-3 : Bolt detection evaluation results 163
Table 7-4 : Hole diameter accuracy measurement 165
Table 7-5 : Translation accuracy measurement 166
Table 7-6 : Rotation accuracy measurement 166
Table 8-1 : Summary of research achievements 171
Table 8-2 : Limitations of this research 173

TABLE OF CONTENTS

ABSTRACT ..... **i**

ACKNOWLEDGEMENT ..... **iii**

LIST OF FIGURES ..... **v**

LIST OF TABLES ..... **ix**

TABLE OF CONTENTS ..... **x**

GLOSSARY OF TERMS ..... **xv**

CHAPTER 1 - INTRODUCTION **1**

1.1 Automation 2

1.2 The Need for Flexibility and Adaptability 3

1.2.1 Freeform automated assembly 4

1.3 Fastener Assembly and Need for Automation 4

1.4 Research Aim 7

1.5 Research Objectives 7

1.6 Research Scope and Scenario 8

1.7 Thesis Outline 9

CHAPTER 2 - LITERATURE REVIEW **11**

2.1 Academic Research Review 11

2.1.1 Flexible assembly systems and concepts 12

2.1.2 Automated assembly with guidance 15

2.1.3 Object pick up task 26

2.1.4 Fastener assembly - Object insertion task 32

2.1.5 Monitoring and correction mechanism 36

2.1.6 Object and feature identification 39

2.2 Existing Industrial Solutions Review 41

2.3 Summary 44

CHAPTER 3 - RESEARCH PROBLEM AND PROPOSED SOLUTION **46**

3.1 Research problem 46
3.1.1 Research hypothesis 47
3.2 Proposed solution 47
3.3 Research plan 50
3.4 Research experimental approach 51
CHAPTER 4 - SYSTEM INTEGRATION AND COMMUNICATION MECHANISM 52
4.1 System Specifications 53
4.1.1 System Controller 54
4.1.2 Manipulator 55
4.1.3 Tightening Mechanism 58
4.1.4 Visual Sensing 60
4.1.5 Test Objects 61
4.2 Communication Mechanism 62
4.2.1 Communication between PC and robot controller 64
4.2.2 Communication between PC and vision sensors 66
4.2.3 Communication between robot and tightening spindle 66
4.2.4 PC and Anybus communicator - DeviceNet network setup 68
4.2.5 PC and tightening spindle - tightening programs 69
4.3 System setup for fastener assembly 70
4.4 Accuracy test for the tightening spindle 71
4.5 Summary 76
CHAPTER 5 - TWO-DIMENSIONAL (2D) FASTENER ASSEMBLY 77
5.1 Assembly Scenario 77
5.2 System Setup for 2D Fastener Assembly 78
5.3 Scope of the Experiment 82
5.4 Bolt Pick Up using Tightening Spindle with Magnetic Socket 83

5.5 Assembly Process 85
5.6 Feature detection in 2D images 91
5.6.1 Hole feature detection 91
5.6.2 Detection of hexagon bolt head 94
5.7 Experiment conditions and data 98
5.7.1 Experiment Conditions 98
5.7.2 Experimental Data under Controlled Lighting (Uniform Lighting) . 98
5.7.3 Experimental Data under Ambient Lighting (Variable Lighting) 99
5.8 Discussion 101
5.9 Results 104
CHAPTER 6 - EVALUATION OF THREE DIMENSIONAL (3D) IMAGING SENSORS 105
6.1 3D Technologies and Sensors Used for Evaluation 105
6.1.1 Ensenso N10 106
6.1.2 PrimeSense Carmine 1.09 108
6.1.3 VC-Nano yr830 109
6.1.4 Micro-Epsilon scanControl 2900-25 110
6.2 Comparing 3D Device Specifications 112
6.3 Comparing Depth Maps and PCD of 3D Sensors 113
6.3.1 Ensenso 115
6.3.2 PrimeSense 116
6.3.3 Micro-Epsilon Laser Scanner 118
6.3.4 Depth Map Comparison Results 119
6.4 Experiment to Determine Accuracy of 3D Devices 119
6.4.1 Experiment with Large Objects - Test Plate 122
6.4.2 Experiment with Small Object - Slip Gauge 131
6.5 3D Positional Device Selection 138

6.6 Summary 139

CHAPTER 7 - THREE-DIMENSIONAL (3D) FASTENER ASSEMBLY 140

7.1 Assembly scenario 140

7.2 System setup for 3D fastener assembly 143

7.3 Assembly process 144

7.3.1 Scanning process and PCD Interpretation 147

7.4 Object and feature identification in 3D 149

7.4.1 Hole Identification Algorithm - Novel feature detection technique 150

7.4.2 Bolt Identification Algorithm 155

7.5 Calibration process 158

7.6 Experimental data 162

7.7 Algorithm evaluation and discussion 163

7.7.1 Bolt identification using surface matching 163

7.7.2 Hole identification using difference in gradient 164

7.8 Results 167

CHAPTER 8 - CONCLUSIONS 168

8.1 Contributions to knowledge 172

8.2 Limitations of this research 173

8.3 Recommendations for future work 175

REFERENCES 176

APPENDIX A - TECHNICAL DATA AND SPECIFICATIONS OF SYSTEM HARDWARE AND DEVICES 186

A1. Motoman SDA20D 186

A2. Schunk PGN-plus 80-1 188

A3. Bosch Rexroth tightening spindle (Size 4 – 150 Nm) 188

A4. Basler Ace 1600-20gm Camera 189

A5. Micro-Epsilon scanControl 2900-50 190

A6. Fastening plate 191

A7. HMS Anybus Communicator 192

A8. OGP SmartScope Flash 200 192

APPENDIX B - TIGHTENING PROGRAMS, 2D IMAGE PROCESSING ALGORITHMS AND 2D CALIBRATION 193

B1. Tightening programs 193

B2. 2D Image processing algorithms 196

B3. 2D Calibration 199

APPENDIX C - POINT CLOUD PROCESSING ALGORITHMS AND 3D CALIBRATION 201

C1. Clarification on acquiring point cloud data from laser scanners 201

C2. Point Cloud Processing Algorithms 202

C3. 3D Calibration 204

APPENDIX D – DISSEMINATION OF RESEARCH 207

GLOSSARY OF TERMS

In the context of this research

Freeform automated assembly : An automated assembly system which is intelligent, flexible, adaptable and robust to perform assembly of a range of products in a non-structured environment with minor modifications to the system.

Non-structured environment : The assembly environment, where the positioning of objects, assembly path and lighting conditions are not structured specifically for assembly process.
In this research the term Non-structured environment is adopted from Niko Herakovic [1], which refers to a not fully structured environment. This is different from unstructured environment, as some order of constrains are applied in non-structured environment

Intelligent assembly : Ability to identify and localize objects for assembly and also monitor the assembly to prevent misalignment.

Flexibility : Handling different size of objects without dedicated fixtures and with less or no robot programming.

Adaptability : Ability to handle variation in product geometry, location and surface finish.

Clutter : Objects (bolts) located one above other and occluded.

Random location : Unknown location of objects within a defined robot workspace.

CHAPTER 1 - INTRODUCTION

This chapter explains briefly about assembly automation, the need for flexibility and adaptability in assembly automation and the need for automating fastener assembly. It also states the aim, objectives and scope of this research.

Assembly automation is one of the prime focus areas of industries in recent years due to increasing market demands and advancement in technologies. Assembly is an important part of the manufacturing process where parts are mated to create a sub-assembly component or a complete product. Automation in assembly has evolved from systems with simple, repeated mechanical actions to systems with cognitive decision making-abilities. At present, in high-volume manufacturing and assembly processes, the programmable, repetitive automated systems are used widely to achieve mass production. On the other hand, in low-volume, high-value manufacturing, components are often produced through a significant amount of manual operations. This is not only due to the difficulties in justifying the cost involved in automating low-volume productions, but also due to the challenges in replacing highly adaptable and dexterous human skills with intelligent machines. For instance, fastening different parts by nuts and bolts may be the simplest form of manual assembly operation, yet is still extremely complex to automate in a non-structured environment.

In recent years, there has been a significant pull from large-scale industries to investigate the possibilities of extending automation to the more traditionally manual processes such as fastening, welding, painting, and polishing. Some of the reasons for such research interests include the high cost of components, the cost of repairs and reworks, and also expensive to use skilled workers [1]. In addition to the demand in large-scale industries for automation, the small to medium sized enterprises (SMEs) are also seeking to develop flexible and sophisticated production methodologies that will enhance the competitiveness of their manufacturing and assembly. Statistical data show that European manufacturing sectors contributes over € 6500 billion in GDP (Gross Domestic Product). The significance of SMEs amongst the European manufacturing

organisations can be understood from the fact that 99% of the manufacturing organisations are SMEs [2]. The large-scale and SMEs sector's interest in modern manufacturing research clearly indicates a research gap in the application of highly developed, automated technologies within highly intense manual processes.

1.1 Automation

In general, automation is defined as '*the creation and application of technology to monitor and control the production and delivery of products and services*' [3]. It can be broadly categorised into two types: repeatable automation, also known as single function automation, and intelligent automation, based on the ability of the implemented control system. A repeatable automation may have open loop control, where process feedback is not implemented and the assembly environment is structured. An example for repeatable automation is a robot performing a pick-and-place operation from a pre-defined position repeatedly, without knowledge of the presence and location of the object.

On the other hand, an intelligent automation system may include closed-loop control, where process feedback is obtained for adaptive control of the assembly process under a non-structured environment. The intelligence referred to in this case is specialised intelligence (i.e. intelligence specific for solving a particular problem) and does not represent general intelligence (i.e. artificial intelligence). Using the same pick-and-place operation example, an intelligent automation system would use a robot with sensing elements to detect the presence and location of objects.

Intelligent automated systems will have this ability to identify and locate objects, as well as monitor and analyse sensor feedback, and make decisions to handle different conditions that occur while performing an assembly. These abilities will make the automated systems self-reliable in decision-making and adaptable to different assembling conditions by obtaining a perception of its environment.

Hence in the near future, intelligent automation will play a critical role in assembly and manufacturing sectors; especially in aerospace and automotive industries. These industries require a higher level of accuracy, adaptability and

flexibility that are crucial for assembling products which will eventually lead to industrial development and growth.

1.2 The Need for Flexibility and Adaptability

A competitive environment has made industries look for highly flexible and adaptable systems to cope with the never-ending product changes. It is important for the industries to meet the customer-orientated market demands. To do so, industries should develop the ability to adapt to the rapidly-changing customer requirements [4]. Based on their customer demands, the industries require smaller batch sizes, lower costs and the flexibility to produce families of products or different parts with the same sets of equipment. At the same time, the industrial solution must also meet the product quality and quantity requirements of the customers.

Owing to this increasing customer-orientated market and stiff competition, industries are going through a transition from mass production to mass customisation, in order to satisfy different customer needs. Currently, flexibility in the most industrial robotic applications are achieved through the automatic change of end-effectors, the efficient programming of robots and by developing component-specific fixtures [5]. For example, in the assembly of large components, creating a dedicated fixture is expensive and difficult to manufacture. According to Bone, the cost of redesigning, manufacturing and installing fixtures for automotive industries is in the region of $100 million per plant, per year [6]. It also consumes a significant amount of time and resources to modify the robot programming and accurate positioning of the fixtures to accommodate product changes. In response, manufacturing companies have deployed various automation systems and production strategies to improve their resource efficiency and move towards right-first-time production.

However, a system is considered to be flexible and adaptable only when it is able to deal with subtle variations in the geometry and location of a product; and also its environment without dedicated fixtures or robot programming. This indicates a strong need for assembly systems that are flexible to accommodate object variability (i.e. geometry, material flexure and surface finish through

sensing) and adaptive in the decision making process. This type of automated assembly system would require less or no modification for product changes; thus providing a low cost solution-in the long term- which will be beneficial to industries. Realising these benefits, industries are likely to demand these highly flexible and adaptable systems that can perform various assembly tasks, without dedicated fixtures and robot programming.

1.2.1 Freeform automated assembly

The term 'Freeform automated assembly' used in this research, indicates an assembly system that is intelligent to identify and localise randomly located components and to avoid misalignment, flexible to assemble a range of products, adaptable to product variation and is robust to work in a non-structured environment with minor modifications to the system. The ability to monitor, analyse and make decisions, enable the automated assembly systems to handle different situations that can arise while performing an assembly task.

1.3 Fastener Assembly and Need for Automation

A fastener is a component that acts as a mechanical joint to affix one component to another. This process of mechanically joining components is called, 'fastening'. Fasteners are widely used for mechanical joining in various industrial sectors. Fasteners are used in assembling industrial products as they ease the maintenance, service, manipulation and disassembly for the recycling of the products [7]. The fastening process can be categorised into different types, based on the method used for affixing components. The most common types of fastening process used in industrial sectors at present are: integral fastening, stapling, threaded fastening and non-threaded fastening [8]. The type of fastening process depends on the application and requirement of industrial assembly sectors. Among the different types of fastening process, threaded fastening is one of the most-used joining methods for assembly due to their simplicity during the assembling and disassembling process [7]. Threaded fastening represents the insertion of threaded fasteners such as bolts into pre-threaded holes or nuts.

Among the various assembly processes, fastener assembly accounts for over a quarter of all assemblies carried out in industries [9]. An industrial statistic shows that out of the 6 million parts used in a particular aircraft, half of them are aircraft fasteners [10]. This shows the significance of the fastening process in the assembly sectors of industries. Due to this sheer number of fasteners used in assemblies, automating fastener assembly will have an immense impact on these industries. Hence any industrial development through automation should primarily focus on automating fastening processes.

Currently most fastener assemblies are carried out either by human operators with tightening tools [11], or by repetitive automation with complicated fixtures [12]. The human-operated manual fastening provides a remarkable degree of freedom to the assembly of fasteners and to the adaptations needed in variations. The fastener and the target component's locations, and the assembling environment need not be structured for carrying out assembly. Thus, manual fastening achieves flexibility and adaptability at the expense of reliability and repeatability. In the context of this work, reliability refers to the consistency in applying a tightening torque and proper fastener insertions. Moreover, it is also a time-consuming and labour-intensive process which may slow down the assembly process significantly.

Alternatively, some industries have implemented repetitive automation to assemble fasteners. This type of automation is more reliable, fast and repeatable, thereby achieving a high production rate with fewer labour requirements. These repetitive, automated systems necessitate the fasteners and other components to be precisely positioned and oriented every time before performing the fastening process. This requires the use of dedicated fixtures to hold the components in precise locations. It also requires supply hoppers and vibratory part feeders to orient the fasteners and to feed it to the fastening tool. These dedicated fixtures and part feeders occupy a large space in the assembly lines, thus lacking the flexibility and adaptability achieved in manual fastening. It is also required to be replaced in case of product change: making it more expensive, time-consuming to redesign and to re-jig the assembly line. These systems usually do not have the error monitoring and correcting abilities which prevent misalignment and cross threading.

In cases of high-value manufacturing and assembly industries such as aerospace, assembly accuracy is an important factor in determining the quality of the product. A small misalignment in aerospace products can have an adverse effect on the aerodynamics of the product which may result in product failure in later stages. They have a very low tolerance for error, which is difficult to accommodate for by either the manual or the repetitive automated fastening method. In aircraft manufacturing, the flexibility and precision of robotic automation have provided a cost-effective solution for drilling and fastening operations on large airframe structures, which had been using huge and fixed monument fixtures [13]. These industrial sectors need flexible automated systems with near-real-time monitoring, inspection and error correction functions to carry out accurate fastener assembly.

This emphasizes a need for a freeform automated assembly system that has the required flexibility and adaptability to perform fastener assembly. Such a system requires precision in identifying the fastener location and the threaded hole in a random (i.e. unknown) workspace. It should also have the ability to manipulate the fastener and have control over the force-torque applied during the fastening process. In addition, the performance of the system should also be considered as a vital part of the assembly solution i.e. cycle time for assembly, cost-efficient solution, and the ability to adapt to industrial conditions such as lighting.

1.4 Research Aim

This research is aimed at developing an automated assembly system to be capable of fastening a range of fasteners (bolts) into their corresponding size holes, located randomly within a defined workspace. Such a system is also required to achieve a high level of robustness, accuracy and repeatability, to reliably implement the system in industrial applications.

1.5 Research Objectives

The objectives of this research are investigated through the development of a prototype automation system to assemble fasteners in a non-structured environment.

The primary objectives of this research can be summarised as below

- ✧ Developing an automated '**BOLT PICK UP'** process - To identify and locate fasteners kept in a random location and also to determine the approach required to manipulate the automation equipment - such as robot and grippers - to pick up and orient the fasteners.
- ✧ Developing an automated '**THREADED HOLE IDENTIFICATION'** method - To identify, localise and determine the size of the threaded holes located in a target component kept in a random location.
- ✧ Formalising a method to automate the process of '**BOLT ALIGNMENT WITH TARGET HOLE AND FASTENING PROCESS'** - To identify the fastening axis so as to align the bolt with the corresponding size threaded hole and to perform a force-torque controlled fastening process with a near real-time monitoring system through closed loop force-torque feedback control.

The secondary objectives focused in this research are summarised as below

- ➢ Identifying and evaluating commercially available hardware devices and technologies required to develop a fastener assembly system
- ➢ Establishing communication between all the system hardware devices to integrate them with a central control unit.

- Investigating and evaluating different three-dimensional (3D) imaging technologies to determine a suitable 3D imaging sensor for obtaining visual perception objects at random environment.
- Minimising the need for dedicated fixtures and robot programming for the research-focused assembly environment

1.6 Research Scope and Scenario

The research is focused on the fastener assembly which is a widely used method in the industrial sectors. The research scope is narrowed to the assembly of threaded fasteners such as bolts that can be fastened into threaded holes or nuts. The threaded fasteners vary in size, shape, length, head drive and the material strength. Thus, the scope of this research is further narrowed down to the specific fastener type, material, size-range and its tightening torque, as illustrated by Figure 1-1.

Industry	• Aerospace and automotive
Assembly Process	• Fastening
Fastener Type	• Threaded fasteners • Hexagonal head drive fasteners (Bolts)
Material	• Ferrous material • Material strength of 8.8 (ISO Standard)
Range	• Bolts size ranging from (M5 to M14) • Pitch size ranging from (0.8 mm to 2 mm) - Standard size
Tolerances	• Bolts - Standard Tolerances of 6g
Tightening Torque	• Tightening torque ranging from 80 Nm to 120 Nm

Figure 1-1 : Scope of the research

The research scenario proposed for freeform fastener assembly involves assembling different size bolts into their corresponding size threaded holes in a non-structured environment (explained in section 7.1). This scenario closely represents certain industrial scenarios such as the assembly of bolts on aircraft wings, fastening involved in the assembly of automobile gearbox casings, or fastening involved in the assembly of wheels on an automobile.

1.7 Thesis Outline

Chapter 2: Literature review

This chapter provides a detailed review of existing assembly automation technologies and work done in the academic and industrial sectors. It explains the research performed to automate fastener assembly and also describes the current automated fastening methods implemented in the industries.

Chapter 3: Research Problem and Proposed solution

The proposed solution chapter describes the research problem and the gap existing in fastener assembly automation. It also provides the research solution proposed based on the determined methodology, and the plan to achieve the research goal.

Chapter 4: System integration and communication setup

The hardware device requirement for the fastener assembly and the reason for selecting the devices are explained in this chapter. The communication protocols used to establish data transmission between all the selected devices are also described. Additionally, it provides the complete system setup developed for this research.

Chapter 5: Two-dimensional (2D) fastener assembly

This chapter describes the automated method developed for assembling hexagon bolts into their corresponding size threaded holes located in a random 2D environment. It also illustrates the experiment setup, 2D image processing algorithm and the fastener assembly experiment results. The findings of the experiment were also summarised in this chapter.

Chapter 6: Evaluation of three-dimensional (3D) imaging devices

An overview of existing three-dimensional imaging technologies and commercially available 3D sensors were provided in this chapter. It proceeds to explain the extensive evaluation carried out to select the most suitable 3D sensor technology for performing fastener assembly.

Chapter 7: Three-dimensional (3D) fastener assembly

This chapter illustrates the automated method developed to assemble bolts from clutter into their corresponding size threaded holes located in a random 3D environment. This chapter also explains the experiment setup, 3D identification algorithms and the fastener assembly experiment results. It also explains the evaluation carried out to analyse the robustness of the developed algorithms. The resulting data and findings were reported in the summary of this chapter.

Chapter 8: Conclusion

This chapter provides an overview of this research, research achievements and the contribution made to the research field. It concludes by summarising the aim and objectives achieved in this research; including recommendations for future work to be carried out in this research project.

CHAPTER 2 - LITERATURE REVIEW

The literature review chapter provides an overview of research carried out in the field of assembly automation. This chapter investigates the existing state-of-the-art methods and technologies developed in this academic field, in order to identify research gaps. It also sheds light on the current industrial solutions available for fastener assembly and elaborates their advantages and shortcomings.

The review on research conducted in the automated assembly field is categorised into the two sections

- ✧ Academic research review
- ✧ Existing industrial solutions review

2.1 Academic Research Review

The mechanical fastening of bolts is the simplest assembly process which is widely carried out in the assembly sectors [7]. Almost all the fastening processes in small-scale industries are performed by manual workers using a torque wrench or other tightening mechanisms. On the other hand, semi-automated assembly systems are implemented in industries that require mass production, where fasteners are orientated and fed to the nut runners or other tightening systems using vibratory bowl feeders to perform fastening. The primary reason for automating the fastener assembly is to achieve a high level of robustness, high production rate, accuracy and quality in industrial assemblies [13]. Fastening is a simple assembly process for a human operator to perform, but it is a very complex process to automate. Due to the difficulty involved in automating threaded fastener assembly, very few studies have been focused on automating threaded fastener assembly [7]. Hence, most research done to date has primarily focused on peg-in-hole insertion and component or part assemblies.

Assembly process can be divided into two major tasks, object pick up and object insertion or mating with target component (assembling). These tasks

may involve one or more sub-tasks such as object identification, feature identification and alignment monitoring and control depending upon the type of assembly application. This research mainly focuses on assembling fasteners located in a random 3D environment. Hence, the academic review is categorised into six sections based on the methods and technologies developed for automating the complete assembly process or a part of the assembly (i.e. the tasks and sub-tasks involved in an assembly process) as illustrated in Figure 2-1.

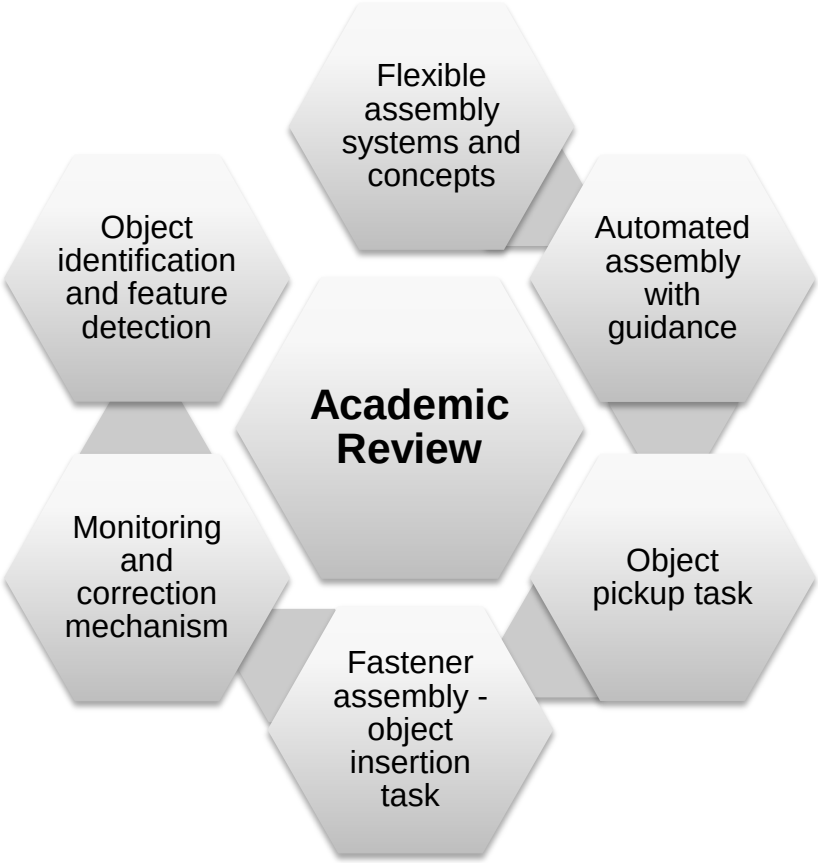

Figure 2-1: Academic review approach based on complete or partial assembly process

2.1.1 Flexible assembly systems and concepts

An assembly process, such as fastening, usually requires the perception of the assembly environment and dextrous manipulation to perform the process effectively. This necessitates an intelligent and flexible assembly system. The importance of such a system has been realised for a long time, hence a

number of studies have been carried out in this area. This includes flexible assembly using multiple collaborative robots, human-robot collaborative assembly and the optimization of assembly cell arrangements with standardised, modular and flexible assembly models.

Multiple collaborative robots or a robot with a dual-arm can perform the assembly operations that are usually performed by human operators. The multi-robot co-operative platform [14] was introduced to carry out dextrous and complex tasks in a dynamic workspace. It is based on a multi-layer control which carries out a task-oriented robot selection. It is done by analysing the suitability and convenience of each robot to perform a particular assembly task. A robust control for collaborating multiple manipulators developed by Esakki [15], focuses on handling flexible components during assembly using two three-link manipulators. The author combined the dynamics of both the flexible components used for assembly and the manipulators to develop the control, based on a singular perturbation technique.

However, the kinematics of multiple robots will result in problems such as singularity and a confined common work area. The synchronisation of multiple robots is also very difficult. On the other hand, a dual-arm robot with bimanual-manipulation provides human-like dexterity for assembly operations with a more common work area. Dual-arm robots can also undertake multi-tasking and are better suited to replicate operations performed by human operators.

More research is also being carried out to utilise the advantages of dual-arm robots to the benefit of handling parts for assembly in highly agile production scenarios. Tsarouchi investigated the use of dual-arm robot for increasing flexibility in automotive vehicle dashboard assembly through efficient robot programming [16]. The dashboard parts include a vehicle traverse, a body computer and screws to fasten it to the traverse. An approach was also developed by Krüger to automate complex assembly tasks using compliance motion control [17]. The robot interaction control was developed through an object-oriented programming approach. This approach requires the decomposition of an assembly task into various bi-manual elemental actions.

These methods can perform complex assembly tasks without dedicated fixtures and clamping, thus paving the way for implementing an increased level of automation in manual assembly stations. Despite this advantage, the adaptability for the variation in geometry of the products and their location are still need to be addressed. In addition, these collaborative robotic assembly methods also require a complicated control strategy to synchronise manipulation in order to prevent collision with each other and with obstacles.

Studies are also conducted on collaborating dual-arm robots with human operators to create a human-robot mixed environment, for the improvement of handling complex assembly operations. Considering the safety of human operators in this scenario, the collaborative strategies were either focused on implementing harmless robots or determining safe robotic behaviour. The ABB dual-arm robot was an example of a harmless robot developed to work alongside human operators without adding safeguards and interlocks [18]. This robot achieves safety through a four layer mechanical design which includes a body without any spikes or pinch points, a lower payload, reduced speed and power, and a software-based collision detection mechanism. The human-robot interaction was also achieved by structuring the collaborative behaviour of industrial robots to assist human operators safely in carrying out assembly tasks [19]. It uses two depth cameras to track the activities of a human operator, in order to control the behaviour of the robot, such as normal action, speed reduction or standstill and protective stop. The robot behaviours are determined based on the distance between the operator and the robot. Another new approach developed was the human body language based interaction with robot, to assist in variety of assembly tasks [20]. This method uses a 3D sensor to identify the operator's skeletal posture; establishing an effective communication between the operator and the robot.

In addition to flexible manipulation methods, research was also focused on developing optimised, flexible assembly line concepts to achieve easy reconfiguration and high productivity without increasing the complexity. Assembly concepts such as Flexible Automatic Assembly (FAA) and Hyper Flexible Automatic Assembly (HFAA) [21] were developed for introducing a high level of flexibility, standardisation and a simplicity in assembly automation.

They deliver effective solutions for improving small batch productions that require frequent reconfiguration through modular, process-oriented assembly approach. Another approach targeting small batch productions without manual assembly is the Fully Flexible Assembly System (F-FAS) concept [22]. An adaptable robotic part feeder system - which uses visual sensing - was proposed in this concept to accommodate different part types. This research was extended with an optimized sequencing algorithm for mixed-model assembly [23] and a framework to evaluate and implement assembly technologies in order to improve performance [24]. These concepts can be implemented to achieve flexibility, compactness and throughput in assembling a variety of products. Consequently, this provides a low cost automated solution for small batch productions by eliminating the need for frequent reconfiguration.

However, achieving flexibility in both the manipulation and assembly concepts for optimising a process flow, together with resource allocation is still insufficient for adapting to product changes and positional variations. It also requires intelligent guidance by obtaining the perception of the environment, analysing the information and making robust assembly decisions to accommodate variation in the product.

2.1.2 Automated assembly with guidance

Generally, assembly using robots involves programming by teaching, to perform an assembly task in a known environment. In a random environment, the fundamental prerequisite for assembly is to identify and locate objects, which can be obtained using any external guidance. According to Herakovic [1], modern industrial assembly processes need advanced, robot-based object detection, recognition and grasping techniques to assemble randomly located objects in a non-structured environment. The detection, recognition, grasping and assembling of objects needs sensor guidance (i.e. visual, tactile or a combination of both). The identification of objects located at random positions and orientation requires a visual perception of the objects. It can be two dimensional (2D), three dimensional (3D) or both -depending upon the assembly application. On the other hand, to accommodate variations such as

positional errors during the final assembly requires force-torque sensing to facilitate the precise insertion or mating.

Selecting suitable sensors for an automated system is an important task, as it is required to provide the perception of the work area in an industrial environment conditions (e.g. variable lighting and shiny surfaces). Hence, most of the automated assembly research uses one or a combination of multiple sensor guidance. Based on the guidance, the review can be categorised into three sections as illustrated in Figure 2-2.

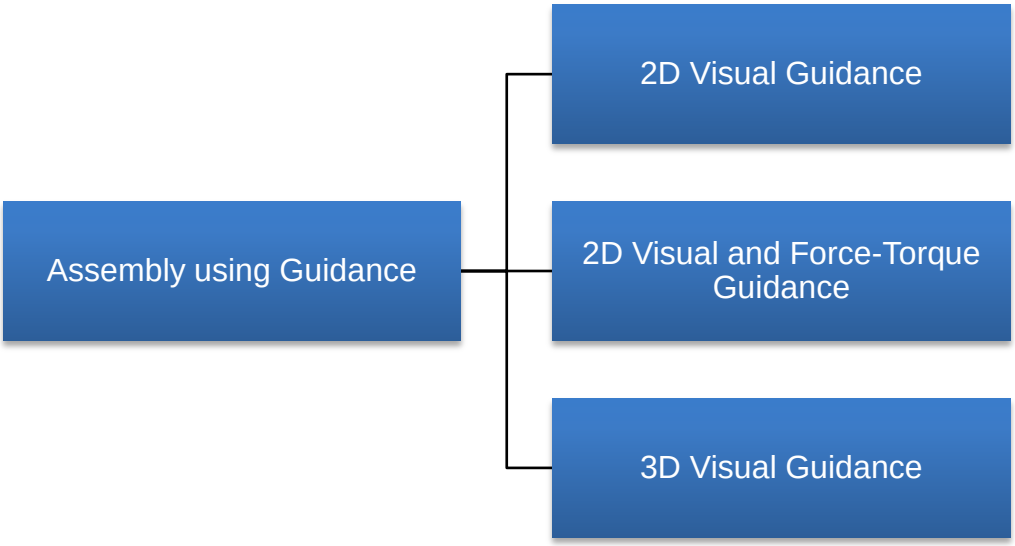

Figure 2-2 : Automated assembly review categorised based on guidance

2.1.2.1 2D visual guidance

The application of machine vision in robot-based assembly introduces an immense potential development in the research field and also in industrial applications. A significant piece of research has been carried out in implementing 2D vision to identify and locate objects in semi-structured industrial environments for assembly. The automated robot-based screw insertion method [25] was developed to insert self-tapping screws into unthreaded holes. The system consists of a 2D camera to acquire the image of the component with different size holes and a screwdriver to insert the screw. An image processing algorithm was developed to identify the circular features representing the holes using Tracking Hough Transform (THT). It also determines the radius and centre of the holes using any three points located on

the circular features. This method is 97% successful with a positional accuracy of 0.5 mm, but requires the surface containing the hole to be flat. Fei [26] developed a 2D automated assembly method to perform jigsaw puzzle assembly which demonstrated its potential in industrial pick-and-place applications. A template matching algorithm was employed to identify puzzle blocks and a corner feature extraction algorithm to calculate the centre point and rotation angle of the blocks. This method can only assemble same shape objects placed at random position and orientation. The intelligent robotic assembly proposed by Jerbic [27], [28] uses machine vision and a CAD model to assemble an artefact. The artefact consists of five parts and their 3D model and 2D drawing on different projections are known beforehand. A 2D vision sensor was used to take images of the parts. An image processing algorithm identifies the 2D edge features and matches them with the 2D drawings of the parts, in order to determine its position and orientation. This method is a proof-of-concept, developed for an autonomous robotic assembly capable of operating in disordered working environment. The 2D drawing projections of parts contains accurate edge-feature information for sharp and planar objects, but are poor in representing smooth and complex shaped objects

Currently in aerospace industries, automated solutions implemented for components in sub-assemblies are mostly based on large dedicated machines. These jigs are usually installed by direct manual labours or with assistance from lifting devices which is a time consuming and labour intensive process. It is also difficult to pre-define positioning of different geometry parts within the working volume. This emphasizes the need for flexible automated assembly solutions. Incidentally, several studies have been conducted to address the aforementioned problems.

Webb [29] proposed a solution for automating the assembly and riveting process of aerospace sub-assembly components. The aerospace components are localised using the part to part hole features as a reference, to measure the position of the component with respect to the robot. This work was carried forward by Jayaweera [30]–[32] to develop an adaptive automated method to assemble aircraft fuselage skin panels and stringers. A specialised re-configurable fixture combined with a metrological system as shown in

Figure 2-3, and a mathematical processing technique was used to guide the robot to handle different skin panels and stringers. A laser seam finder was used as a non-contact metrological system which projects laser line on the holes to identify its location. These locations of accurately positioned hole features are used to measure the position deviation of components from their desired position using a best-fit placement algorithm. This deviation is then used for component pick up and also to assist in aligning the component with its target. The results of the experiment reported in this paper claim that the assembly of aero structures is possible with an accuracy of 0.6 mm tolerance range. Despite the high accuracy achieved by the methods mentioned above, they require a specialised fixture and an approximate location of the components in order to measure the position deviation, thus is not suitable for freeform assembly.

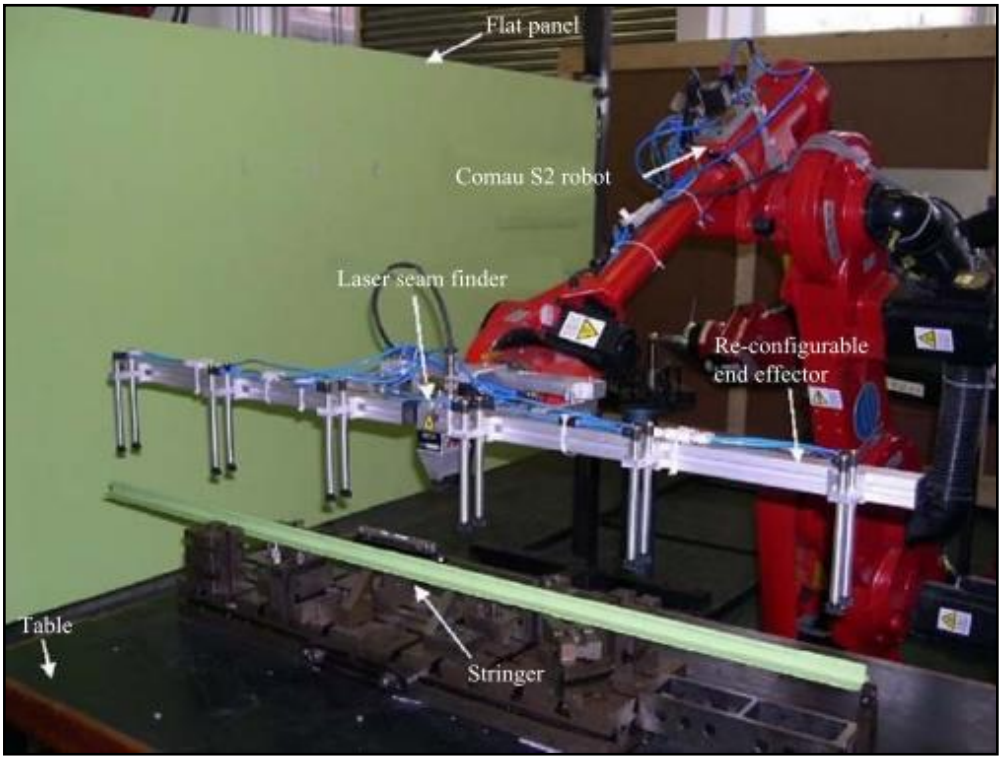

Figure 2-3 : A reconfigurable fixture and laser seam finder used for aerospace skin panel assembly [30]

Research was also carried out in automating automotive sub-assemblies, to achieve flexibility and high productivity. The insertion strategy proposed by Su was aimed at assembling automotive engine components [33] and air-

conditioning components [34]. The goal is to perform sensor-less (i.e. no force-torque sensor or mechanical compliance) manipulation to carry out peg-in-hole assembly. The strategy for automotive engine components shown in Figure 2-4 (a) involves tight tolerance (2 µm - 7.5 µm) fitting of a peg into both an unfixed hole of a piston and a hole located at the end of a rod. The latter involves fitting an eccentric crankshaft into a bearing hole of the automotive air-conditioners as shown in Figure 2-4 (b). Both strategies use a 2D vision sensor for identifying the automotive components and a 6-DOF (Degrees of Freedom) robot to pick up and place component in their respective target location. The insertion of the peg into hole is based on the attractive region formed by contact constraints. A special mechanical fixture was also required to hold the component with hole in both cases (i.e. piston and rod in engine sub-assembly and bearing in air-conditioner sub-assembly). The positions of the components are presented at their desired orientation, the pick-up approach is predefined and also it requires dedicated fixtures, thus limiting the flexibility of the system.

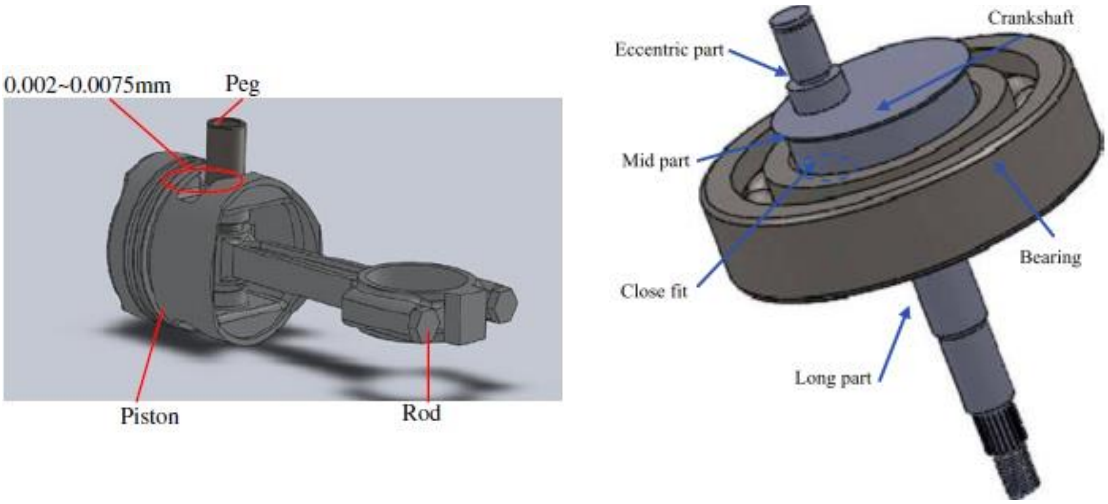

a) Engine components [33]

b) Air-conditioner components [34]

Figure 2-4 : Peg-in-hole assembly involved in automotive sub-assemblies

The review of the automated assembly systems using 2D vision shows that these systems are prone to lighting effects and calibration issues existing in industrial environment. Hence, these systems can be implemented only in limited industrial applications where the environment is structured.

2.1.2.2 2D visual and force-torque guidance

To overcome the positional errors in determining the parts location in 2D, additional sensing elements such as force-torque sensors were used to compensate the errors. This combination of sensing elements was mainly realised in high precision automotive sub-assemblies.

The research on high-precision assembly of automotive transmission components [35], [36] used a combination of sensors to accomplish successful assembly. This method was developed to assemble a piston into a valve body hole in a semi-structured environment. A 2D vision was used to identify the predetermined features in the valve body using a pattern-matching technique to locate the piston. The insertion of the peg into the valve body is accomplished using the input from the force-torque sensor. A 6-DOF robot is then used to pick up the piston and guide it to the desired position of the hole. A search algorithm using the force feedback controls the robot with the piston to rotate spirally near the valve hole, until it reaches a radius of 1.2 mm. At the same time, a continuous and controlled force is applied on the piston to facilitate successful insertion. The author claims that the method was able to achieve the tight tolerance assembly without any misalignment.

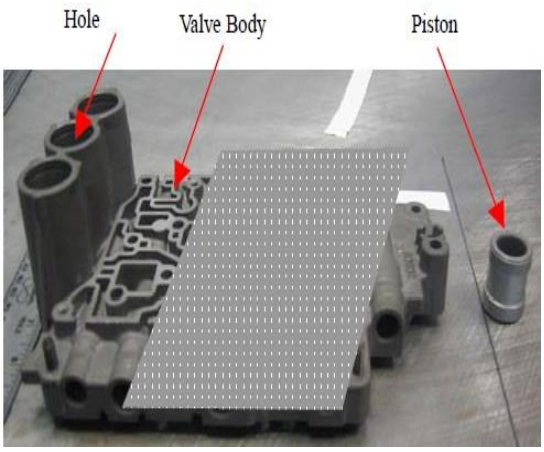

a) Automotive transmission components

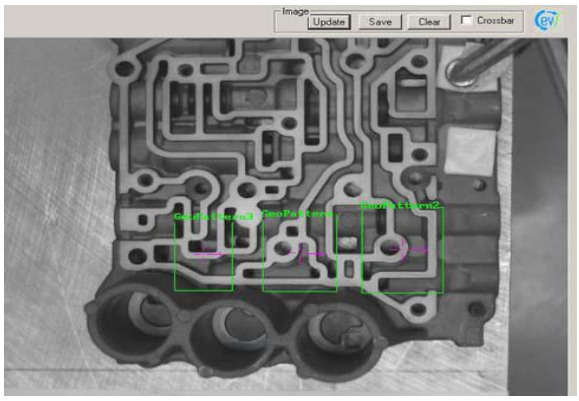

b) Feature identification using pattern matching

Figure 2-5 : Automotive sub-assembly in a semi-structured environment [35]

The major limitations of this method are that the location of the valve hole is identified by a predefined feature and the geometry of the hole is known beforehand. The piston is also required to be close (i.e. within 1.2 mm) to the valve hole in order to perform the force control search and insertion, otherwise assembly is not possible.

Vision guided robotic automatic assembly proposed by Huang [37] was developed for assembling parts in random environments. Distributed control architecture was introduced to integrate the system consisting of a 3-DOF SCARA robot with each joint controlled by a microprocessor, a 2D camera system and a force-torque sensor. The part location and geometry was obtained from the 2D image data processing which includes filtering, digitalizing, edge-detection and boundary line-slimming operations respectively. The force-torque sensor was used to compensate the error in determining the height of the object that occurs during 2D image processing. The assembly of simple models with a predefined sequence was achieved with an accuracy of 0.15 mm in determining the object size. The objects used are simple shapes such as rectangles, squares and circles with planar surface; hence this method is not suitable for objects with non-planar surfaces.

Using sensors for introducing flexibility and intelligence in automated assembly systems were discussed in the aforementioned methods. Studies were also conducted to achieve flexibility and intelligence through learning and maintaining a knowledge base, to adapt to different objects and assembly conditions. Lopez [38] developed an intelligent strategy based on the fuzzy ARTMAP neural network controller (NNC) for knowledge acquisition and learning in an unknown environment. The robot was provided with the contact force information and a primitive knowledge base (PKB). The robot enhances its knowledge progressively by adding new contact force patterns encountered during its assembly operations, only if it contributes to the success of the assembly. By this way the robot performs the learned tasks faster and also avoids the mistakes made earlier. The PKB was increased further by introducing 2D representation of the parts and also by the initial contact force-action mapping recorded for the robot actions to constrained forces [39]. The learning is based on a neural network which uses 2D vision to detect and learn

different shape parts and a force-torque sensor to correct and learn error patterns.

Based on the learning strategies developed by Lopez, an intelligent fixtureless assembly method was proposed [40]. It was aimed at acquiring assembly skills from scratch without much prior information. The information for assembly such as object type, position and orientation are acquired using a vision sensor. The initial knowledge about the directions of the motion of the parts (Contact states) is embedded into the NNC as fuzzy logic rules and is updated online when encountering new parts. The neural network is trained with 12 defined motion directions for each part which includes linear, combined and pure rotation as illustrated in Figure 2-6. The training of different size parts to the NNC consumes time, thereby making it difficult to introduce new parts.

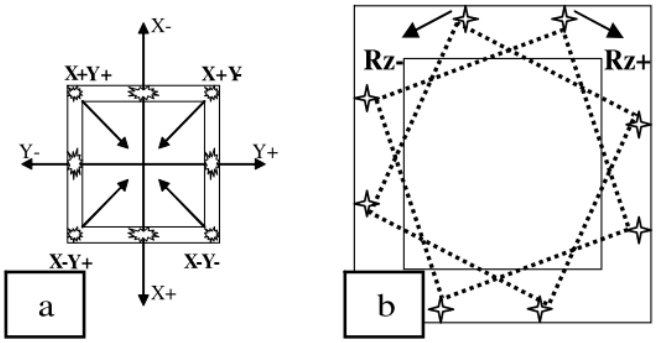

Figure 2-6 : Contact forces for components a) Linear movements and b) Pure rotation Rz+ and Rz- [40]

Cabrera [41] proposed a methodology for online object recognition and classification for robotic assembly tasks. The method includes an object recognition technique for fast recognition, classification and estimation of pose of the objects. An algorithm is developed to obtain various parameters of the part such as orientation, perimeter, centroid and boundary functions from a 2D image. This information is then fed to the artificial neural network (ANN) for recognition and estimation of pose of an object. The concept was experimentally verified with peg-in-hole assembly with different geometry and shapes. The results achieved as stated by the author, shows an error of ± 3

mm in position and ± 9 degrees in orientation; it is therefore not suitable for fastener assembly application.

All reviewed methods using 2D vision can be implemented only in specific real industrial applications with many constraints. For instance, the objects have to be in one plane perpendicular to the vision sensor plane in order to identify them. Therefore many of these methods are not sufficiently flexible and adaptable for industrial applications.

2.1.2.3 3D visual guidance

The constraints in 2D vision as explained in the previous sections - and the requirement of the 3D pose information to identify objects located at a random workspace necessitated the use of 3D vision. Much research has been carried out to make the automated systems robust, flexible and intelligent for assembling different objects without fixtures and robot programming. The Robotic Fixtureless Assembly (RFA) is a concept which aims to replace fixtures used in the automated assemblies with sensor-guided robots. This solution can adapt to product and position variation occurring during the assembly without much modification; thereby saving time, space, cost and materials in making mechanical fixtures.

Assembling in a non-structured environment is always difficult because it needs to handle variation in the geometry of objects and their location in the workspace. Even with the help of 3D visual guidance only a limited perception of the objects can be obtained, thereby making the object identification process difficult. An efficient solution to tackle this problem is to utilise prior information of the objects such as features, markings or 3D models (CAD).

The vision-guided fixtureless assembly stated by Bone [6], and the fixtureless spatial alignment method for assembly developed by Fleischer [42], describe a vision-guided work cell for assembling automotive components using markings for identification. The former used a 2D vision sensor and programmable flexible grippers to identify, locate and pick up the components with an accuracy of ± 1 mm position and ± 0.2° in orientation. This method implements a new 3D system (a pan-tilt camera and two laser projectors) to correct the alignment of components during assembly. One vertical and one horizontal

laser line are simultaneously projected onto the component and the 3D edge points of the projected laser lines are obtained to correct the alignment, as illustrated in Figure 2-7 (a), with an accuracy of ± 2 mm. The latter uses a stereo camera system to locate the components in 3D space. The complex-shaped cylindrical profiles are marked with component-inherent markings (multiple circles with known size and distance between them as shown in Figure 2-7 (b)). An image processing algorithm extracts the circular features from the images of both assembly components. This information was then used to determine the position in a longitudinal axis and rotation about the same axis in 3D co-ordinates with high accuracy.

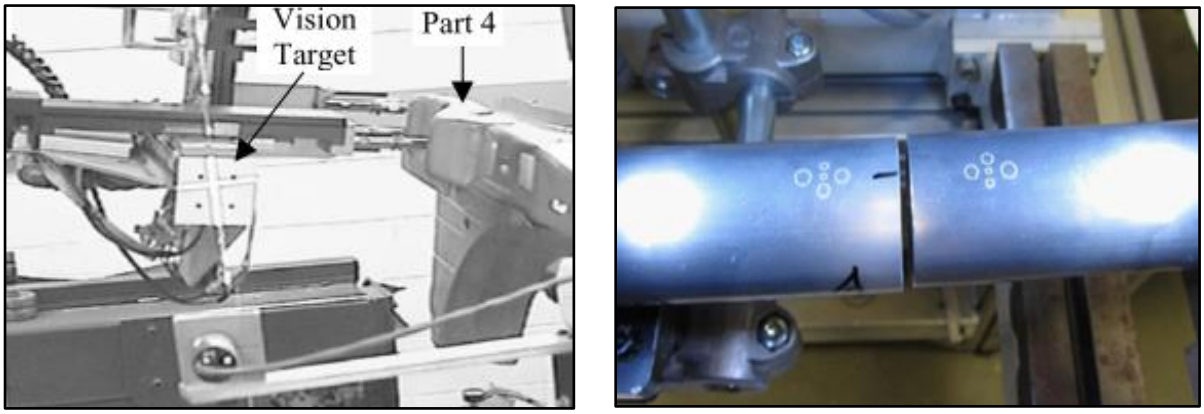

a) Laser line tracking [6] b) Multiple circle feature tracking [42]

Figure 2-7 : Tracking component markings for 3D alignment

Both methods described above acquire the 3D position for alignment by tracking the markings drawn or projected onto the component. This requires the markings to always be visible and the physical location of markings on the part has to be calculated beforehand, which is not an ideal solution for flexible assembly.

The remote robotic assembly method [43] used 3D models of the objects as a reference, to identify and localise objects placed at random locations in the workspace, with the entire operation being controlled by an operator. The 2D camera system was used to take multiple images of the objects at different angles. The silhouettes of these images are projected in 3D space. A 2D trimming process was applied to these projected images to determine the outer bounding polygon which approximates the actual dimensions of the object. This

information was then used to obtain the geometric centre and orientation of the objects. The generated 3D object models - and their locations - are integrated into a virtual robotic cell for identifying the assembling sequence. The robot commands are generated automatically in the virtual cell and are transmitted to the real robotic cell to accomplish the assembly. The experiment conducted to assemble three primitive components takes 22 seconds with a 3D modelling accuracy of less than 1 mm. Despite the high accuracy achieved, this method is computationally expensive and also not suitable for complex-shaped components.

Aerospace components usually have complex shapes and require high precision, thus at present, most of the assemblies are performed manually due to the challenges involved in automating this assembly process. Robotic assembly automation has, in recent years, become a popular research topic, owing to product demand and the advancement in technologies. The robotic assembly using closed loop alignment [44], the robotic assembly using non-contact measurement guidance [45] and the visual sensor guided robotic adaptive assembly [46] are some of the methods focused on assembling aerospace components.

Both the robotic assembly using closed loop alignment method [44] and the visual sensor guided robotic adaptive assembly method [45] are focused on assembling aircraft engine components. These methods used vision system to locate and align deformable and complex shape components for assembly. The former uses a laser triangulation system (a camera and a laser line projector) and two industrial robots to reduce the reliance on fixtures to hold the components. One robot with the laser system measures the weld seam between aerospace components (strut and panel). The offset calculated is sent to the second robot; based on the offset value the robot pushes or pulls the components in order to align them. The latter uses two laser sensor systems and an industrial robot to replace the part holding fixtures. One sensor was mounted on the robot to locate components edge positions relative to robot base and the other was placed static to locate the component position relative to the robot tool. The components were scanned on a number of points located at all the side edges. A mathematical algorithm was implemented to best-fit line

and curve features on the edge points. The intersection of these features renders the true position of the components. This position was then used for assembling the fabricated engine components.

The assembly accuracy for the methods explained is 0.12 mm and 0.5 mm respectively. These methods are highly accurate, but are component-specific as they obtain a laser profile of the components at known locations and also require approximate positioning of the components beforehand.

Assembly of aero aluminium alloy tubes proposed by Zhang [46], aims to accomplish adaptive robotic assembly through a non-contact sensing system. The system includes two robots, a laser vision sensor and a flexible fixture to assemble an aero tube and a flange. The laser light interaction with the cylindrical tube structure provides information about the curvature of the tube (i.e. an elliptical arc). The posture information of the tube or flange in 3D was acquired based on the eccentricity of the elliptical arc. The components are then transformed onto the plane parallel to laser plane for carrying out TIG welding. The accuracy of this method is ±0.2 mm in translation and ±0.5˚ in rotation, but this method requires the objects to be cylindrical.

The review on research using 3D vision for automated assembly shows a promising result, as they are highly accurate and able to identify objects in random 3D workspace. Despite this advantage, the aforementioned methods are not adaptable to product variation as they depend upon component specific features for identification and also require a semi-structured environment where the objects are positioned at a relatively known orientation.

2.1.3 Object pick up task

One of the major tasks in a freeform automated fastener assembly is to pick up bolts placed at random locations within the workspace. This task involves identifying and determining the position and orientation of the bolts. This information is then used to determine the approach required for manipulating the robot with a gripper for grasping and picking up the bolts.

In manual assembly scenarios, the bolt is picked up by human operators to be fastened into a threaded hole or nut either by using a torque wrench or a

tightening tool. Alternatively, in a repetitive automated (semi-automated) scenario, a larger supply hopper coupled with a vibrating bowl feeder is used for orienting and feeding bolts to the tightening tools to carry out fastening. The challenges in fastener pick up, such as the different size of bolts and the way the fasteners are presented (separated or clustered in a bin) to the system will have a great impact on the identification, localisation and grasping of fasteners. The human operator can adapt to these challenges with their high dexterity hand and intelligence to handle objects. On the other hand, the repetitive automated systems require major modification to their feeding unit so as to adapt to the aforementioned challenges. Thus, there is a strong need for advanced object detection, recognition and grasping methods to assemble objects located at random positions and orientations.

Since less academic research work is carried out in fastener applications, works on grasping different objects are reviewed in this section. This review is further categorised based on the visual guidance used for object identification as illustrated in Figure 2-8.

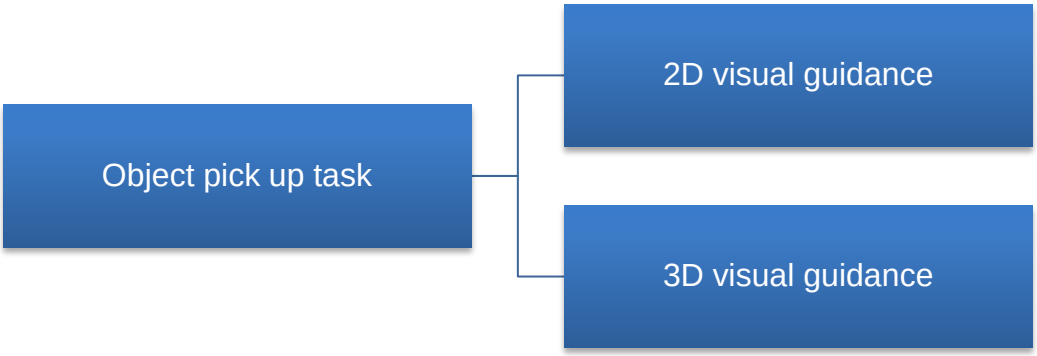

Figure 2-8 : Categorising review on object pick up task

2.1.3.1 Object identification using 2D visual guidance for pick up

Using 2D vision to identify objects for pick-and-place application is a well-established research area. At present in industries, most of the vision-based automated pick-and-place applications use 2D vision. These systems use calibrated 2D image processing technique for identifying and localising the objects and this technique is highly successful in many industrial applications. This section describes the research focused on implementing 2D vision for

assembly such as the un-calibrated visual servoing methods [47], [48], the method to obtain 3D pose from 2D images [49], [50] and object learning methods [51], [52].

The term ‘visual servoing’ represents the use of machine vision to develop a closed-loop control for a manipulator such as a robot with an end-effector. Both the fixtureless assembly automation method [47] and the robotic arm control method for assembly [48] used the un-calibrated 2D visual servoing technique for robot manipulation in order to reach the target object. Both methods used a planar object as the target and identify the displacement of the object in the camera image, in order to move the robot towards it. The former drives the manipulator, using target object position in discrete steps, by tracking the object and maintaining it at the centre of the image. The latter determines the target object location through linear matrix inequality and drives the manipulator towards the object in a direct trajectory. Both methods can only work for objects placed on a flat surface and require a tolerance of ±5 pixels and ±6 pixels respectively.

Studies were also conducted to estimate the 3D pose of the objects using their 2D images. The method to enhance industrial robot intelligence [49] and the method for guiding the robot for picking up objects [50] used a 2D vision sensor for identifying and localising objects in 3D. Both methods captured multiple images of the objects from different 3D poses beforehand to generate a knowledge database. The former used a pattern-matching technique to identify the location of the object. The later used the silhouettes to find a coarse 3D pose of the objects. These methods requires uniform lighting in order to identify and localise objects, as both uses light intensity based matching technique.

Several research works were also focused on developing random object recognition and learning techniques for automated assembly using 2D vision sensor and fuzzy based artificial neural network. Lopez [51], [52] developed a fuzzy controlled neural network for classifying different objects and approaching their locations in random conditions. Learning and a fast object recognition approach [51] was developed for learning manipulative skills to assemble objects without much prior information. This approach used artificial neural

network (ANN) for object learning and invariant object recognition, which is provided to the robot for making them self-adaptive to perform different assembly tasks. The neural network (Figure 2-9) was created using the recurrent pattern vectors, obtained from a collection of 2D images of the objects. Only two image patterns from each object are collected to learn and recognise that object location, invariant to rotation, translation and scaling. This work was developed further [52] into a fast-recognition and localisation method for grasping objects in a non-structured environment. The recognition time was reduced to 1 millisecond with 100% recognition and 93.8% efficiency. Orientation of the object in x-axis and y-axis is fixed, and the z-axis information is predefined in the 3D data. In addition, the objects used were primitive shapes, thus these methods are not suitable for identifying and classifying complex-shaped objects.

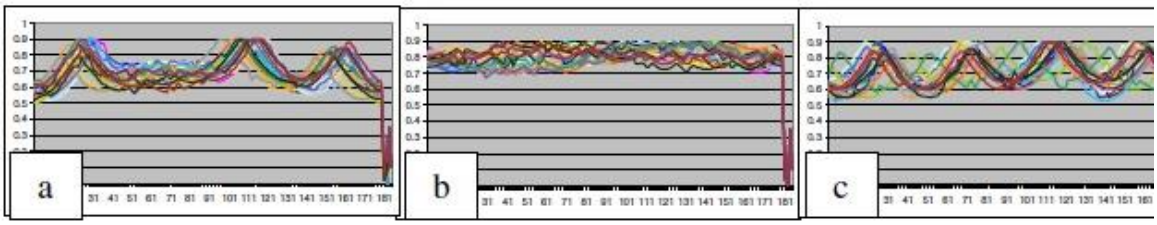

Figure 2-9 : Training patterns for different shapes a) radiused-square b) Circle c) Square [51]

2.1.3.2 Object identification using 3D visual guidance for pick up

Objects that are complex in shape with non-planar surfaces or objects that are stacked up in a clutter form and located randomly in the workspace require a 3D perception of the environment for identification and localisation. The object pick up from random locations will add flexibility and adaptability to the automated systems.

In real industrial scenario, objects for assembly could be placed in a clutter (one above other) form or in a bin. Objects lying in clutter are a great challenge to identify, localise and pick up due to the problems such as occlusion and overlapping. The picking up of objects from a bin in an industrial robotic application offers a high degree of flexibility in automation, meanwhile also reducing the need for special purpose feeders and containers to supply objects

(fasteners). Accurate 3D information of the object is needed for the versatile object picking systems to be capable of performing picking up from bin. The major sub-tasks involved in 3D object pick up are object identification and localisation, path planning and grasp point determination. Apart from identification and localisation, determining the right approach to grasp the overlapping object (fastener in this case) plays an important role in the picking up task. This prompted more research on identifying and picking up objects from a bin, commonly referred as 'Bin-Picking' problem. Currently, this is one of the most researched topics. The bin-picking methods based on primitive shape-based matching [53], [54], global features-based matching [55]–[57], local features-based matching [58], template matching [59] and spectral highlight-based matching [60] are some of the solutions developed to address this problem.

The bin-picking method developed for automotive sub-assembly automation [53] and the mobile robot bin-picking method [54], identified and localised objects from a bin using the geometric primitives on the surface of the object. This approach involves the decomposition of the reference 3D models (CAD) and the input point cloud data into known simple geometric primitives such as planes, cylinders or cones for matching. The former method is robust in detection but inaccurate with more than a 10 mm error in translation and 1.5˚ in rotation. The latter method is accurate to a level of less than 1 mm but failed to detect some objects mainly due to occlusion. Both methods are computationally expensive and only suitable for a specific type of components that can be decomposed into geometric primitives.

The global feature matching methods identify and localise objects based on the features such as edges, chamfers or partial surfaces. The fast object registration method [55], combined the 2D image matching algorithm with the improved iterative closest point (ICP) algorithm for object localisation. The objects in the bin are roughly identified through contour-based matching and then the pose refinement was performed using the progressive mesh based ICP. This method is faster as it requires only 1 second for object identification, but only accurate to a level of ± 2.5 mm in translation and ± 1.5˚ in rotation.

The bin picking method based on a modified RANSAC approach [56] and the fast object localisation method [57] are developed to identify objects from random clutters. The method based on modified RANSAC referred to as ‘random sample Matching’ (RANSAM) localised objects by matching reference CAD data with the input point cloud data obtained from the laser scanner. The matching algorithm used the oriented point-pair relation to find the pose of the reference object on the input point cloud. The major drawback of this method is the position error, which is about 3 mm, and also the high processing time of 4 seconds. The fast object localisation method identifies and localise objects using a fast directional chamfer matching (FDCM) algorithm. It used a multi-flash camera, which generates differential illumination on the surface of the object by casting a shadow for imaging. The chamfer matching technique involves finding the best possible alignment between the reference template edge map and the input query edge map. This method is much faster and has a processing time of 0.71 seconds for object detection, but is inefficient in detecting objects that are occluded by more than 5%.

The stereo vision-based bin-picking solution [58] determines the 3D pose of the objects in clutter using the local key geometric features such as holes. Initially, the image from one of the camera was used for identifying the objects approximately by a 2D pattern matching technique. Then the accurate measurement of 3D pose of the object was then obtained from the 3D position of the holes features in the object. This method has an accuracy of 1 mm in translation and 0.3˚ in rotation. Despite its high accuracy, the method depends upon the local object features and requires significant modification of the algorithm to adapt to a different object.

The bin picking method using the 3D template matching technique [59] was developed to recognise freeform objects from clutter form. It includes three main tasks: 3D data acquisition, segmentation and object identification to determine the pose of the object. The segmentation involves the clustering of points based on density and classifying the clusters by calculating the smallest rectangular bounding box that can fit the clusters. After segmentation, template matching was used to identify each and every object from the input point cloud.

This method is accurate and faster, but the object detection is affected by occlusion.

The bin-picking method to pick up coil springs from a pile [60] used spectral highlight information for object detection. The spring coils are illuminated by area-based highlight technique (i.e. side highlight and end-face highlight) before imaging. These images are converted into binary and then the highlights found in the binary image are group based on area, direction and the distance between the two highlights, in order to segment individual coil springs. The 3D positions of the springs are obtained using the stereo correspondence. This method has stated an accuracy of 1 mm and processing time of 1.7 seconds, but the average success rate of coil spring detection is only 77%.

2.1.4 Fastener assembly - Object insertion task

The fundamental step in a fastener assembly is the process of fastening a bolt into its corresponding size threaded hole. The major factors that contribute to a successful fastening are:

1) Approach and alignment
2) Fastener insertion (helical transition) and
3) Torque control.

Approach and alignment determine the path and approach required to guide the manipulator with a fastener to align with the threaded hole (i.e. aligning with the fastening axis). The path is the best possible way to reach the point where the threaded hole is located. The approach of the fastener should always be in the direction perpendicular to the hole plane in order to avoid misalignment or cross threading. After aligning the fastener with the hole, the fastening of bolt into the hole is carried out with appropriate amount of torque - depending upon the size and condition of the bolt. The torque-controlled fastening process can be divided into three steps: initial breakthrough, smooth threading and final tightening. The torque value for each step varies based on the size, pitch, lubrication condition and material strength of the bolt used.

Considering the amount of fastening performed in industrial assemblies, not much research has been performed in automating threaded fastener assembly.

Most of the reviewed research works were focused on the peg-in-hole insertion process. The insertion of a peg into a hole is similar on the aspect that both requires identifying the hole feature and approaching the hole on the axis perpendicular to it. But it follows a quite different path for insertion, which involves a vertical displacement, contrary to threaded fastening which involves helical translation.

Studies conducted on automating fastener assembly are mainly focused on developing a control strategy for fastening, given that the fastener is already identified and picked up by a manipulator. The automated fastening method by Dhayagude [61], and the tightening control for wind turbine bearing assembly methods by Deters [62], [63] implemented fuzzy logic to control the torque applied during the fastening process. Klingajay [7], [64] contributed a series of research work to develop an analytical model of torque vs. insertion depth to control fastening. Fan [65] studied a distributed control for a multi-axial tightening machine to intelligently control multiple fastening processes. Wiedmann [66], [67], proposed a full kinematic model and a spatial kinematic model to determine the nature of the contact happening between bolt and nut at the initial stage of the fastening process.

The automated fastening method [61] described an intelligent control strategy to fasten a screw into a hole. This method categorises the fastening process into three steps which includes engagement, draw-in and torquing. An integrated closed loop control was developed using fuzzy-logic control to perform and monitor torque controlled fastening in a simulated environment. The control logic is simple and was carried out in a virtual environment. The author himself stated that the simulated environment has a lot of variables and uncertainties, therefore is not suitable for real industrial applications.

The bolt tightening control method for wind turbine bearing assembly [62], [63] used a model-free fuzzy control for monitoring and controlling fastening process. It aimed to replace the manual fastening operation due to the relatively high degree of variability and repeatability involved in the fastening process. The control strategy using fuzzy logic divided the fastening process into four stages: bolt-nut alignment, partial engagement, full engagement and final

tightening. The membership functions and fuzzy rules are derived separately for all four stages. The fuzzy error detector used the input from the torque and angular encoder for error detection. This method was able to perform fastening with an accuracy of 1.5 Nm in applying torque and ±184˚ in angular rotation for a complete cycle of rotation (i.e. 2100˚). This method is also capable of monitoring and detecting torque error accurately, but has a large rotational error.

The parameter estimation of threaded fastener operation [64] monitored the screw insertion process and also determined the friction and hole depth parameters by an analytical model. The screw inserting system shown in Figure 2-10 (a) consists of three parts an electric screw driver for inserting screws, torque sensor with optical encoder for measuring torque values and rotation angle, and a monitoring system. The work done above was carried forward [7] to develop a method to co-ordinate the fastening process by obtaining their torque vs depth graph. The entire process is divided into five steps as shown in Figure 2-10 (b) with different torque vs. depth value.

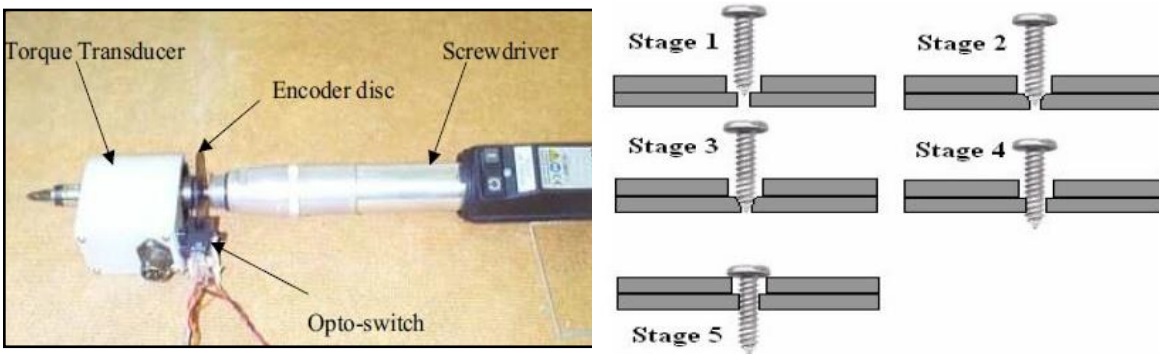

a) Screw insertion system b) Stages in fastening process

Figure 2-10 : Monitoring and controlling of screw insertion process

The analytical model presented in this paper is obtained using the analytical model of ngemoh; with torque signature signals determined by using the Newton-Raphson method. It also determined the estimation of friction and hole depth online, through a simulation. Using this model and the properties of the screw such as material and mating plate, an effective control strategy was presented to perform automated screw fastening. The analytical model needs

multiple input parameters, such as screw properties and plate properties, which are difficult to obtain and not practical.

Distributed multi-axial control [65] was developed to handle the tightening operation of bolts using multiple tightening machines. The tightening torque and angle to achieve the desired clamping force for bolts are incorporated into the control. The complete system and the tightening device controllers are integrated using a fieldbus network. The full kinematic model of thread starting in an assembly method [66] provided the details of the threaded fastener insertion and the nature of contact between a bolt and a nut at the initial phase of the insertion. The two-dimensional contact point analysis, illustrated in Figure 2-11, was made by locating the contact occurring while inserting the bolt into the nut in a counter clockwise direction. Using the nature of contact, the wedging and jamming that can occur during fastening may be prevented.

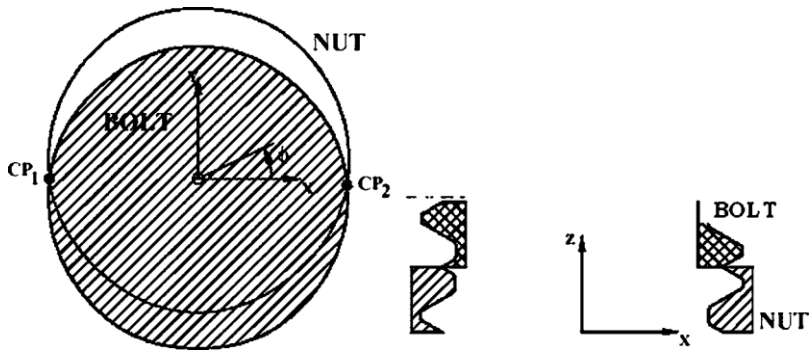

Figure 2-11 : Contact points anlaysis of bolt and nut (CP1 and CP2) [66]

The spatial kinematic model [67] was focused on a 3D collision analysis of tessellated solid models in simulation. The result of the analysis was then used to determine the approximate initial contact point of the bolt and the nut. The analysis of the vertical movement of the bolt for the every movement of the bolt into the nut revealed three types of contact states: unstable two points, quasi-stable two points and stable three points. The contact point analysis simulation was carried out for 81 potential orientations with each having their own contact points. This simulation proved that the contact state history of the bolt and the nut during fastening can be found with certainty. It also stated that this contact state history can be used to develop a passive compliance or an algorithmic motion control to assist proper fastening.

These fastening methods were based on mathematical models and contact point estimation in a virtual simulated environment, therefore may not be applicable to real industrial scenarios.

2.1.5 Monitoring and correction mechanism

In assembly, the monitoring and correction is also an important aspect which makes the system intelligent and robust. A near real time monitoring should be carried out in parallel to the picking up process and the fastener assembly process for ensuring successful assembly operation. The sensors such as vision systems and force-torque can be used to monitor the entire assembly process. To obtain optimum result in a freeform automated assembly the monitoring has to be in near real-time and the feedback obtained from the sensors also has to be processed in near-real time for applying corrective actions.

In fastener assembly, the alignment error and the positional error can lead to the misalignment of threaded parts which will further result in cross threading. Much research has been conducted to analyse and correct the position and the alignment of the fasteners before and during the fastening operation. The work carried out by Diftler and Walker [68] was focused on aligning threaded parts of the bolt and the nut with a special fixture arrangement and a force-torque sensor. Pitipong [69] proposed a visual servoing method using two cameras to monitor the screw alignment. These methods are developed to correct the fastener alignment before the fastening process.

The experiment in aligning threaded parts [68] was introduced to determine and correct the misalignment occurring during the threaded fastening process using feedback sensors (i.e. force-torque and angular position feedback). The alignment detection and correction technique was determined by monitoring and analysing the axial force data obtained by back spinning a nut into a bolt. The experimental setup consists of a nut plate with a steel helical thread at the bottom and a vertical sliding bolt holder with a force-torque sensor coupled to it. The bolt holder is further connected to a rotating slide with ± 15 degree angle on top and the bottom of the bolt holder with the bolt facing the nut thread. This setup can provide the drop azimuth angle needed to correct the misalignment

when the bolt drops in the nut. Pitipong [69] introduced an automated robot screw fastening using vision to track the fastener alignment. This method used a 4-DOF robot and two 2D cameras to determine the screw alignment with respect to the hole plane and correct them before fastening. The position values are significantly affected by their surrounding environment conditions and also by the object surface finish.

The most preferred method of monitoring the threaded fastening process is using the force-torque sensor feedback. The research carried out by Althoefer [70] and Klingajay [71] monitored the self-tapping screw fastening process using neural networks and analytical control models. Chumakov [72] proposed a fault detection method in thread forming screws using neural network by analysing the force-torque sensor feedback.

Althoefer [70] developed an artificial neural network (ANN) to monitor the screw insertion process using the torque vs. insertion depth. It divided the self-tapping screw insertion process into five stages which include the start of insertion, initial breakthrough, advancement of the screw, the tightening stage and the final stage. The analytical model developed for defining torque vs. insertion depth signals for each stage [71] was used to design the ANN for monitoring screw insertion in a generalised way.

The fault detection in thread forming screw assembly [72] aimed to develop a two layer dynamic Elman Neural Network for detecting faults in the assembly of thread forming screws using force-torque feedback. The Elman neural network has a recurrent layer and a linear layer. The modelling of neural network is developed by defining the torque vs depth values for various states of occurrences that can be identified during the thread forming process. For each torque signal, an output error code is generated. The control system can use these error codes to carry out necessary actions such as to stop the fastening process, to increase or to decrease the amount of torque applied. A study [73] was also performed to find the grip length of the fasteners in real time using the Mahalanobhis-Taguchi system (MTS) and also to check the quality of the fasteners (re-used fasteners).

In addition to the fastener alignment monitoring in robot-based automated fastening systems, research was also carried out in monitoring the fastening tool used in the manual fastening assemblies to improve efficiency and accuracy. Rusli and Luscher [74] used Infra-Red (IR) cameras and torque feedback to monitor a manual fastening tool and Seong [75] used an inertial measurement unit and a 3D position sensor to assist the manual fastening process.

The fastener identification and monitoring method [74] used a IR tracking system and a force-torque sensor to monitor the fastening tool used by a manual worker. Tracking markers are placed on the fastening tool and also on the target hole location. Six IR cameras were placed at predefined locations to track the marker on the fastening tool. The 3D position of the tool and the fastening hole was obtained by control software which uses the relative position of the marker and the IR camera to triangulate the location (Figure 2-12). The torque sensor was attached to the tool and its feedback is sent to the fastening tool controller. Using the position of the tool and the nominal control of torque value, the fastener assembly was carried out. The precision for tracking the fastening tool is 2-3 mm with more than a 99% tracking success rate.

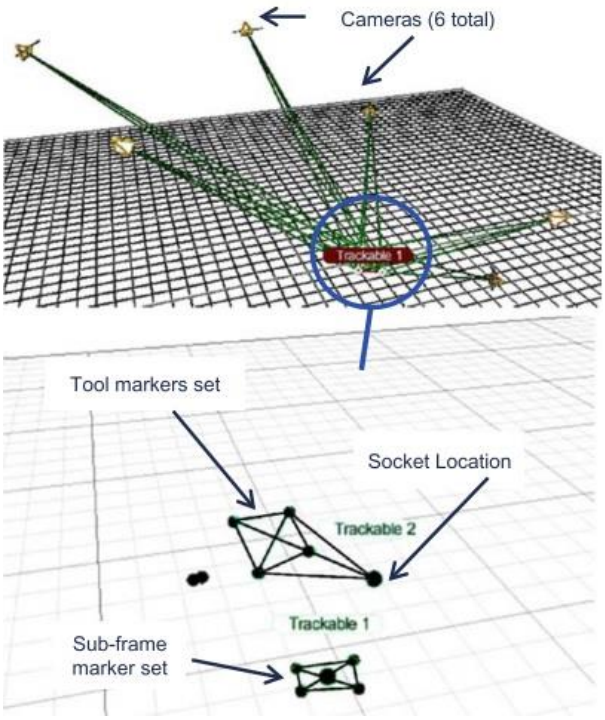

Figure 2-12 : Fastening tool identfication using IR cameras

At least four markers have to be tracked on the tool to localise it, which limits the flexibility of using the tool. Placing markers on all the target holes is not an ideal automated fastening solution for industrial applications.

A method for tracking the fastening tool and the position of the fastened bolt was proposed [75]. It used an Inertial Measurement Unit (IMU) and a position sensor for tracking the tool. The IMU was used to obtain the tilt angles of the tool. The kalman filter was used to estimate the orientation of the tool using the IMU measurements and the position sensor (a 3D sensor-Spaceage Control Inc) to identify the 3D position. The bolt position was recorded after every time a bolt was fastened into a hole. The previous position of fastened bolt was then compared with the tool tip position before carrying out the next fastening to check the orientation and position errors. An experiment was carried out to fasten eight bolts and the results showed that this method was able to track the tool with a precision of 6 mm. The position of the fastening hole is predetermined and only the tool is positioned and oriented with respect to the hole.

2.1.6 Object and feature identification

For the assembly system to be flexible, it needs to have the ability to identify and classify objects located at random workspaces. Usually the object identification is based on the shape, size or any feature on the surface of the object. Several advanced methods are already used for object recognition [76]–[80] in industrial applications such as visual inspection, bin picking, object tracking and face recognition. Object recognition methods can be broadly categorised into global and local methods based on the type of feature descriptors used for the recognition process. The global object recognition methods [77], [78], can only detect primitives shapes such as planes, spheres and cylinders from the input point cloud data (PCD). These methods are slow and also require segmentation of objects, if they are in clutter form. On the other hand, the local object recognition methods [79], [80], are using point to point correspondence between the reference model and the input PCD using regional information of the surface. Because of using local information for detection, these methods are prone to noise and occlusion which can affect the

object detection. The model global and match local method [76] used the oriented point pair features for creating a global model descriptor. These features were then used to match the reference model with the input PCD locally using a voting system. This method groups similar features of the reference model and compares them with the input PCD to find the best match without coarse information, thus can be implemented in occluded and noisy input data. Hence, this method is used in this research to detect bolts that are located in clutter form. Despite the good level of accuracy and reliable object detection, this method is typically slow. Hence, this method is not suitable for dynamic manufacturing and assembly systems. In order to enhance performance of this method, a modified CAD model is used for generating global model descriptors, thereby reducing the computation time considerably (explained in section 7.4.2.1). This method is referred to as 'Surface Matching Technique', as it involves grouping of similar surface point pairs for matching the reference model with the input PCD obtained from a vision sensor.

One of the major challenges in this research is to identify threaded holes located at multiple planes with chamfered edges and visible internal threaded edges. In addition to that, the circular feature (i.e. the outer edge of the threaded hole) geometry and location in 3D space has to be determined for selecting appropriate size bolt. There are very few 3D hole feature detection methods available, the hole detection method developed by Wang [81], finds solid holes by detecting planes and their boundary relationship. This method cannot be implemented to identify chamfered non-solid holes. The method to detect holes in point set surfaces [82] used the angle between the points on the surface of the objects to detect edges. This method is very slow and also cannot differentiate the threaded edges and chamfered edges from the outer edge of the threaded hole. The feature detection methods based on RANSAC [83] and Hough Transform [84] are computationally expensive and also effective only in detecting planes.

Therefore, a new hole feature detection algorithm is needed to be developed to identify and localise the threaded holes with chamfers located at random position and orientation in 3D, which reflects closely the applications in industries.

2.2 Existing Industrial Solutions Review

This section focuses on the information about existing automated fastening systems available in industries. This review is conducted to understand the level of robustness, flexibility and precision exists in commercially available industrial automated systems for assembling threaded fasteners. The threaded fastener assembly generally used in industries include human workers with hand held tightening tools or torque wrench, repetitive automated systems and flexible automated systems.

Currently, most of the small scale industries are using hand held nut runners or electric screwdrivers for threaded fastener assembly performed by a manual operator. These tightening tools will have force-torque control and in some cases the axial control of the fasteners. An example of a commercial pneumatic nut-runner is the QA4 series illustrated in Figure 2-13 used by the 'New Era Ohio' a major manufacturer of diaphragm and piston pumps, for installing fluid caps on a small pump which requires 24 separate bolts [85]. This method is time consuming and also needs extensive inspections due to reliability issues. Automating the threaded fastening operation can increase productivity, reliability and also saves valuable time by avoiding re-work.

Figure 2-13 : QA4 series Pneumatic Nut-runner [85]

Typical repetitive fastening systems used in industries, comprise of a bowl feeder or other mechanical feeding systems for arranging, orientation and feeding the fasteners into nut runners or electric screwdrivers. General Motors Corp (Detroit) implemented a semi-automated fastening system to install the Rivnut fasteners into vehicle bodies. The system consists of a supply hopper for bulk fastener supply, vibratory bowl to align fasteners in a particular orientation for feeding and an integrated electric screwdriver which is operated by human worker [86]. The feeding system used in this solution occupies large

spaces. The feeding units may require extensive modification in case of product change, thus lacking flexibility.

JMP engineering developed a flexible automated assembly system for assembling thread protector on the oil pipes to protect its threads from damage during packing and transit [87]. The solution includes two industrial robots and a machine vision to locate and manipulate the thread protectors. One robot moves towards the thread protector located in a bin, the camera in the hand of the robot takes a picture, to identify, localise, pick up and places a thread protector at a known position near the second robot as shown in Figure 2-14 (a). The second robot picks up and carries the thread protector towards the pipe positioned in a fixture as shown in Figure 2-14(b). An image of the pipe is obtained using the camera in hand to located the pipe and measure its hole geometry. A compliant device is also fixed to its end-effector which adjusts to the pull created while fastening the thread protector into the pipe. The thread protectors come in various sizes and all are assembled through one system which increases the flexibility and also the productivity. The localisation of the thread protectors are in 2D and the pipe hole need to be perpendicular to the camera for the system to identify and localise it. This automated solution defers substantially from the fastening of threaded fasteners in a random environment where bolts are in a clutter and threaded holes are located in 3D.

a) Bin-picking thread protector

b) Robot approaching threaded pipe

Figure 2-14 : Thread protector assembly using machine vision [87]

In a particular aerospace company, there are over 400 different types of fasteners used for manufacturing aircrafts. The sorting processes for such a large number of fasteners are usually done by manual workers. The use of mechanical vibratory bowl feeders are not cost effective in this circumstance as they are only capable of handling one family of parts, or they need a large number of feeders to handle the fasteners. Thus they implemented an automated solution from the Rixan Associates termed as RFS-1000 (Figure 2-15 (a)) with flexible vibratory bowl feeder which costs around $45000. The solution potentially provided a significant increase in productivity [12]. The system has a vibratory bowl for handling fasteners, shown in Figure 2-15 (b) (aerospace fasteners are replaced with chocolates due to confidentiality) and a Cognex In-Sight 5401 vision system to identify the position and orientation of fasteners in the vibratory bowl.

a) Rixan RFS-100

b) Vibratory bowl used in RFS-100

Figure 2-15 : Rixan aerospace fastener sorting and pick up system [12]

If a fastener with the right orientation is found, then the bowl feeder is stopped and the camera takes an image again to localise the fastener. This location is then sent to the Mitsubishi Electric RV-6SL-S11robot to pick up the fastener. If the fasteners are not oriented properly it will be sent again into the vibratory bowl feeder. The fasteners are required to be in a particular orientation to be picked up by the robot, if not, it goes into the vibratory bowl. Despite the flexibility achieved by handling different types of fasteners, this solution can

only identify objects that are separate and located in 2D. The process of orienting the fasteners completely depends on the vibratory feeder and can take more time to change the orientation.

Another industrial example is the F-35's J450 Wing Overlap drilling facility at Lockheed, which uses an automated drilling and fastening method [13]. In this example, the external metrology for positional guidance is obtained using a laser triangulation scanner and a non-contact probe attached to the end-effector. The metrology data is used for measuring the countersink quality, hole diameter and grip length as shown in Figure 2-16. The FILLS (Fastener Installation Live Link System) is an automated hole measurement system that carries out accurate insertion of roughly 30,000 fasteners in the F-35 centre fuselage. The entire process uses a digital thread manufacturing technique which creates a list of fasteners brought to the work area automatically. The Delta Sigma's ProjectionWorks 3D projector is then used to display a 3D colour coded map which provides information about location of the target holes where the fasteners are to be installed. It also displays the assembly sequence, part number and direction for fastening on the component.

Figure 2-16 : Kuka robot automatic drilling and inspection [13]

2.3 Summary

Based on the reviews carried out on the academic literatures and also on the existing industrial solutions, it was understood that the existing technologies and ongoing research are not suitable for assembling objects in a non-

structured environment. It was also found that the existing solutions are mainly focused on component assembly and peg-in-hole insertion, but none focus on the automation of fastener assembly. Most of the research methods investigated is either based on semi-structured 2D environment automation or component-specific, flexible 3D assembly automation, which may to some extent have addressed specific industrial needs. Current industrial solutions include employing manual workers with hand-held tightening tools, robotic assembly using feeders and vibratory bowls for sorting and orientating fasteners. However, these existing assembly methods have not been tested in a random environment for industrial application. Such capability is essential to provide an automated fixtureless assembly solution. Eliminating the need for knowledge of accurate positioning of components is a key benefit for this research that can potentially save significant amount of investment on equipment and tools.

The review was also conducted on research carried out to automate individual assembly tasks and sub-tasks such as object pick up, object insertion, assembly alignment monitoring and control, object identification and feature detection. It was found that the object pick up methods are affected by factors such as occlusion, accuracy and also have a high processing time due the complexity of the algorithms. The object insertion methods are not applicable for fastening, as they involve simple insertion rather than the torque-controlled helical transition required for fastening.

Among the various object identification methods investigated, the surface-based matching method with the required enhancement is found to be more suitable for bolt identification from clutter. The literature also showed that there is no method available for detecting threaded hole features with chamfer located at random 3D position and orientation. Clearly, there is a requirement for a new hole detection method that has yet to be developed as a part of this research. Further important findings based on the literature review, is the time and efficiency of the existing methods which are not suitable for industrial assembly processes. Thus, the object and feature identification methods required for this research should be robust and fast, in order to be implemented in industries.

CHAPTER 3 - RESEARCH PROBLEM AND PROPOSED SOLUTION

This chapter describes the research problem in the field of assembly automation and also the hypothesis put forward based on the problem. It states the solution proposed to automate fastener assembly, along with the research plan and the approach.

3.1 Research problem

The fastener assembly accounts for over a quarter of all assemblies carried out in industries. Currently most of the fastening operations in industries are carried out by manual operators or repetitive automated systems. The manual fastening is not reliable and is time consuming. Contrary to that, repetitive automation is not flexible and adaptable, as it requires component-specific fixtures and extensive robot programming to adapt to product changes.

Despite the significance of fastener assembly in industries, not much research has been focused on automating the fastening process (as explained in section 2.1.4). Most of the research is focused on achieving fixture-less component assemblies and solving a typical peg-in-hole problem. A comprehensive review on the existing literature was carried out and reported in CHAPTER 2 - . This review clearly shows that existing automated solutions are not suitable to perform the assembly of a range of bolts located in clutter form into their corresponding size threaded hole in a non-structured environment.

The primary reasons for not automating fastener assembly are mainly attributed to the cost factor and also the difficulty involved in automating the process [11]. The difficulty is due to the requirement of flexibility, adaptability and intelligence to perform the fastening operation (a manual operator has the intelligence and dextrous hands to perform fastening). This strongly emphasizes the need for a freeform automated system that has the required flexibility and adaptability to perform fastener assembly. In addition, freeform automation can also play a

critical role in manufacturing industries such as aerospace and automotive where a high level of accuracy, adaptability and productivity are crucial for their development. However, to restrict the research efforts to a manageable size, the scope of this research is limited to metallic hexagon drive bolts with a standard pitch size (explained in section 1.6).

3.1.1 Research hypothesis

The research hypotheses stated for this research include:

1) Machine vision guided robots can provide high flexibility and adaptability to assemble different size fasteners in a non-structured environment.
2) Enhancing the surface model creation process in the surface matching technique can identify and locate fasteners from clutter robustly, with less processing time and high accuracy than the existing method.
3) Feature identification based on a difference in gradient between neighbouring points can detect sharp edge features from point cloud data (PCD). These edge features provide significant information, which is sufficient to identify and localise the outer edge of a 3D feature (hole) on a component with high robustness and accuracy.
4) Integrating commercially available systems and technology with novel algorithms can be used to develop a robust automated fastening system.

3.2 Proposed solution

The research is focused initially on the assembly of metallic bolts into a fixed component with threaded holes. The bolt represents any sub-assembly component that may be accessible to an automated handling mechanism, for example the assembly of two sub-components before fastening onto a third component. The required precision for identifying the size of bolts and hole features is required to be 1 mm (minimum difference between two standard metric bolts) for accurate size classification. At the same time, the required translational and rotational accuracy are considered to be less than 1 mm and 1° respectively for the robust assembly process without misalignment or cross-threading.

In the proposed fastener assembly solution, the initial step is to identify and localise the components (in this research - different size threaded holes in the target component) placed at a random location within the workspace. Then, it needs to identify and localise different size bolts located in clutter. The size of the identified threaded hole feature dictates the size of the bolt required for fastening. Hence the system determines the assembly sequence automatically by allocating the right size bolts to the threaded holes. After matching bolts and holes based on their size, the system picks up the right size bolt from the clutter by manipulating a robot with an appropriate end-effector.

Once the right size bolt is picked up, the system identifies the assembling axis (i.e. the orientation and the axis perpendicular to the centre of the threaded hole plane) and approaches the hole in that direction. The final and fundamental step in fastener assembly is the fastening of the bolt into the corresponding threaded hole with right amount of torque. The torque applied is monitored continuously in near real-time. The proposed monitoring system is influenced by the way human operator performs the fastening processes. By doing so, the system is able to retain high level of robustness and precision, at the same time being able to avoid misalignment and cross threading. A mechanism is required to distinguish between the tightening torque and the miss-alignment torques (e.g. cross threading). Figure 3-1 illustrates the steps involved in proposed automated freeform assembly method.

In this research, commercially available technologies and equipment are used, but significantly enhanced to be suitable for industrial assembly applications. A laboratory prototype automated assembly system is developed to replicate the industrial environment and investigate the applicability of the proposed solutions. Different 3D imaging devices are evaluated under different lighting conditions and surface qualities to select a suitable imaging device for this research application. To improve performance, prior knowledge such as CAD models of the bolts are utilised for determining bolts located in clutter. A novel hole feature detection algorithm has been developed to identify threaded holes. The entire assembly processes and systems were integrated in the form of an automated assembly prototype system. Control and monitoring mechanisms

are developed and deployed to prevent any component misalignments such as cross threading.

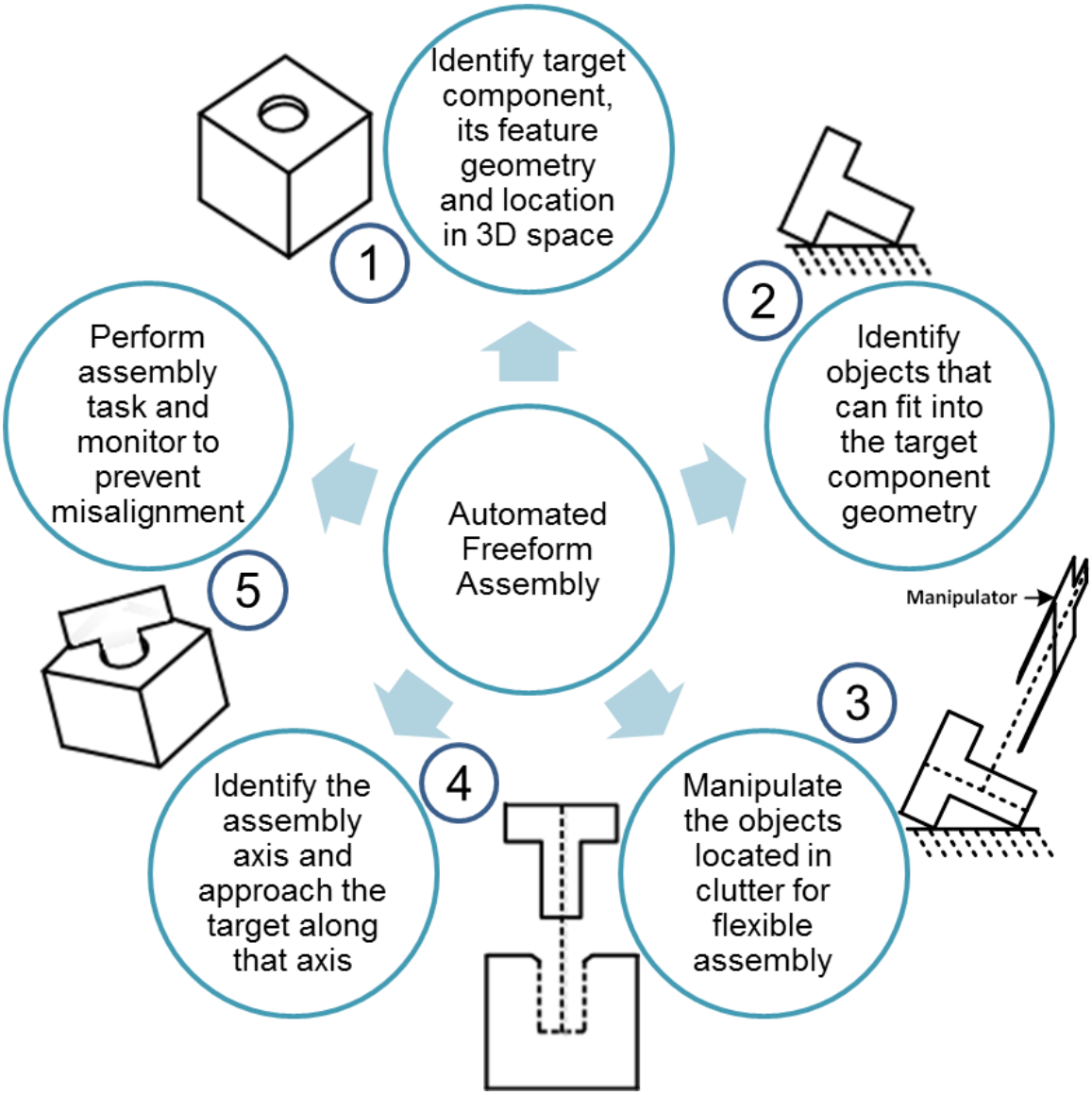

Figure 3-1 : Process involved in automated freeform assembly solution

The steps explained in the proposed solution are the fundamental processes required to assemble different size fasteners in a non-structured environment. These steps make the automated system flexible and adaptable to product and position variation in industries without the need for fixtures and robot programming.

3.3 Research plan

The research plan to achieve the proposed solution, to perform an automated freeform fastener assembly, includes the following stages as shown in Figure 3-2.

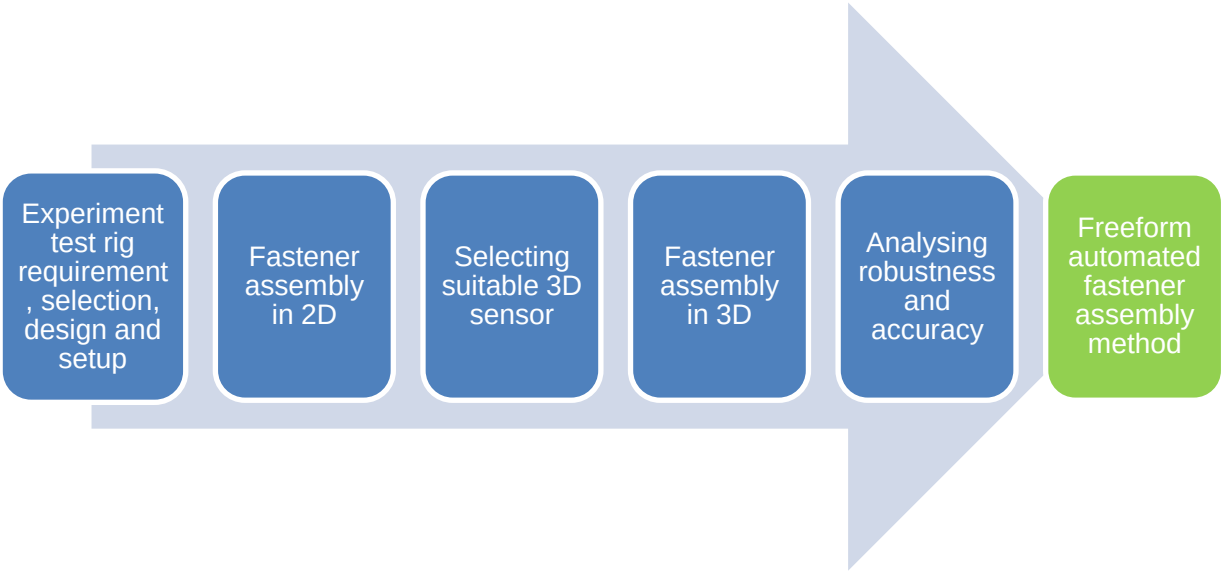

Figure 3-2 : Different stages of research plan

The first stage involves setting up an experimental test rig by identifying and integrating commercially available technologies required for performing fastener assembly. The second stage is to perform an automated fastener assembly of different sizes of hexagonal fastener with their corresponding fastening hole in two-dimensional (2D) environment (third dimension is assumed to be known). Example of this scenario is delivering parts (or bolts in this research) to a flat surface or the use of shadow boards to eliminate further complication of the part location.

The third stage focuses on evaluating different 3D imaging technologies to identify a suitable 3D sensor for fastener assembly which is capable of providing visual perception of the workspace in industrial environment conditions (i.e. variable lighting and object surface reflectivity). The fourth stage is to perform fastener assembly in 3D by identifying and localising fasteners from clutter and the fastening hole in a component located at a random position and orientation in a three-dimensional (3D) workspace. The final stage of the

plan is to evaluate and validate the level of robustness and accuracy achieved by the bolt and hole feature identification algorithms developed. For instance, picking up bolts from a bin and assembling the part to an approximately located component, such as a large aircraft wing.

3.4 Research experimental approach

A test rig is developed for the experiments to replicate an industrial environment, as there was no industrial partner available. Hence, an assembly scenario was developed to closely resemble industrial fastening in automotive and aerospace industries. The capabilities of the existing technologies are assessed based on the specifications provided by the manufacturers and enhanced by new and innovative mathematical algorithms.

The enhanced technologies are then assessed under variable lighting conditions, random positioning, similar to those required in industrial applications.

The complexity of the assembly scenarios are gradually increased from a 2D positioning environment to a 3D freeform localisation. At each stage, various types of identification technologies (e.g. vision systems and laser scanners) are used and the success rate of the assembly process is recorded.

An empirical approach is taken to measure and assess the enhancement made to the existing technologies and evaluate the robustness of the solution for industrial application domains.

CHAPTER 4 - SYSTEM INTEGRATION AND COMMUNICATION MECHANISM

In this chapter the hardware devices required for the fastener assembly system and the communication setup established for the integration of these hardware are explained. In addition, the justification for selecting the hardware devices, their working procedures and specifications are described. This chapter also provides the analysis of tests carried out for evaluating the hardware suitability to be used in fastener assembly system.

The hardware and devices required for fastener assembly depends on the approach taken for assembly automation. The automation approach for assembly is determined based on different parameters such as type of assembly components, automation level, sensing element and the workspace as shown in Figure 4-1. It also depends upon the level of robustness and accuracy required for the application. In the assembly scenarios, fastener assembly can be performed by either repetitive automation or intelligent automation. The repetitive automation represents performing a number of tasks repeatedly in a structured environment, thereby lacks adaptability to variation. This type of automation does not require any active sensing elements as the position and orientation of the assembly components are fixed. On the other hand, the intelligent automation needs to obtain perception of the objects to identify and also make a cognitive decision to perform successful assembly. The object perception can be obtained using sensing elements such as visual and tactile sensing. This type of automation can be adaptable to variation in objects and also to the work environment. Selecting suitable sensing elements depends on the type of assembly components used and also the environment conditions such as lighting in which the assembly is carried out.

Currently, industries are focused in developing intelligent and flexible approaches for assembly automation. This involves identifying and optimising manual skills for assembly that can be implemented through automation systems. Thus the approach taken for this research is to emulate human

operator to perform robust and intelligent automated fastening. In manual fastening scenarios, human operators utilise their vision and tactile sensing for fastening a fastener (bolt) into a threaded hole.

In this research, visual sensing (using cameras or scanners) is required to identify fasteners and threaded holes located in an unknown position and orientation. Initially, bolt assembly is carried out in two-dimensional workspace to start with less complexity. Then the assembly is carried out in a three-dimensional workspace (i.e. more complex condition) which is the case in most real industrial scenarios.

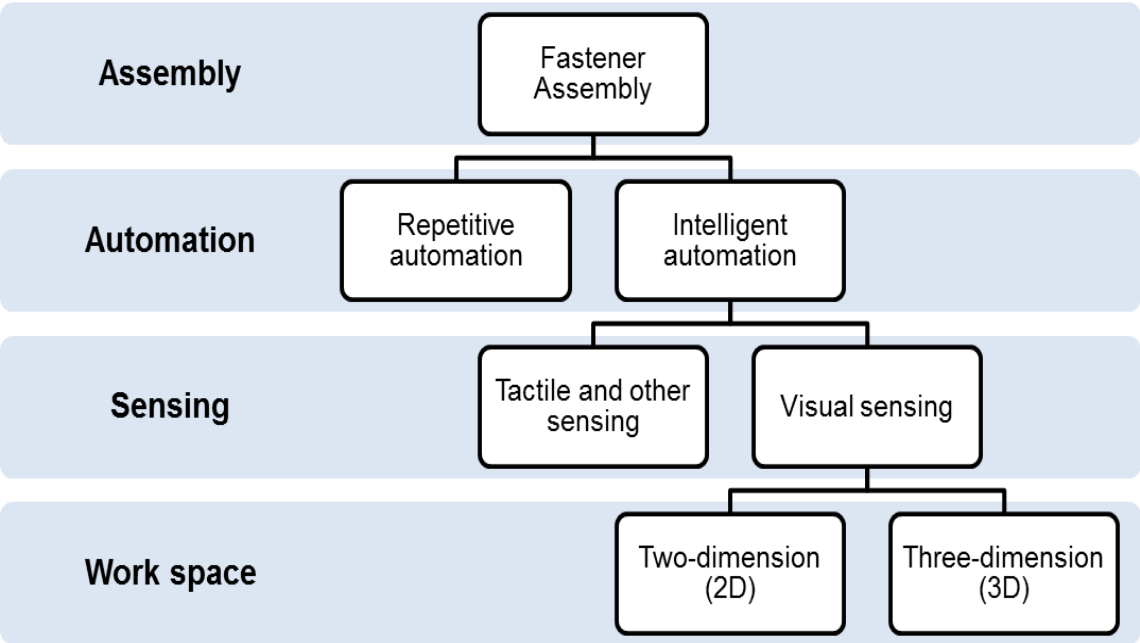

Figure 4-1 : Automation Approach

4.1 System Specifications

The fastener assembly system proposed in this research is a unit developed by integrating different technologies and devices required to perform various tasks involved in fastener assembly. This integrated system requires a centralised unit for controlling and monitoring the entire assembly process. The system requires a visual sensor for identifying the fasteners and threaded holes in the target object located in random positions. It also needs a manipulator (such as a robotic arm) to pick up the fasteners and manipulate them to reach the test

object in the work space. After reaching the target object with threaded holes, the system requires a tightening mechanism to perform torque-controlled fastening. The final requirement is a test object with fastening holes on a different dimensional space to represent the real industrial fastening conditions and different size fasteners (i.e. hex bolts).

The hardware requirement for the fastener system to perform automated assembly of fasteners is illustrated by Figure 4-2.

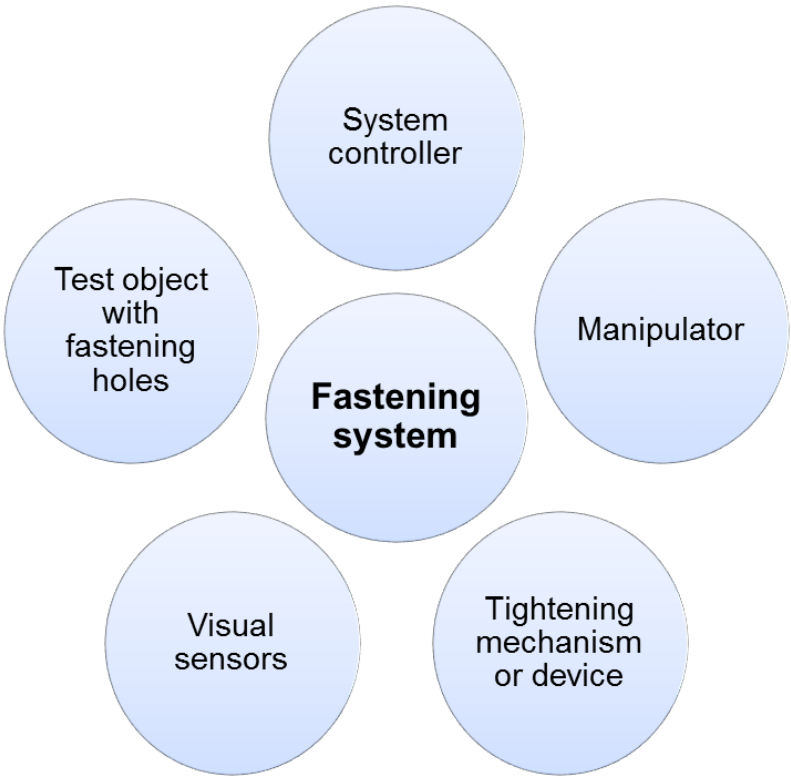

Figure 4-2 : System hardware requirements

The criteria for selection were based on the availability and compatibility of system hardware with future collaborators (i.e. aerospace and automotive industries) and to transfer this system to industries without many modifications.

4.1.1 System Controller

The system controller is a device that can be programmed to control and monitor the entire automated fastening process and also the individual devices. It acts as a master unit to control all other system hardware such as manipulators, sensing elements, tightening mechanism and also the algorithms

developed for object and its target identification. The system controller represents any programmable device such as personal computer (PC). The performance of the system control, which includes data-processing speed and communication speed, depends on the processing capacity[1] of the computer.

4.1.2 Manipulator

The manipulator required for the fastener assembly depends upon the work area reachability and type of objects used for assembly. The task of the manipulator in this research is to pick up and carry the hex bolts from their initial location to the corresponding target location using the position and path information provided. The manipulators required for the assembly includes an industrial robot for moving the bolts, an end-effector for gripping actuation and gripping fingers for grasping the bolts in the workspaces.

The industrial robot used for bolt manipulation in the workspace is a Yasakawa Motoman SDA20[88] shown in Figure 4-3. Any industrial robot with one arm or two arms can perform the task required for this research. The Motoman robot is used because of its two arms which provide additional flexibility for manipulation within the workspace required to replicate human operators; it is also readily available in the lab.

Figure 4-3 : Yasakawa Motoman SDA-20[88]

[1] The PC used in this fastening project includes an Intel Core i7 processor with processing speed of 3.40GHz and an internal memory of 16GB.

The Motoman robot is a two-arm industrial robot with 15 degrees of freedom (DOF) in total with 7 DOF on each of its arm and one DOF on its body waist region. The robot controller type used for controlling the Motoman SDA20 robot is DX100. The robot arms can carry a payload of 20kg each. The repeatability of the robot is in the range of ±0.1 mm and the maximum speed ranges from 125 °/s to 400 °/s varying between the joints. The complete specifications of the robot and controller are provided in appendix A1.

The end-effector can be any commercially available two-finger gripper which is capable of generating an actuation for the gripping fingers to grasp an object. The Schunk PGN-Plus 80-1 pneumatic gripper[89] shown in Figure 4-4, is used as the end-effector along with two gripping fingers. The pneumatic actuation is preferred over the electric actuation due to its cost advantages and robustness.

The gripper has a closing force of 415 N and is capable of carrying an object with a weight of 0.5 kg. The maximum stroke for the fingers is 8 mm with an accuracy of 0.01 mm and the other technical data are given in appendix A2. At the initial stage the tightening mechanism described in section 4.1.3 is used for picking up bolts from a cradle. The gripper is used at later stages where the bolts are in clutter form - and fingers are required to grasp bolts for picking up.

Figure 4-4 : Schunk PGN-Plus 80-1 Gripper[89]

The fingers are required to grasp the objects located in the work space. In this case, the gripping fingers need to hold the cylindrical threaded section of the hex bolt for grasping and picking up. The bolts are of different sizes and may be

lying on a flat surface or in a clutter form. Therefore the fingers designs are required to be capable of adapting to the conditions mentioned above.

The task of the gripper with fingers, in this research, is to pick up bolts from a flat surface or clutter and place them at their intended target position. For designing the gripping fingers, factors such as minimum clearance for picking up the bolt and minimum surface contact with the cylindrical surface, required for proper pick up, are taken into account.

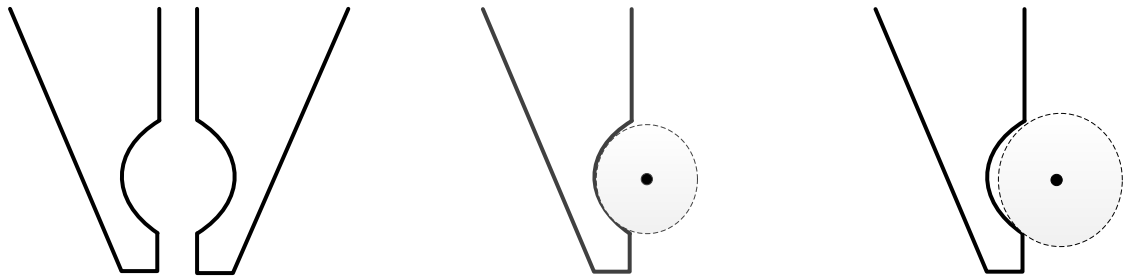

a) Fingers with arc cut b) Bolt size equal to arc c) Bolt size larger than arc

Figure 4-5 : Gripping finger design with arc cut

Among the different finger designs analysed, the gripping finger with an arc cut at the tip was designed as shown in Figure 4-5. The arc cut will provide a minimum of four contact points (i.e. two contact points for each finger) on its surface for grasping cylindrical threaded section of the bolts.

When the size of the bolt is equal to the finger arc surface or slightly larger than the arc as shown in Figure 4-5 (b) and (c), the bolts can be grasped at their cylindrical thread section. This ensures that the bolt position is located exactly at the centre of the arc surface between the two fingers of the gripper. However, for smaller bolt sizes, there is no guarantee that the bolt might remain at the same position at every pick up. Similarly, the condition where the larger bolt size is grasped using smaller size arc fingers might result in a failure to grasp the bolt. This is due to smaller arc surface (contact surface) available for grasping larger bolt sizes.

Therefore to cover a range of bolt sizes within the research scope (i.e. M5 to M14) and minimise the potential positioning error, two differently sized arc

fingers are designed, as shown in Figure 4-6. The finger with 5 mm arc radius indicated in Figure 4-6 (a) is designed to grasp the smaller sizes ranging from M5 to M8 bolts. Another finger with 10 mm arc radius, as illustrated in Figure 4-6 (b) is designed to grasp larger bolts ranging from size of M10 to M14. Since this finger design has a minimum of four point contact, it provides a firm grasp of bolts, thereby ensuring successful assembly. Several trials were carried out to test and validate the design by grasping the bolts from clutter which provided a successful grasping.

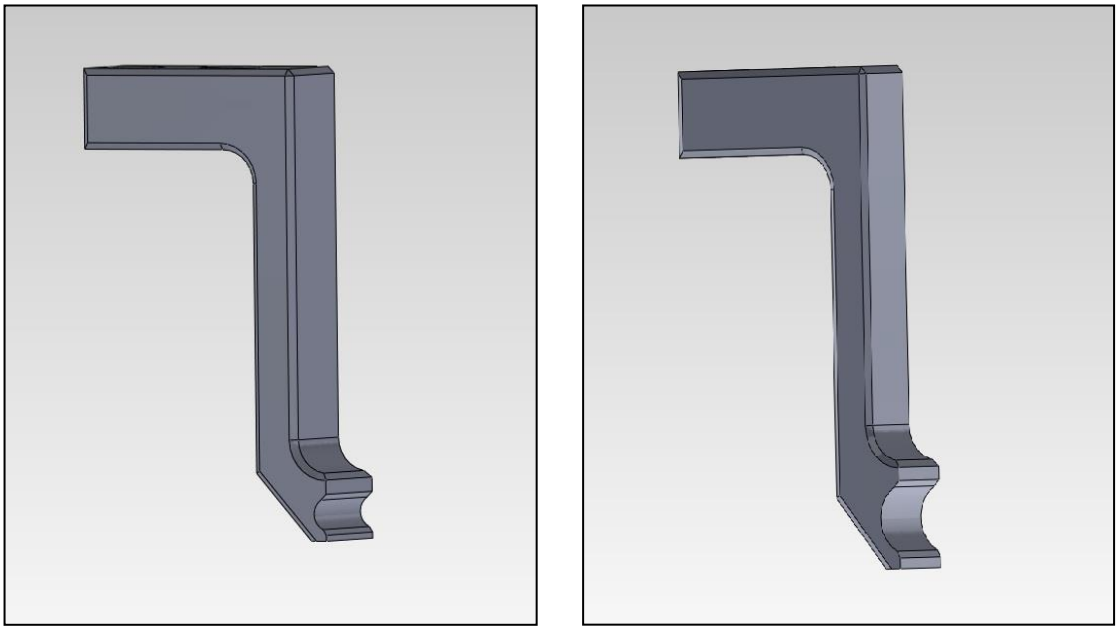

a) Finger with arc size of 5 mm b) Finger with arc size of 10 mm

Figure 4-6 : Finger design CAD model

4.1.3 Tightening Mechanism

An automated fastener assembly system requires a tightening mechanism to fasten the hex bolts into the corresponding threaded holes with appropriate torque. The tightening device is required to have a continuous and controllable rotating drive mechanism to fasten the bolts. It also needs to meet the maximum tightening torque requirement of 120 Nm to cover the bolt sizes specified in the research scope.

The other requirements of a tightening device for an industrial application include an acceptable speed and a compact size. It also has to be capable of

controlling the torque applied during fastening, as the amount of torque applied for fastening varies depending upon the size of the bolts. The amount of torque required for fastening also varies at different stages of fastening, for instance: the initial contact, running down and then the tightening. The control system for the drive should be compatible to enable the physical integration with a tightening mechanism for communication and power supply. The tightening mechanism is also required to have a gripping mechanism for handling the bolts and fastening them into a threaded hole. An analysis of existing systems for bolt tightening resulted in identifying the Bosch Rexroth tightening spindle [90] shown in Figure 4-7.

Figure 4-7 : Bosch Rexroth tightening system[90]

The tightening spindle has a measurement transducer, servo drive, gear mechanism and spindle bearing as depicted in Figure 4-8. It meets all the requirements stated for the tightening mechanism in this research, except the gripping mechanism for handling bolts.

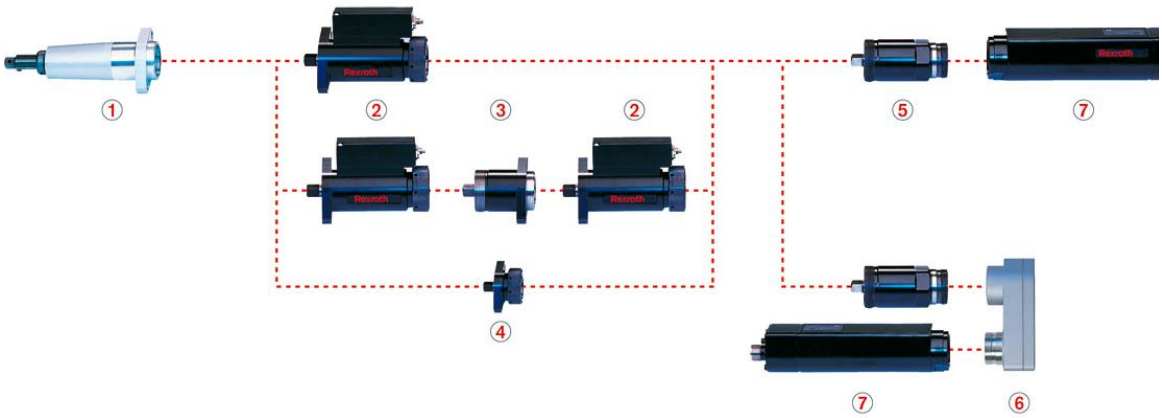

1- Spindle bearing 2- Measurement transducer 3- Redundant adapter 4- Adapter
5- Planetary gearbox 6- Transverse gearbox 7- EC motor (Electronically Commutated)

Figure 4-8 : Tightening spindle exploded view[90]

The accuracy of the spindle in delivering the required torque is less than 1 Nm, as noted in the manufacturer specification (see appendix A3). For the initial stage which is to demonstrate automated fastening of single type of fastener in 2D, this device is a suitable option. For handling bolts, a magnetic socket is attached to the spindle to facilitate bolt pick up from a cradle. At the later stages where the bolts are required to be picked up from the clutter, the gripper with two fingers described in section 4.1.2 is used.

4.1.4 Visual Sensing

Visual sensing is one of many technologies used for locating an object in a workspace for assemblies. Visual sensing can provide the perception of the work area in both two and three-dimensional space depending upon the assembly requirement. This research involves three stages, the initial stage focuses on assembling bolts in two dimensional space (the third dimension is known to the system) and requires a 2D visual sensor to identify co-ordinates. The Basler ace[91] given in Figure 4-9, is used as the visual sensor to obtain the 2D visual perception of the work area with objects. The later stages focus on assembling bolts in three-dimension and require a 3D visual sensor for detecting bolts in a completely random location. The Micro-Epsilon scanControl [92] laser scanner shown in Figure 4-9 (b), is used for obtaining a 3D visual perception of the randomly located objects. Selection and specifications of 2D and 3D sensors are discussed in CHAPTER 5 - and CHAPTER 6 - respectively.

a) 2D sensor - Basler ace 1600-20gm[91]

b) 3D sensor - Micro-Epsilon scanControl 2900-50[92]

Figure 4-9 : Visual sensors

4.1.5 Test Objects

The primary objective of the fastener assembly is to pick up different size bolts and fasten them into corresponding threaded holes. Thus the test objects required for this task includes different size hexagon head bolts and a target component with different size threaded holes, as explained in the research scope.

At the initial stage, the hex bolts are considered to be located in random 2D space and identified using their head shape and size. For this, the bolts are placed on a cradle with their head section on top. A cradle that can hold hex bolts with size ranging from M5 to M14 was designed and made to represent semi-structured 2D environment as shown in Figure 4-10.

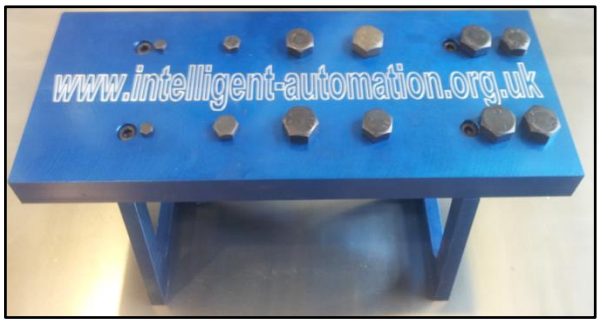

Figure 4-10 : Cradle with different size bolts

To represent the threaded holes in multi-dimensional space, a fastening plate was designed with different size threaded holes as shown in Figure 4-11. The threaded holes on the target component are located in both flat surface and also at different angled surface to emulate the 2D and 3D fastener assembly conditions. It is a circular steel plate of 250 mm in diameter and 25 mm in thickness mounted on a fixed holder (Figure 4-11). The fastening hole plate has eight threaded holes of four different sizes (M5, M6, M10 and M14), two of each size on the top surface of the plate to represent the holes located in 2D space. The dimensions of the fastening plate are provided in appendix A6.

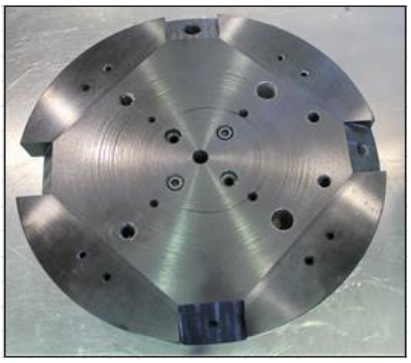

Figure 4-11 : Fastening plate with different size holes mounted on a holder

The fastening plate also has four threaded holes of sizes M5, M6, M10 and M14 on its angled surface, located at an angle of 60, 45, 30 and 15 degrees respectively to represent the holes in 3D space. The plate was designed to represent different fastener assembly conditions that may exist in industries.

The fastening plate holder is designed in such a way that the fastening plate can be mounted both horizontally and vertically. The fastening plate can also be rotated around its centre, giving it the flexibility to represent the threaded holes at random positions in 2D and 3D space.

4.2 Communication Mechanism

Communication setup is a vital step in developing the fastening system, as it integrates the individual hardware devices together into one complete system. The communication setup was developed with a centralised control for all the hardware devices to synchronise their functioning within the system. It is also required to provide a near real-time feedback control to the system's devices, for instance, the stopping of a fastening operation in case of cross threading. In fastener assembly system setup, the PC acts as the centralised control to the robot, the tightening spindle and the vision sensor, as shown in Figure 4-12.

The communication mechanism required for integrating the devices used in this research did not exist as an off-the-shelf solution. It had to be developed using a program written in C# programming language in the PC. The communication link between all the devices in the fastener assembly system is categorised into two types, active data transmission connection and passive device connection.

In active connection, the system exchanges data actively during the entire assembly process which includes communication between

- PC and robot controller
- PC and vision sensors (2D and 3D sensors)
- Robot controller and tightening spindle

The passive connection is the communication link established only to setup the connection with devices and to store predefined parameters or programs which includes:

- PC and Anybus communicator - DeviceNet network setup
- PC and tightening spindle - tightening programs

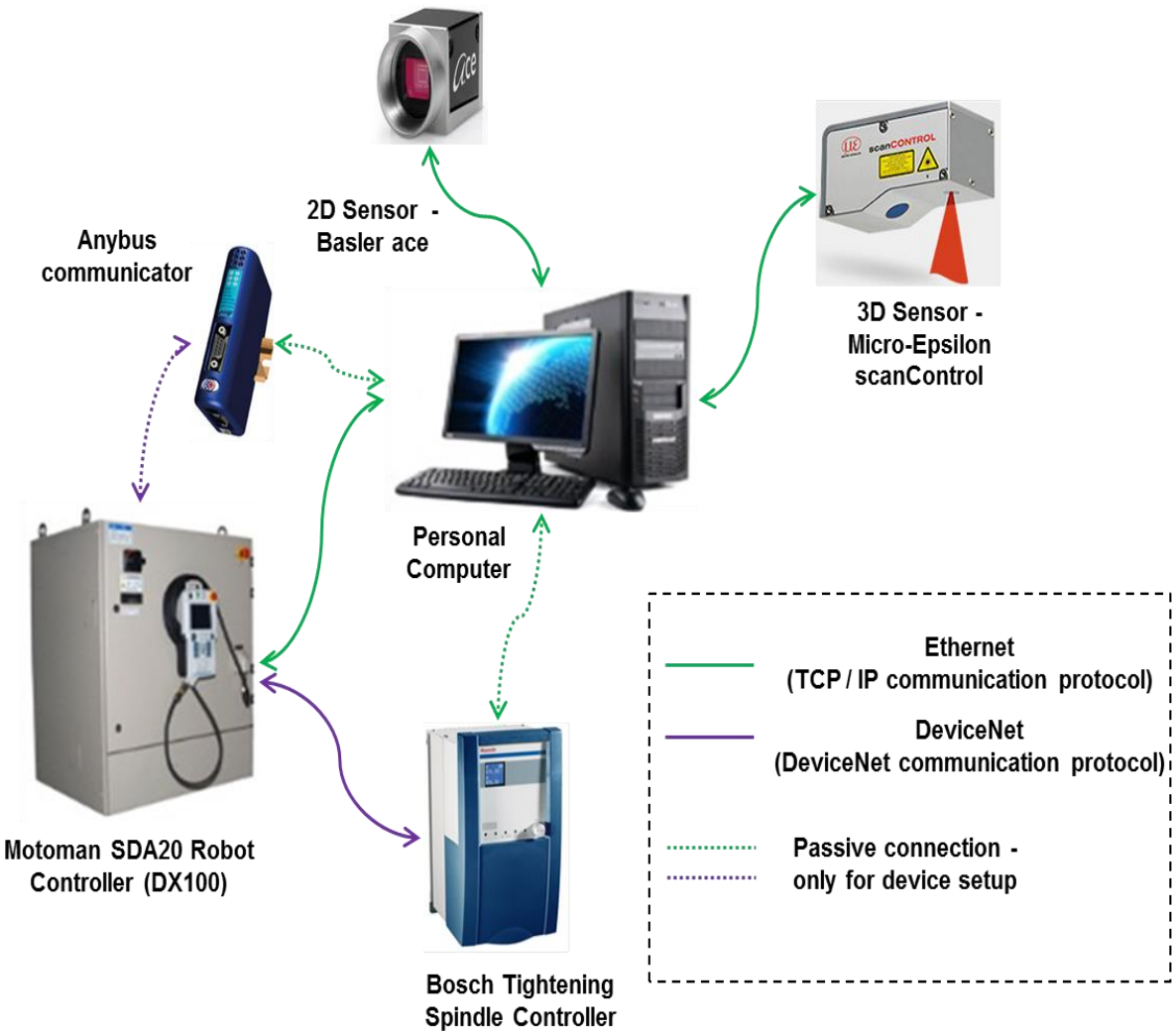

Figure 4-12 : Communication setup for the fastener system

4.2.1 Communication between PC and robot controller

DeviceNet protocol

Initially, DeviceNet protocol [93] was investigated as a potential communication protocol between the control PC and the robot. This is due to the communication link between tightening spindle and robot which was established first through DeviceNet protocol as described in section 4.2.3. Hence to bring all the devices under single network for effective communication, DeviceNet protocol was considered. Since the PC does not have a DeviceNet module for communication, a network bridge is required to enable communication between the DeviceNet network and the Ethernet network (available in PC). For this purpose, the HMS Anybus X-Gateway[94] provided in Figure 4-13) was identified which acts as a bridge between the Ethernet/IP and DeviceNet networks.

Figure 4-13 : HMS Anybus X-Gateway[94]

Even though the Ethernet/IP network uses Ethernet cable for communication, its host layer uses Common Industrial Protocol (CIP). This is similar to DeviceNet but is different from the TCP/IP protocol which is the network communication in PC.

Following a number of trials, it was realised that the Ethernet/IP protocol requires a data frame converter to interpret communication from one network protocol to another. At the time of this research, there was no open support available for both Ethernet/IP and DeviceNet communication protocol that can be utilised using any open-source programming language. Therefore an

alternative protocol was considered to reduce the complexity involved in establishing DeviceNet communication.

Ethernet Protocol

The DX-100 controller of the Motoman robot has a built-in Ethernet server function [95] which enables communication with any devices acting as a client. Therefore this communication method was used for the data transmission and the controlling the robot using the PC through the Ethernet. The Ethernet server function in the robot controller is a simple protocol that supports the sequential processing of requests. It uses TCP protocol for the lower levels of communication which simplifies the connection control in a network. The PC can communicate to the robot controller by establishing a connection using the IP address and port number. The outline of the data request and transmission using Ethernet server function is illustrated by Figure 4-14.

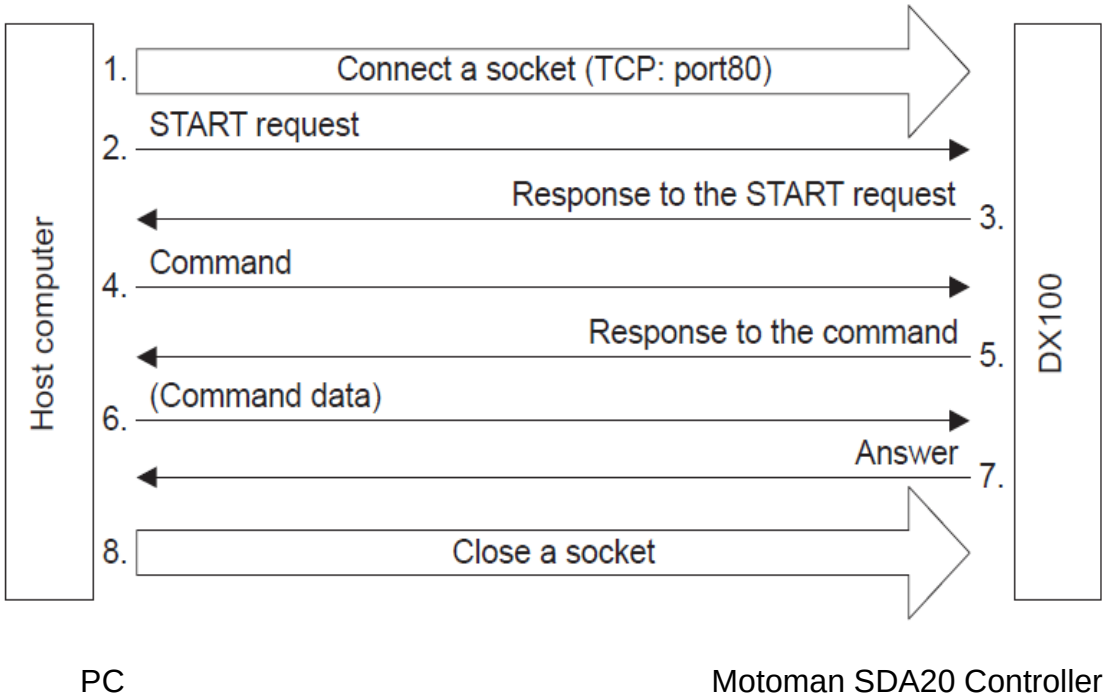

Figure 4-14 : Ethernet server communication outline

The command transmission in the Ethernet server function follows a simple 'Handshaking' technique. In this technique, first the client (i.e. the PC) has to send a request and the server (i.e. the robot controller) will respond to the request by sending back an acknowledgement. This process is repeated

throughout the communication between the devices. If the request is not in the correct format or structure, the server will send a response code depending upon the error. Figure 4-14 depicts that the PC is required to connect to the robot controller through a fixed port to establish a communication link. After that, the PC acting as a client sends a START request to start the data transmission with the robot controller acting as a server. Once the acknowledgement for the request is received from the server, the client can send or receive data. The number of commands to be sent to the robot controller can be predefined to avoid data losses. The command's details and the information to structure the data are provided by the Motoman communication manual. With the help of this information, a program was developed to establish a communication link. After the communication is completed, the PC has to close the socket port and it has to start again by repeating the above explained process if needed.

4.2.2 Communication between PC and vision sensors

The communication between the PC and the vision sensors (i.e. Basler camera and Micro-Epsilon laser scanner) are through TCP/IP protocol. These sensors have an open source libraries provided by the manufacturer. Using these libraries functions, program has been developed to establish connection and acquire data. The data acquisitions from the 2D and 3D sensors are explained in CHAPTER 5 - and CHAPTER 7 - respectively.

4.2.3 Communication between robot and tightening spindle

The tightening spindle and the robot can use the DeviceNet module as a common platform for communication. This type of communication allows one device to be a master and other devices to be in slave configuration. Since the robot has more control than the spindle, it was equipped with a DeviceNet master card. The tightening spindle was connected as a slave device in the DeviceNet network to enable communications with the robot. The DeviceNet protocol was developed for industrial application and it follows the OSI model. It contains Common Industrial Protocol (CIP) at the host layers, which is used for the communication session management and structuring the data format sent

to the receiver. It uses Controller Area Network (CAN) protocol at the media layers, which is used for the network routing and for reliable data transmission.

The tightening spindle works according to the programs stored in its controller. The tightening programs with required parameters such as torque, rotational angle, time and speed are predefined and stored in the controller. The program can have multiple parameter conditions in a single program step. For example, the program can have a threshold limit to torque, time and angle and if the tightening spindle exceeds any one of the limits the program will terminate the rotation of the spindle.

The tightening spindle controller only allows the master device in the network to select a program from a list of pre-stored programs. But the output of the encoders such as torque and angle values connected to the motor drive can only be obtained after a program has been executed.

The robot controller acting as the master device in the DeviceNet network can select a program stored on the tightening spindle controller by just sending the program number. The structure of the data frame representing program number has to be constructed using the following information:

- Total bits to be sent has to be 8 (bit 0 to 7)
- First six bits (bit 0 to 5) represents the program number
- The bit 6 represents program enable function
- The bit 7 represents clockwise or anti-clockwise rotation.

It was found that the six bits to enable program number restricts the maximum number of program that can be selected to 64, even though the total number program that can be stored in the controller is 100.

The output received by the master device (robot controller) from the tightening spindle controller can be configured to include program number, torque and angle value (obtained from an encoder) after executing a program. The output data structure is arranged in a format as described below:

- Program number (1 byte)
- Torque value (4 bytes)

- Angle value (4 bytes)

The output received does not represent the values of the program number, torque and angle in decimal numeral system, as it is in the Fieldbus communication format. Therefore the output has to be processed to convert it into the decimal numbers by following the steps shown below:

- Read the 4 bytes of information into 4 separate decimal numbers
- Reverse the order of the 4 decimal numbers
- Convert individual decimal numbers into binary
- Combine all the binary bits together into a single 32 bits string
- Convert the 32 bits string into a decimal number
- Multiply the decimal number by
    1. Factor of 0.0001 for torque values in N/m.
    2. Factor of 0.0001 for angle values in degrees.

The result obtained by the steps explained above gives the actual torque and angle values in a decimal numeral system. The output values obtained are then used to verify the input values provided through the tightening program.

4.2.4 PC and Anybus communicator - DeviceNet network setup

In order to setup the DeviceNet network and add the master device (i.e. the robot controller) and the slave device (i.e. the tightening spindle) to the network a communicator device and commercial software is required. The HMS Anybus Communicator for DeviceNet [96] shown in Figure 4-15, which has a DeviceNet module interface at one end and a Ethernet module interface on the other end, is used for setting up the network. This device along with the Anybus Netool software is utilised for adding new devices and also to categorise the devices into master and slave devices (see appendix A7 for technical information).

Figure 4-15 : HMS Anybus Communicator for DeviceNet [96]

The reason for selecting this device is its ability to allow any device with Ethernet network to control the DeviceNet network. In this case, the PC with Ethernet port is programmed to set up and modify the devices connected to DeviceNet network. It was also used for setting up the parameters such as the number of devices in the network, allocating input and output memory in the master device for data transmission with other slave devices connected in the network. A total of 64 devices can be connected to the DeviceNet network, but only one master can be in the network and the remaining devices can be added as slaves.

4.2.5 PC and tightening spindle - tightening programs

The PC and tightening spindle controller are communicating through the Ethernet connection as indicated in Figure 4-16. The tightening spindle is equipped with PC interface software which is used to develop tightening programs.

The PC interface has drag and drop function modules which allows the user to program multiple steps with different parameter conditions. The functions available in the interface are user-friendly and can be programmed easily, but with limited flexibility (i.e. programming steps are pre-defined and cannot be changed during the process).

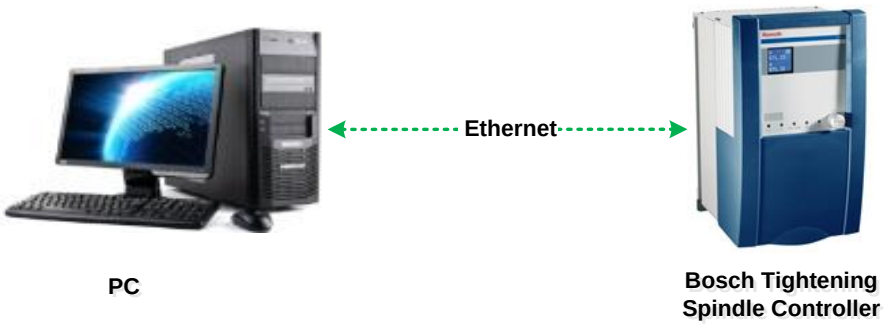

Figure 4-16 : Communication between PC and tightening spindle controller

The communication made by PC with the tightening spindle controller is an offline process. The tightening spindle controller cannot be programmed once it is connected to DeviceNet network. It only allows the selection of a pre-stored program by using the program number. Therefore, programs required for the fastening process has to be pre-programmed and stored in the tightening spindle controller.

After creating the programs with required torque, angle, time and speed parameters in the PC interface provided by the manufacturer, it is then sent to the tightening spindle controller. The connection between the PC and tightening controller has to be disconnected after storing the programs. The tightening spindle can be controlled from the software interface provided by the manufacturer by logging into the 'Online mode'. The programs developed using the interface can be tested by running them directly from PC. The output of the programs after completion can be visualised on the interface. This interface shows the output values of the torque, the angle and the time of the tightening spindle after executing a program. These data can also be used to analyse the tightening program.

4.3 System setup for fastener assembly

The hardware devices required for performing fastener assembly are integrated into one system with PC as their master control. The communication links between all the devices are established to facilitate control and data transmission. The tightening spindle and the Schunk gripper are mounted on the robot, one in each arm to assist in picking up and manipulating the bolt to

carry out fastening. Figure 4-17 illustrates the system setup developed for automated fastener assembly.

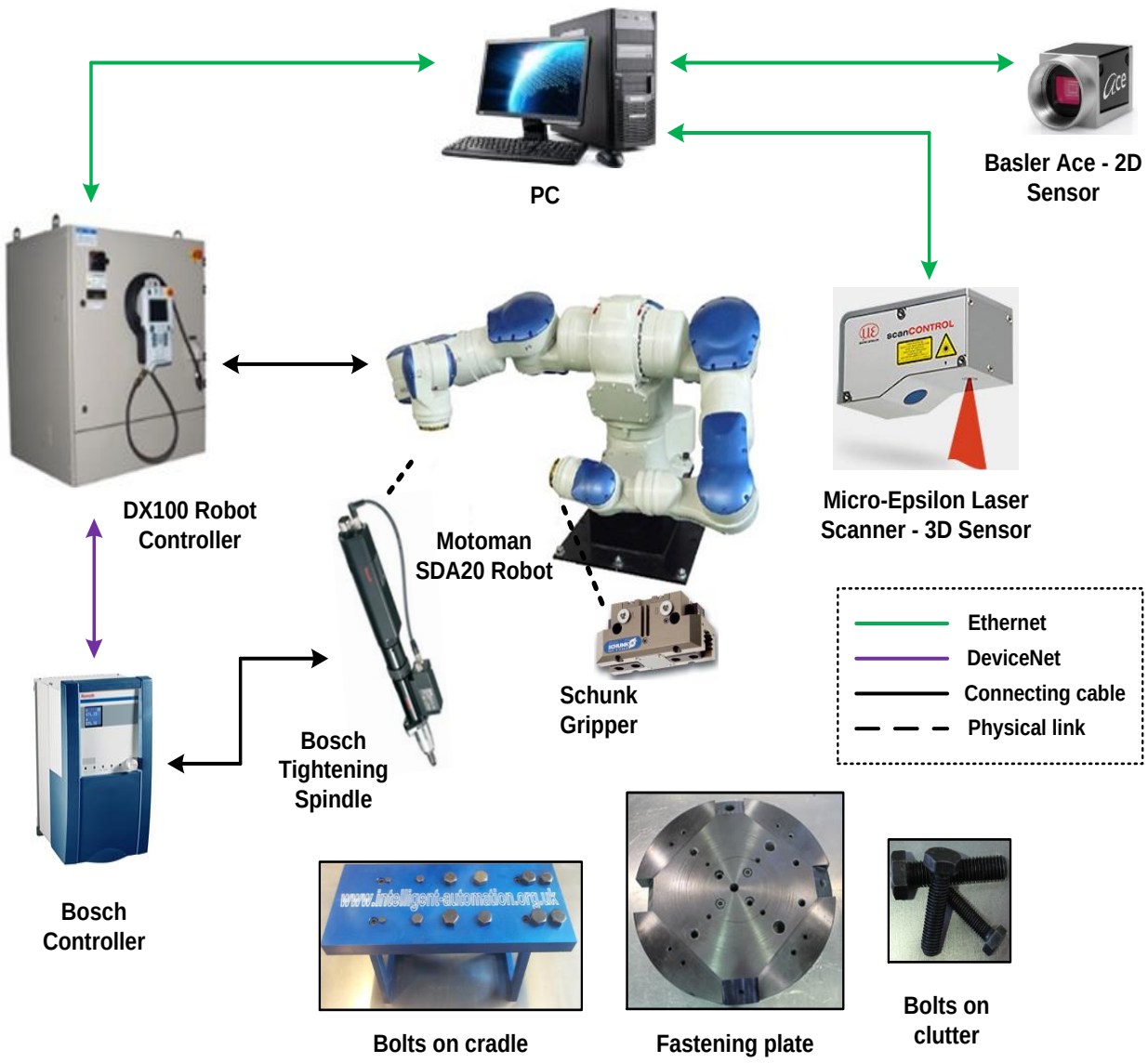

Figure 4-17 : System setup for fastener assembly

4.4 Accuracy test for the tightening spindle

At the initial stage of the research, a hexagonal magnetic socket was attached to the tightening spindle for picking up the bolts located in the bolt cradle. For facilitating successful pick up of the bolt by the socket, the tightening spindle with the socket has to be aligned with the hex bolts. This requires accurate rotation of the spindle in order to align within the bolt head. Therefore a number of experiments were carried out to determine the rotational accuracy of this

device. It was also understood that the success rate of the pick-up process depends upon the rotational accuracy of the spindle.

A plan was devised to find the angle deviation of the bolt head with respect to a reference line, considering the magnetic socket in the spindle has to be aligned to the reference line. The angle between two sides of a hexagon is 60° which is the case in both the socket and the bolt head. Considering that the reference line is a horizontal line: any two corners of the hexagonal magnetic socket in the spindle align with the reference line. The best case scenario for bolt alignment will be that any two corners of the hex bolt are located on the reference line; therefore angle correction is not required. The worst case will be that any two sides of the hex bolt are perpendicular to the reference line which needs an angle deviation correction of ± 30° as explained in Figure 4-18.

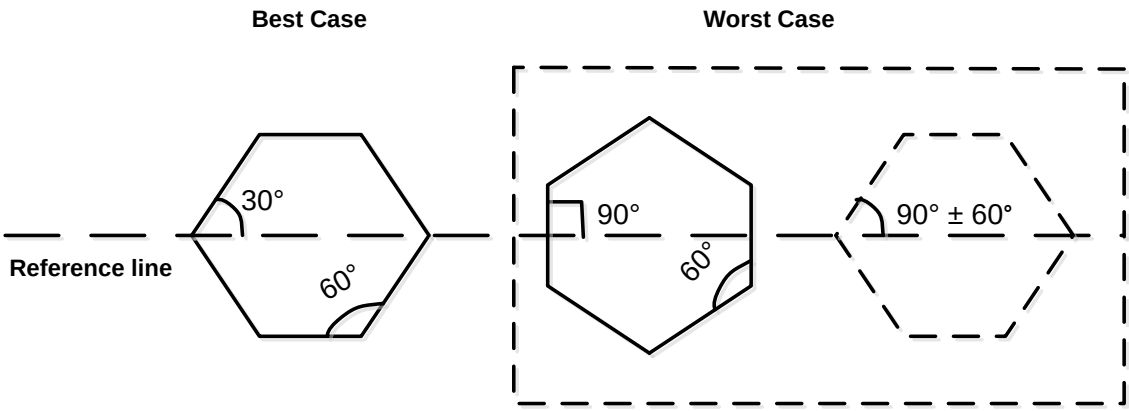

Figure 4-18 : Maximum angle deviation of hex bolt head

Therefore, the deviation of the bolt head with respect to reference line may fall between 0° and 30°. This required the tightening spindle to be rotated to increment angles in order to correct the deviation of socket with respect to bolt head. The tightening spindle accuracy in delivering the required torque is stated by the manufacturer as 1 Nm with a repeatability of 0.30 Nm. But the accuracy of rotational angle for the tightening spindle has not been specified by the manufacturer. An experiment was devised to calculate the accuracy of the tightening spindle rotation angle.

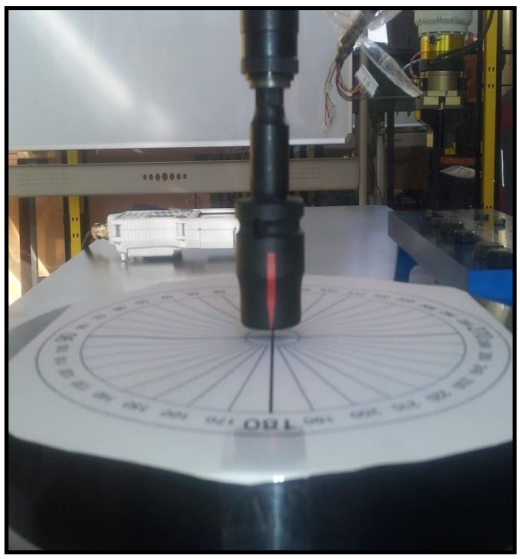

a) Socket with red marker

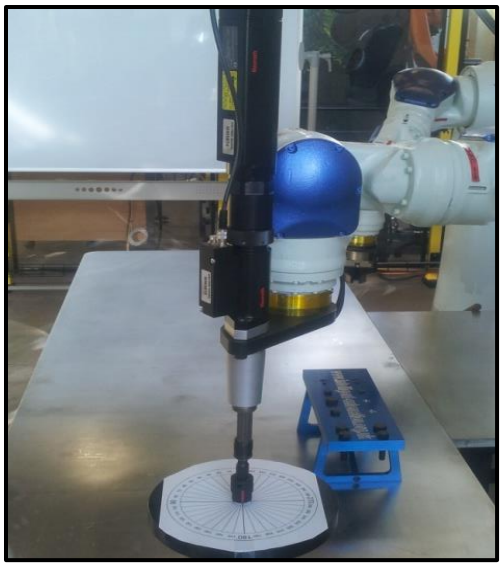

b) Spindle positioned above a protractor

Figure 4-19 : Accuracy test

Initial tests with a marker on the socket to indicate the starting point and protractor (Figure 4-19) showed the inaccuracy of the spindle to rotate small angles but less error while rotating large angles. This is the reason for conducting an angle accuracy test over three different ranges, as described below. The experiment was carried out to find the accuracy at three different ranges of angles:

- Small range angles (5°, 10°, 15°, 20° and 25°)
- Medium range angles (30°, 40°, 50°, 60°, 70° and 80°)
- Large range angles (100°, 150°, 200°, 300° and 360°)

The spindle is made to rotate five times for each angle in all three angle ranges. This is to test the accuracy of the angle at all ranges and also for the repeatability of the spindle for each angle.

Table 4-1, Table 4-2 and Table 4-3 show the encoder value of the rotated angle, the average error and the repeatability of each angle in the small, medium and large ranges respectively.

Table 4-1 : Small angle range rotation

Angle Given (degree)	Encoder Value - Angle rotated (Degree)					Average error (degree)	Repeatability (degree)
	Trial 1	Trial 2	Trial 3	Trial 4	Trial 5		
5	11.7	12.0	11.9	11.9	12.1	6.9	0.1
10	16.3	16.1	16.3	16.1	16.0	6.2	0.1
15	20.1	20.1	20.0	20.3	20.4	5.2	0.2
20	25.2	25.1	25.1	24.9	25.2	5.1	0.1
25	29.9	30.0	29.9	29.9	30.0	4.9	0.1

Table 4-2 : Medium angle range rotation

Angle Given (degree)	Encoder Value - Angle rotated (Degree)					Average error (degree)	Repeatability (degree)
	Trial 1	Trial 2	Trial 3	Trial 4	Trial 5		
30	34.7	34.9	34.9	34.8	34.8	4.8	0.1
40	44.3	44.0	44.0	44.3	44.1	4.1	0.2
50	53.9	53.6	53.5	53.7	53.9	3.7	0.2
60	63.3	63.5	63.2	63.3	63.2	3.3	0.1
70	72.9	72.9	72.7	72.8	72.9	2.8	0.1
80	82.4	82.5	83.4	82.3	82.3	2.6	0.5

Table 4-3 : Large angle range rotation

Angle Given (degree)	Encoder Value - Angle rotated (Degree)					Average error (degree)	Repeatability (degree)
	Trial 1	Trial 2	Trial 3	Trial 4	Trial 5		
100	101.7	101.7	101.9	102	101.9	1.8	0.1
150	151.3	151.2	151.2	150.1	150.2	0.8	0.6
200	201.2	201.1	201.2	201.2	201.2	1.2	0.1
300	301.1	301.2	301.1	301.3	301.1	1.2	0.1
360	361.2	361.3	361.2	361.3	361.2	1.2	0.1

The encoder signal has an angle resolution of ≤ 0.25° and therefore the values are rounded to one decimal point. The average error is shown in Figure 4-20, for the small range angles (5° to 25°) rotation by the tightening spindle is 5.7° and for the medium range angles (30° to 80°) rotation is 3.6°. The repeatability is ± 0.1° and ± 0.2° for small and medium angles, indicated by a black line on the bar chart (Figure 4-20).

Even though the rotation of the tightening spindle to a specified angle is repeatable, the average error for each angle is considerably larger and varies for different angle ranges. Because of these large angular errors of the tightening spindle for angle ranges from 0 to 80°, applying a small deviation correction for aligning the socket corners with bolt head corners is not a viable solution.

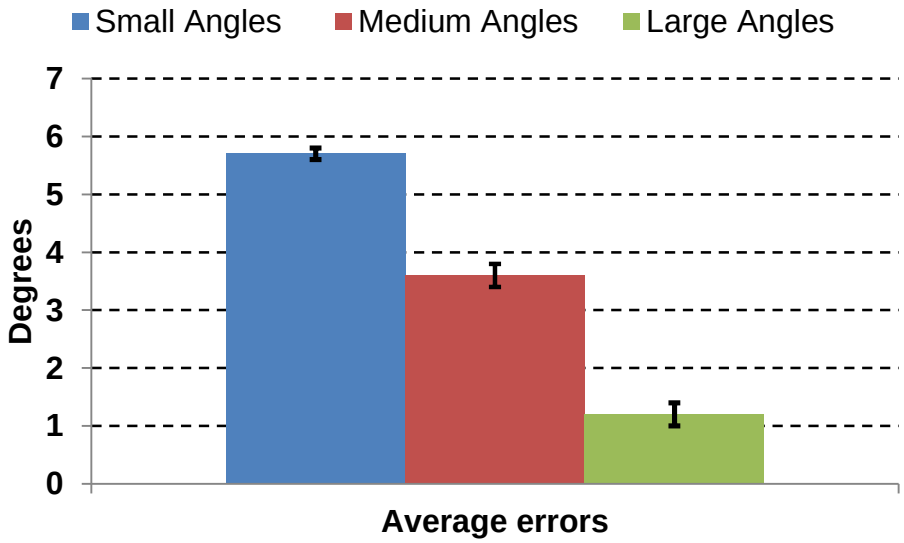

Figure 4-20 : Average error and repeatability for all ranges

In contrast, the average error for rotating the tightening spindle at large range angles shown in Figure 4-20 is 1.2°. It shows that the tightening spindle has less error when rotated to large angles (more than 100°) and also has high repeatability of ± 0.2°. So the deviation correction can be applied by adding a large angle with actual deviation to minimise the error.

The bolt head orientation with respect to a reference line can be obtained using the vision system. The deviation of bolt head will be dealt with rotating the tightening spindle to align it with the bolt. As a result of the tightening spindle rotational accuracy test, it was found that rotating a spindle to angles less than 100° will augment the error. Thus, the angle correction, if required, can be applied by adding a large angle 120° (twice the angle of hexagon corner) to the correction angle.

4.5 Summary

The suitable system hardware devices required to setup an experimental test rig for automated fastener assembly were identified. The communication setup required to integrate these hardware was established. A series of tests were carried out for evaluating the suitability of the identified hardware devices and their results were analysed. The complete system setup developed for the freeform automated assembly has been described in this chapter. The fastener assembly in 2D using the experimental test developed is described in the next chapter.

CHAPTER 5 - TWO-DIMENSIONAL (2D) FASTENER ASSEMBLY

To simplify the process of identification of objects and to understand parameters that affects identification of objects in 2D, initially the bolts and threaded holes are assumed to be located in a two-dimensional (2D) workspace (from an identification point of view). In reality, however in most real industrial scenarios, bolts and the threaded holes on the target component may be located in two or three-dimensional space. Assembling bolts in random 3D environment is described in CHAPTER 7 - .

The 2D approach for assembly is to start with simple scenarios which may exist in industrial fastener assemblies. Initially, an experimental setup with test components located in 2D was created. This chapter explains the experimental setup and the automated fastening method developed to assemble a bolt into a threaded hole using 2D vision system. It also describes the investigation carried out to determine the level of robustness achieved for industrial applications.

5.1 Assembly Scenario

The assembly scenario considered for fastener assembly is to identify and assemble objects located at a random position in a 2D environment. The bolts are placed in a cradle with their top surface of the head visible to the vision system as shown in Figure 5-1. This requires the hexagon shape of the bolt head to be identified and measured to determine the size of bolt and its location. The target component is a fastening plate and for this scenario, the holes located on the flat top surface of the plate are considered as illustrated in Figure 5-2. It is required to identify and classify holes accurately based on their size, where the size of holes varies from a minimum of 1 mm (i.e. difference between a 5 mm and 6 mm hole). Thus the assembly scenario pose a difficult challenge to determine features (i.e. circle and hexagon) with an accuracy of less than 1 mm in order to perform successful fastener assembly.

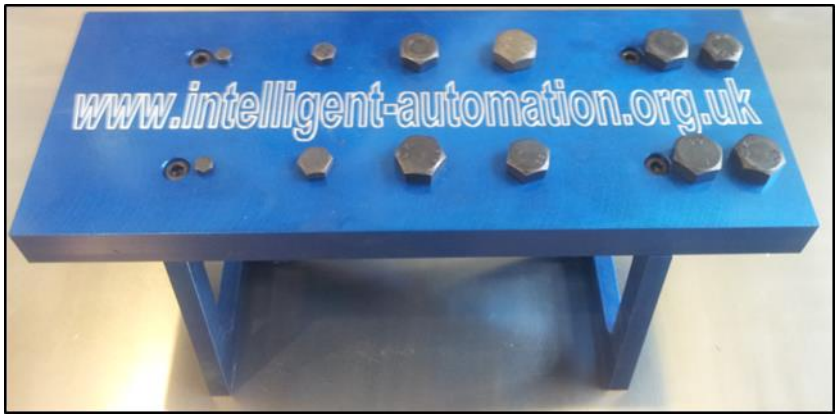

Figure 5-1 : Bolts in cradle

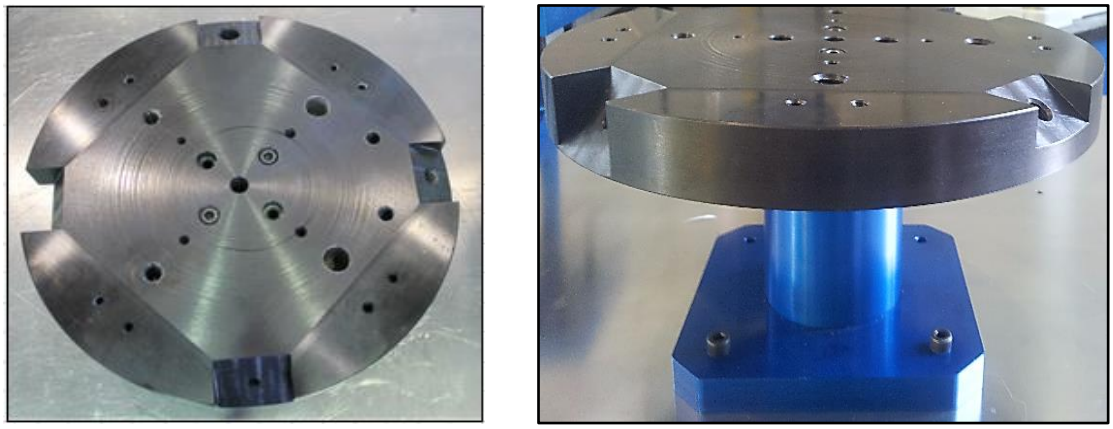

Figure 5-2 : Fastening plate mounted on a holder

The solution developed for this scenario has to identify bolts, holes which are located in a random 2D space, then it must pick up the bolts and perform fastening with high accuracy.

5.2 System Setup for 2D Fastener Assembly

In CHAPTER 4 - , the system and communication setup to integrate a robot, a tightening spindle, a vision sensor and a PC as one system were described. The Motoman robot is used as the manipulator and the Bosch tightening spindle with a hexagonal head magnetic socket is used for picking up the bolt using the magnetic force, thus no additional gripper is required at this stage. The tightening spindle provides a maximum torque of 150 Nm that allows the fastening of bolts up to the size of M14.

The vision sensor required for the fastener assembly in this case is a 2D camera. The primary specifications considered for finding a suitable 2D camera are resolution, stand-off distance and a field of view (FOV). The camera was integrated with the robot arm along with the tightening spindle. This allowed the camera to be mobile and move between the location of the fastening plate and the bolt cradle. The stand-off distance is the distance between the camera focal point and the object. The 2D camera needs a minimum of 300 mm of stand-off distance, as the length of the spindle after the robot hand is 260 mm (additional 40 mm is the clearance between the spindle and object to avoid collision).

The 2D camera FOV should cover the entire fastening plate and the bolt cradle to identify bolts and holes located on it. The fastening plate is a circular plate with 250 mm in diameter and the bolt cradle is rectangular structure with the length and breadth measured at 320 mm and 120 mm respectively. The FOV required for covering the fastening plate and bolt holder separately is obtained by taking the largest size values between them (i.e. the length of the bolt cradle is 320 mm as the horizontal length and the diameter of fastening plate is 250 mm for the vertical length of the camera FOV) as shown in Figure 5-3 (a).

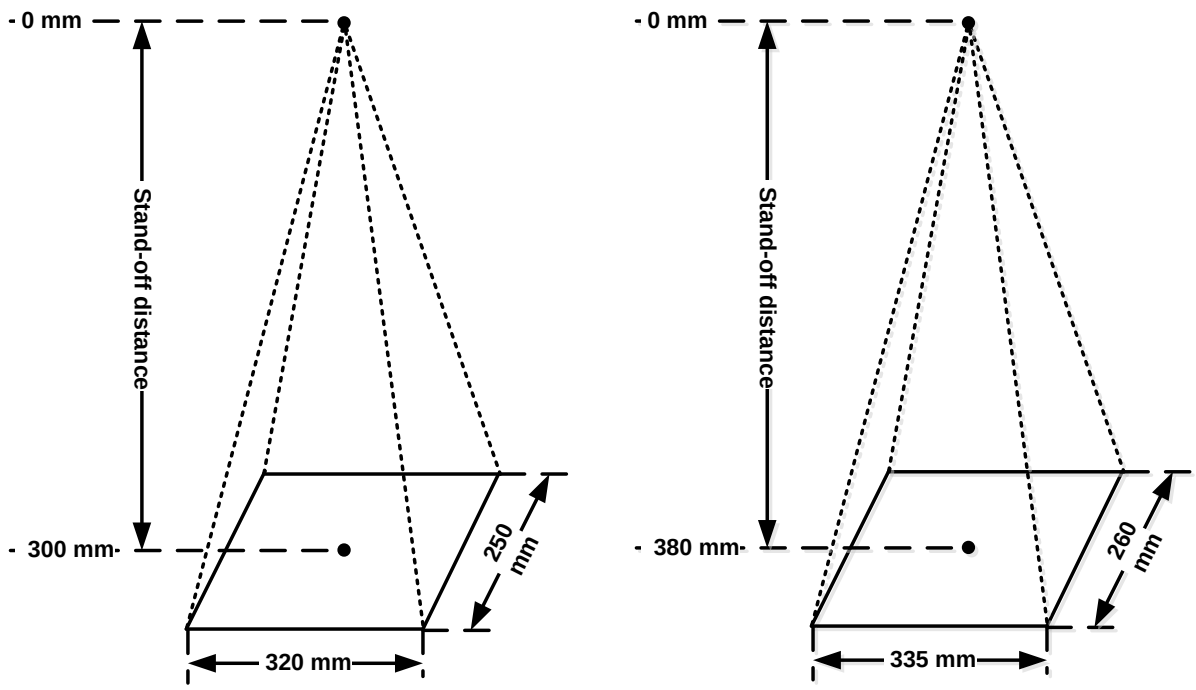

a) Minimum requirement

b) Basler Ace camera

Figure 5-3 : Field of view and Stand-off distance of the 2D camera

The Basler Ace 1600-20gm [91] shown in Figure 5-4 (a), is a 2D monochrome camera possessing a 8 mm focal length lens, which is selected to take 2D images of the bolt holder and fastening plate (specifications are provided in appendix A4). It is a gigabit Ethernet camera and communicates with the PC through TCP/IP protocol.

The camera is used at a stand-off distance of 380 mm from the object plane to cover the entire object into its field of view (FOV). The FOV achieved at this stand-off distance is 335 mm (horizontal length) and 260 mm (vertical length), as shown in the Figure 5-3 (b). The illumination for the camera is provided using the CCS blue ring light with a diffuser [97] as shown in Figure 5-4 (b) and (c).

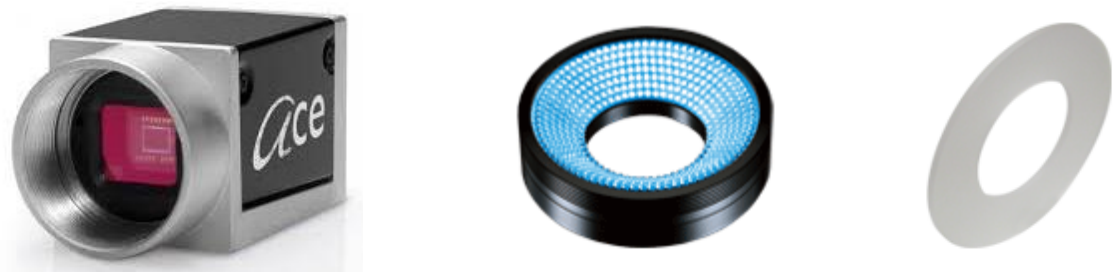

a) Basler Ace 1600-20gm[91]

b) CCS Blue ring light[97]

c) Diffuser[97]

Figure 5-4 : Basler camera[91] **with illumination**

The blue light was used because it has the property to scatter due to its smaller wavelength than other light colours. This provides better results while taking images of shiny objects under variable lighting conditions. The blue light with diffuser will flood the work area to diffuse the external lighting, thereby providing better illumination for the objects in the work area. This illumination is also affected by ambient lighting; the extent to which it gets affected will be discussed at the end of this chapter.

The system setup developed for 2D fastener assembly includes Motoman SDA20 2-arm robot, Bosch tightening spindle, 2D camera, bolt cradle, fastening hole plate and PC as shown in Figure 5-5. The fastening hole plate and the bolt

cradle are bolted down to a table placed in front of the robot. The tightening spindle is mounted on arm 2 (R2) of the Motoman SDA20 robot with the help of mounting plates. The camera along with the blue ring light is also mounted on the same arm of the robot using an adapter plate. Thus only one arm (R2) is required to carry out the assembly task in this case.

Figure 5-5 also shows the communication protocol used between the devices. The PC, camera and robot controller communicate through Ethernet cable. The DeviceNet communication protocol is used between robot controller and the tightening spindle controller to facilitate control and data transfer.

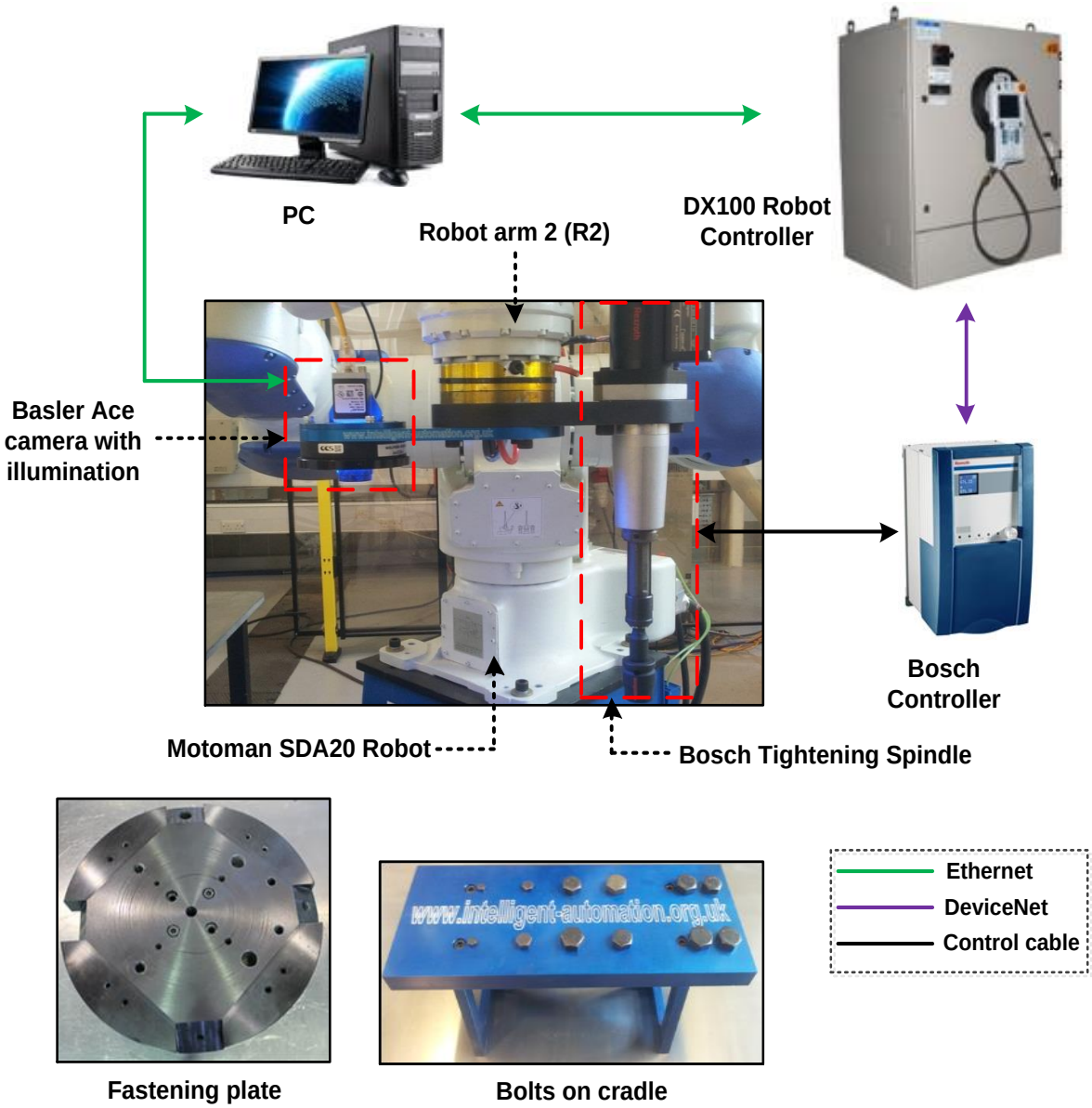

Figure 5-5 : System setup for 2D fastener assembly

5.3 Scope of the Experiment

This experiment is focused on fastening of bolts ranging from M5 to M14 placed at a random location into their corresponding size fastening holes whose position is also not known. The range of bolt size is limited due to the limitations in the equipment used and can be extended depending upon the requirement. Figure 5-6 shows the general dimensional attributes of bolts. In this experiment the length across the head ($L_{a/c}$) is used to identify the bolt size.

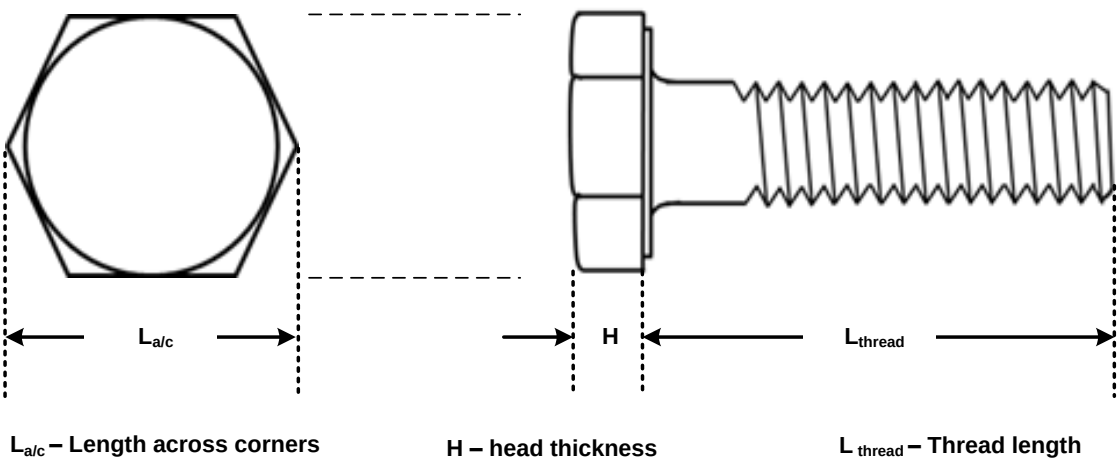

Figure 5-6 : Bolt dimensional attributes

Initially as a proof of concept, the experiment involved two M10 bolts and their corresponding size holes for carrying out fastening. The length of the M10 bolts thread section used in this experiment is 50 mm. The bolt head size and the threaded hole diameter are shown in Table 5-1.

Table 5-1 : Physical Measurement values

Bolt head - $L_{a/c}$		**Threaded hole - Outer diameter of hole**	
M10 Bolt 1 (mm)	**M10 Bolt 2 (mm)**	**M10 Hole 1 (mm)**	**M10 Hole 2 (mm)**
19.77	19. 92	11.50	11.38
Measured using a Vernier scale			

5.4 Bolt Pick Up using Tightening Spindle with Magnetic Socket

The tightening spindle selected for fastening bolts has a 1/8 inch female output drive at the end. The lack of gripping fingers is compensated by a magnetic socket with 1/8 inch male drive at one end and hexagonal socket at other end. The socket provides the spindle with the ability to hold the bolt by its head using the magnetic force during pick up – and the manipulation of the bolt.

The bolt located in the cradle has to be picked up using the tightening spindle and this requires the magnetic socket corners to be aligned with the bolt head. The spindle will fail to pick up the bolt if the socket and the bolt head are not aligned.

Initial test to make the tightening spindle to rotate at slow speeds and approach the bolt in perpendicular direction was not a success. This is because, the bolt in the cradle also rotates along with the spindle, as the bolt head is not properly fitted into the socket. So the experiment was modified to make the spindle to rotate and approach the bolt at low speed like before, but this time at an angle in different directions. This was inspired by human approach to that condition (i.e. if the socket does not align with the bolt head, the socket is rotated at an angle until it aligns with the bolt head).

The experiment involves three conditions based on the manual approach

- Only in Y-axis - Tilting the socket 5° at one axis (-Y and +Y)
- Sequence 1 - Tilting the socket 5° at each of the axis (-Y, +Y, +X and –X)
- Sequence 2 - Tilting the socket 5° at each of the axis (-Y, +X, +Y and –X)

On all these conditions the socket will be 5 mm away from bolt head centre in the Z-axis and will also be rotating at a speed of 100 rpm. Figure 5-7 shows the axis involved in the experiment conditions and one of the conditions in which the spindle is tilted by 5° to the negative x-axis.

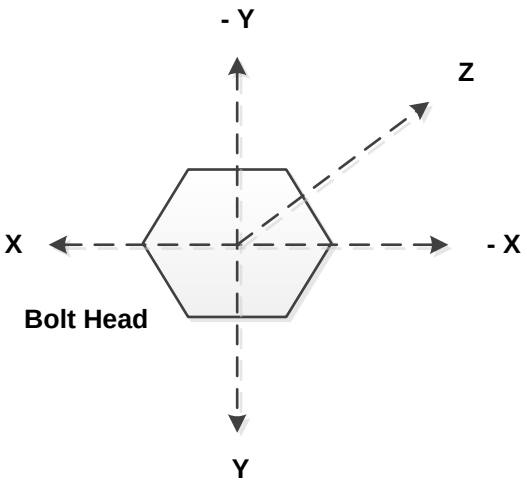

a) Bolt head with positive and negative axis

b) Tilting 5° in negative x-axis

Figure 5-7 : Axis used in the experiment conditions

The tilting in the y-axis involves moving the socket between the positive and negative y-axis (180° movement). In sequence 1, the socket moves between a negative to positive y-axis which is 180°, the negative y-axis to positive x-axis which is 90° and positive x-axis to negative x-axis which is 180°. But in sequence 2, the socket moves at 90° between all the axes and transits between the x and y axis. The experiment was carried out 20 times and the results were tabulated in Table 5-2.

Table 5-2 : Socket alignment results

Experiment condition	No of trials	No of successful alignment of socket	% Success
Only Y-axis	20	12	60
Sequence 1	20	18	90
Sequence 2	20	20	100

The results showed that tilting the socket at one axis (only Y-axis) and approaching the bolt has a success rate of 60% and therefore not reliable. The results also showed that tilting the socket at two axes and following sequence 1 provided a better success rate of 90%. This is due to the nature of the sequence, as it involved approaching the bolt at four different directions which increases the probability of successful alignment. On the other hand, Table 5-2

also shows that using sequence 2 for tilting the socket results in a 100% success. This is because in sequence 2, the socket transits between the x and y axis making a sharp 90° movement. It was found that the success of aligning the socket with the bolt is higher and more reliable when there is a sharp transition in the approach of the socket.

Despite the success and reliability of this condition in aligning the socket with the bolt head, this technique has a number of drawbacks. The drawbacks include the material wear and tear that may happen in the socket and the bolt head during the alignment process. Therefore, this alignment method was not implemented in this research and an alternate method was developed, as explained in the next section.

5.5 Assembly Process

The 2D fastener assembly method developed involves identifying the hexagonal head bolts by its head size, the threaded holes diameter and their locations in a random 2D workspace. With the positional information obtained using the 2D vision sensor, the robot with the tightening spindle is programmed to pick up the right size bolt and fasten it into the corresponding size threaded hole in the fastening plate. The entire assembly is divided into three major steps which involve imaging the work area, the image processing algorithm and then the fastener assembly, as illustrated by the Figure 5-8.

The first step in the automated assembly method is imaging the work area, containing the bolts and the threaded holes. The images obtained from the 2D vision system are then sent to the PC. The second step is to process the images using the algorithm developed to identify and locate the bolts and holes. Their positional information is then passed on to the robot for assembly. The final step is to assemble the right size bolt with the corresponding size threaded hole.

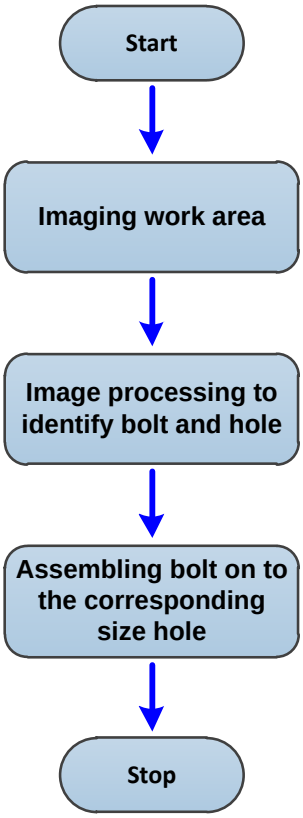

Figure 5-8 : 2D fastener assembly steps

The process involved in imaging the work area is shown by Figure 5-9. It starts with the PC initiating a communication request with the robot controller and then sending a request to access robot arm 2 (R2) to the robot controller.

The PC drives the arm R2 to move to a pre-defined position on top of the fastening plate area. At this point the robot sends a signal to the PC to confirm that it has reached the position. The PC then triggers the camera to take an image of the fastening plate with holes located at a random position and orientation as shown in Figure 5-10. The images are transferred from the camera to the PC. After receiving the image, the robot is then commanded to move arm R2 to a pre-defined position on top of the bolt cradle. While the robot is moving, the PC executes the hole detection algorithm on the fastening plate image to identify and locate the different size holes.

After reaching the fastening plate area, the robot sends a signal to confirm that the imaging location is reached. Then the PC triggers the camera to obtain the image of the bolt cradle with bolts located at a random position and orientation. The bolt area image is sent to the PC for further processing. After receiving the

image, the PC executes bolt detection algorithm on the image. The algorithm identifies the bolts from the image and also their size and position in 2D.

The image processing is the second step involved in the fastener assembly method. The feature detection algorithms developed to identify and localise bolts and holes are explained in section 5.6.

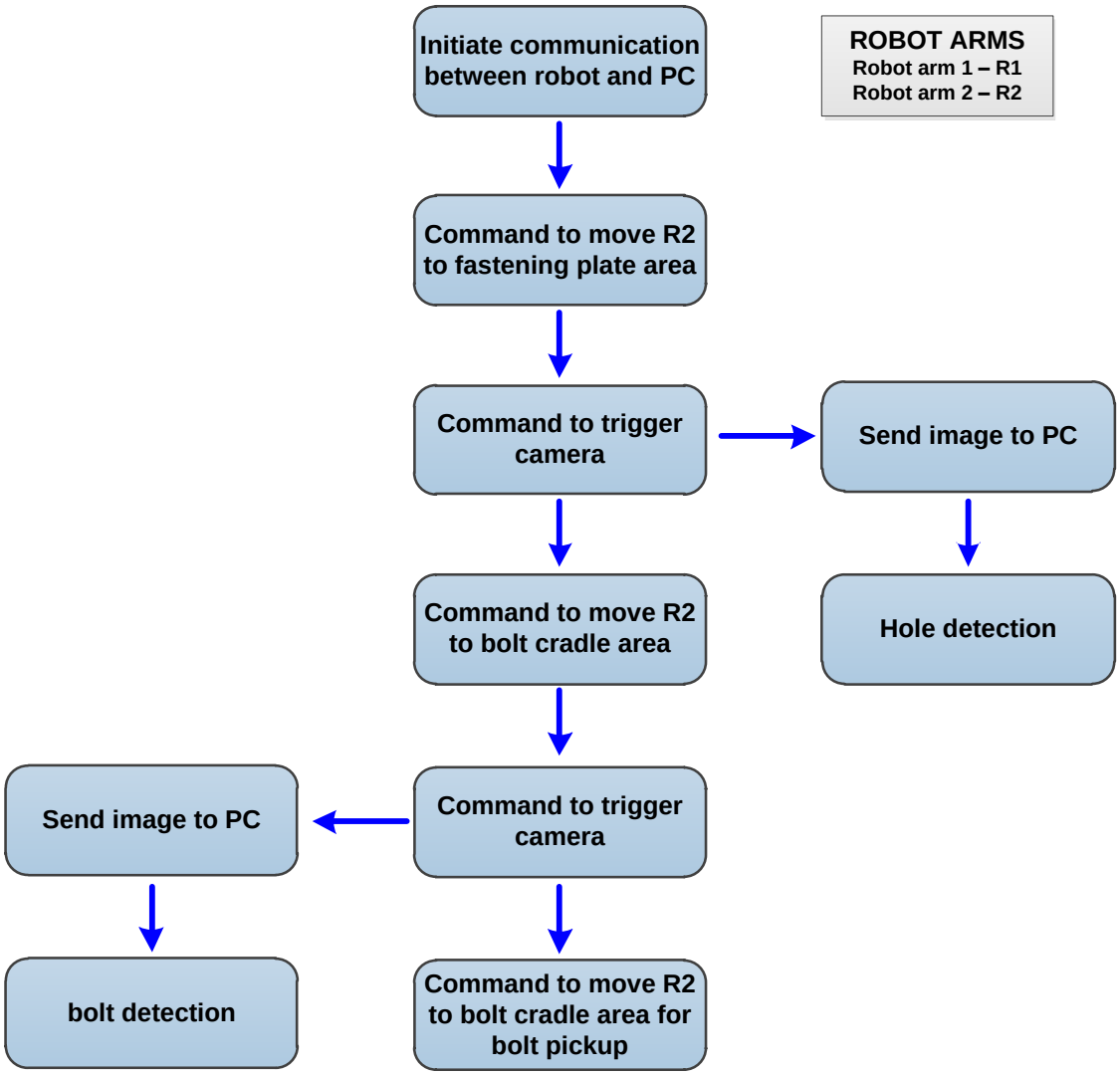

Figure 5-9 : Imaging work area

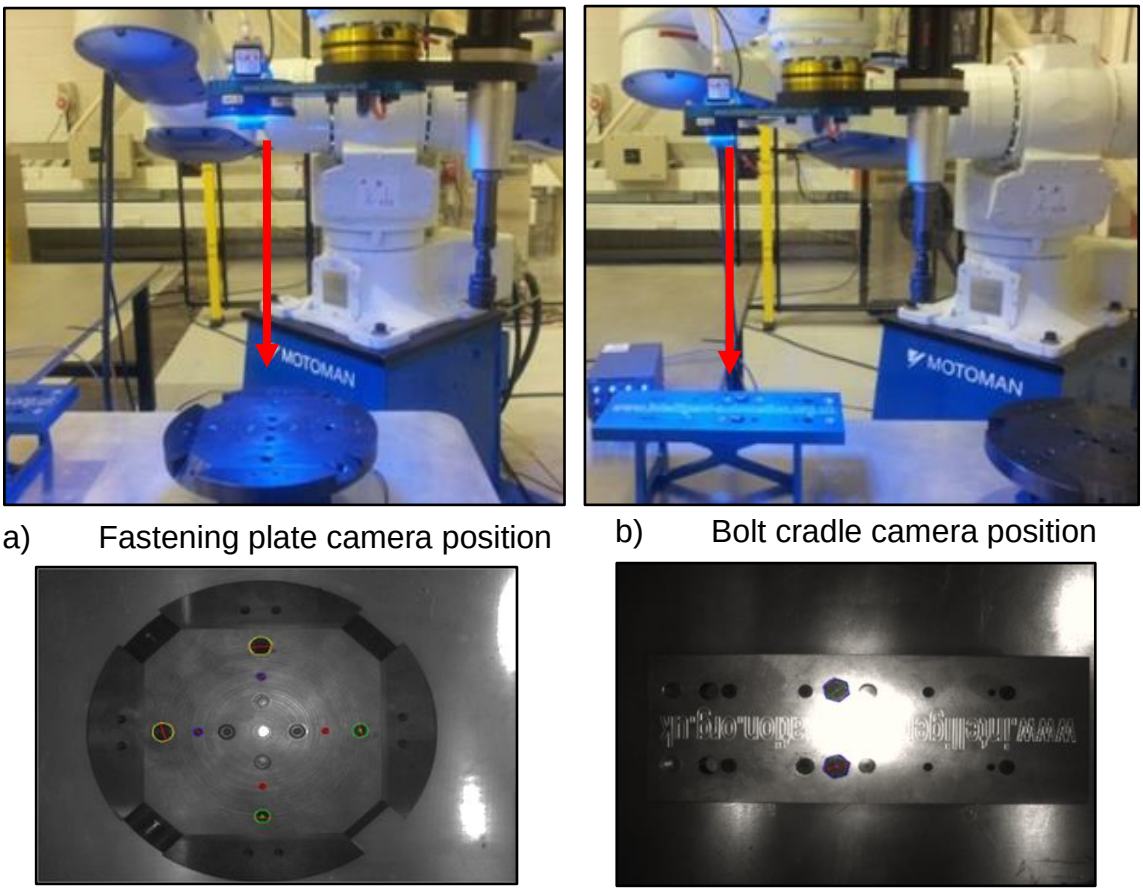

a) Fastening plate camera position

b) Bolt cradle camera position

c) Hole identification

d) Bolt identification

Figure 5-10 : Fastening plate and bolt cradle imaging

The final step in the fastener assembly method is the assembly of bolts into threaded holes. It involves picking up the bolt, reaching the location of the hole and performing fastening using the tightening spindle as describe in Figure 5-11.

The algorithm classifies the bolts and holes based on their size. If the size of the bolt matches the hole size, the position information of both the bolt and hole are sent to the robot controller and saved as a variable. In this case there are two bolts, thus the PC looks for two holes matching the bolts sizes. If there is no match found for the bolt size, the PC ignores that bolt.

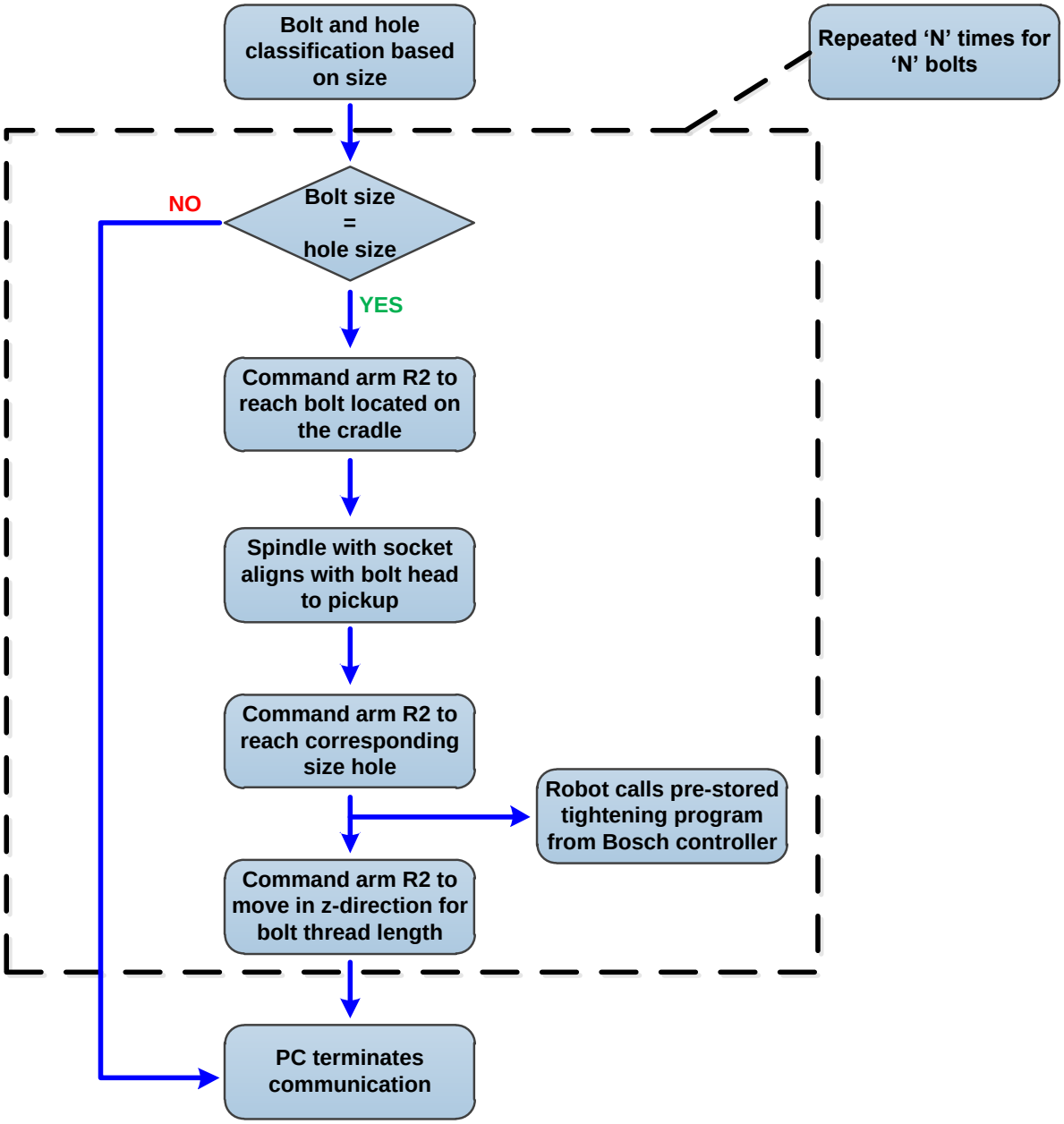

Tightening programs are explained in appendix B1

Figure 5-11 : Assembling bolts into corresponding size threaded hole

After identifying a size match, the PC directs the robot to reach the bolt location in the cradle. Then the spindle with a magnetic socket is aligned with the bolt head by rotating the spindle at slow speed in a counter clockwise direction - approaching the bolt head. This method was also realised from the way a human operator will carry out such a task. This alignment approach locks the bolt into the magnetic socket, thereby picking up the bolt as illustrated in Figure 5-12.

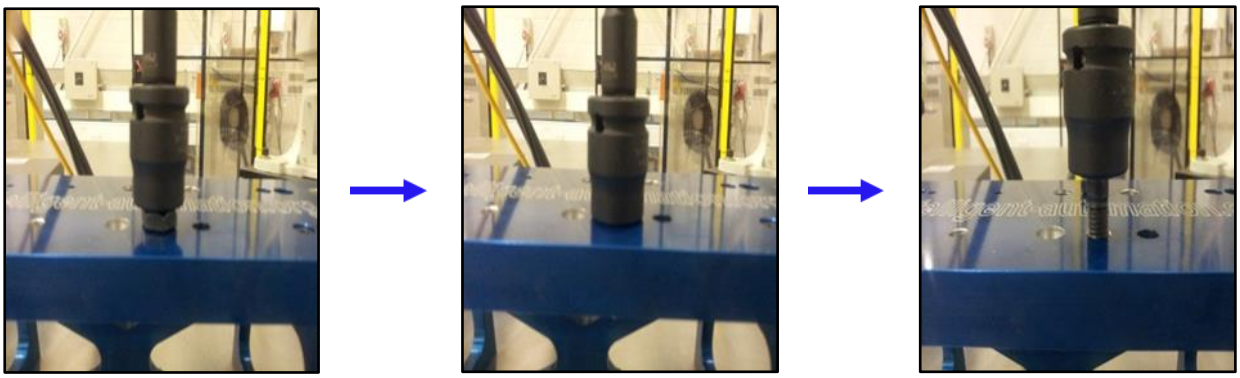

Reaching the bolt | Socket alignment with bolt head | Bolt pick up

Figure 5-12 : Bolt pick up process

After bolt pick up, the tightening spindle with the bolt is moved to the hole that matches the size of the bolt. The bolt is slowly inserted into the threaded hole. At the same time, the robot initiates the tightening program developed in the tightening spindle controller (provided in appendix B1). During the fastening process, the robot is also made to move in z-axis (assembling axis) in relation with the bolt insertion to synchronize the fastening process. The tightening program - which is pre-defined - rotates the tightening spindle to fasten bolt into the threaded hole for the time, torque and angle value specified to carry out the fastening for this particular bolt size. If the bolt and hole alignment are accurate, the fastening process is carried out without any cross-threading as illustrated in Figure 5-13 . On the other hand, the fastening process will be terminated if the alignment is not accurate.

Reaching hole | Fastening | Fastened bolt

Figure 5-13 : Steps invovled in fastening a bolt into a threaded hole

During the fastening process, if the value of the torque exceeds the set threshold limit, the tightening spindle is programmed to terminate the rotation. This may either represent the completion of fastening or an occurrence of cross threading error. Thus a monitoring system is in place to prevent the misalignment or cross threading by terminating the assembly process to prevent damages to the thread. The correction mechanism required to solve this problem was not developed, as it is not within the scope of this research.

5.6 Feature detection in 2D images

The 2D image of bolt holder and fastening hole plate obtained from the camera are subjected to several image processing steps - to identify the bolt and the fastening hole. In the images, threaded holes are represented by circular-shaped features and the head of the bolts are represented by hexagon-shaped features. Thus a feature detection algorithm was developed using HALCON Image processing libraries [98], to process the images of bolts in the cradle, and of the fastening hole plate to obtain features such as hexagonal and circular shapes.

5.6.1 Hole feature detection

The fastening plate image is used as the input image for the hole feature detection algorithm. The output of the algorithm is the circular features (threaded holes), their geometry and location as illustrated in Figure 5-14. The input image is first subjected to a sharpening process, which enhances the difference in grey values in the image to emphasize sharp edges, thereby making them distinctive (explained in appendix B2 (a)). The enhanced image is then used for detecting edge features.

There are several edge detection techniques available to identify sharp features (i.e. edges in an image). A review of the existing edge detection technique was carried out and an evaluation of different techniques was conducted (appendix B2 (b)). The results of the review and evaluation showed that the Canny edge detection technique [99] is the most effective edge detection method and was implemented in this research due to its compatibility for industrial applications.

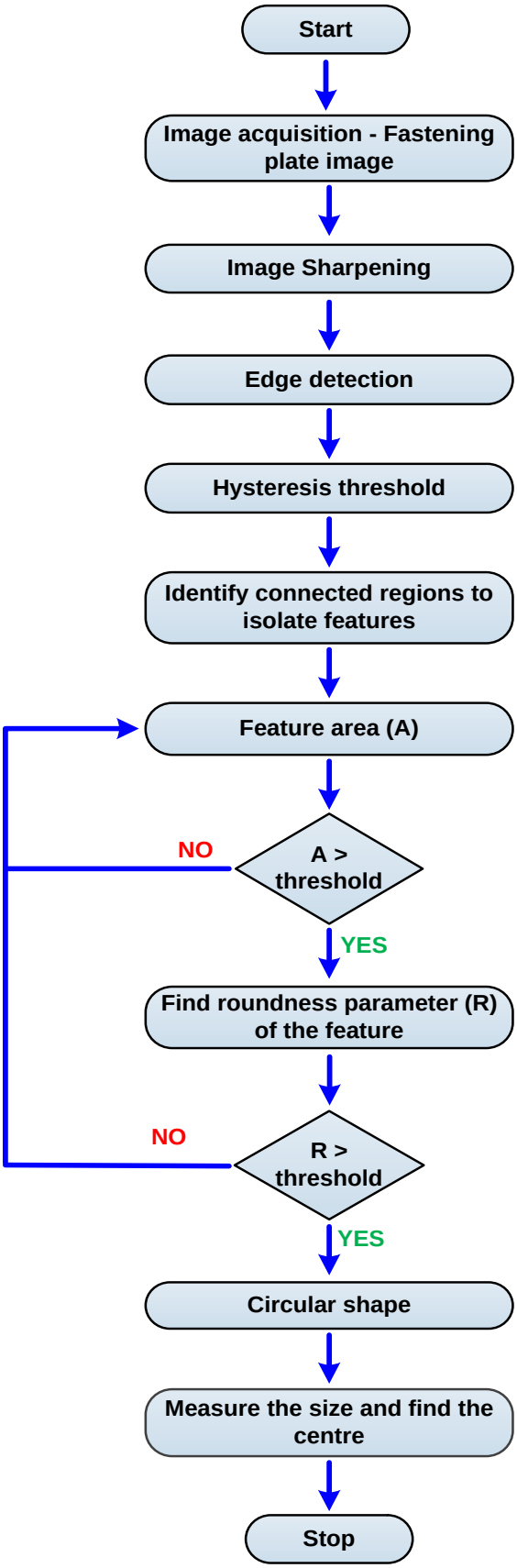

Figure 5-14 : Process involved in hole feature detection (2D)

It uses Gaussian filter to smooth the image and remove noise, then it finds the magnitude of the image gradient and tracks it for detecting the edges. The Canny edge detection is used to detect sharp features in the image without a definitive threshold value to obtain an edge amplitude image as shown in Figure 5-15. This image is then subjected to a hysteresis threshold to determine the definitive edges. The hysteresis threshold has two threshold levels, maxima and minima. The grey values of a region that are above the maxima and also the regions between the maxima and minima are considered as potential edges. The remaining part of the regions are set to zero, thereby only providing the edges presented in the image. In this research, the canny edge detection technique combined with a hysteresis threshold was implemented and it has also proved to provide better and more defined edge in an image.

After obtaining the edges, a region of interest is introduced to keep the edge features of the object and to remove the edge features representing the background for efficient processing. The edges in the interested region are fitted with boundary marking technique to enhance the edges. From the marked boundary, the edges pixels that are continuous and connected to their neighbours are grouped together to form connected features as explained in appendix B2(c)).

After separating the connected features in the fastening plate image, the algorithm looks for circular features (i.e. holes). This involves determining the area of all the connected features and removing the features that have an area smaller or larger than the required size of holes. The remaining connected features are subject to the roundness parameter process (appendix B2 (e)) and the output of this process provides a potential circle feature that represents threaded holes in the image.

Then the smallest circle that can fit into the circular region is defined to measure the diameter of the hole. The holes are then classified according to their size, which have been obtained from the diameter measurement. The centre point of the fitted circle is determined to obtain its location on the image as shown in Figure 5-15.

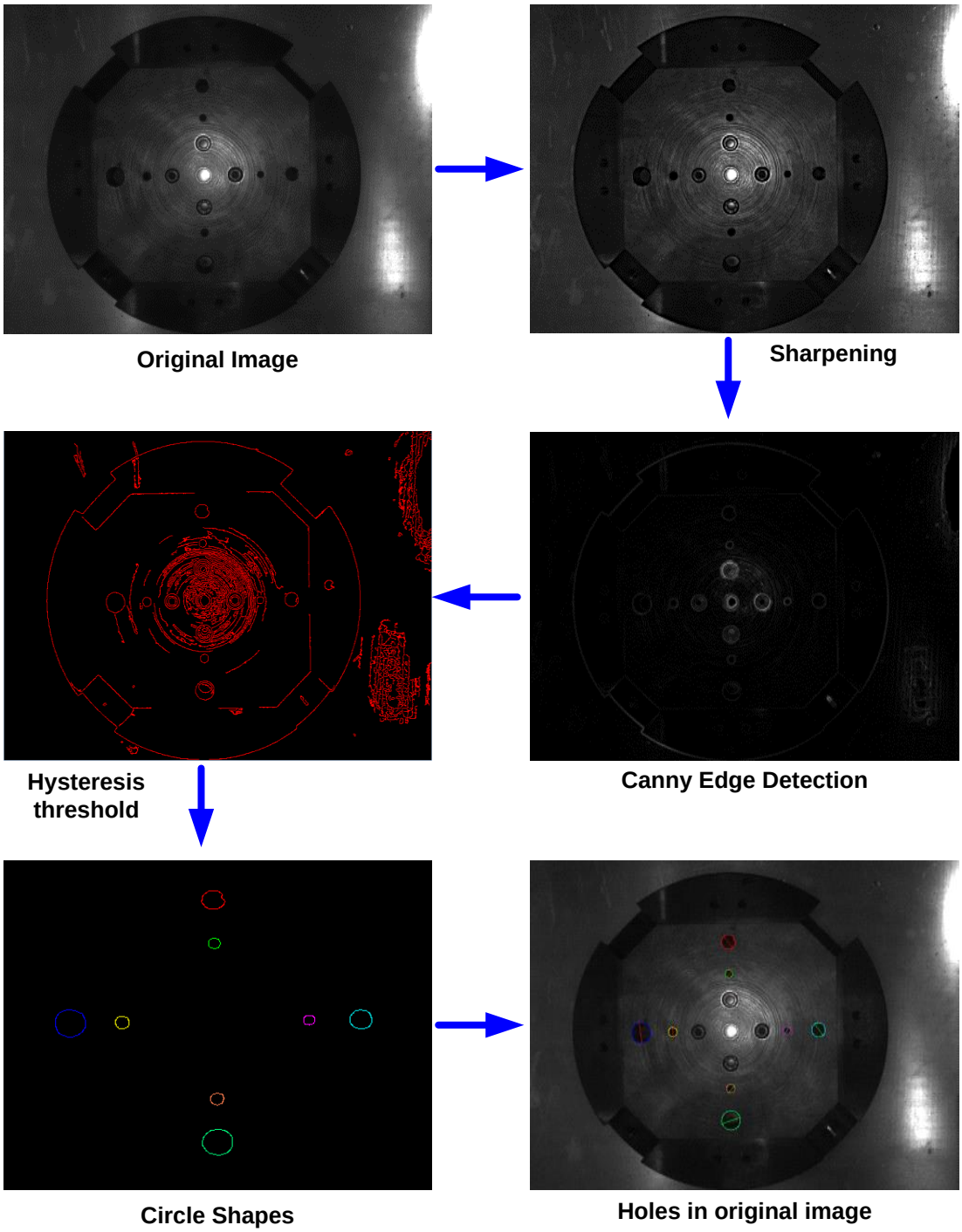

Figure 5-15 : Image processing - hole feature detection

5.6.2 Detection of hexagon bolt head

The image of bolts in the cradle is acquired from the camera and is used as the input for bolt detection algorithm. The output of this algorithm provides the bolt head size and location as given in Figure 5-16. The input image is subjected to image processing steps which include a sharpening process, canny edge

detection with a hysteresis threshold and identifying connected features in the same order as described in the hole feature detection.

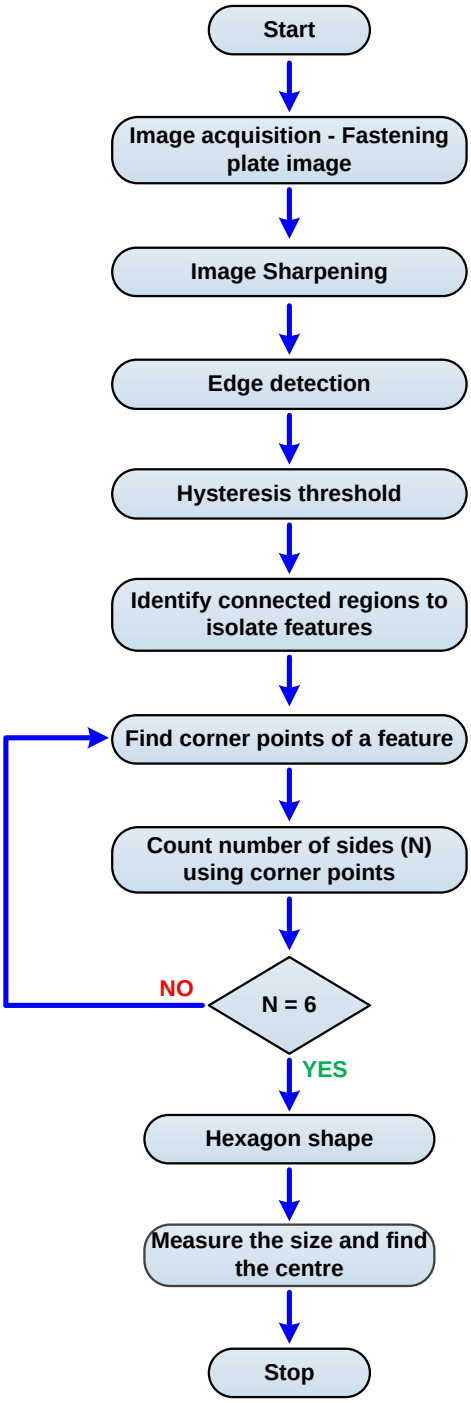

Figure 5-16 : Process involved in bolt head detection

These are the common steps required to identify a feature regarding its shape and size (explained in appendix B2).The difference between the two algorithms is the method to detect the shape of a feature. In this case, the algorithm

searches for hexagonal shapes that represent the bolt heads. After separating the connected features in a bolt cradle image, the algorithm determines the hexagonal-shaped features as shown in Figure 5-17 .

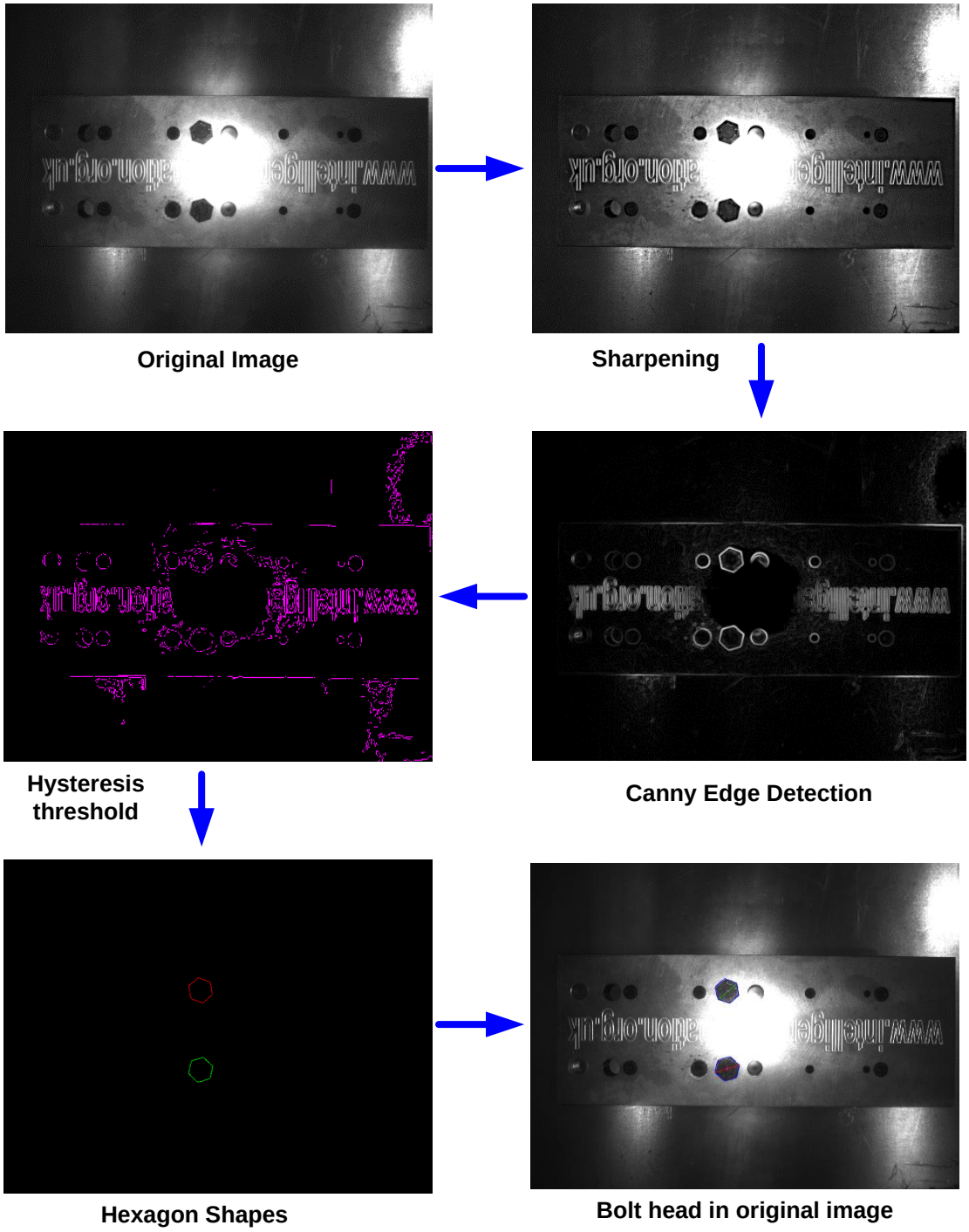

Figure 5-17 : Image Processing - bolt head detection

It is obtained by identifying the corner points of the connected features and then connecting the corner points with each other to form a polygon. The number of

sides of each polygon is counted (the equation to determine the number of sides is explained in appendix B2 (f)) and the polygon features with 6 sides are considered as hexagonal shapes. The hexagonal shapes representing bolt heads are then classified into different sizes by measuring their length across any two corners. The centre point of the classified hexagonal heads provides the location of the bolts in the image.

The information obtained from the images has to be converted into real world measurements and co-ordinates. The method developed for this purpose includes calibrating the 2D camera with a reference model plate containing equidistance dots of known size and distance. Figure 5-18 illustrates the process flow for the calibration process.

This calibration provides a transformation matrix which represents the transformation of camera plane to the object plane in the work area (appendix B3). The transformation matrix will change if the position of camera from where the image is obtained changes, and also if the object plane changes.

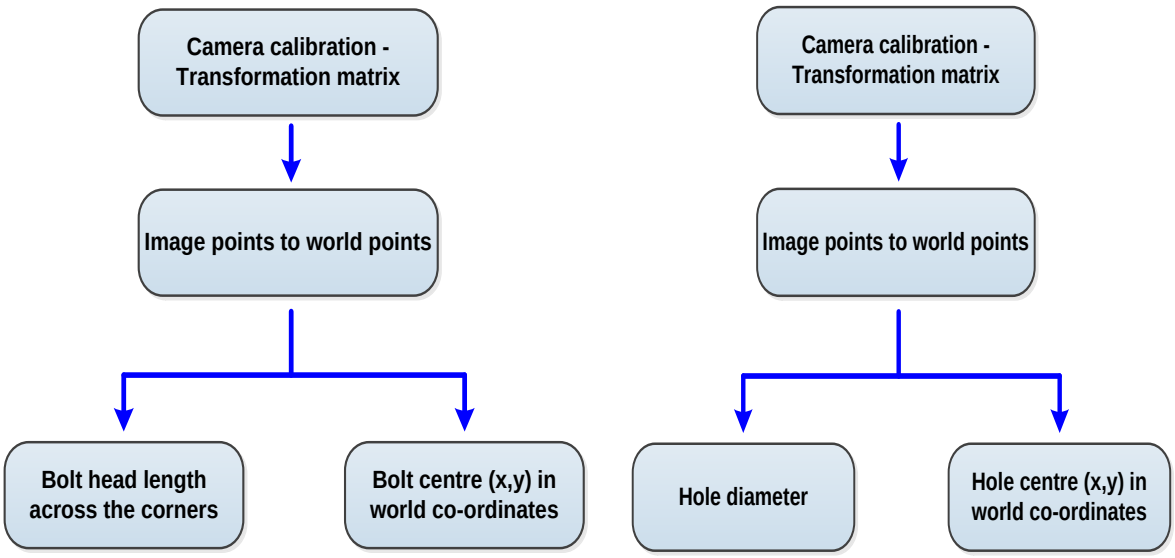

a) Bolt holder calibration b) Fastening plate calibration

Figure 5-18 : Camera calibration

5.7 Experiment conditions and data

5.7.1 Experiment Conditions

The experiment for detecting bolt and the threaded hole is carried out in two different lighting conditions, controlled and ambient lighting conditions as shown in Figure 5-19. The reason for using different lighting conditions is to investigate the robustness and applicability of the developed assembly method in an industrial environment.

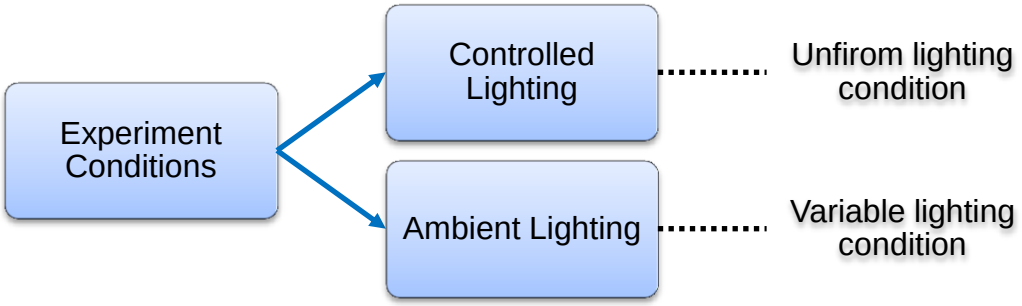

Figure 5-19 : Experiment condition

5.7.2 Experimental Data under Controlled Lighting (Uniform Lighting)

The controlled lighting condition for this experiment is considered as the lighting in the laboratory without ambient light. The camera has been integrated with blue LED light in its lens to project diffused light on the workspace. Under uniform lighting condition, the lighting variation in the workspace is negligible.

The camera image taken under this condition was processed to obtain the size of the bolt head (i.e. length across the corner) and the threaded hole diameter. This experiment was carried out 15 times to measure the success and also the repeatability of the size measurement data obtained as a result of image processing. The bolt head and threaded hole size measurements for all 15 trials are tabulated, as shown in Table 5-3.

The experiment conducted shows that the influence of light is insignificant (due to less variation in lighting) and the edges in the images had very little variation in the grayscale values.

Table 5-3 : Measured values of bolt and threaded hole - controlled lighting

S .No	Bolt head - length across corners (mm)		Threaded hole - outer diameter of the hole (mm)		Fastener assembly completion
	M10 bolt 1	M10 bolt 2	M10 hole 1	M10 hole 2	
1	19.49	19.70	11.62	11.51	Yes
2	19.49	19.72	11.65	11.45	Yes
3	19.47	19.70	11.59	11.49	Yes
4	19.47	19.70	11.70	11.59	Yes
5	19.51	19.74	11.59	11.59	Yes
6	19.47	19.74	11.69	11.64	Yes
7	19.55	19.70	11.62	11.50	Yes
8	19.47	19.71	11.70	11.54	Yes
9	19.48	19.70	11.65	11.54	Yes
10	19.47	19.73	11.66	11.59	Yes
11	19.46	19.76	11.63	11.60	Yes
12	19.48	19.74	11.69	11.51	Yes
13	19.52	19.72	11.56	11.54	Yes
14	19.46	19.71	11.49	11.61	Yes
15	19.48	19.74	11.54	11.58	Yes

Due to less variation in greyscale values, edges in the image are sharp, thus the size measurement and fastener assembly process were not affected. Hence, the success rate of identifying the bolt and the hole geometry and location to carry out the fastening is 100%.

5.7.3 Experimental Data under Ambient Lighting (Variable Lighting)

The ambient lighting is the lighting condition which is influenced by the sunlight. The lighting condition may vary depending upon the amount of sunlight (or any indirect, strong natural light) entering the workspace where the bolt holder and the fastening plate are located. To minimize the influence of sunlight on the workspace, a blue LED light was integrated with the camera which projects diffused blue light on the objects. The measured values of bolt head size and hole diameter under the ambient lighting condition are provided in Table 5-4.

Table 5-4 : Measured values of bolt and threaded hole - ambient lighting

S .No	Bolt head - length across corners (mm)		Threaded hole – outer diameter of the hole (mm)		Fastener assembly completion
	M10 bolt 1	M10 bolt 2	M10 hole 1	M10 hole 2	
1	19.47	19.44	11.31	11.29	Yes
2	19.38	19.27	11.28	11.04	Yes
3	19.64	19.36	11.31	10.89	Yes
4	ND	19.58	11.64	11.43	No
5	19.01	19.82	ND	11.56	No
6	ND	ND	11.74	ND	No
7	18.73	19.58	10.91	11.42	Yes
8	ND	ND	ND	ND	No
9	19.49	19.19	ND	11.2	No
10	19.23	19.32	11.34	10.85	Yes
11	19.46	19.61	11.25	11.43	Yes
12	19.24	19.38	ND	11.14	No
13	ND	ND	ND	11.19	No
14	19.44	19.06	10.89	11.2	Yes
15	19.32	19.33	11.28	11.47	Yes
ND – No Data					

When the sunlight influence is higher than the illumination provided, the obtained images had different grayscale values and therefore resulted in the failure of the algorithm to detect the edges in the image. This sometimes affects the identification of bolts and the threaded holes, thus the developed automated fastener assembly method was not always successful.

The real industrial scenario where the assembly is performed is represented by the variable lighting condition. The 2D automated assembly experiment was carried out in variable lighting condition for evaluation of its application in industries. The experiments were conducted for 15 times and the results showed that the success rate of the assembly process was only 53%. This is due to the influence of external lights on the input image.

5.8 Discussion

The 2D fastening process in controlled lighting conditions with negligible sunlight interference has a success rate of 100%. The M10 bolts and holes are correctly identified, measured and their positions are obtained with minimal error. On the other hand, in variable lighting condition where external light interference is high, the success rate of the experiment falls to 53%.

In addition, it was also found that the success rate may decrease further, if the objects or surrounding environment have reflective surfaces. The reflective surfaces tend to emit more light affecting the edge detection process, which is crucial in identifying and measuring the bolt head and the threaded hole.

Table 5-5 : Mean and standard deviation of errors - controlled lighting

Parameter	Bolt 1 (mm)	Bolt 2 (mm)	Hole 1 (mm)	Hole 2 (mm)
Mean error	-0.29	-0.20	0.13	0.17
Standard deviation	0.02	0.02	0.06	0.05

As shown in Table 5-5, the mean error in measuring the length across the corners of the M10 bolt head is 0.29 mm and 0.20 mm respectively for the two bolts used in the experiment in uniform lighting condition.

In addition, the mean error in measuring the M10 threaded hole outer diameter is 0.13 mm and 0.17 mm respectively, for the two threaded holes. As indicated in Table 5-5, the mean errors are within the limit for differentiating two different size holes which are 1 mm apart (i.e. the difference between a M5 and a M6 hole).

Another important factor to look for is the degree of closeness between the errors which is very small in this case. This closeness factor is determined by the standard deviation of error values. The standard deviation of bolt head measurement errors is 0.02 mm and 0.02 mm respectively for bolt 1 and bolt 2. On the other hand, the threaded hole outer diameter measurement error

standard deviation is 0.06 mm and 0.05 mm for hole 1 and hole 2. Both standard deviation measurements show that the method is highly repeatable.

The standard deviation is marked by a black line indicator on Figure 5-20 and Figure 5-21 for the bolt and the hole measurement respectively. Thus, the error occurring in the bolt and the threaded hole measurements can be traced and rectified, as the deviation in the repeatability of error is negligible.

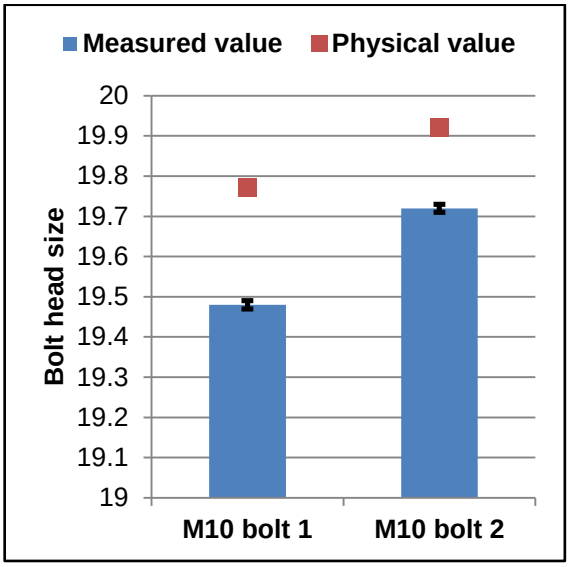

Figure 5-20 : M10 bolts mean error and standard deviation - controlled lighting

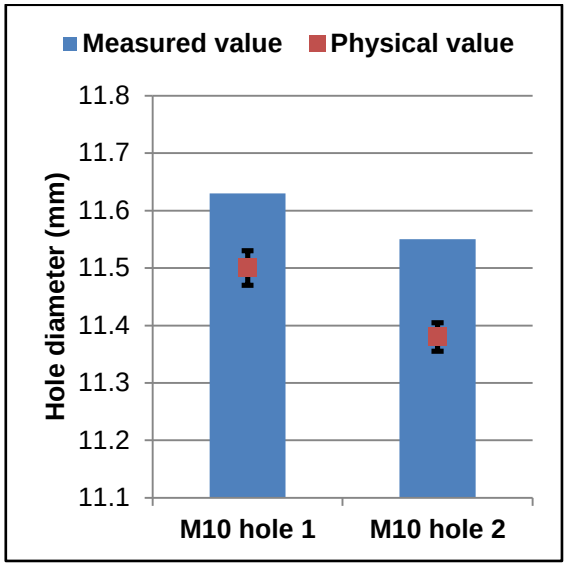

Figure 5-21 : M10 holes mean error and standard deviation - controlled lighting

As indicated by Table 5-6, in variable lighting condition, the mean error in measuring the M10 bolt head size (i.e. length across the corners) is 0.46 mm and 0.51 mm respectively for the same two bolts used in uniform lighting condition. The mean error in measuring the M10 threaded hole outer diameter stands at 0.20 mm and 0.14 mm respectively for two threaded holes. The error calculation is performed only for the successful iteration where measurement data are obtained.

Table 5-6 : Mean error and standard deviation - ambient lighting

Parameter	Bolt 1 (mm)	Bolt 2 (mm)	Hole 1 (mm)	Hole 2 (mm)
Mean error	-0.46	-0.51	0.20	0.14
Standard deviation	0.25	0.21	0.27	0.22

Even though the errors are less than 0.5 mm for the bolt head and threaded hole measurements, the degree of closeness of the errors are large. For the bolt head measurement errors, the standard deviation is 0.25 mm and 0.21 mm respectively; for the two bolts and for the threaded hole measurement error, standard deviation is 0.27 mm and 0.22 mm respectively for the two threaded holes.

The standard deviation is marked as a black line indicator on Figure 5-22 and Figure 5-23. This shows that the measurements are not repeatable and the error margin is large. Because of this large deviation, measurement errors are not predictable and error correction cannot be applied.

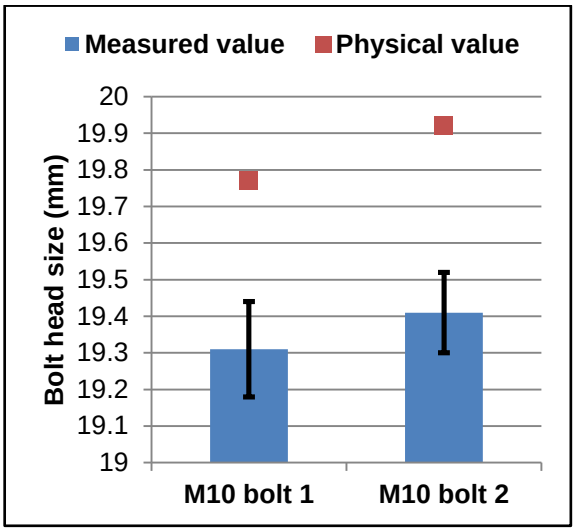

Figure 5-22 : M10 bolts mean error and standard deviation - ambient lighting

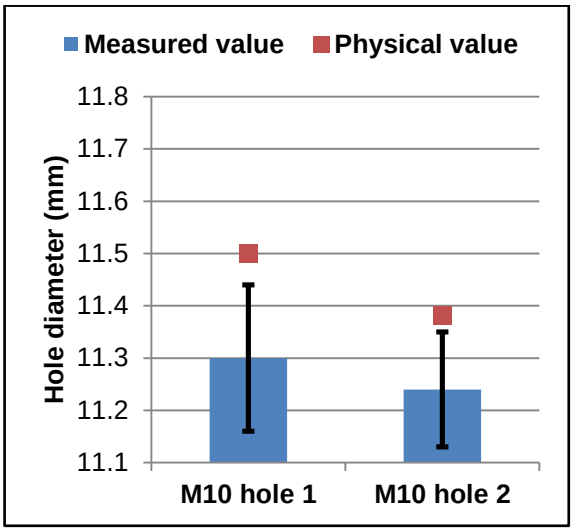

Figure 5-23 : M10 holes mean error and standard deviation - ambient lighting

In addition to the lighting conditions, the camera resolution and stand-off distance are some of the main parameters that affect the accuracy of the size and position measurements of the bolt head and threaded hole. The resolution of the camera used in this experiment is 1626 x 1236 (2 MP) and the standoff distance of the camera to cover the objects into the camera field of view is 380 mm.

5.9 Results

The experimental data collected shows that the developed 2D fastener assembly method is sensitive to the external lighting conditions. This method can be used only in uniform lighting conditions where the environment is structured and not suitable for non-structured environment which is the case in most industries. Despite the fact that the mean error is less than 0.5 mm in variable lighting condition, the rate of success in successfully assembling a bolt into a fastening hole falls to 53%. This may vary depending upon the amount of light entering the work area. These limitations make the 2D fastener assembly method less robust for being used in industrial automation.

In addition, the 2D fastener assembly is performed with a constraint that bolts and holes are located in two-dimensional space (i.e. fixtures are used to present the bolts and component with threaded holes to the vision system in a defined orientation). But in industries, the bolts are brought in bins and the components may have threaded holes at different angled surfaces, thus making this method less flexible.

The results of the experiments proved that the 2D fastener assembly is less flexible and less robust for implementation in industrial applications. These are the main reasons for moving from 2D sensors to 3D sensors for assembling bolts and holes.

One efficient solution is to use 3D sensors which are not sensitive to variable lighting conditions and reflection problems. The next step in this research is to identify the most suitable 3D sensor for assembly, with better accuracy and less sensitivity to environmental conditions.

CHAPTER 6 - EVALUATION OF THREE DIMENSIONAL (3D) IMAGING SENSORS

For simplification, fastener assembly was investigated initially in a two dimensional environment - with the bolts and mating components located at flat surfaces, as described in CHAPTER 5 - . However, in an industrial assembly scenario, fasteners may be located at random positions (i.e. in 3D) and therefore require 3D location information.

There are different types of 3D imaging technologies and sensors that already exist commercially, which can provide a 3D visual perception of objects or work area. The 3D imaging sensors can be categorised into two major categories: contact and non-contact sensors. The contact sensors provide 3D information through physical contact for example, a coordinate measuring machine (CMM). The non-contact sensors use electromagnetic radiation or ultrasound to obtain 3D information: stereo cameras, structured light 3D scanners, time-of-flight scanners, depth-from-focus and laser triangulation scanners all function in this way. Each method of 3D measurement is suitable for certain industrial application. The purpose of evaluating commercially available 3D sensors as a part of this project is to select the most suitable sensor for the fastener assembly application.

This chapter will discuss different 3D imaging technologies and their working principle, specifications and merits. It also describes the experiments carried out to evaluate the 3D sensors under different conditions, such as variation in lighting and surface finishing.

6.1 3D Technologies and Sensors Used for Evaluation

Among various technologies used for 3D measurements, three distinctly different technologies are selected for evaluation. These include depth sensor with IR (Infra-Red) pattern projector, stereo camera with pattern projector and laser profile scanner. The time-of-flight and stereo camera are not involved in the evaluation due to their sensitivity to ambient light in typical industrial

environment. Figure 6-1 illustrates the four commercial 3D sensors of three different technologies evaluated at this stage of the project. For laser scanner technology, two different sensors are selected based on their laser line width (i.e. Micro-Epsilon with 25 mm and VC- Nano with 300 mm)

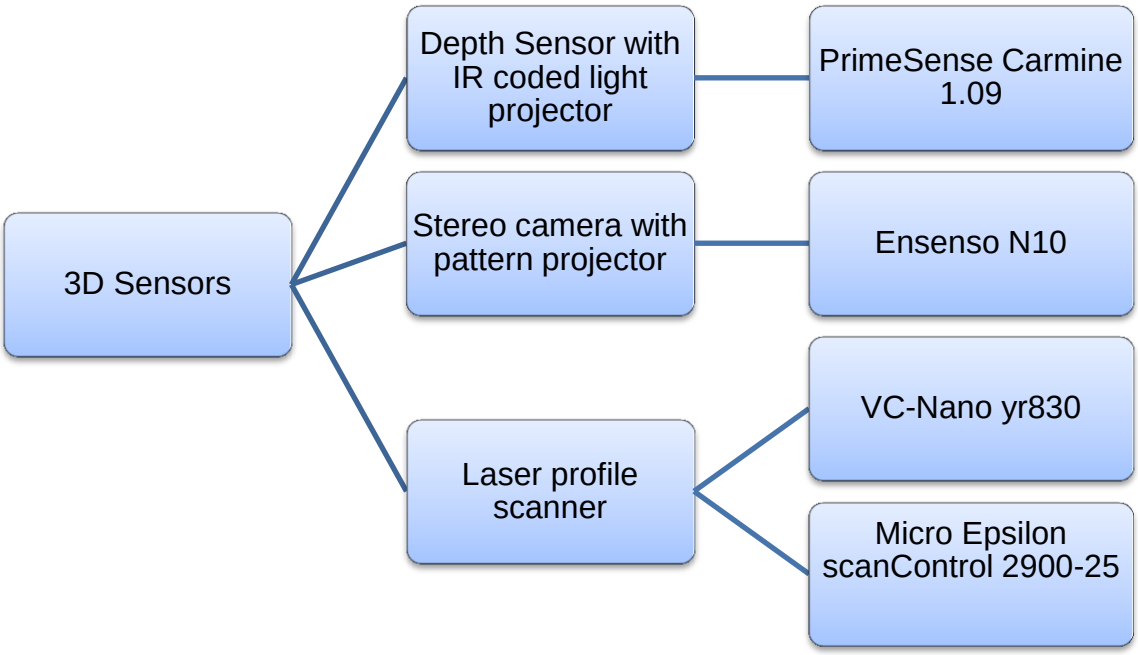

Figure 6-1 : 3D sensors used for evaluation

6.1.1 Ensenso N10

The Ensenso N10 sensor manufactured by Imaging Development Systems (IDS)[100] uses the stereo camera with pattern projector technology to obtain 3D information. It has two CMOS (Complementary metal oxide semiconductor) image sensors and a dotted light pattern projector, as shown in Figure 6-2. The projector projects a highly structured, dotted pattern on the object scene. The left and the right cameras capture that scene as shown in Figure 6-3 (a). The sensor determines the correspondence between each point on the left and the right images, thereby determining the depth and the spatial co-ordinates of all the points in the scene. Consequently, a point cloud data (PCD) is generated using the information obtained through stereo correspondence.

The manufacturer of Ensenso has stated the resolution as 752 x 482 pixels with a spatial resolution of 0.8 mm and a depth resolution of 0.5 mm at its optimum

working distance (500 mm). The minimum stand-off distance required is 166 mm from the object, the measurement range is from 166 mm to 2000 mm and the working volume of the camera is shown in Figure 6-3 (b).

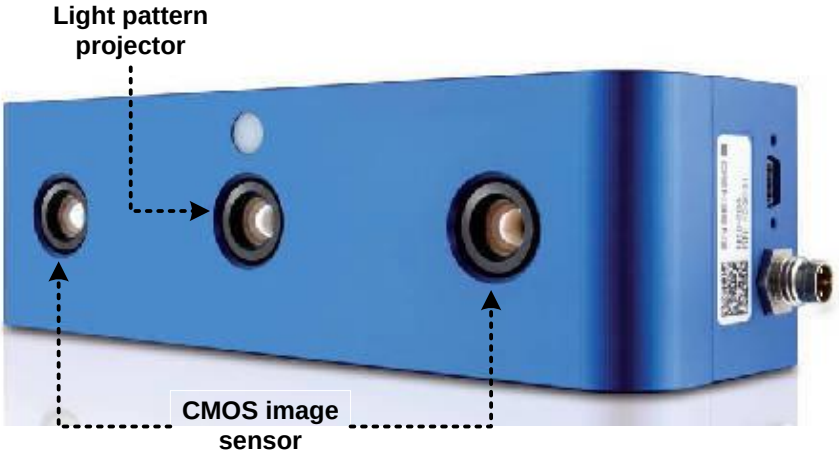

Figure 6-2 : Ensenso N10 [100]

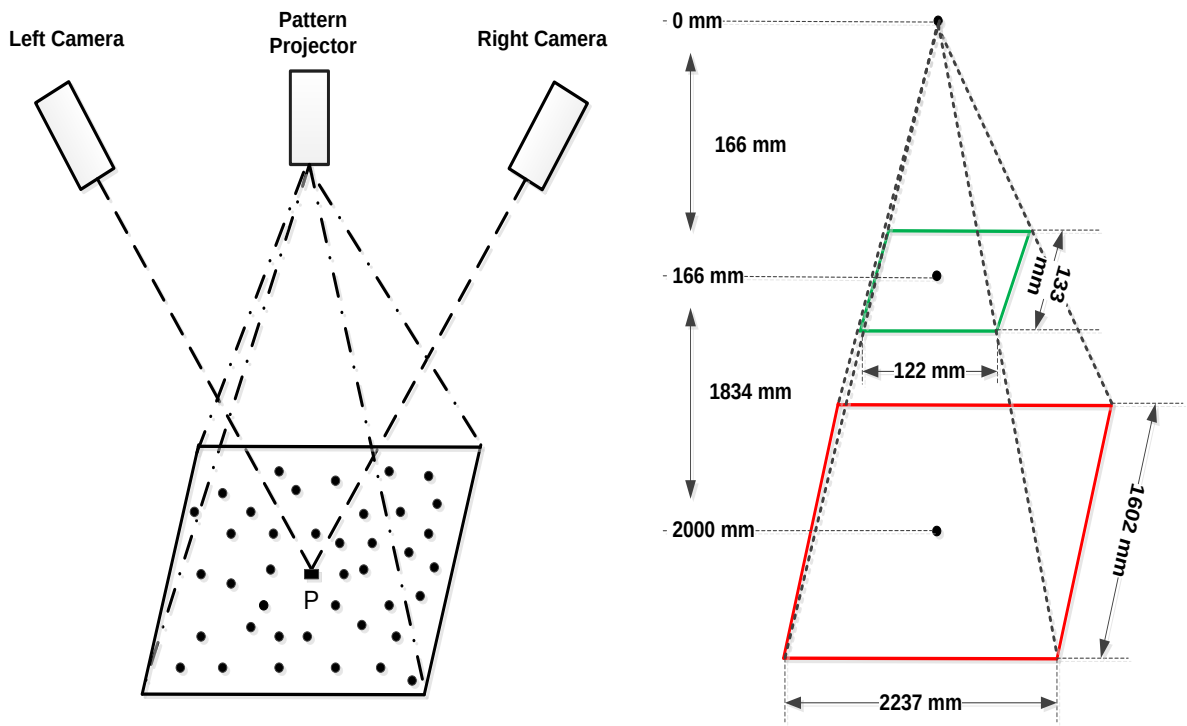

a) Working principle

b) Working volume

Figure 6-3 : Enseno technology

6.1.2 PrimeSense Carmine 1.09

The Carmine 1.09 sensor developed by PrimeSense [101] is equipped with a colour image sensor, depth image sensor and infra-red coded light projector as shown in Figure 6-4. The principle in which the sensor works is known as 'Light coding technology'. The projector in the sensor projects coded dots of infra-red light and the depth image sensor, with infra-red filter, captures the image, as shown in Figure 6-5 (a).

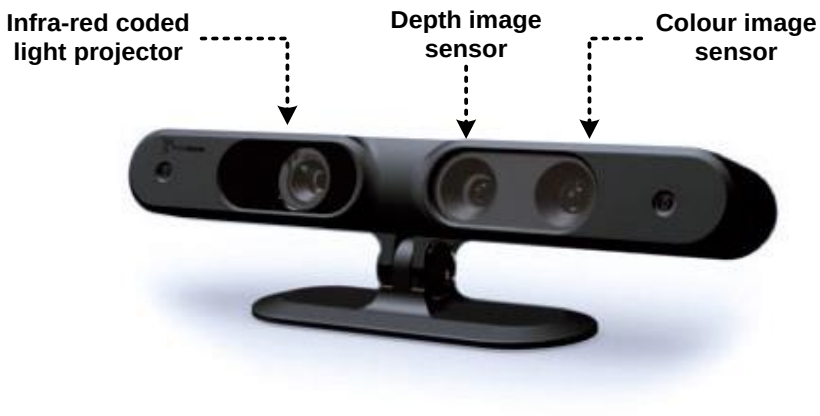

Figure 6-4 : PrimeSense Carmine 1.09[101]

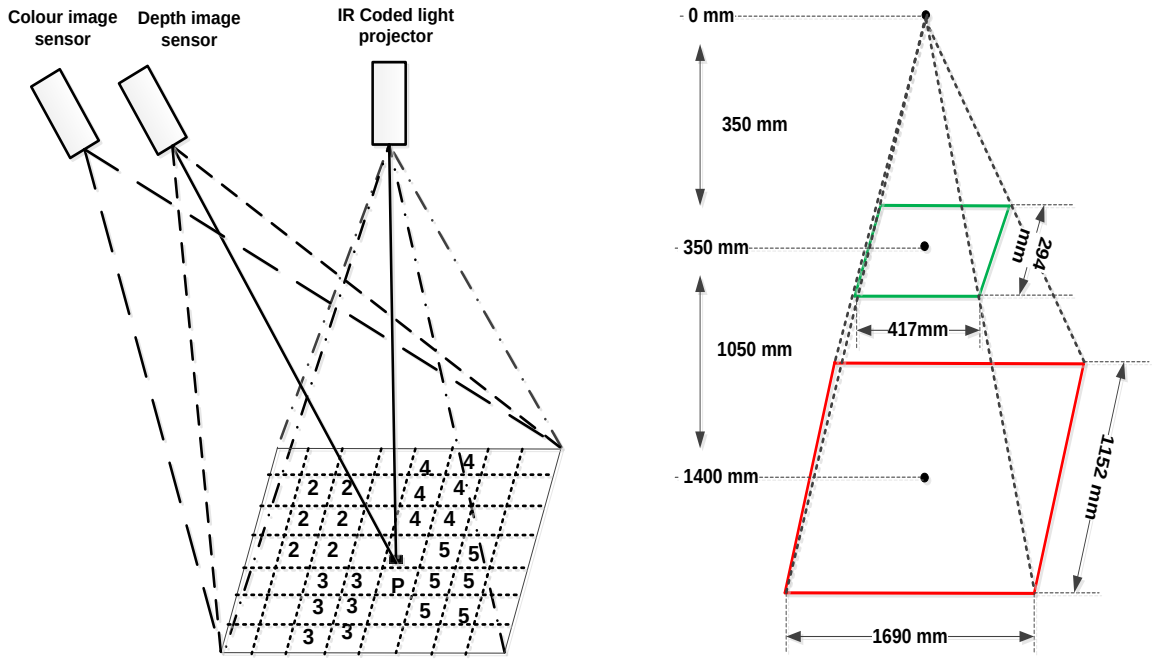

a) Working principle b) Working volume

Figure 6-5 : PrimeSense technology

The obtained pattern of infra-red dots varies depending upon the distance of the object and its shape, which is then translated into depth information. The technology used in this sensor is inferred from an online website source, as the original information is not provided by manufacturer.

The manufacturer of the Carmine 1.09 device has stated the resolution as 640 x 480 pixels with a spatial resolution of 0.9 mm and a depth resolution of 0.523 mm at 500 mm working distance. The minimum stand-off distance required for this sensor is 350 mm from the object, the measurement range is from 350 mm to 1400 mm and the working volume is shown in Figure 6-5 (b).

6.1.3 VC-Nano yr830

The Nano yr830 sensor manufactured by Vision Components (VC) [102] works on the principle of laser triangulation technology. It includes a CMOS image sensor and a Class 2M laser line projector as shown in Figure 6-6.

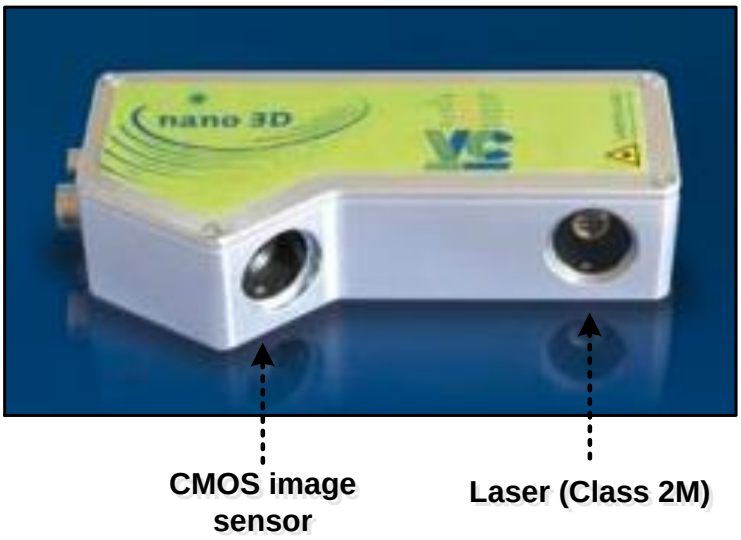

Figure 6-6 : VC-Nano yr80[102]

The laser line is projected on the object or the work area and the reflected laser light is captured by the image sensor as shown in Figure 6-7 (a). The laser triangulation principle involves determining the depth and spatial information by forming a triangle between the CMOS sensor, the laser projector and the object. The depth information and x-axis information is calculated from the relative change in the position of the reflected laser line on the image sensor

matrix with respect to calibrated reference position. The image sensor can also be used to take 2D images of the scene separately.

The Nano yr830 sensor has a resolution of 1280x1024 pixels as stated by the manufacturer. This device has a spatial resolution of 0.08 mm and depth resolution of 0.04 mm at a 240 mm working distance. The rate of laser scan is up to 1 kHz and the line width of the laser line is 340 mm as described in Figure 6-7 (b). This large line width with compact size is the main reason for considering this sensor for evaluation, as other commercially available laser scanners do not have this advantage. Usually, the laser scanners with a large line width will not be compact.

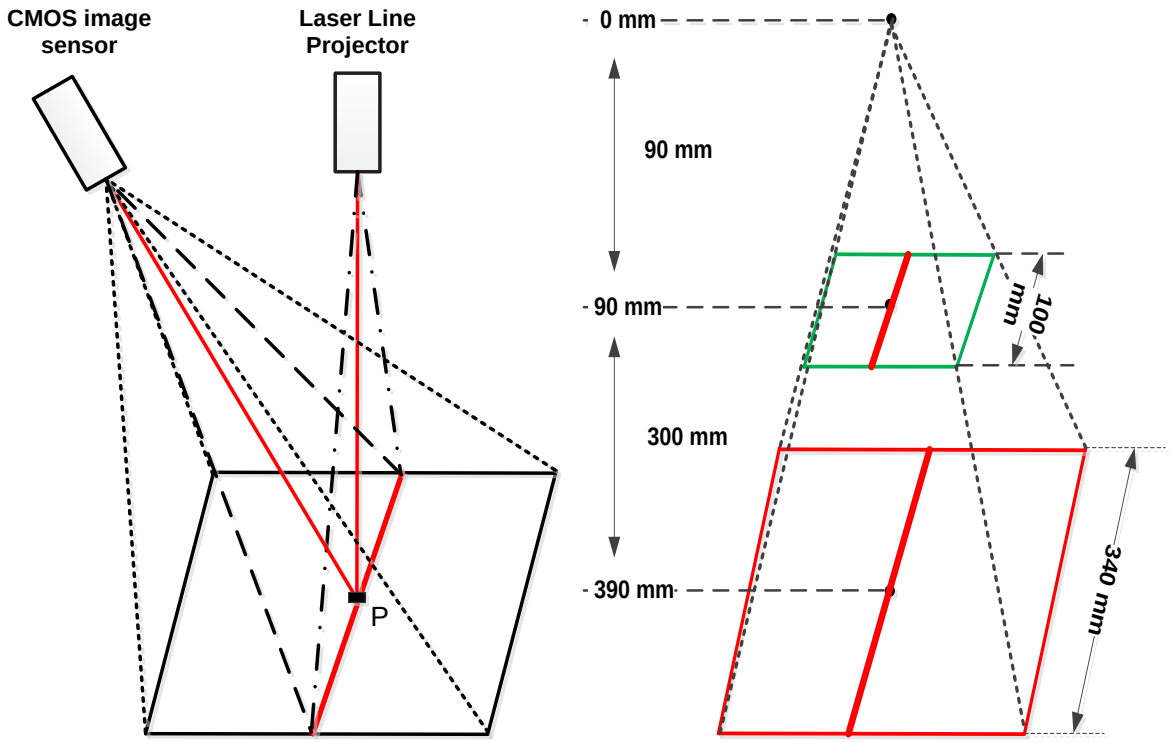

a) Working principle b) Working volume

Figure 6-7 : VC-Nano technology

6.1.4 Micro-Epsilon scanControl 2900-25

Micro-Epsilon[92] also works with the principles of laser triangulation technology, which were explained in the previous section. It includes a CMOS image sensor and a Class 2M laser line projector as shown in Figure 6-8. The

laser line is projected on the object or workspace and reflected laser light is captured by the image sensor, as illustrated in Figure 6-9 (a).

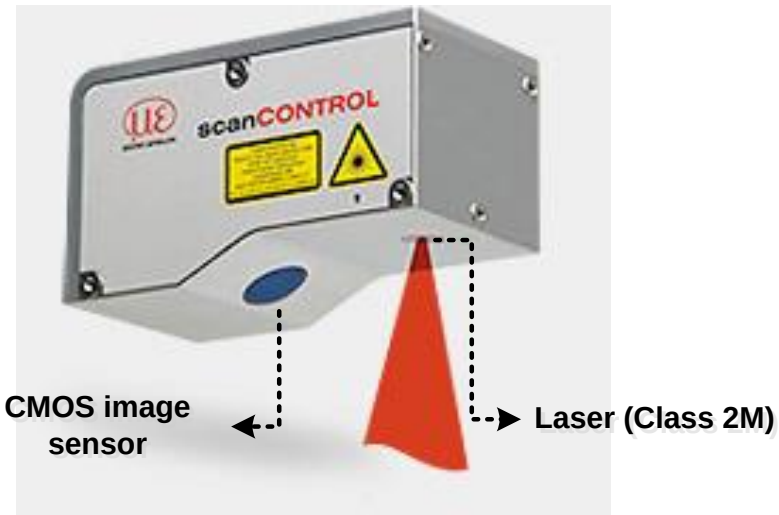

Figure 6-8 : Micro-Epsilon scanControl 2900-25[92]

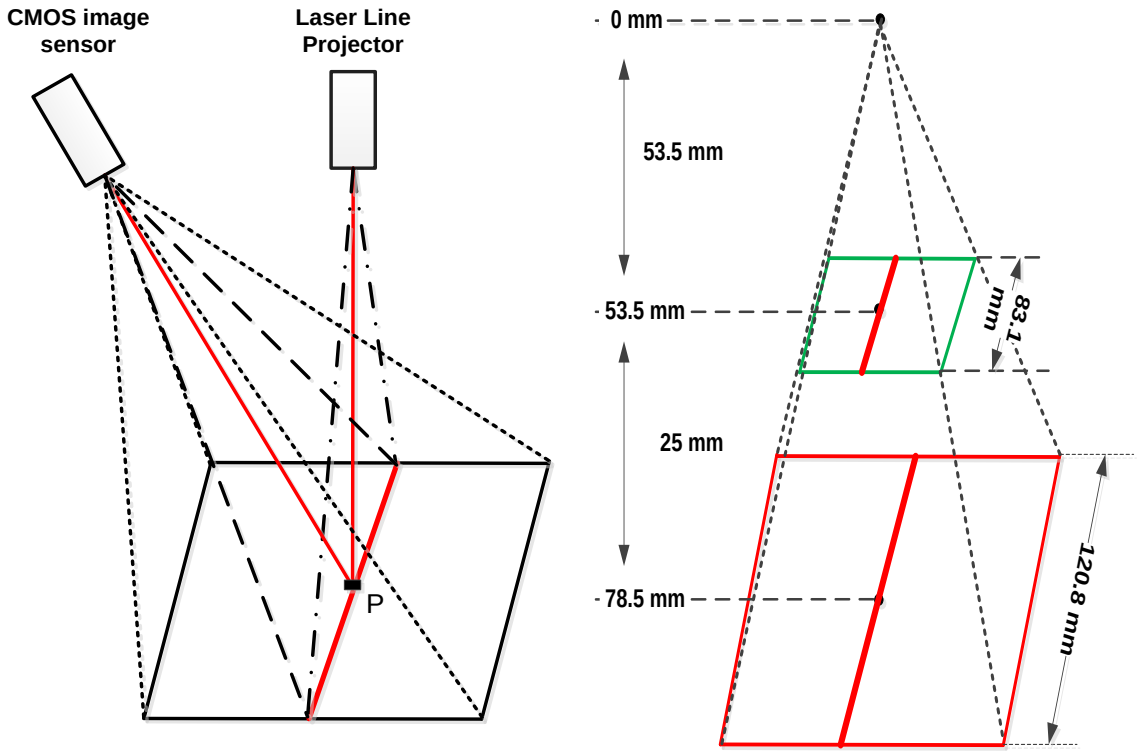

a) Working principle b) Working volume

Figure 6-9 : Micro-Epsilon laser scanner technology

The depth information and x-axis information is calculated from the reflected laser line position on the image sensor matrix. The manufacturer has stated a resolution of 1280 pixels per profile for this device. Both the spatial resolution and the depth resolution of the sensor is 0.02 mm and the rate of scan is up to 2 kHz. The stand-off distance is 53.5 mm from the object, the measuring ranges from 53.5 mm to 78.5 mm and the laser line width is 29.3 mm as shown in Figure 6-9 (b).

6.2 Comparing 3D Device Specifications

Table 6-1 gives the specifications provided by the manufacturers of 3D devices.

Table 6-1 : 3D sensors manufacturer specification

3D Sensor	Resolution	Working distance (mm)	Spatial Resolution (mm)	Depth Resolution (mm)	Scan Rate (kHz)
Ensenso	752 x 482	500	~0.8	0.523	n/a
PrimeSense	640 x 480	500	0.9	1	n/a
VC- Nano	1280 x 1024	240	0.08-0.3	0.04	Up to 1
Micro-Epsilon	1280*	78.5	~0.02	~0.02	0.2 to 2

*resolution in points/profile

The spatial resolution of the PrimeSense and Ensenso sensors are 0.9 mm and 0.8 mm respectively and the depth resolution are 1.0 mm and 0.5 mm respectively, as per the manufacturer specifications. This limits the sensors on the application where accuracy has to be less than 0.5 mm. In fastener assembly, the error has to be less than 0.5 mm to differentiate between different diameter threaded holes, for example differentiating a M5 from a M4 and M6 threaded hole which has a 1 mm diameter difference. In addition, the positional accuracy has to be less than 1 mm for the prevention of cross threading while fastening. Despite this disadvantage, the working distance and working volume of the sensors are greater as shown in Figure 6-5 (b) and Figure 6-3 (b). Thus, these sensors can be used to obtain 3D information from a larger object or work area.

On the other hand, the VC-Nano and Micro-Epsilon sensors have a spatial resolution of 0.02 mm and 0.3 mm respectively and a depth resolution of 0.04

mm and 0.02 mm respectively. With this resolution, the threaded holes which are 1 mm apart can be easily identified and the positional accuracy of less than 1 mm can be achieved. Despite this advantage, their working distance and the working volume are smaller as shown in Figure 6-7 (b) and Figure 6-9 (b)

With a small field of view, these sensors will not be able to provide the 3D information of a large object or work area, and need multiple scans to completely map them. For an efficient bolt assembly, the sensor requires a larger working volume, but at the same time, needs to provide an accurate perception of the object or the work area.

6.3 Comparing Depth Maps and PCD of 3D Sensors

The 3D sensors comparison has to take into account the working volume of the 3D sensors, which dictates the imaging time. The PrimeSense and Ensenso can view a large work area and subsequently view the large object completely with less time for imaging. The VC-Nano and Micro-Epsilon sensors have less working volume and cannot completely view large objects or work area, thereby taking more time for imaging multiple times to cover an entire object or work area. Thus, for evaluating the sensors a common size test object is used.

An initial depth comparison was conducted for PrimeSense and Ensenso to determine the effectiveness of these devices in imaging differently sized objects (Figure 6-10, Figure 6-11 and Figure 6-12). This is performed to select a test object that best suits all the sensors. The effectiveness of the 3D sensors in imaging the reflective and masked (i.e. with white spray coating) surfaces will also be considered for comparing depth maps.

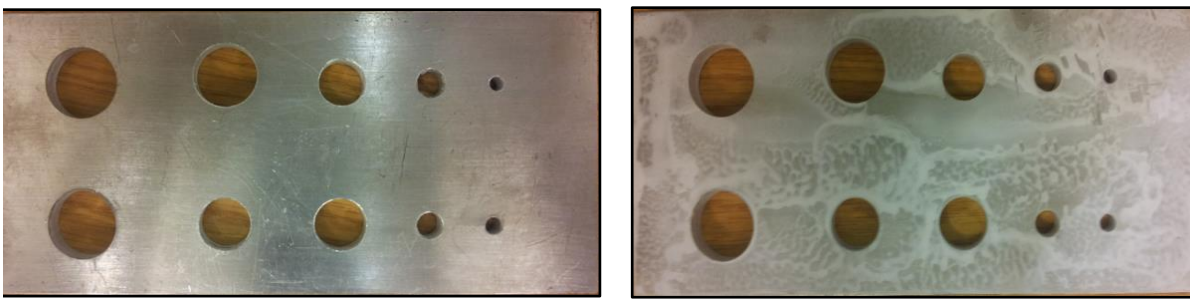

a) Normal test plate b) Test plate with white spray

Figure 6-10 : Test Plate

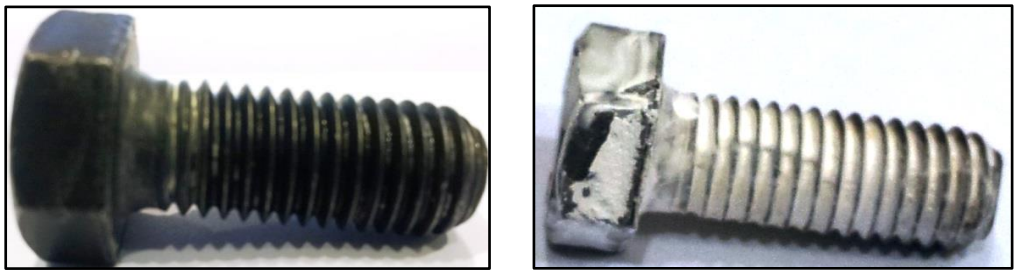

a) Normal M12 bolt b) M12 Bolt with white spray

Figure 6-11 : Bolt M12

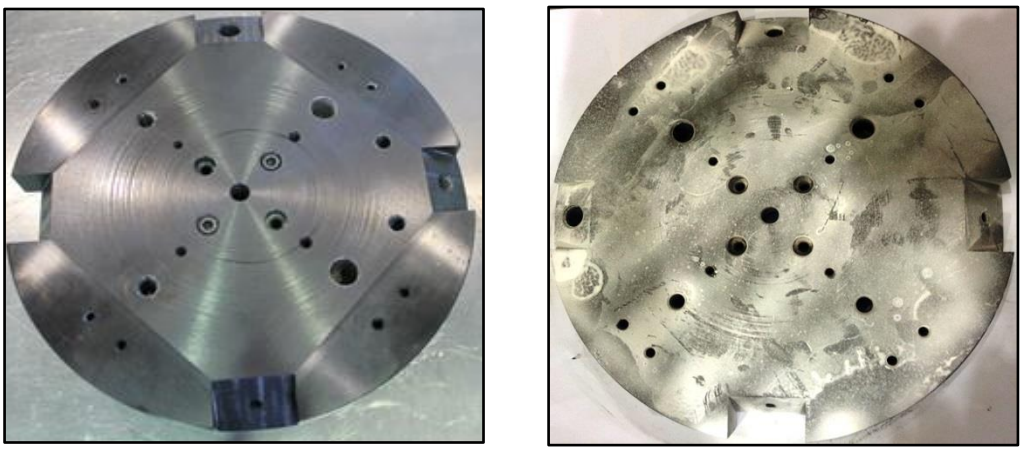

a) Normal Fastening Plate b) Fastening Plate with white spray

Figure 6-12 : Fastening Plate

The depth map evaluation is carried out on shiny objects, which may well be the case in the real industrial applications. The objects are also coated with ARDROX 9D1B[103], a non-chlorinated solvent-based spray developed by Chemetall group. The spray will form white particles on the surface of the objects which suppress the specular highlights formed due to surface reflectivity. The test object used for evaluation is a rectangular aluminium plate with differently sized holes and the same object with white spray coating as seen in Figure 6-10. In addition, a M12 bolt and the fastening hole plate are also used for this test (i.e. the objects used in this research for assembly). These objects are evaluated to understand the amount of information that can be obtained using these sensors in different conditions. The M12 bolt and the fastening hole plate and the same objects with white spray coating are shown in Figure 6-11 and Figure 6-12 respectively.

6.3.1 Ensenso

The depth maps of the test objects are obtained through the PC interface provided with the Ensenso 3D device.

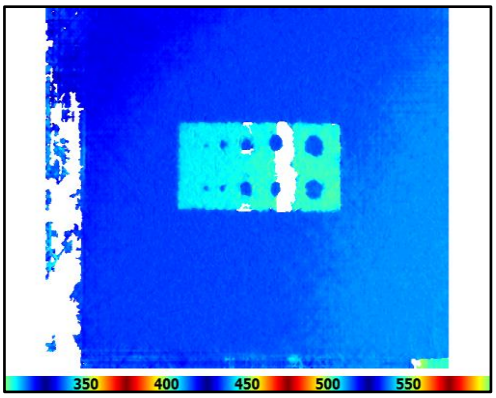

a) Test plate depth map

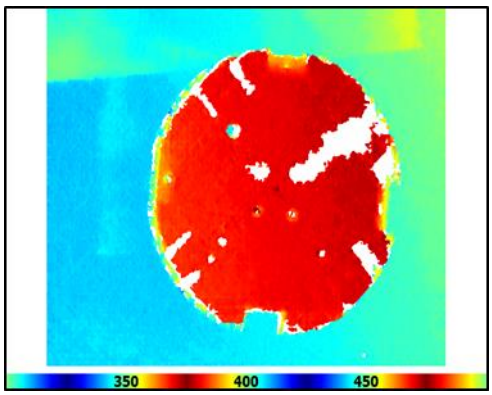

b) Fastening plate depth map

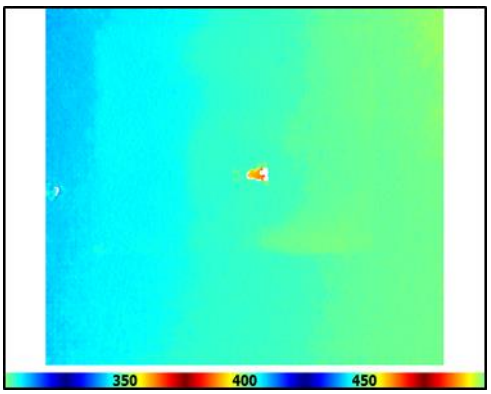

c) M12 Bolt depth map

Figure 6-13 : Depth map of normal objects - Ensenso

The depth maps of the objects shown in Figure 6-13 have some missing data points which are represented by white colour patches on the object images. The missing data points are attributed to the bright spots (specular highlights) occurring on the objects due to the influence of external lighting and also due to the reflection of its own light projector from the shiny surface of the objects.

After spraying the white spray coating on the surface of the objects, the depth information of the objects was obtained, as illustrated in Figure 6-14. The white spray on the surface of the objects masks the specular highlights, thus providing better depth information. The information obtained clearly shows the small object (Bolt M12 shape) as indicated by Figure 6-14 (c) and also provides

rich information on the features presented in the larger objects (i.e. the test plate and the fastening plate), as shown in Figure 6-14 (a) and (b).

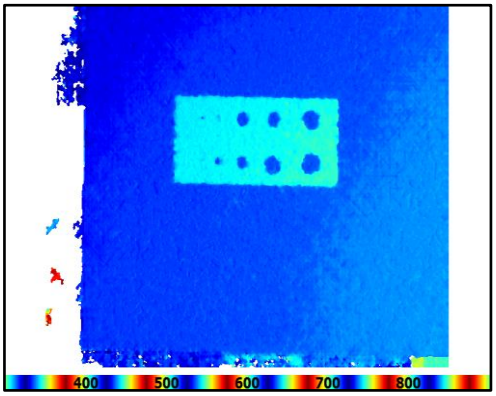

a) Test plate depth map

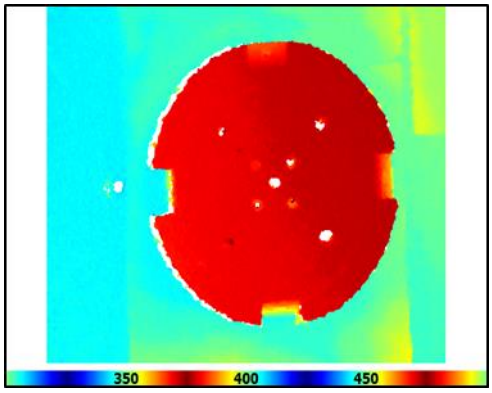

b) Fastening plate depth map

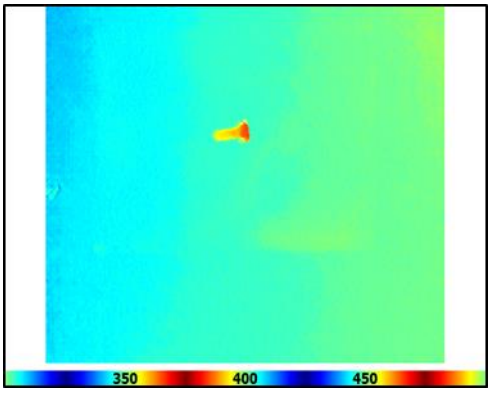

c) Bolt M12 depth map

Figure 6-14 : Depth map with ARDROX white spray - Ensenso

6.3.2 PrimeSense

The depth maps of the objects from PrimeSense are obtained using the PC interface provided by its manufacturer. The depth map information of all the test objects is shown in Figure 6-15. Even without the white spray on the objects, this sensor was able to provide clearer and better depth map information when compared to the Ensenso 3D sensor.

This shows that the sensor was not affected by specular highlights formed on the objects. This is because, it uses an infra-red (IR) coded light pattern instead of visible light for imaging. The reflected IR-coded light pattern is filtered by infra-red filters, thus only the IR light is captured back by the image sensor. Therefore, the sensor is not affected by the visible light.

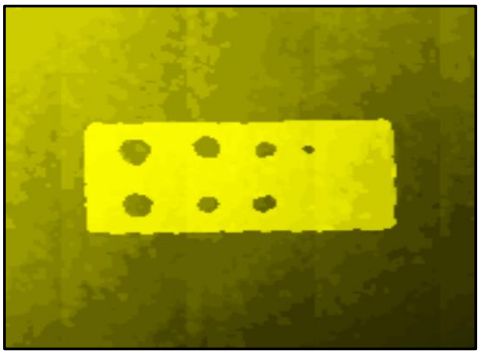

a) Test plate depth map

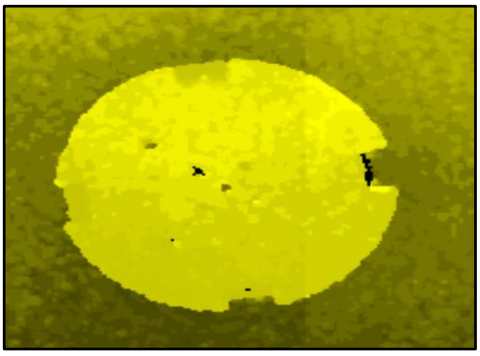

b) Fastening plate depth map

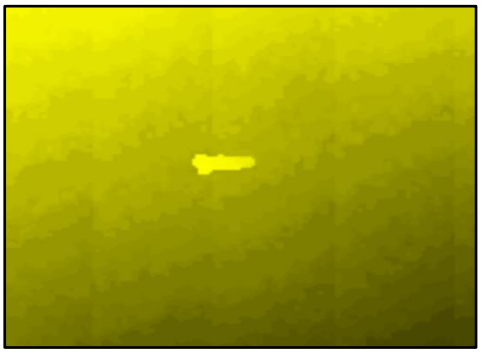

c) Bolt M12 depth map

Figure 6-15 : Depth map of normal objects - PrimeSense

But the depth map of the smaller object such as M12 bolt has less information about its shape and size as shown in Figure 6-15 (c). In addition, the depth maps of larger objects do not provide much information about the small features such as holes.

After spraying the surface of the objects with the white spray, by visual analysis, the depth maps of the objects are little better than without spray - as the small objects like the bolt M12 have little more information. But still the small object features cannot be obtained from this depth map, as shown in Figure 6-16 (c). This is similar to the large objects such as test plate and fastening plate; the spray has added less information as shown in Figure 6-16 (a) and (b), and the features such as holes are still not clear on the objects.

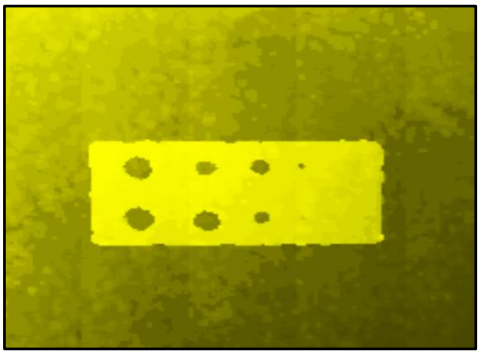

a) Test plate depth map

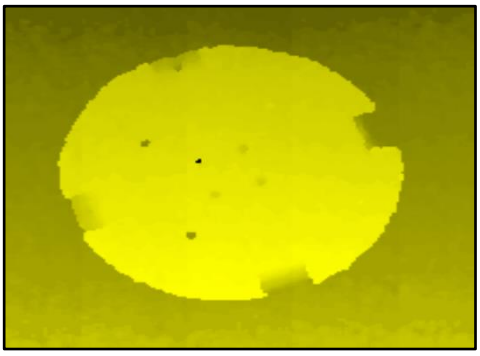

b) Fastening plate depth map

c) Bolt M12 depth map

Figure 6-16 : Depth map with ARDROX white spray – PrimeSense

6.3.3 Micro-Epsilon Laser Scanner

The laser scanner has a smaller field of view, hence only the bolt which is small enough to fit into the FOV of the laser scanner is used for acquiring PCD. The PCD of the bolt with and without white spray is shown in Figure 6-17.

The PCD obtained showed that the shape of the M10 bolt is clearly visible. In addition, it was observed that the bolt with white spray provided a slightly better PCD than the bolt without the spray, but the difference is not significant. Thus, the PCD of the object is less affected by the specular highlights on the surface, due to external lighting interference.

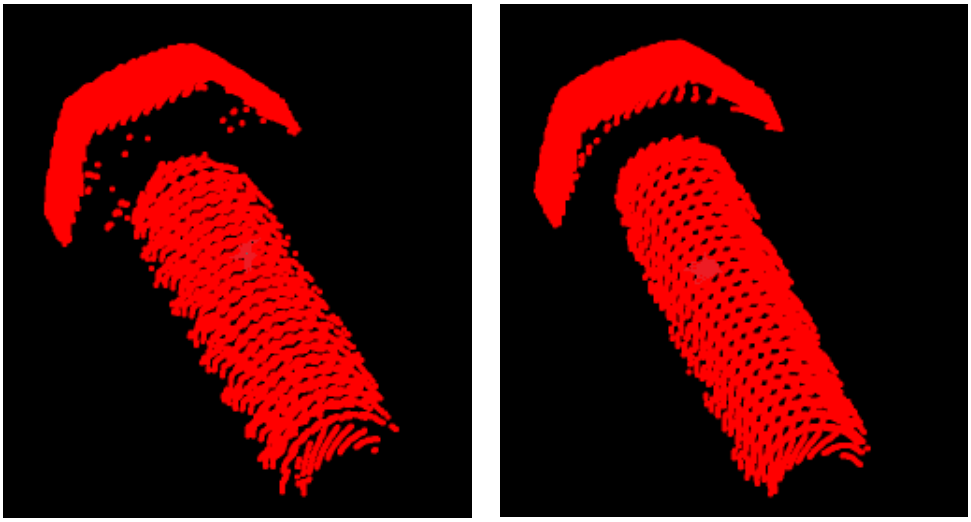

a) Bolt M10 b) Bolt M10 with white spray

Figure 6-17 : PCD comparison of Bolt M10 with and without white spray

6.3.4 Depth Map Comparison Results

The visual comparison of depth maps of the objects showed that PrimeSense and Ensenso with large field of view (FOV) were not able to obtain much information from smaller object. This is due to the limitation in the spatial and depth resolution of the sensors. On the other hand, the Micro-Epsilon with small field of view can provide more information about the smaller sized objects, but require additional scanning to view larger objects. Hence, the Micro-Epsilon is not advisable for scanning large size objects, and the PrimeSense and Ensenso are not suitable to provide accurate information of objects.

To further evaluate the 3D sensors, two different size objects have been considered. The plan is to use a large object of known size for evaluating PrimeSense and Ensenso sensors, as they have large FOV and low resolution i.e. greater than 0.5 mm. A small object of known size that is within the FOV laser scanners was used to evaluate Micro-Epsilon and VC-Nano 3D sensors.

6.4 Experiment to Determine Accuracy of 3D Devices

The experiment to determine the accuracy of all four 3D sensors has to involve two differently sized objects as discussed in the previous section. This experiment is conducted in two different categories, one with a large object for PrimeSense and Ensenso devices and the other with small object for Micro-

Epsilon and VC-Nano. The accuracy of the 3D sensors is determined in both spatial (X and Y) and vertical (Z) axis for a complete 3D evaluation.

Both the categories involve determining the spatial accuracy of the 3D devices by measuring the size (length and breadth) of a known object. The vertical height accuracy (z-axis) is determined by measuring a range of known height increment made using a depth micrometre. The experiment categories and their accuracy measurement steps are described below:

1) Experiment with large object - PrimeSense and Ensenso
    a. Object size measurement
    b. Z-axis accuracy measurement
2) Experiment with small object - Micro-Epsilon and VC-Nano
    a. Object size measurement
    b. Z-axis accuracy measurement

To achieve the robustness required for industrial application, the 3D sensors have to obtain visual perception of the objects or the work area accurately in different environment conditions such as variation in lighting and surface finishing. Hence, this experiment was carried out in different environment conditions and the accuracy measurement results are analysed for selecting the suitable technology for the fastener application. The measurement conditions used in this experiment are shown in Figure 6-18.

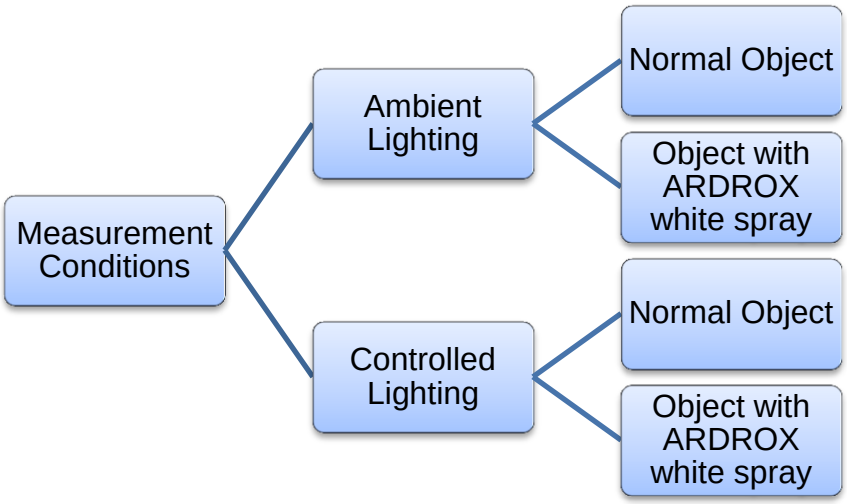

Figure 6-18 : Measurement Conditions for evaluating 3D sensors

The experiments were conducted in two different lighting conditions which include the ambient and controlled lighting. Apart from using the objects normally for measurement, it was also coated with ARDROX white spray and subject to accuracy measurement. This is carried out to determine the effect of surface finish of the object on the measurement accuracies of the 3D sensors. The large object used in this experiment is a 10 mm thick test plate (shown in Figure 6-19 with its physical dimensions).

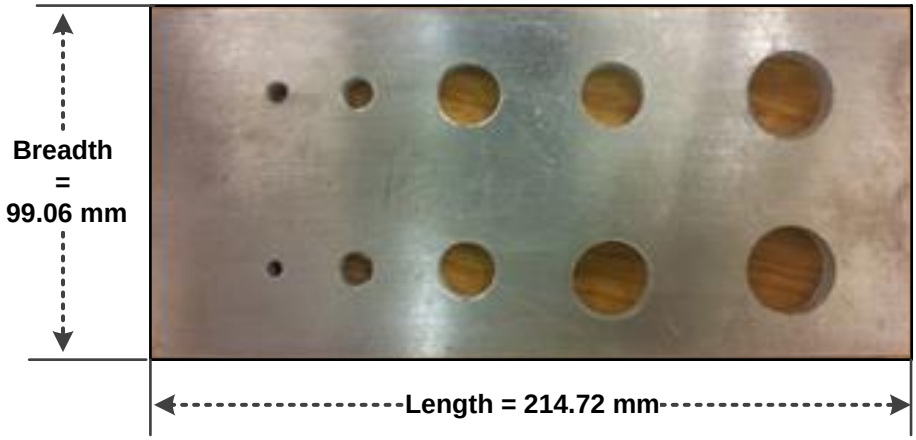

Figure 6-19 : Test plate with physical size

The small object used in the experiment is a 20 mm slip gauge which is shown in Figure 6-20 with its physical dimensions.

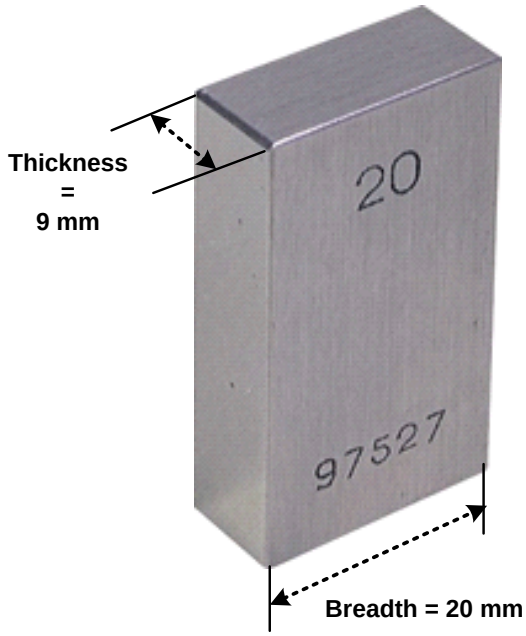

Figure 6-20 : Slip gauge bar (20 mm)

6.4.1 Experiment with Large Objects - Test Plate

This experiment category is for the 3D sensors, PrimeSense and Ensenso with larger FOV, to measure the large object i.e. test plate (Figure 6-19). The length and breadth of the test plate are measured using the sensors and are compared to the physical values - to obtain the accuracy and repeatability. It also involves a z-axis accuracy measurement experiment to determine the 3D sensors depth accuracy.

6.4.1.1 Object Size Measurement

The measurement accuracy of the sensors in *x-axis* and *y-axis* are determined by measuring the length and breadth of the test plate. The length of the test plate is 214.72 mm, representing the measurement of the larger side of an object, and the breadth is 99.07 mm, representing the measurement of the smaller side of an object. Thus two different sizes are measured on the same object.

The point cloud data (PCD) of the test plate is obtained from the PrimeSense and Ensenso 3D devices and processed by a program developed in C# for this experiment. Both the PrimeSense and the Ensenso are mounted next to each other and all the measurements in different lighting conditions are performed simultaneously. This is to ensure both the sensors are subjected to similar conditions while taking measurements.

The processing information for measurement accuracy involves plotting the PCD of the test plate obtained from the sensors and fitting the smallest bounding box on the PCD of the object i.e. the test plate. The bounding box length and breadth obtained from the developed program represents the measured test plate dimensions.

a) Ambient Lighting Condition

The ambient lighting represents the daylight interference on the experiment setup and thus represents the variable lighting condition. The test object is measured with and without the white spray applied to its surface. Table 6-2

gives size measurements of the test plate without white spray under ambient lighting condition.

Table 6-2 : Test plate size measurement - Normal object

Trial No	PrimeSense 3D		Ensenso 3D	
	Length (mm)	Breadth (mm)	Length (mm)	Breadth (mm)
1	215.8	100.5	216.0	104.1
2	215.5	100.1	215.2	104.2
3	216.0	99.9	216.3	103.9
4	214.9	99.7	215.4	104.4
5	215.2	99.5	216.0	103.2
6	215.8	100.2	215.6	104.4
7	215.0	100.6	216.7	104.1
8	215.3	100.0	216.6	104.3
9	215.8	100.5	215.5	104.2
10	216.2	100.0	216.0	103.6
Average	**215.6**	**100.1**	**215.9**	**104.0**

Table 6-3 : Test plate size measurement - object with spray

Trial No	PrimeSense 3D		Ensenso 3D	
	Length (mm)	Breadth (mm)	Length (mm)	Breadth (mm)
1	215.5	100.5	215.5	102.6
2	215.9	101.1	215.5	102.0
3	215.1	100.8	216.7	102.4
4	215.2	100.5	216.2	102.5
5	216.1	100.0	216.4	103.0
6	215.6	101.5	216.5	102.8
7	216.1	100.7	215.4	102.8
8	215.6	101.0	216.2	101.5
9	216.5	100.7	215.5	102.0
10	216.0	100.1	215.7	101.3
Average	**215.8**	**100.3**	**216.0**	**102.3**

Table 6-3 illustrates the size measurement of the test plate with ARDROX white spray applied to it under the ambient lighting condition.

b) Controlled Lighting Condition

The controlled lighting condition does not have any daylight interference; therefore the variation in lighting is negligible. Table 6-4 gives the size measurements of normal test plate under controlled lighting obtained from the PrimeSense and Ensenso 3D devices.

Table 6-4 : Test plate size measurement - Normal object

Trial No	PrimeSense 3D		Ensenso 3D	
	Length (mm)	Breadth (mm)	Length (mm)	Breadth (mm)
1	213.8	100.5	216.3	104.1
2	213.6	100.1	215.6	104.0
3	213.5	100.8	216.3	104.3
4	214.1	100.3	215.6	104.0
5	213.2	100.2	216.3	104.1
6	213.7	100.2	215.7	104.0
7	214.2	100.4	216.4	104.1
8	214.0	100.0	216.9	103.8
9	213.6	100.7	216.2	103.8
10	213.5	100.1	216.4	104.2
Average	**213.7**	**100.4**	**216.2**	**104.0**

Table 6-5 : Test plate size measurement - object with spray

Trial No	PrimeSense 3D		Ensenso 3D	
	Length (mm)	Breadth (mm)	Length (mm)	Breadth (mm)
1	215.6	100.1	215.1	101.3
2	215.5	100.6	215.4	101.0
3	216.0	100.3	215.3	101.4
4	215.2	101.0	216.0	102.0
5	215.7	100.3	215.8	101.3
6	215.9	100.4	215.6	101.5
7	215.4	100.2	216.0	100.9
8	215.6	100.0	215.2	101.6
9	216.0	100.4	216.1	101.2
10	215.8	100.0	215.7	101.1
Average	**215.7**	**100.3**	**215.6**	**101.3**

Table 6-5 illustrates the size measurement data of test plate with ARDROX white spray under controlled lighting.

6.4.1.2 Object Size Measurement Result Analysis

The data obtained under ambient lighting conditions show that the average error in determining the length (larger side) of test plate with normal surface, and the surface with white spray is 0.9 mm and 1.1 mm respectively for the PrimeSense sensor. The average error in measuring the breadth (smaller side) of test plate with normal surface and surface with white spray is 1.0 mm and 1.2 mm respectively as shown in Figure 6-21. This indicates that the PrimeSense sensor is not affected by surface finish as the errors in length and breadth measurements are not significantly different for both normal surface and surface with white spray (lies between 0.9 mm to 1.2 mm).

In addition, the object size difference i.e. measuring the larger and smaller side also does not make much difference in accuracy. The measurement accuracy of around 1.0 mm is attributed to its spatial resolution of 0.9 mm. The standard deviation of the size measurement lies between 0.3 mm to 0.4 mm under ambient lighting, represented by the black bar in Figure 6-21.

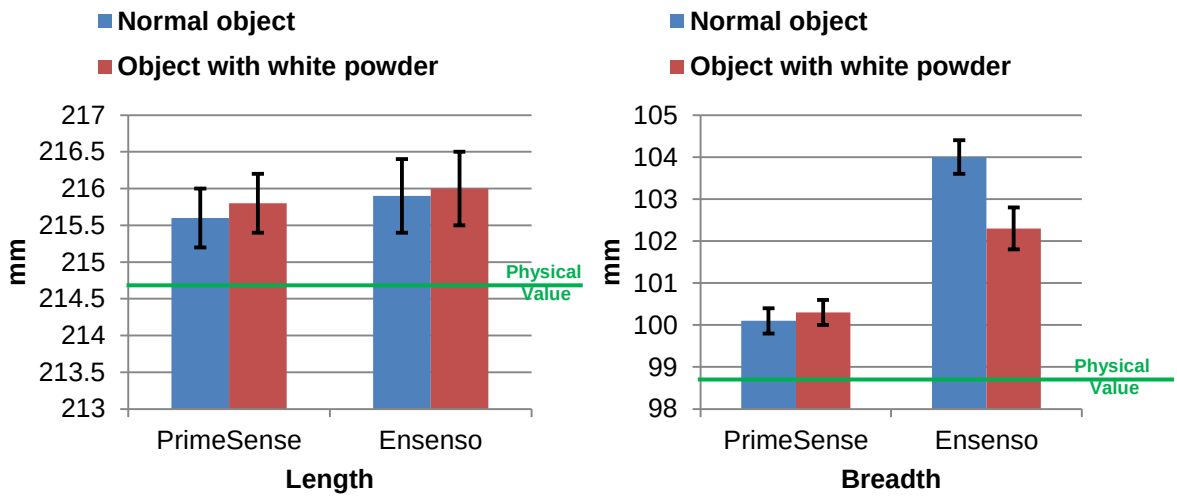

Figure 6-21 : Test plate measurement error in ambient lighting

On the other hand, the average error in measuring the length of test plate with normal surface and surface with white spray is 1.2 mm and 1.3 mm respectively for the Ensenso sensor.

The average error in breadth measurement of the test plate with normal surface and surface with white spray is 4.9 mm and 3.2 mm respectively as shown in

Figure 6-21. These results show that the Ensenso has an average error of around 1.2 mm for measuring the larger side (length) irrespective of the surface condition. But there is a 1.7 mm difference in the average error for measuring smaller sides for normal surface and surface with white spray. This is due to the specular highlights occurring on the surface of the test plate. The standard deviation of the Ensenso lies between 0.4 mm and 0.5 mm in ambient lighting condition.

The data obtained under the controlled lighting shows that the PrimeSense has an average error of -1.0 mm and 1.0 mm for measuring the length of test plate with normal surface and surface with white spray respectively. The average error in measuring the breadth of test plate with normal surface and surface with white spray is 1.3 mm and 1.2 mm respectively as shown in Figure 6-22. The error measurement shows that the PrimeSense average error in measuring larger side (length) is ±1.0 mm and smaller side (breadth) is around 1.2 mm. Thus it is not affected by the surface finish (with or without white spray).

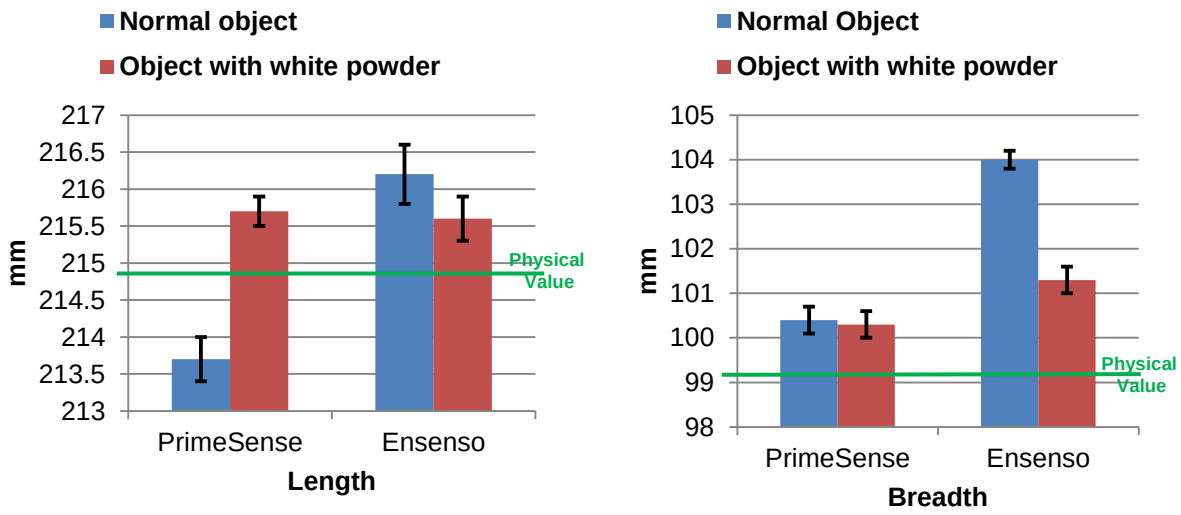

Figure 6-22 : Test plate measurement error in controlled lighting

The measurement accuracy in controlled lighting condition is around 1.2 mm which is similar to the results obtained in ambient lighting conditions. The standard deviation for PrimeSense lies between 0.2 mm to 0.3 mm shown as black line bar in Figure 6-22, which is similar to ambient lighting condition.

On the other hand, the Ensenso sensor average error in controlled lighting condition for measuring the length of the test plate with normal surface and surface with white spray is 1.5 mm and 0.9 mm respectively. The average error in measuring the breadth of test plate with normal surface and surface with white spray is 4.9 mm and 2.2 mm respectively, as shown in Figure 6-22. This data shows that the average error for measuring length and breadth has improved by 0.6 mm and 2.7 mm respectively for the Ensenso, when compared to the average errors of test plate with normal surface. However, the measurement accuracy in controlled lighting condition is found to be very similar to the accuracy obtained in ambient lighting conditions. The average errors for length and breadth are in the range of 0.9 mm to 4.9 mm respectively. The standard deviation of the Ensenso in controlled lighting conditions is 0.2 mm to 0.3 mm, which is a 0.2 mm improvement than the ambient lighting condition.

6.4.1.3 Z-axis Accuracy Measurement

The Z-axis accuracy for PrimeSense and Ensenso 3D sensors are determined by the height accuracy measurement experiment. The experiment involves incrementally increasing the height of a square shape plate placed on top of a depth micrometre, and measuring the known height increment using all the 3D sensors. The setup developed for this experiment is shown in Figure 6-23.

The depth micrometre used in this experiment is capable of increasing the height of the square plate by 2.54 µm for each revolution. The known height increment made for this experiment includes 1 mm, 2 mm and 5 mm. These large increments are due to the fact that the PrimeSense and Ensenso have a depth resolution of more than 0.5 mm and it is not capable of registering depth information less than their stated resolution.

The depth micrometre with the square plate on top (Figure 6-23) is kept within the FOV of all the 3D sensors (the initial Z-value can be any value), then the actual height of the square plate is increased to 1 mm, 2 mm, 3 mm, 5 mm, 10 mm, 15 mm and 20 mm one after other. Both the PrimeSense and Ensenso are subject to this z-axis measurement under ambient and controlled lighting conditions.

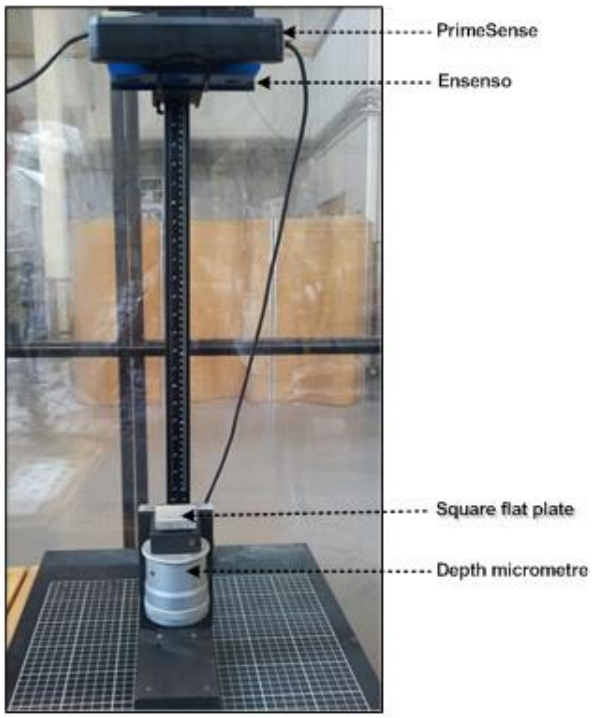

Figure 6-23 : Z-axis accuracy measurement setup

a) PrimeSense 3D

The initial z-axis value provided by the PrimeSense 3D device is 443.1 mm, this value indicates the height between the PrimeSense and centre point of the square plate. The results after measuring each height increment made using the depth micrometre are tabulated and shown in Table 6-6.

Table 6-6 : Z-increment measurement for PrimeSense 3D

Actual Height (Increment Value) (mm)	**Z- Value from the point cloud data (mm)**		**Measured height Increment (mm)**		**Error in Z-value increment (mm)**	
	Ambient Lighting	Controlled Lighting	Ambient Lighting	Controlled Lighting	Ambient Lighting	Controlled Lighting
1	442.8	442.7	0.3	0.4	-0.7	-0.6
2 (+1)	440.6	440.7	2.2	2.0	1.2	1.0
3 (+1)	438.8	439.4	1.8	1.3	0.8	-0.7
5 (+2)	436.2	437.8	2.6	1.6	0.6	-0.4
10 (+5)	429.9	431.0	6.3	6.8	1.3	1.8
15 (+5)	426.4	427.0	3.3	4.0	-1.7	-1.0
20 (+5)	420.0	421.3	6.4	5.7	1.4	0.7

b) Ensenso 3D

The initial z-axis value provided by the Ensenso 3D device is 437.4 mm, this value indicates the height between the device and centre point of the square plate. The data obtained after each height increment is tabulated as shown in Table 6-7.

Table 6-7 : Z-increment measurement for Ensenso 3D

Actual Height (Increment Value) (mm)	**Z- Value from the point cloud data (mm)**		**Measured height Increment (mm)**		**Error in Z-value increment (mm)**	
	Ambient Lighting	Controlled Lighting	Ambient Lighting	Ambient Lighting	Ambient Lighting	Controlled Lighting
1	437.1	436.9	0.3	0.4	-0.7	-0.6
2 (+1)	435.2	435.6	1.9	1.3	0.9	0.3
3 (+1)	434.8	434.5	0.4	1.1	-0.6	0.1
5 (+2)	433.2	433.1	1.6	1.4	-0.4	-0.6
10 (+5)	429.0	426.8	4.2	6.3	-0.8	1.3
15 (+5)	422.7	423.0	6.3	3.8	1.3	-1.2
20 (+5)	416.1	417.2	6.6	5.8	1.6	0.8

After each height increment, the z-axis value is measured by the PrimeSense and Ensenso sensors are noted simultaneously before the next increment is made. This simultaneous measurement is made to ensure that both 3D devices are subject to similar lighting conditions.

6.4.1.4 Z-Axis Accuracy Measurement Result Analysis

Figure 6-24 shows the actual height versus measured height values. The average z-axis measurement error for PrimeSense in ambient and controlled lighting condition is 1.1 mm and 0.9 mm respectively.

Since the depth resolution of the PrimeSense is 1.0 mm, it means that it cannot obtain information less than 1 mm. The difference of 0.2 mm between ambient and controlled lighting is negligible and therefore it can be concluded that the PrimeSense depth (z-axis) measurement is not affected by external lighting conditions.

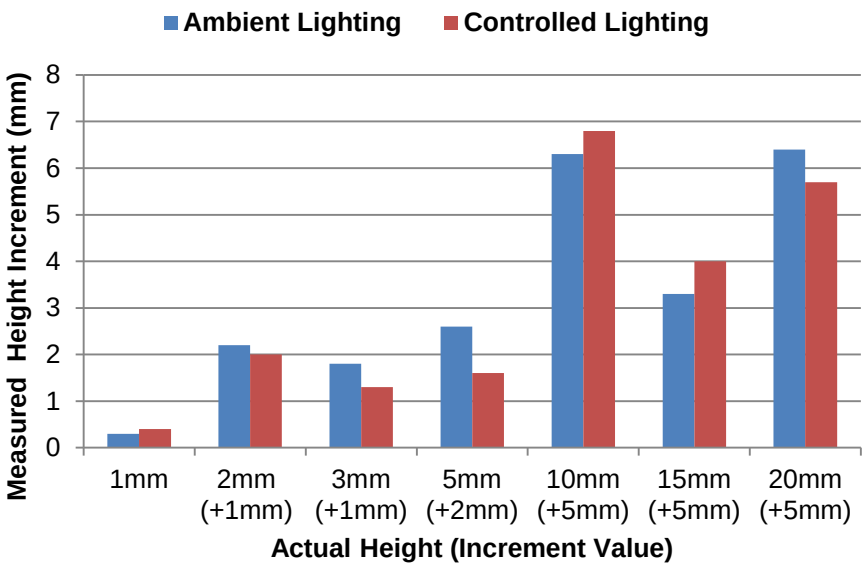

Figure 6-24 : Actual increment vs. measured increment - PrimeSense 3D

On the other hand, the average z-axis measurement errors for Ensenso in ambient and controlled lighting conditions are 0.9 mm and 0.7 mm respectively. Figure 6-25 provides the actual value versus measured valued of Ensenso. The 0.2 mm difference in the height measurement in controlled lighting condition is considered as a small improvement, because of its depth resolution i.e. 0.5 mm.

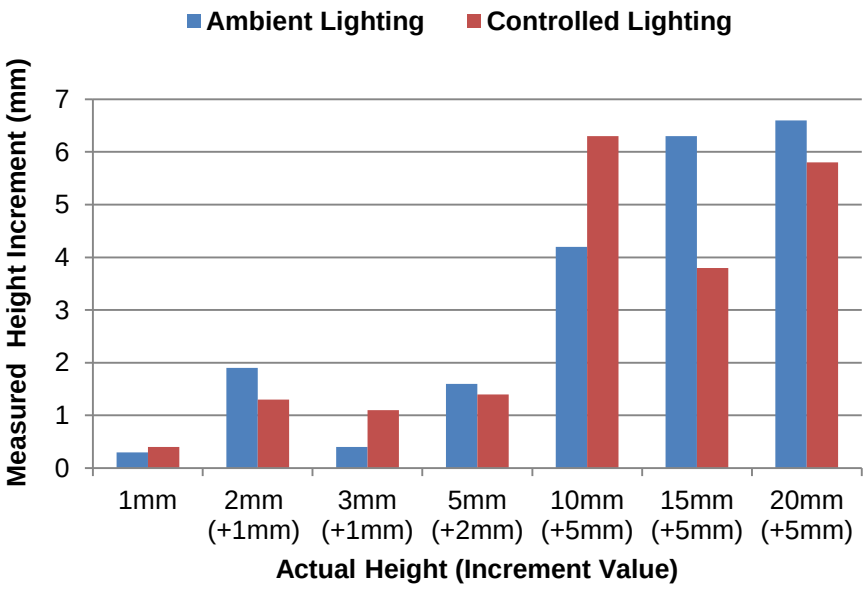

Figure 6-25 : Actual increment vs. measured increment – Ensenso 3D

The standard deviation of both PrimeSense and Ensenso in ambient and controlled lighting lies between 0.4 mm and 0.5 mm. This shows that the measurements made using these devices are not highly repeatable and an error correction cannot be applied.

6.4.2 Experiment with Small Object - Slip Gauge

This experiment was carried out to evaluate the 3D sensors, Micro-Epsilon and VC-Nano. It involves measuring the length and thickness of a slip gauge (small object) which is shown in Figure 6-20, and comparing it with its physical value, thereby calculating the accuracy and repeatability of the 3D sensors. It also involves z-axis measurement experiment to determine the depth accuracy of the sensors.

Figure 6-26 : Straight laser line reflection obtained through VC-Nano

The initial test carried out using the VC-Nano device showed a distorted point cloud data. The laser line projected from the scanner on a horizontal surface is observed using the camera image (the device can trigger the camera separately). The resulting line on the image sensor is curved as shown in Figure 6-26.

The PCD of the test plate obtained using VC-Nano sensor is shown in Figure 6-27. The PCD of the test plate is plotted in X-Z axis graph (Figure 6-27 (b)). It shows that the x-axis is curved and there are lot of noises on the PCD.

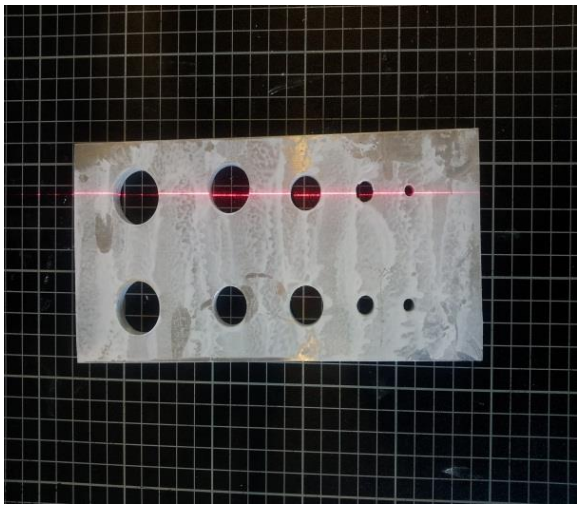

a) Test plate in flat surface

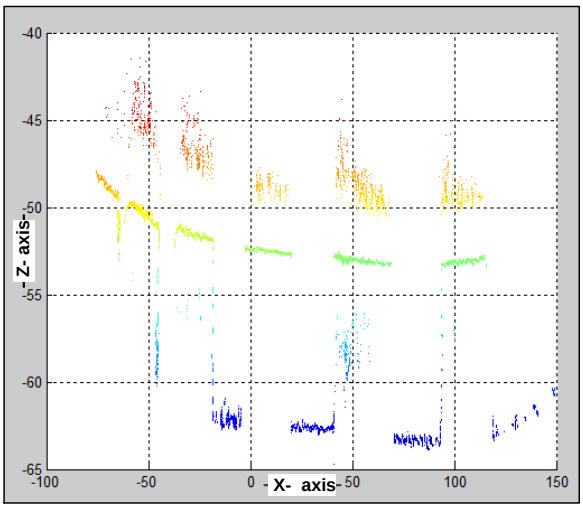

b) Test plate PCD plot

Figure 6-27 : VC-Nano initial test

It was concluded that the curvature of the reflected straight laser line is due to the lens distortion and it has not been corrected. The lens has to be factory calibrated for distortion by the manufacturer. The error is also attributed to the large laser line width which is 340 mm. The VC-Nano is not able to measure any object until the problems are sorted out.

A query has been made with the manufacturer and the response was very limited. Hence the evaluation of laser scanner technology on object measurement is carried on forward with Micro-Epsilon (The VC-Nano manufacturer has not solved the lens distortion problem which affects the measurement of objects).

6.4.2.1 Object Size Measurement

The slip gauge is a rectangular object with 20 mm breadth and 9 mm thickness. In this experiment the Micro-Epsilon 3D sensor is made to measure the breadth and the thickness of the slip gauge. Since the laser scanner measures only one spatial co-ordinate (x-axis), the slip gauge breadth and thickness are measured by scanning each side, one after the other.

The PCD of the slip gauge obtained from Micro-Epsilon is plotted using a program developed in C#. Then a boundary box is fitted to the PCD of the slip gauge for measuring the breadth and thickness. The slip gauge is presented to

the laser scanner two times, first showing the breadth side and then showing the thickness side, as the scanner measures only one spatial axis at a time.

a) Ambient Lighting Condition

The Micro-Epsilon was made to scan the slip gauge at two different views, one view showing the breadth side and other view showing the thickness side. The measurements of the slip gauge with a normal surface and a surface with white spray are made in ambient lighting conditions. The breadth and thickness was measured ten times and the measurement data were tabulated, as shown in Table 6-8.

Table 6-8 : Size measurements under ambient lighting condition – Micro-Epsilon

Trial No	Normal object		Object with white spray	
	Breadth (mm)	Thickness (mm)	Breadth (mm)	Thickness (mm)
1	20.22	9.19	20.07	9.15
2	20.26	9.26	20.15	9.07
3	20.19	9.15	20.12	9.16
4	20.21	9.14	20.04	9.11
5	20.08	9.17	20.11	9.03
6	20.25	9.10	20.13	9.12
7	20.18	9.22	20.08	9.05
8	20.17	9.16	20.06	9.10
9	20.13	9.17	20.14	9.09
10	20.24	9.22	20.16	9.13
Average	**20.19**	**9.18**	**20.11**	**9.10**

b) Controlled Lighting Condition

The Micro-Epsilon was also made to obtain the PCD of the slip gauge with a normal surface and a surface with white spray in controlled lighting condition. The measurement data of slip gauge (i.e. breadth and thickness) in controlled lighting conditions were obtained and tabulated, as shown in Table 6-9.

Table 6-9 : Size measurements under controlled lighting conditions – Micro-Epsilon

Trial No	Normal object		Object with white spray	
	Breadth (mm)	**Thickness (mm)**	**Breadth (mm)**	**Thickness (mm)**
1	20.21	9.11	20.03	9.09
2	20.11	9.21	20.05	9.09
3	20.23	9.07	20.09	9.12
4	20.19	9.18	20.08	9.10
5	20.22	9.22	20.04	9.09
6	20.14	9.19	20.08	9.09
7	20.14	9.19	20.09	9.06
8	20.12	9.13	20.08	9.06
9	20.23	9.11	20.08	9.07
10	20.20	9.15	20.12	9.15
Average	**20.18**	**9.16**	**20.07**	**9.09**

6.4.2.2 Object Size Measurement Result Analysis

Figure 6-28 shows the plot of average measurement value of the breadth and the thickness of the slip gauge. In ambient lighting conditions, the average error for measuring the breadth of the slip gauge with normal surface and surface with white spray is 0.19 mm and 0.11 mm respectively. The average error in measuring the thickness of the slip gauge with a normal surface and a surface with white spray is 0.18 mm and 0.1 mm respectively. These results show that the Micro-Epsilon is less affected by surface finish than Ensenso and PrimeSense. The surface with white spray has only improved the average error by 0.08 mm for both breadth and thickness. On the other hand, the size of the object (i.e. breadth 20 mm and thickness 9 mm) does not influence the average error, as the average error difference between the breadth and thickness is minimal (i.e. 0.01 mm).

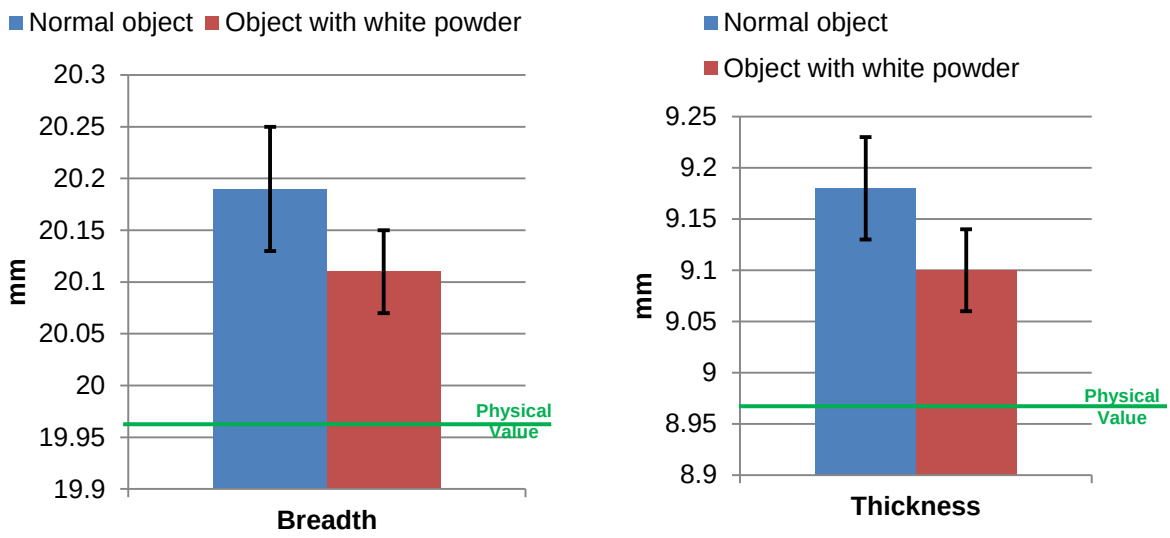

Figure 6-28 : Size measurement under ambient lighting

Figure 6-29 shows the average values of breadth and thickness measurement plot in controlled lighting. The average error in measuring the breadth of the slip gauge with a normal surface and a surface with white spray is 0.18 mm and 0.07 mm respectively. The average error in measuring the thickness of the slip gauge with normal surface and surface with white spray is 0.16 mm and 0.09 mm respectively.

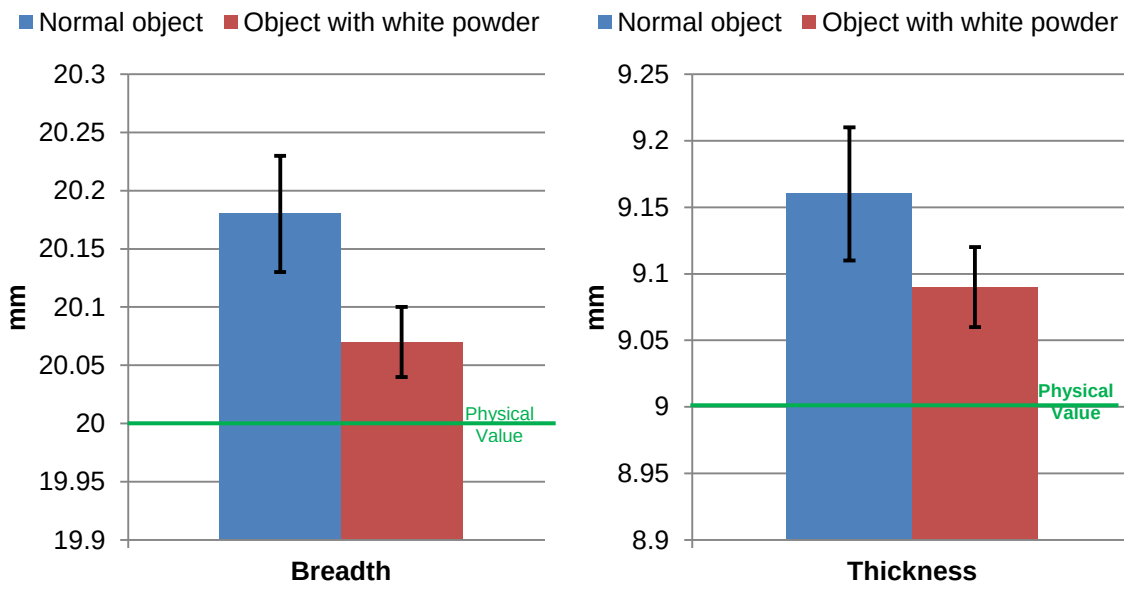

Figure 6-29 : Size measurement under controlled lighting

These results show that the Micro-Epsilon was not affected by external lighting conditions as the average error difference between two lighting conditions is minimal (i.e. less than 0.03 mm). In addition, the surface finish also has a less influence on the average error obtained while measuring the size. The average error difference for different surface finish is only 0.07 mm.

6.4.2.3 Z-Axis Accuracy Measurement

The z-axis accuracy of Micro-Epsilon was obtained through the height increment experiment. It involves measuring a known height increment made by the depth micrometre which is capable of increasing the height by 2.54 µm.

This experiment was carried out in two different lighting conditions i.e. ambient and controlled lighting. The known height increments made includes 0.025 mm, 0.05 mm, 0.4 mm, 0.5 mm, 1 mm and 3 mm. The actual height values are 0.025 mm, 0.05 mm, 0.1 mm, 0.5 mm, 1 mm, 2 mm and 5 mm.

a) Ambient Lighting Condition

The initial height value obtained from Micro-Epsilon was 76.149 mm from the micrometre centre point. The measured height values for each increment were tabulated, as shown in Table 6-10.

Table 6-10 : Z-axis increment measurement in ambient lighting condition

Actual height (Increment value) (mm)	Z-axis height value from PCD (mm)	Measured increment value (mm)	Increment error (difference) (mm)
0.025	76.123	0.030	0.005
0.05 (+0.025)	76.091	0.032	0.007
0.1 (+0.05)	76.061	0.030	-0.020
0.5 (+0.4)	75.635	0.426	0.026
1 (+0.5)	75.163	0.472	-0.028
2 (+1)	74.126	1.037	0.037
5 (+3)	71.086	3.040	0.040

b) Controlled Lighting Condition

The initial height value of the micrometre centre point measured from Micro-Epsilon was 76.401 mm. Table 6-11, shows the measured height increment values under controlled lighting condition.

Table 6-11 : Z-axis increment measurement in controlled lighting condition

Actual height (Increment value) (mm)	Z-axis height value from PCD (mm)	Measured increment value (mm)	Increment error (difference) (mm)
0.025	76.365	0.036	0.011
0.05 (+0.025)	76.335	0.030	0.005
0.1 (+0.05)	76.310	0.025	-0.025
0.5 (+0.4)	75.901	0.409	0.009
1 (+0.5)	75.386	0.515	0.015
2 (+1)	74.369	1.017	0.017
5 (+3)	71.301	3.068	0.068

6.4.2.4 Z-Axis Accuracy Measurement Result Analysis

Figure 6-30 shows the plot between the actual height increment and the measured height increment values. The average error in the measured height increment in ambient and controlled lighting condition is 0.023 mm and 0.022 mm respectively. This result shows that the height measurements are not affected by the lighting conditions as the error difference between two lighting condition is minimal.

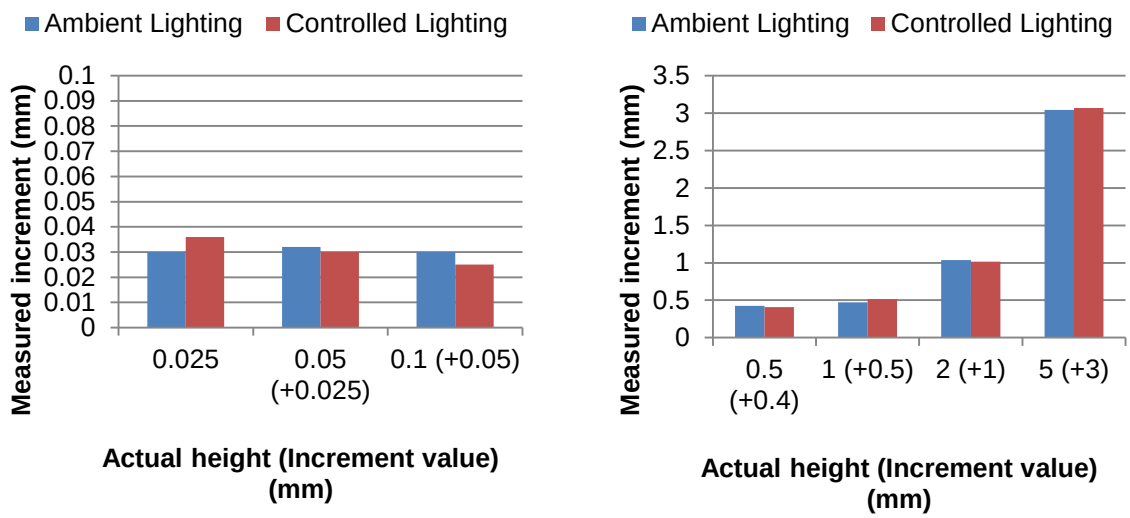

Figure 6-30 : Z-axis accuracy measurement results

The standard deviation of the height increment is less than 0.020 mm for both conditions. The depth resolution of Micro-Epsilon is 0.020 mm and the height measurement results indicate that the 3D sensor is more accurate.

6.5 3D Positional Device Selection

The evaluation of 3D sensors was performed to select the suitable 3D sensor for the fastener assembly application. The fastener assembly requires a sensor that is accurate to differentiate fastening holes of 1.0 mm difference. The sensor is also required to find the location of an object accurately to avoid misalignment and cross threading.

Table 6-12, provides an overview of the comparison made on the 3D imaging sensors, based on the evaluation conducted in different conditions. The spatial accuracy of both PrimeSense and Ensenso in best case condition is 0.9 mm. Hence, these sensors will have a serious limitation in determining the holes with 1.0 mm difference and also affects the accuracy of the 3D location of the objects.

Despite the large error margin, the PrimeSense is affected by lighting condition to only a minimal effect. In addition, the surface smoothness and reflectivity affects the accuracy to only to a minimal level and the PrimeSense has same error margin for different size objects (i.e. large and small size) within its FOV.

Table 6-12 : 3D imaging sensor comparison

Device	Measurement accuracy (mm)				Affected by		Object size
	Spatial axis		Z-axis		Lighting condition	Surface finish	
	Best	Worst	Best	Worst			
PrimeSense	0.9	1.3	0.9	1.1	Minimal	Minimal	No
Ensenso	0.9	4.9	0.7	0.9	Minimal	Yes	Yes
Micro-Epsilon	0.070	0.190	0.022	0.023	Minimal	Minimal	No

The Ensenso spatial accuracy is also affected by lighting condition to a minimal effect. But the Ensenso is greatly affected by the surface smoothness, reflectivity and also to the size of the object. The larger objects have better accuracy then the smaller objects within its FOV. However, the test results indicate that Ensenso has better z-axis accuracy when compared to PrimeSense. The major advantage of Ensenso over PrimeSense is the PCD

quality and density which can be seen from the depth map comparison made in section 6.3.

In contrast, the Micro-Epsilon has both a better spatial accuracy and depth accuracy (z-axis), which meets the fastener assembly requirements. The lighting condition and the surface smoothness affect the Micro-Epsilon measurement accuracy only to a minimal effect, which makes it suitable for industrial applications. It is also not affected by the object size within its FOV, as the accuracy remains almost same. But one major disadvantage of Micro-Epsilon over other two 3D sensors is the FOV. The FOV in the spatial plane for Micro-Epsilon is 25 mm, compared to 1.4 metres for PrimeSense and 2 metres for Ensenso. This may require a manipulator to enable additional scanning action to cover large surface of an object or work area.

The 3D sensors evaluated as a part of this research have a trade-off between accuracy and the field of view (FOV). Thus, 3D sensor selection completely depends upon the type of application. The fastener assembly planned for this research requires a 3D sensor which is accurate and also has acceptable FOV. Hence the Micro-Epsilon laser scanner is considered the most suitable 3D imaging sensor for the fastener assembly. It has the accuracy required for the fastener assembly but with limited FOV which is the trade-off made for this application.

6.6 Summary

As a result of the evaluation of 3D technologies and sensors carried out, it was found that the Micro-Epsilon laser scanner was more suitable to perform the fastener assembly in a non-structured environment. It was also found that the laser scanners have high accuracy and minimal effect to external lighting and surface speculation making it suitable for industrial applications. The next step in this research is to use this laser scanner to identify fasteners located in clutter, thereby assisting the robot to pick up and fasten the bolt into their corresponding size threaded holes located at random 3D workspace. The 3D fastener assembly is explained in the following chapter.

CHAPTER 7 - THREE-DIMENSIONAL (3D) FASTENER ASSEMBLY

Assembling fasteners in a 2D workspace is discussed in CHAPTER 5 - with an assumption that the threaded holes and bolts are placed in a single plane perpendicular to the 2D camera. But in most industrial scenarios the bolts and the fastening holes could be located in a random 3D workspace. For example, the bolts may be placed in clutter form in bins and the target component with threaded holes on multiple planes located at random positions and orientation. To identify and localise these objects requires a 3D imaging sensor capable of providing accurate information of the objects located in the work area. The Micro-Epsilon laser scanner was found to be the suitable 3D sensor after an extensive evaluation of three different imaging sensors, as explained in section 6.5 (see appendix A5 for specifications). This chapter describes the automated 3D assembly method, the algorithms developed to identify bolts located at random position in clutter and the threaded holes at random locations in 3D. It also explains the experiment results of the assembly carried out in a non-structured environment. In addition to that, the evaluation results of the developed 3D object and feature identification algorithms were also discussed in this chapter.

7.1 Assembly scenario

The experiment scenario proposed for 3D fastener assembly involves assembling different size bolts into their corresponding size threaded holes in a robot workspace where the location of bolts and threaded holes are not known. The bolts of different sizes in clutter form are then placed at a random location within a defined workspace as shown in Figure 7-1. The challenge in this case is to identify and segment the bolts based on their size and also to determine its location in 3D space for picking up. The target fastening component has different size threaded holes located at different angled surfaces (Figure 7-2). Each threaded hole is chamfered and the internal threaded section of the hole is visible during imaging if the viewing angle is not perpendicular. These

additional sharp features greatly affect the edge detection and segmentation process for the existing feature detection algorithms, making threaded hole detection difficult. This assembly scenario represents an environment which is not structured completely for automated assembly and this is the case in many industrial applications.

The research aim is to carry out bolt assembly in this kind of non-structured environment robustly and accurately with a minimal need for prior information, without fixtures and also without any major modification to the assembly system.

Figure 7-1 : Bolts in clutter

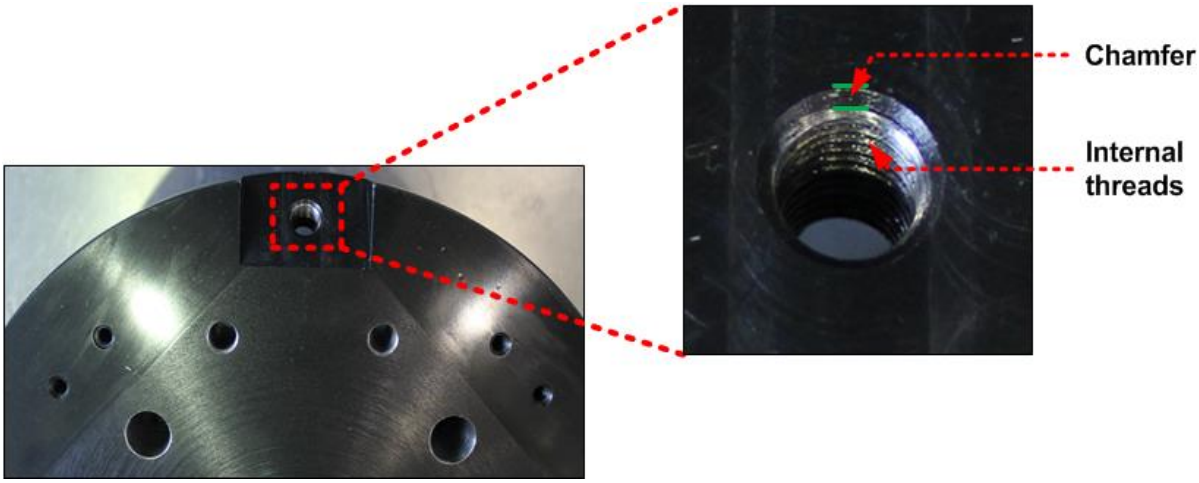

Figure 7-2 : Hole on angled surface with chamfer and internal threads

Since there are many complex technical challenges involved in this scenario, it was further divided into two stages based on the complexity of the process involved. The first stage, as illustrated by Figure 7-3, is to identify bolts placed

on a cradle by detecting its head size and fasten them into the threaded hole located on the surface of the fastening plate in single plane (Figure 7-3 (c)). This is same as the 2D fastener assembly, but the height of the surface containing bolts and fastening plate can be varied, making it a 3D challenge. Some of the real industrial scenarios will be similar to the initial experiment, as the bolts are kept in semi-arranged condition.

On the other hand, the second stage as shown in Figure 7-4 focuses on the increasing complexity of the fastener assembly. In this stage, the bolts are placed in clutter form at a random location (Figure 7-4 (a)) and the fastening plate is mounted on a tilting table which can be pitched at different angles, as represented in Figure 7-4 (b). The increased complexity of this stage is introduced to push the technology further and also to add more flexibility to the fastening system.

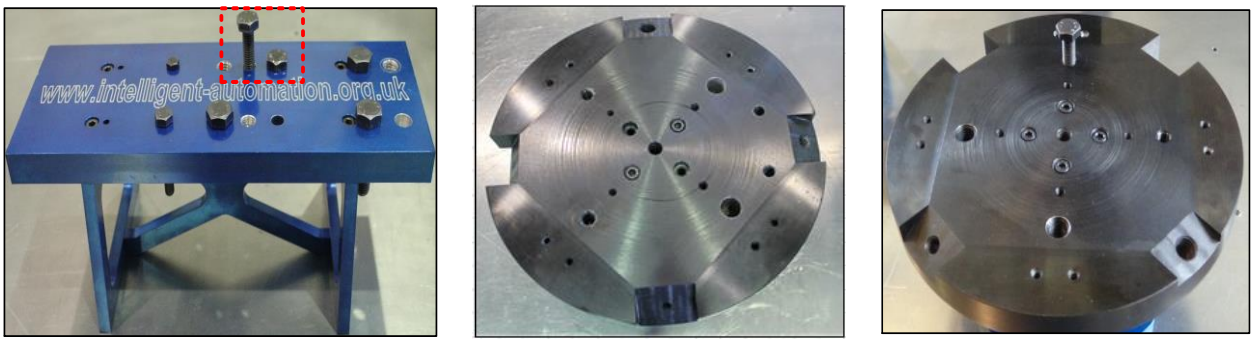

a) Bolts in cradle **b) Fastening plate** **c) Bolt fastened to hole in flat surface**

Figure 7-3 : Scenario first stage - less complex assembly

The second stage represents a non-structured environment where the assembly process is carried out without the positional information of the bolts and the fastening plate.

a) Bolts in clutter

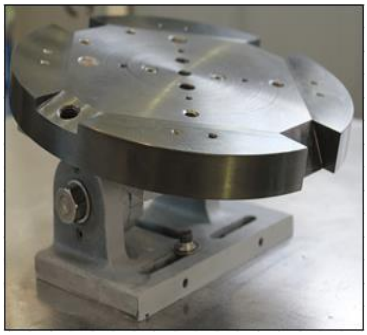

b) Plate mounted on tilt table

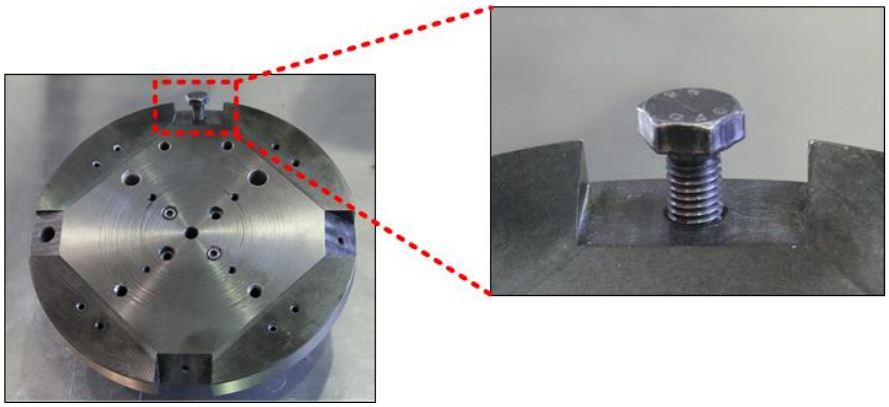

c) Bolt fastened to angled surface

Figure 7-4 : Scenario second stage – non-structured assembly

7.2 System setup for 3D fastener assembly

The test rig setup for 3D fastener assembly is almost the same as the test rig used for 2D fastener assembly, with the 2D camera being replaced by a 3D imaging sensor. Figure 7-5 shows the system setup developed for 3D automated freeform fastener assembly.

The Micro-Epsilon scanControl 2900-50 laser profile scanner was selected as the 3D imaging sensor and a Schunk PGN Plus 80 two finger gripper with pneumatic actuation was selected as the end-effector for robot arm 1 (R1). The fingers for the gripper are designed to grasp the cylindrical bolt as explained in section 4.1.2. The fixed support used for the fastening plate is replaced by a tilting table, so that the fastening plate can be placed at a random 3D position and orientation.

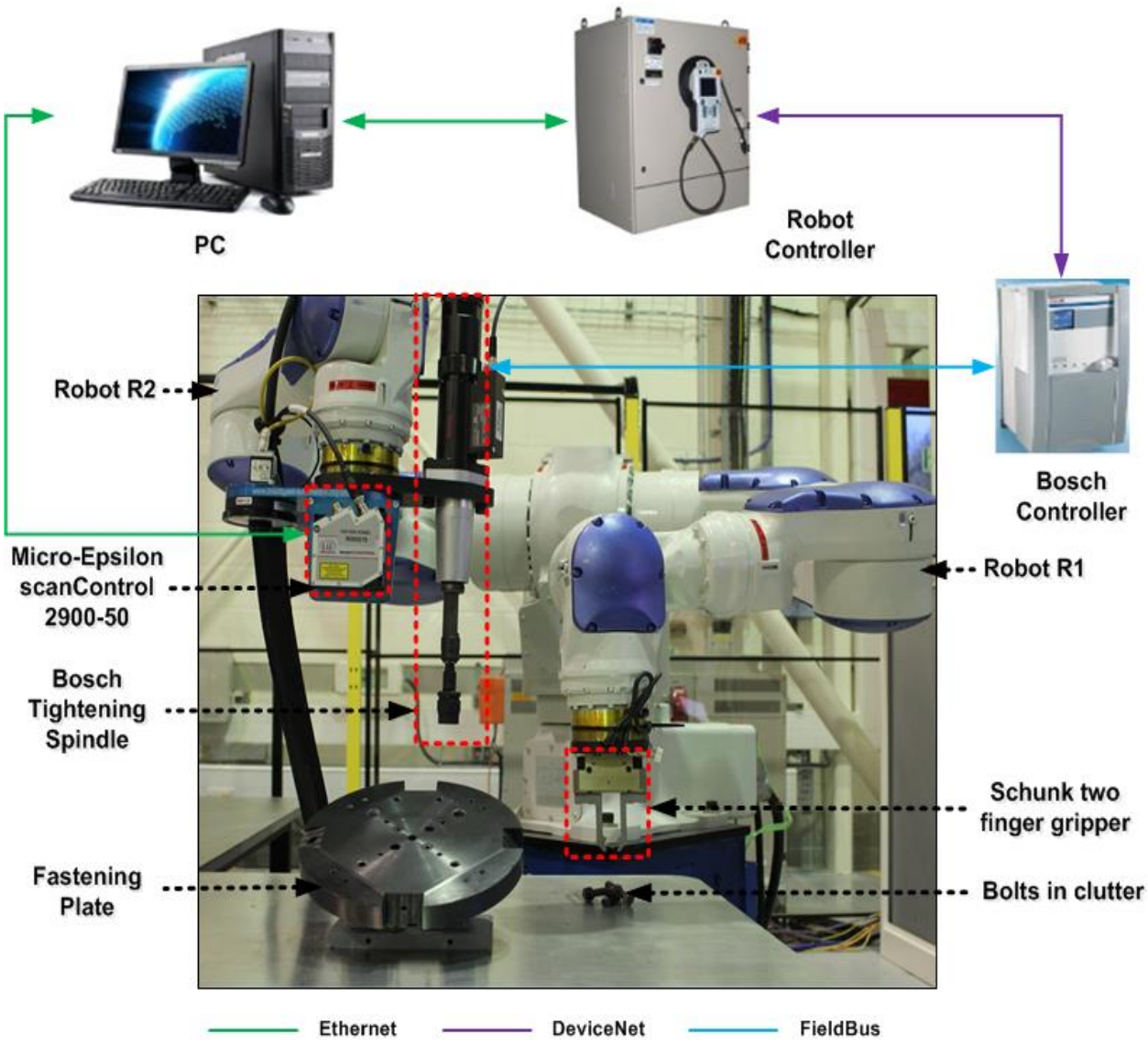

Figure 7-5 : Test rig developed for 3D fastener assembly

7.3 Assembly process

The automated freeform assembly method obtains the 3D data of the work area, identifies the objects and its location and then carries out the torque-controlled fastening. Figure 7-6 illustrates the process flow involved in assembling fasteners.

The master control PC initiates the connection with the robot and laser scanner - to establish a communication link. After initiating the communication, the PC commands the robot arm R2 (shown in Figure 7-5) to move to the fastening plate area for scanning.

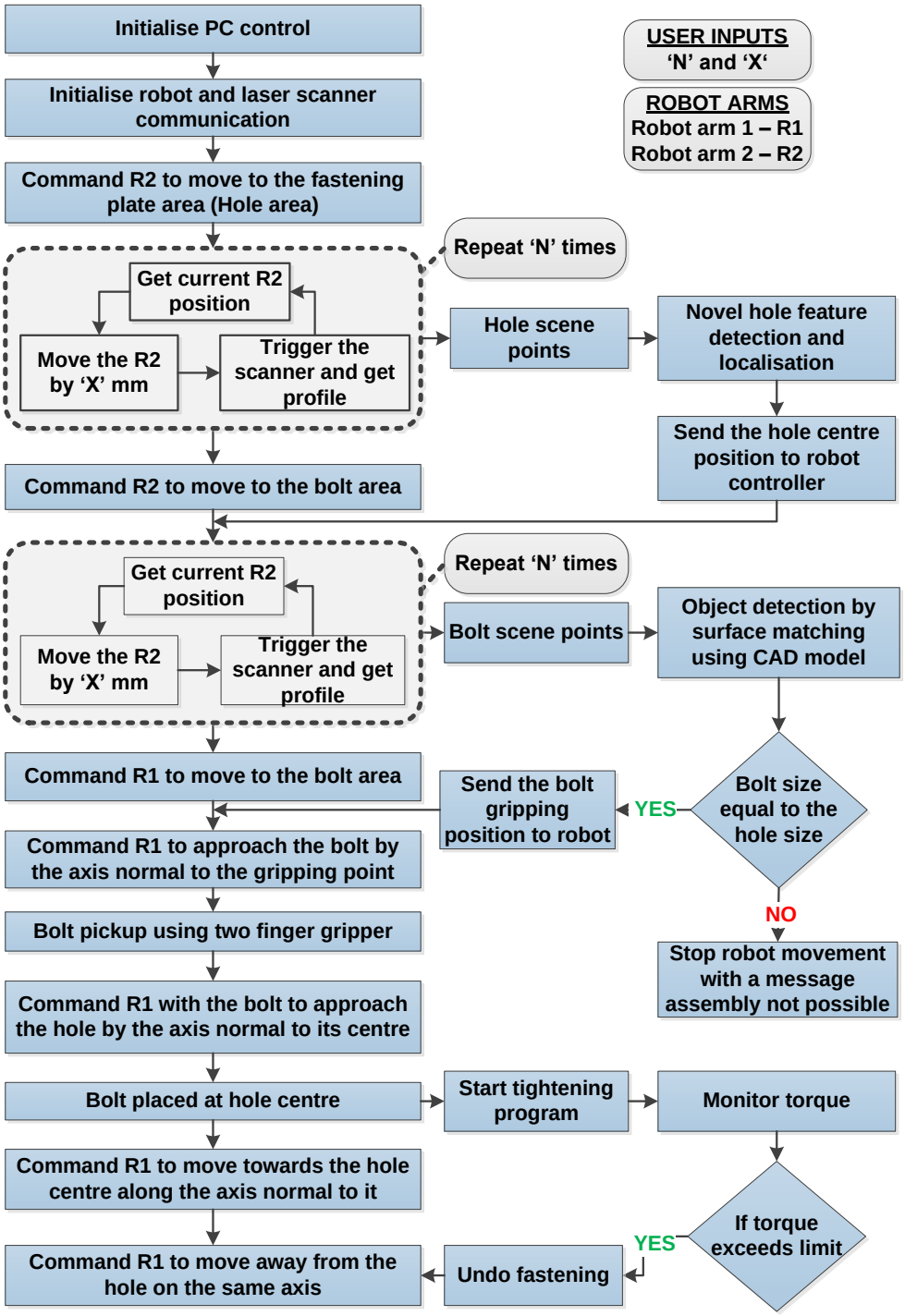

Tightening programs are explained in appendix B1

Figure 7-6 : Automated assembly step by step process

The output data obtained in the form of PCD (point cloud data) after scanning (as explained in section 7.3.1) is converted into a 3D object model referred as the 'hole scene points'. After creating the 3D object model, the robot arm R2 is moved to the region where the bolt is located for scanning. In parallel, the PC executes a novel hole feature detection algorithm developed as a part of this

research, to detect the threaded holes, its size and its pose in 3D, as described in section 7.4.1.

The hole pose obtained is sent to the robot controller and saved in a position variable to be used during the final part of the assembly process. After the robot arm R2 reaches the bolt area scanning location, the area is then scanned to obtain PCD information, referred as the ‘bolt scene points’. The bolt located in the region is then identified from the bolt scene using the surface matching technique explained in section 2.1.6).If the bolt size matches the hole size, the bolt gripping position is sent to the robot controller. The robot arm R1 is guided to approach the bolt in an axis perpendicular to the gripping point, as indicated in Figure 7-7 (a). The bolt is then picked up using the two finger gripper mounted on the arm R1. Since the robot arm cannot be rotated more than 360° and can only provide a maximum torque of 30 Nm, the bolt cannot be fastened using the robot arm. Thus, the bolt in the robot arm R1 is transferred to the tightening spindle with a magnetic socket mounted on the arm R2 as shown in Figure 7-7 (b). The arm R2 - with the bolt - is then moved to the hole location in an axis perpendicular to the hole plane as highlighted in Figure 7-8 (a).

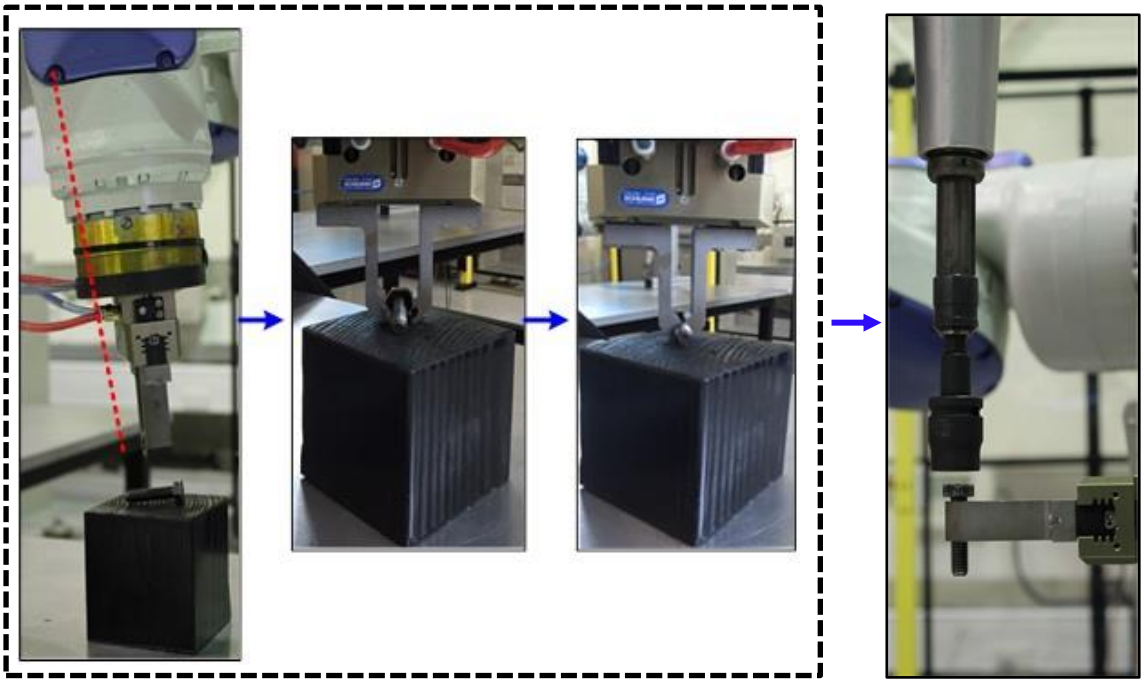

a) Bolt pick up

b) Bolt exchange

Figure 7-7 : Bolt manipulation

At this point, a predefined program in the tightening tool is activated to turn the spindle clockwise for fastening. Simultaneously, the robot arm R2 is also moved towards the hole on the perpendicular axis with a speed relative to the pitch and the rotation of the bolt to perform successful assembly (Figure 7-8(b)). Different tightening programs are stored in the Bosch controller for a range of bolt sizes that will control the parameters such as torque, speed, time and direction of rotation. This applied torque for fastening process is continuously monitored using a built-in torque sensor on the Bosch spindle (tightening programs are explained in B1).

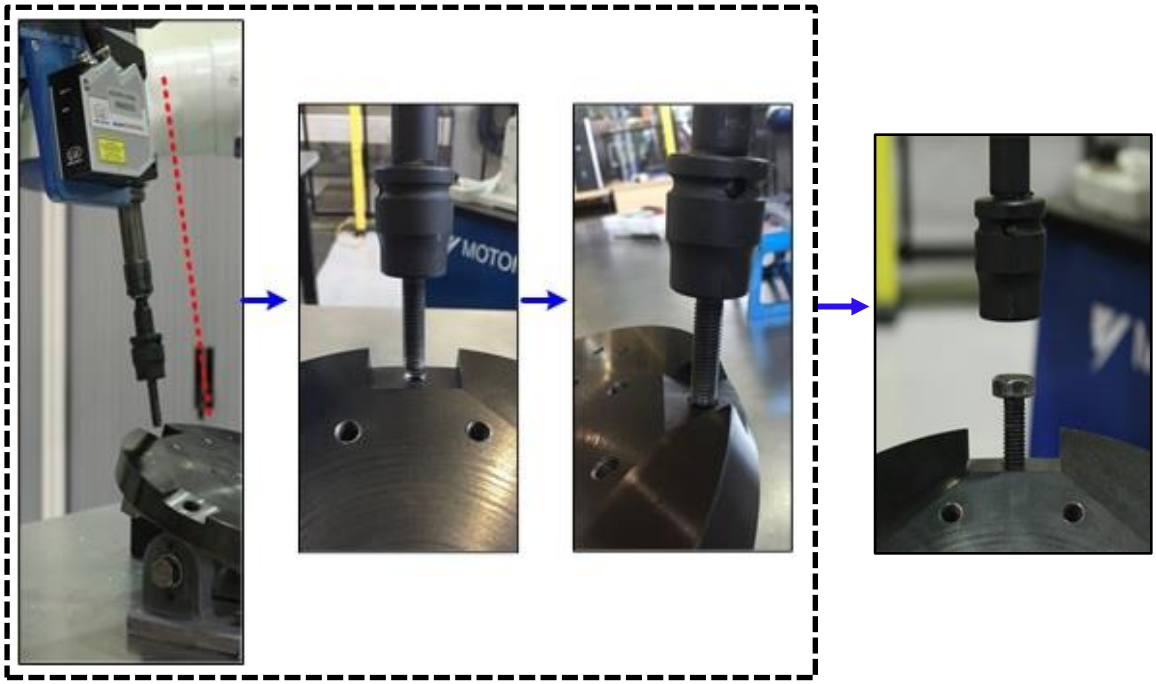

a) Bolt insertion into hole

b) Successful assembly

Figure 7-8 : Bolt assembly

If the torque exceeds the limit set for this operation, the process is terminated and the bolt is removed from the hole by reversing the process to prevent cross threading. The torque limit has been linked to the axial position of the bolt to distinguish cross threading from the final tightening process.

7.3.1 Scanning process and PCD Interpretation

The scanning process is performed to obtain a 3D representation of objects located within the work area. It can be performed either by moving an object

within the field of view of a stationary scanner or by moving the scanner over a stationary object. In this research, the scanner is mounted on the robot in order to achieve more flexibility to scan any region within the robot workspace. The scanner mounted on the robot is swept across the region where the bolts and the fastening plate are located as indicated in Figure 7-9. For every defined movement of the robot, the scanner is triggered to obtain a profile of that region. The total distance required for covering the work area and the distance between each trigger dictates the number of times the scanner has to be triggered (i.e. number of profiles). The scanning process is a continuous cycle in which the scanner is triggered after every defined distance moved by the robot. Each step in a scanning cycle involves moving the robot by a defined distance of 0.5 mm and triggering the scanner. The distance between each trigger and the number of times the scanner has to be triggered are defined by the user.

a) Section of fastening plate **b) Bolt in flat surface**

Figure 7-9 : Scanning regions

Since the minimum difference between threaded hole and bolt sizes varies in the range of 1 mm, the scanner has to capture information of the work area containing bolts and holes with a small triggering distance (i.e. less than 1 mm). A small triggering distance provides a large number of data points, thereby increasing the computation time for processing. At the same time, a triggering distance close to 1 mm results in losing the information necessary to differentiate between the size of bolts and holes. This resulted in selecting a

triggering distance of 0.5 mm which provides a balance between resolution and number of points (i.e. for reducing the computation time).

For every scanner trigger, points representing a single laser line profile on the scanning region are obtained as output. These points represent the depth information ('*z*' value) for every '*x*' value on the laser line profile. The direction of scanning is the y-axis direction and the line profile number is the '*y'* value. The PCD of all the profiles representing the object or the work area is stored in a 3D array format as shown in Table 7-1. An example of a laser line projected on a cylindrical surface and the PCD acquired from the laser scanner are explained in appendix C1.

Table 7-1 : Point Cloud Data (PCD) representation

Profile No	***X* Value**	***Y* Value (Profile No)**	***Z* Value**
0	x_0	y_0	z_0
1	x_1	y_1	z_1
. . .	. . .	. . .	. . .
n	x_n	y_n	z_n

n – number of profile scans

7.4 Object and feature identification in 3D

The two major challenges involved in this research include identifying bolts located in clutter and threaded hole features with chamfer on the target component located in random 3D space. The bolts can be different sizes and may lay one above the other. On the other hand, the target component with threaded holes may have chamfered edges which overshadow the inner edge of the hole as highlighted in the assembly scenario (section 7.1). This section describes the novel algorithm developed using HALCON image processing libraries [98], for identifying a hole feature on the fastening plate and also the enhanced object detection technique for identifying bolts located in clutter.

7.4.1 Hole Identification Algorithm - Novel feature detection technique

An algorithm was developed for hole feature detection in 3D PCD and also used to obtain the geometry of the hole and its location in a random 3D environment, as described in Figure 7-10.

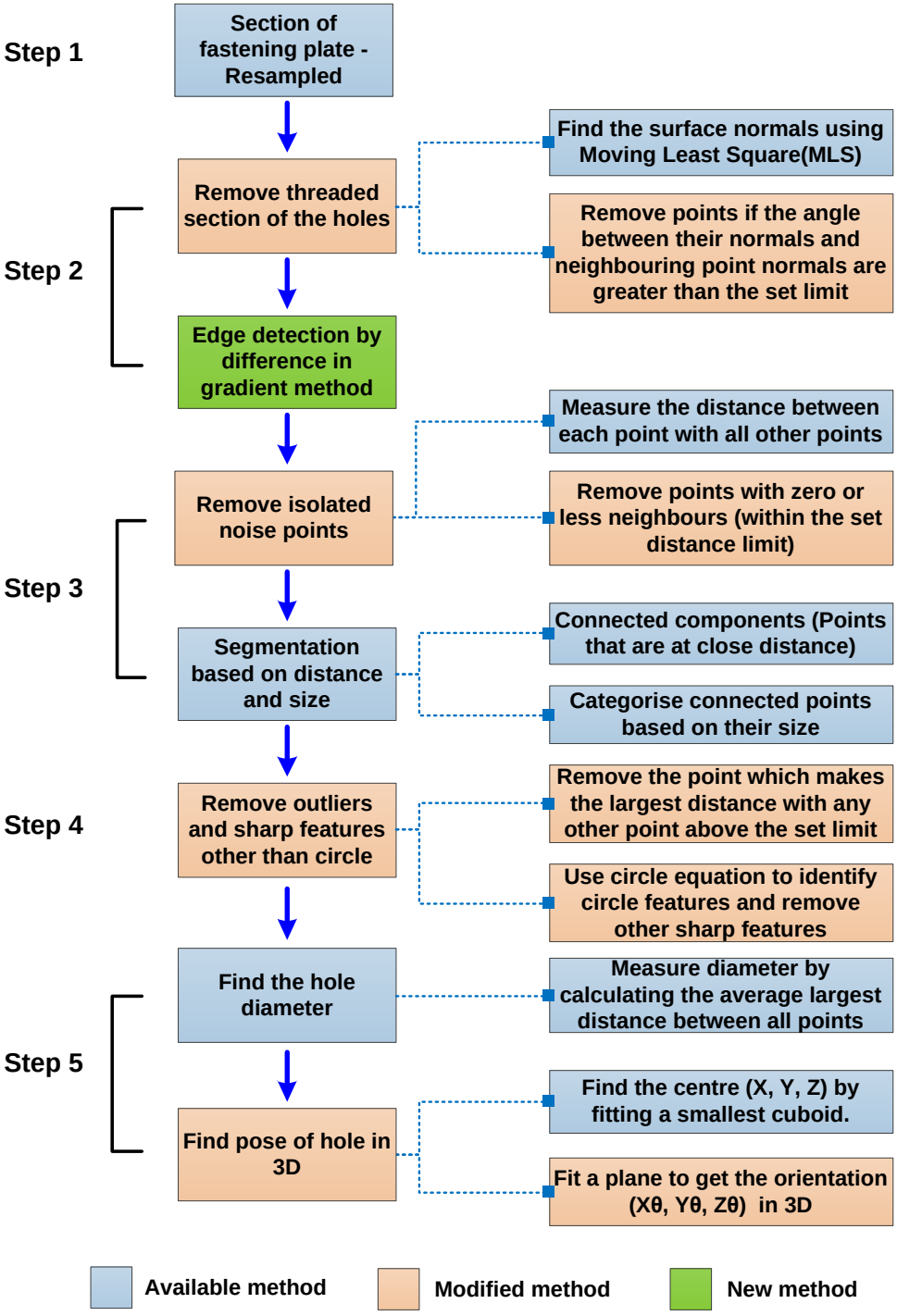

Figure 7-10 : Process involved in hole feature detection (3D)

Following a surface scan of a section of the fastening plate, the output - in the form of the point cloud data (PCD) - is stored as a 3D model referred to as the ‘hole scene’. The resulting data contains the hole with a chamfer and an internal thread section on the component located at random position and orientation. The first step is to resample the input hole scene to make the points equidistant for further processing (appendix C2 (a)). The second step in the process is to remove the points that represent the threaded section of the hole. This is to eliminate the negative impact of these points on the edge feature identification process. It is carried out by finding a surface normal (perpendicular axis to the surface of object) of all the points using the moving least square method (appendix C2(b)). After finding the surface normal of the points, it is then required to find a difference in angle between each surface normal of the points and its local neighbours. The angle differences of points which exceed the set limit are considered to be a threaded section and can be removed.

The second step also involves identifying the points that represent sharp edge features in the hole scene using the proposed feature identification algorithm (section 7.4.1.1). The resulting edge points may represent any sharp features such as outer and inner edge points of the hole, planar edge points and noise points (i.e. unwanted points or discrepancies) present in the hole scene. The noise points in the data affect the classification of the edge features. Thus the third step is to remove isolated noise which is not near the edge features by identifying a point or small group of points which have fewer neighbours within the set distance limit (i.e. 1 mm in this case), as explained in appendix C2 (c). This limit depends upon the scanning distance (i.e. 0.5 mm in this case). After removing the isolated noise points, the remaining points are grouped into connected regions if the points are at close distance. This segmented group of points are helpful in categorising the features based on their size.

The fourth step is to check for outliers in the segmented edge features by identifying the points that have a larger distance than the average maximum distance between the points in the group. After removing outliers, the features which satisfy the circle equation are considered a hole edge (provided in

appendix C2 (d)). The point cloud processing involved in determining the hole feature is explained in Figure 7-11.

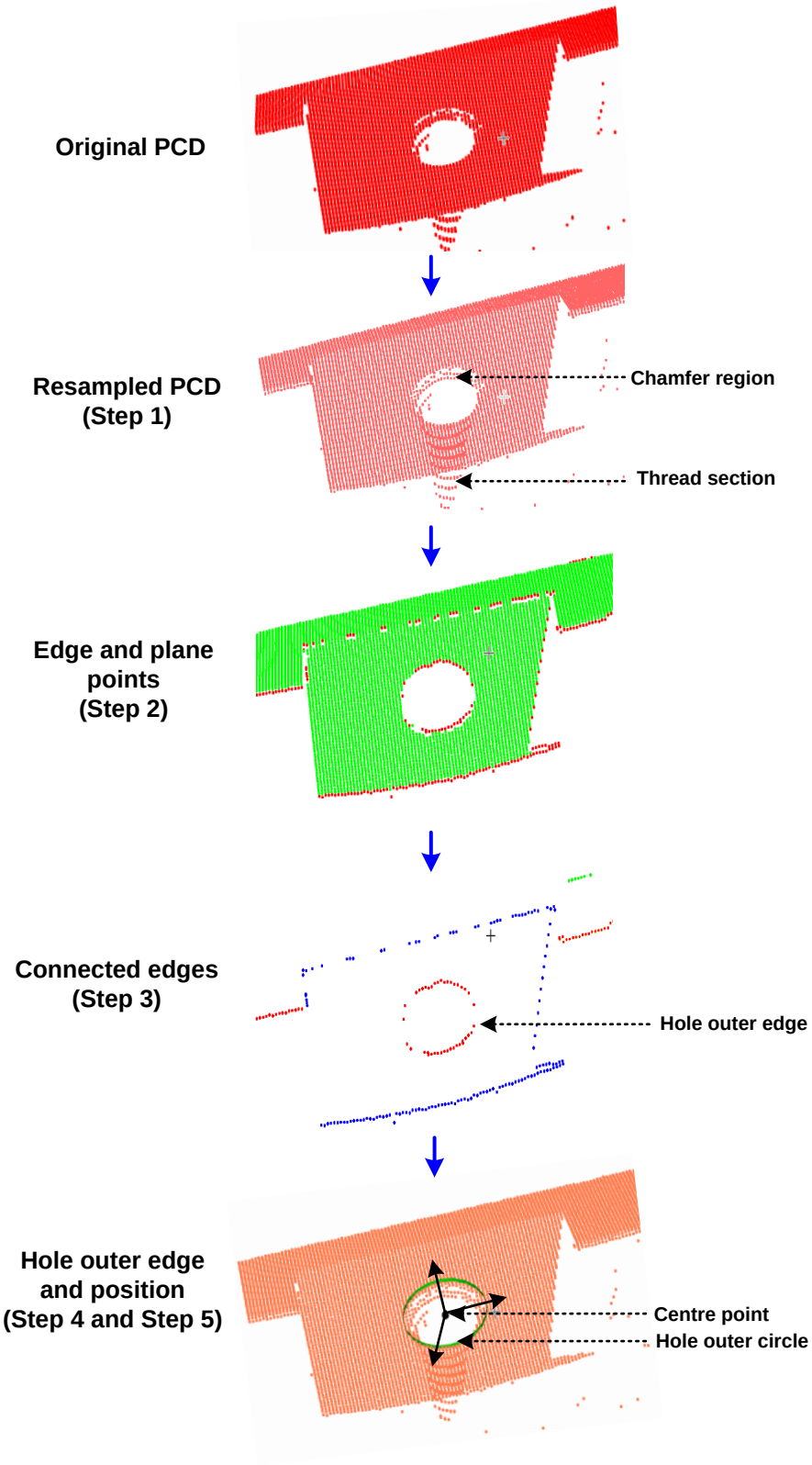

Figure 7-11 : Step by step process involved in hole feature detection

The resulting circular edge features represent the total number of holes present in the hole scene. The fifth and final step is to obtain the diameter and pose of the hole in 3D. The diameter of each circle feature is calculated by taking the average of the largest distance between each point with all other points of the feature. The centre point (*x*, *y* and *z*) of each circle feature in 3D can be obtained by fitting a smallest cuboid possible and calculating its centre point. To determine the orientation in 3D, a plane is fitted to the points and the orientation along all three axes (θ_x, θ_y and θ_z) is obtained. The centre point and the orientation along all three axes together constitutes the final pose of the hole feature.

7.4.1.1 Edge detection by difference in gradient method

Edge detection is a process by which sharp features are identified in a point cloud data. This method involves finding gradient differences between three consecutive points in the point cloud. If the difference is greater than a set threshold, the points are then subject to a series of conditions to be considered as an edge point. The threshold is set based on some prior knowledge of the surface roughness of the target component. The conditions used are developed based on the different arrangements of points in the 3D scene representing a sharp change in gradient. It also considers the relation with immediate neighbouring points to avoid false edge points caused due noise spikes in point cloud.

The selection of points for processing is traversed along any axis to cover the entire point cloud data. The algorithm eliminates most of the plane points at the initial gradient difference stage and only the points which have greater difference are subject to the remaining conditions to be considered as an edge. Selecting the key points for determining the edge makes this algorithm significantly faster and highly accurate.

The gradient difference between any three consecutive points is given by the equation 1,

$$\boldsymbol{Gradient\ Differnce} = |\boldsymbol{\nabla}_{i,i+1} - \boldsymbol{\nabla}_{i+1,i+2}| \quad \textbf{(1)}$$

where,

$$\nabla_{i,i+1} = \frac{dz_{i,i+1}}{dx_{i,i+1}} = \frac{z(i) - z(i+1)}{x(i) - x(i+1)}$$

$$\nabla_{i+1,i+2} = \frac{dz_{i+1,i+2}}{dx_{i+1,i+2}} = \frac{z(i+1) - z(i+2)}{x(i+1) - x(i+2)}$$

Where '∇' denotes gradient, '*dz*' denotes difference in *'z'* points and '*i* 'denotes index of a point

If the gradient difference between three points is greater than the set threshold as given in the equation 2, then the points are subject to a series of conditions (equation 3 - 5). If a point satisfies any one of the conditions illustrated below, then the point is a potential edge point.

$$Gradient\ Difference > threshold \qquad (2)$$

$$dz_{i,i+1} < 0 \qquad (3)$$

$$z(i) \neq 0 \rightarrow \begin{cases} z(i+2) \neq 0 \rightarrow \{z(i-1)\ and\ z(i+3) \neq 0 \rightarrow \{|\nabla_{i-1,i} - \nabla_{i+2,i+3}| > threshold \\ z(i+2) = 0 \rightarrow \begin{cases} z(i+3)\ and\ z(i+4) = 0 \\ z(i+3) - z(i+4) > 0 \rightarrow \{|\nabla_{i,i+1} - \nabla_{i+1,i+3}| > threshold \\ z(i+3) - z(i+4) < 0 \rightarrow \begin{cases} z(i+3) \neq 0 \rightarrow \{|\nabla_{i,i+3} - \nabla_{i+3,i+4}| > threshold \\ z(i+3) = 0 \rightarrow \{|\nabla_{i,i+1} - \nabla_{i+1,i+4}| > threshold \end{cases} \end{cases} \end{cases}$$

$$z(i) = 0 \rightarrow \begin{cases} z(i-2) - z(i-1) = 0 \\ z(i-1) \neq 0 \rightarrow \begin{cases} z(i+2) \neq 0 \rightarrow \{|\nabla_{i-1,i+1} - \nabla_{i+1,i+2}| > threshold \\ z(i+2) = 0 \rightarrow \begin{cases} z(i+3) \neq 0 \rightarrow \{|\nabla_{i-1,i+1} - \nabla_{i+1,i+3}| > threshold \\ z(i+3) = 0 \rightarrow z(i+4) \neq 0 \rightarrow \{|\nabla_{i-1,i+1} - \nabla_{i+1,i+4}| > threshold \end{cases} \end{cases} \end{cases}$$

$$dz_{i,i+1} = 0 \qquad (4)$$

$$z(i-1) \neq 0 \rightarrow \begin{cases} z(i+2) - z(i+3) < 0 \rightarrow \{|\nabla_{i-1,i+2} - \nabla_{i+2,i+3}| > threshold \\ z(i+2) - z(i+3) > 0 \rightarrow \{z(i+3)\ and\ z(i+4) \neq 0 \rightarrow \{|\nabla_{i-1,i+2} - \nabla_{i+2,i+4}| > threshold \end{cases}$$

$$z(i-1) = 0 \rightarrow \begin{cases} z(i+2) - z(i+3) < 0 \\ z(i+3 - z(i-4) \neq 0 \rightarrow \{z(i+2) - z(i+4) < 0 \\ z(i+3) - z(i+4) = 0 \rightarrow \{i = i+2 \end{cases}$$

$$dz_{i,i+1} > 0 \qquad (5)$$

$$z(i+2) \neq 0 \rightarrow \{z(i+1) \neq 0$$

$$z(i+2) = 0 \rightarrow \{z(i+1), z(i+3)\ and\ z(i+4) = 0$$

7.4.2 Bolt Identification Algorithm

In this assembly scenario, the bolts are considered to be located in clutter form at random location within the work area. To identify and localise bolts in clutter, an enhanced CAD based surface matching technique is implemented. The bolt detection process includes a pre-processing step which is to provide prior knowledge to the system and a post-processing step for detecting bolts from the work area.

7.4.2.1 Pre-processing - Preparing reference surface model

Since the bolts are in clutter, they are prone to occlusion and also may have noise due to external interference during the scanning process. Thus the object detection method used has to identify and localise objects which are affected by occlusion and noise. After studying different methods illustrated in the literature review, the model global and match local method (Surface matching technique) [76] was found to perform better in identifying bolts in clutter. This method requires prior knowledge of the bolt in the form of CAD model for identifying objects from the work area PCD (i.e. bolt scene).

The pre-processing step is performed to prepare a CAD model of a bolt as a reference model as indicated in Figure 7-12, which will be used to identify the bolts from the bolt scene. The CAD model which is in the form of a triangulated surface, defined by the unit normal and the vertices of triangles, is sampled at the distance of 0.5 mm to convert the model into equally spaced points for processing. After sampling, a gripping region is identified from the CAD model. The gripping region is a section of the bolt which is used to grasp the bolt using the two finger gripper. A centre point of this region in 3D is the final position which needs to be sent to the robot to pick up the bolt. Thus, the co-ordinates representing the CAD model in its initial stage is then transformed to this final position (as explained in section 7.5).

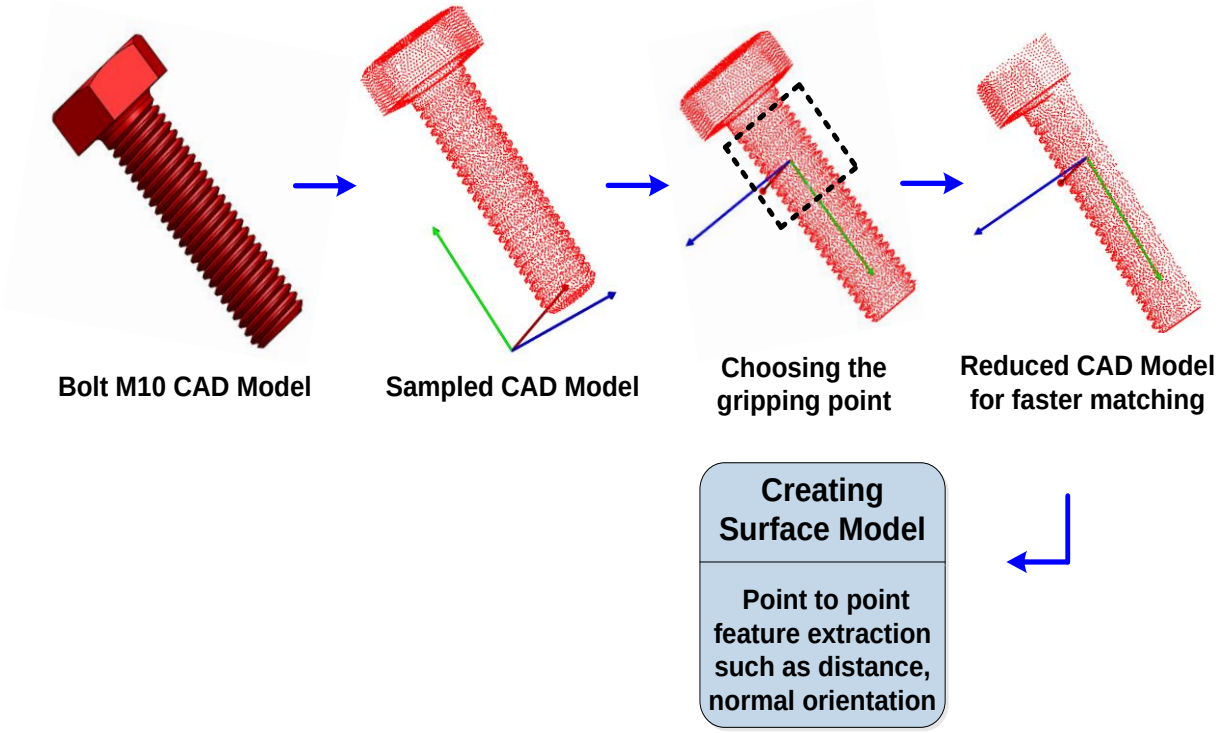

Figure 7-12 : Preparing reference surface model for matching

To reduce the computation time for the surface matching process and to concurrently maintain important features for efficient matching, the model is reduced (a cut along the longitudinal axis of the bolts). This modification reduces the computation time roughly by 3 times. To create the reference surface model for matching, the point to point relations such as distance, the normal and its orientation are mapped and stored as described in Figure 7-12.

7.4.2.2 Post-Processing - Surface Matching Technique

The post processing involves obtaining the PCD of the work area, which contains bolts in clutter, referred to as the 'bolt scene'. The distance between points in the bolt scene along the y-axis is 0.5 mm (i.e. triggering distance in scanning process) and in the x-axis is nearly 40 µm (i.e. resolution on the scanner spatial axis). To obtain an equidistant point model, the bolt scene is then resampled with the same sampling distance of 0.5 mm that has been used to create reference surface model. The surface model created during the pre-processing step is used as a reference to search for the bolt inside the sampled bolt scene using the surface based matching technique as illustrated in the Figure 7-13.

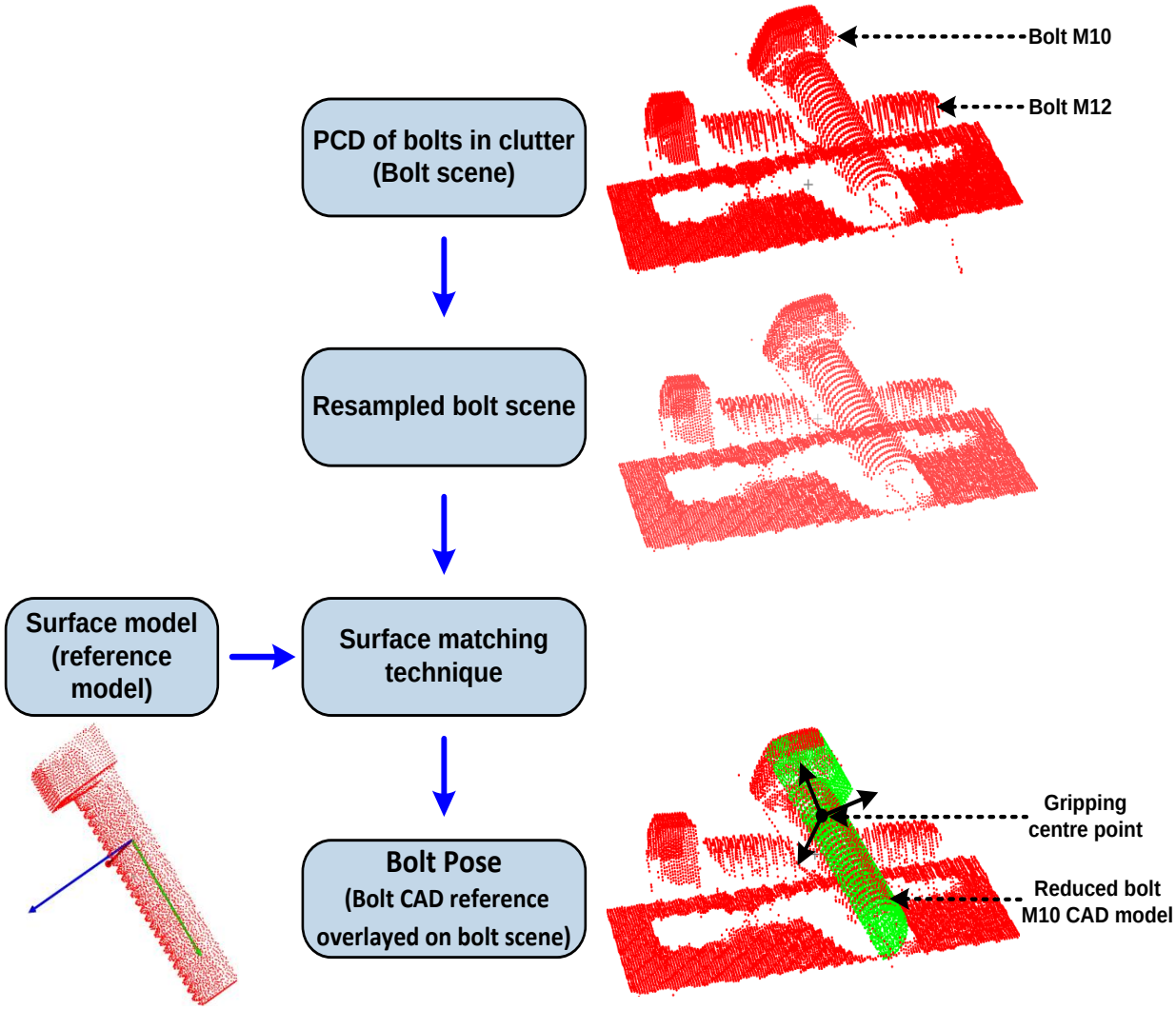

Clarification of point cloud data acquired from laser scanner on a cylindrical object is explained in appendix C1

Figure 7-13 : Detecting bolt from the scene using surface matching

The basic principle of the matching technique is to use a set of key points (such as edge points and corner points) selected from the reference surface model and to try to match the model within the bolt scene. The result of this matching is a set of 3D poses of the surface model in the bolt scene co-ordinate system (i.e. scanner co-ordinate system) and a matching score which depends upon approximate number of key points from reference model match with the surface of the bolt scene.

The final bolt poses are determined by selecting the poses that have a matching score value greater than the set limit. The number of objects with

same size, present in the bolt scene is determined from the total number of poses qualified as an optimum final pose.

The final bolt poses obtained as a result of surface matching represents the transformation of the gripping points with respect to the bolt scene. The z-axis information from the final poses is used to identify the bolt which is located on top of the clutter. This pose is then sent to the robot for picking up the bolt from the work area.

7.5 Calibration process

The 3D calibration is a process of registering the perception of the object or work area obtained using a 3D sensor (i.e. the laser scanner in this case) with respect to the robot co-ordinate system. The bolt pose obtained from the bolt detection algorithm provides the position of the bolt with respect to the laser scanner. Similarly the hole pose obtained using the hole detection algorithm gives the position of hole with respect to the laser scanner. To carry out an assembly using a robot requires the position of the bolt and the hole to be transformed to the robot co-ordinate system.

In this case, the robot has two different tools; one on each arm of the robot. The tool on arm 1 (R1) is the two finger gripper used for picking up the bolt and the tool on arm 2 (R2) is the tightening spindle used for tightening the bolt into the threaded hole. Thus, the calibration process for fastener assembly involves two transformations, one from the laser scanner to robot arm R1 (i.e. the bolt position) and one from scanner to robot arm R2 (i.e. the hole position). This enables the bolt to be picked up and manipulated for fastening accurately within the workspace as required.

The calibration is performed by using a common reference object for both the robot tools and the laser scanner. This object should represent a 3D space with defined dimensions to be used as a reference. Figure 7-14 shows the co-ordinates representing the robot tools, scanner and the reference object.

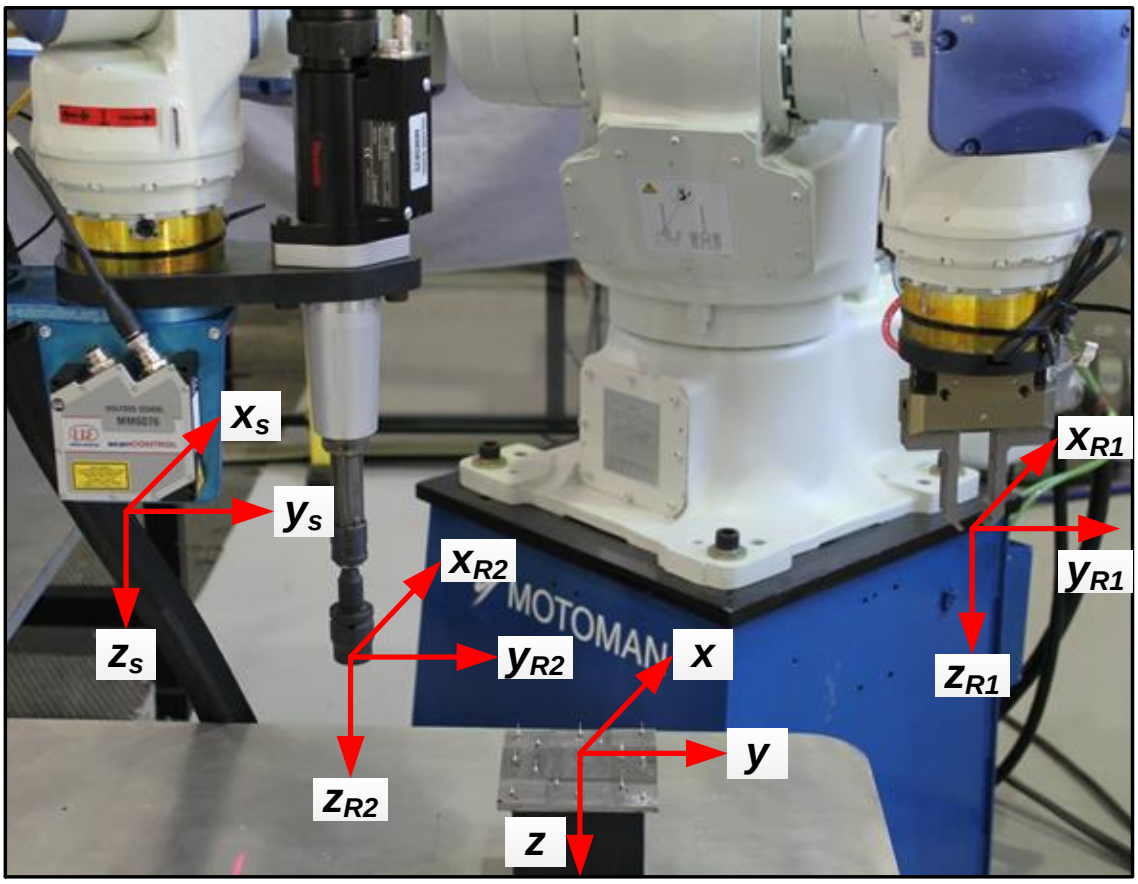

's' - scanner **'R1' - Robot arm 1 tool** **'R2' - Robot arm 2 tool**

Figure 7-14 : Co-ordinates of robot tools, laser scanner and reference object

A reference object given in Figure 7-15 was developed as a common reference to be used for calibration. It is a multistep metal plate which represents the defined 3D space. The multistep plate represents planes at different heights, which is to calibrate the robot and scanner at different heights (i.e. a defined 3D space). The height of the planes on the plate varies from 1 mm to 5 mm. The plate has threaded holes, equidistance at 15 mm apart, for mounting the stylus (the dimensions of the reference object is given in appendix C3 (a)). The styli are used as pointers which have a 1 mm diameter ruby ball at its tip, as shown in Figure 7-15**.**

There are 15 ball styli mounted at the threaded holes located at different planes of the calibration plate. The distance relation between the stylus mounted at the centre and the remaining stylus are measured using a Co-ordinate Measuring

Machine (CMM). This is to obtain precise distance relation between the stylus in *x*, *y* and *z* (i.e. 3D space).

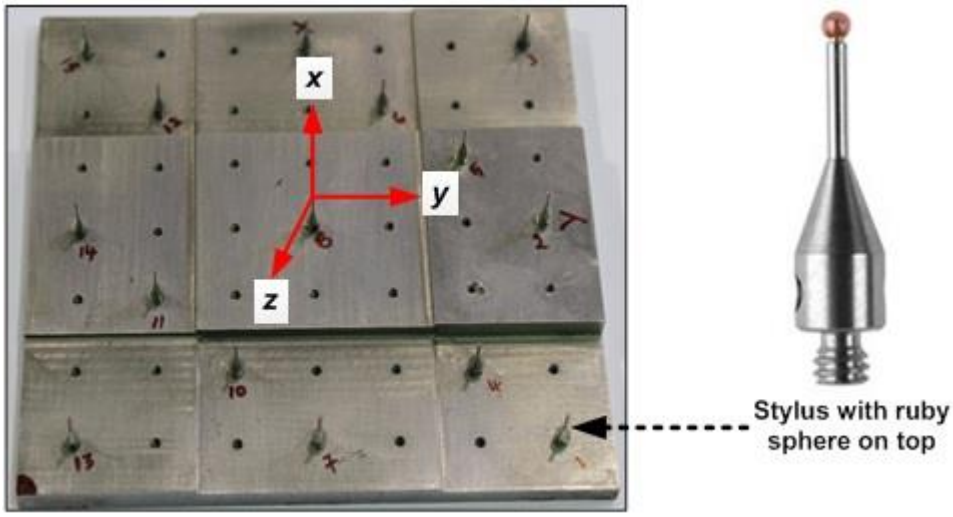

Figure 7-15 : Calibration artefact with stylus

The transformation of the pose with respect to the laser scanner to the pose with respect to the robot tool is calculated using the reference co-ordinate - located at the centre of the calibration plate as shown in the Figure 7-16. Initially, a user co-ordinate for the robot with the tool is defined using the reference co-ordinate. Thus any pose with respect to the reference co-ordinate is the same as with respect to the user co-ordinates of the robot with the tool as illustrated in the equation 6.

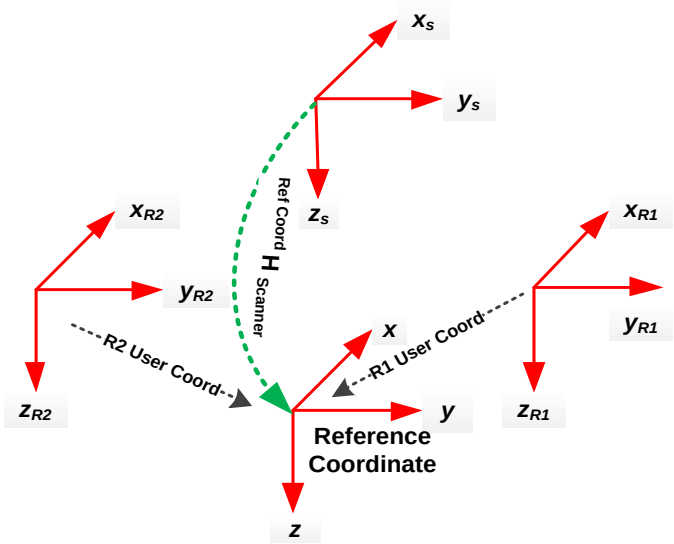

Figure 7-16 : Transformation of co-ordinates

Then the pose with respect to the scanner is transformed to the reference co-ordinate using the equation 7.

$$^{Ref\ Coord}\mathbf{Pose} = {}^{R\ User\ Coord}\mathbf{Pose} \tag{6}$$

Where '*Ref Coord*' denotes reference co-ordinate and '*R User Coord*' denotes the robot user co-ordinate.

$$^{Ref\ Coord}\mathbf{Pose} = {}^{Ref\ Coord}\mathbf{H}_{Scanner}\ \mathbf{x}\ {}^{Scanner}\mathbf{Pose} \tag{7}$$

The 'H' denotes the transformation matrix and the above can be expanded into a 4x4 matrix (equation 8)

$$\begin{bmatrix} P_x^T \\ P_y^T \\ P_z^T \\ 1 \end{bmatrix} = \begin{bmatrix} r_{11} & r_{12} & r_{13} & T_x^{S\ Org} \\ r_{21} & r_{22} & r_{23} & T_y^{S\ Org} \\ r_{31} & r_{32} & r_{33} & T_z^{S\ Org} \\ 0 & 0 & 0 & 1 \end{bmatrix} \begin{bmatrix} P_x^S \\ P_y^S \\ P_z^S \\ 1 \end{bmatrix} \tag{8}$$

Where '*r*' - rotational elements, '*T*' - translational elements, 'P^T' - point with respect to robot tool and 'P^S' - point with respect to scanner

Equating each row of the matrix will give the following three equations (equation 9-11)

$$P_x^T = P_x^S r_{11} + P_y^S r_{12} + P_z^S r_{13} + T_x^{S\ Org} \tag{9}$$

$$P_y^T = P_x^S r_{21} + P_y^S r_{22} + P_z^S r_{23} + T_y^{S\ Org} \tag{10}$$

$$P_z^T = P_x^S r_{31} + P_y^S r_{32} + P_z^S r_{33} + T_z^{S\ Org} \tag{11}$$

From the above equations, for each position values of the 15 styli noted from the laser scanner and the robot, a total of 45 simultaneous equations can be derived (see appendix C3 (b) for information about registering the laser line with a styli). These equations are solved to get the rotational and translational elements of the transformation matrix required to transform the scanner pose into a robot tool pose (i.e. $^{Ref\ Coord}\mathbf{H}_{Scanner}$).

Thus the bolt pose obtained from the bolt detection algorithm is transformed into the robot R1 user co-ordinate for picking up the bolt by using equation 12

$$^{R1\ Tool}\mathbf{Pose}_{\text{Bolt}} = {}^{Ref\ Coord}\mathbf{Pose}_{\text{Bolt}} = {}^{Ref\ Coord}\mathbf{H}_{Scanner} \times {}^{Scanner}\mathbf{Pose}_{\text{Bolt}} \quad (12)$$

Similarly the hole pose has to be transformed into the robot R2 user co-ordinate for carrying out fastening. The transformation is done by using equation 13

$$^{R2\ Tool}\mathbf{Pose}_{\text{Hole}} = {}^{Ref\ Coord}\mathbf{Pose}_{\text{Hole}} = {}^{Ref\ Coord}\mathbf{H}_{Scanner} \times {}^{Scanner}\mathbf{Pose}_{\text{Hole}} \quad (13)$$

The output transformation matrix and the pose of the laser scanner with respect to the reference co-ordinate is given in appendix C3 (c).The accuracy of the calibrated transformation matrix depends upon the accuracy of the laser scanner and the robot.

7.6 Experimental data

The bolts are kept at random position in the clutter and the fastening plate mounted on the tilting table is also pitched up at a random orientation. The position of the bolts and the position of the fastening plate are randomly changed each time before carrying out the fastener assembly. The fastener assembly was carried out 25 times and the assembly was successful 24 times with one failed assembly. The failure is due to the noisy data, where the hole detection algorithm could not identify the hole in 3D. Hence the 3D fastener assembly is 96% successful.

Table 7-2 illustrates the results of the 25 assembly trials that were carried out by placing the bolts one above other and also positioning the fastening plate in different orientation each time using the tilt table. Only the successful data from the trials are used for calculating the hole diameter accuracy, as there is no data obtained during failures.

Table 7-2 : Summary of fastening experiment

No of trials	Average no of points in 1000's	Average hole accuracy (mm)	Bolt		Average Identification time (s)	
		Diameter	Size	Pick up	Hole	Bolt
25	175	0.62	M10	Successful	0.9	1.1

7.7 Algorithm evaluation and discussion

The algorithms developed for this research were able to identify the bolt and the hole feature successfully along with its location in 3D. In order to evaluate the developed algorithms, a series of tests were carried out to analyse the accuracy and robustness. The following sections elaborate the evaluation method for the algorithms and also analyse the results obtained.

7.7.1 Bolt identification using surface matching

The bolt identification algorithm was able to identify a M10 bolt from a group of different size bolts (M10 and M12) placed in the clutter form. The 3D pose of the gripping section obtained as a result of the matching was accurate, as the robot with the gripping fingers was able to pick up the bolt successfully each time. To evaluate the bolt identification algorithm, three different clutter forms of bolts (M10 and M12) were used as shown in Figure 7-17.

Clutter form 1 Clutter form 2 Clutter form 3

Figure 7-17 : Three different clutter forms of bolts used for evaluation

The bolt identification method was used to find the M10 bolt on each clutter form ten times. The results are shown in Table 7-3.

Table 7-3 : Bolt detection evaluation results

Clutter formation	Trials	Bolt size detection	Position repeatability	
			Translation (±)(mm)	Rotation (±) (degree)
1	20	M10	0.11	0.2°
2	20	M10	0.07	0.1°
3	20	M10	0.09	0.2°

The repeatability of the algorithm in determining the 3D pose of the bolt on average is about ±0.09 mm in translation and ±0.2˚ in rotation. These results illustrate that this method is highly accurate and repeatable. Hence, the developed algorithm is robust enough to support its applicability for freeform automated assemblies in industries.

7.7.2 Hole identification using difference in gradient

The developed hole feature identification algorithm was able to determine the top edge of the chamfered threaded holes located on the fastening plate. The algorithm was proved to be sufficiently accurate and fast enough to be used for industrial applications. For further evaluating the algorithm, four holes of two different sizes (M10 and M14) were drilled into the fastening plate on a single plane. The size of the holes and the distance between them are measured using a precision metrology device (SmartScope Flash 200 [104]) to an accuracy of 10 µm (see appendix A8). Figure 7-18 shows the holes, their size and the distances between them.

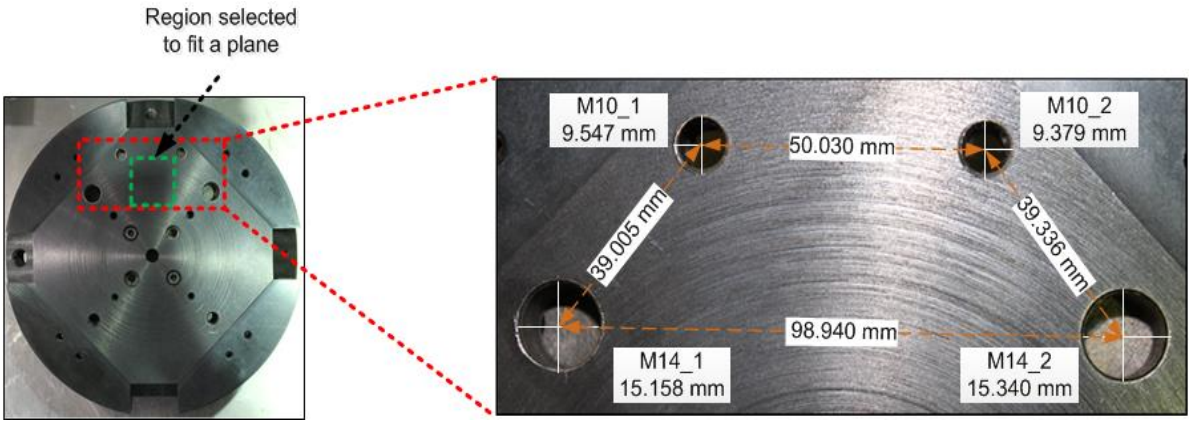

Figure 7-18 : Hole identification algorithm - accuracy measurement setup

The section of the fastening plate where the holes are located is scanned to get the point cloud data. This data is then processed using the hole feature detection algorithm to detect the holes, its diameter, position and orientation in 3D space. The diameter and the distance between holes measured using the algorithm was compared with the reference measurement obtained using the metrology equipment.

The result provides the translation accuracy of the algorithm in 3D (i.e. *x, y* and *z* accuracy). To obtain the rotational accuracy, a planar region (shown in the inner square on Figure 7-18) located near the holes was selected and a 3D plane is fitted to the planar region data. The pose of the plane representing the planar region was used as the reference to analyse the rotational elements of the holes location in 3D space (i.e. θ_x, θ_y and θ_z accuracy). The evaluation process for the rotational accuracy is carried out by pitching the tilt table at different orientation (0° to 30°) along the *x*-axis of the scanner.

Table 7-4 : Hole diameter accuracy measurement

Tilt angle	Trials	Measured diameter (mm)				Average error (±) (mm)
		M10_1	M10_2	M14_1	M14_2	
0	20	10.01	9.97	15.37	15.52	0.35
10	20	10.39	10.28	15.54	16.03	0.71
20	20	10.44	10.23	15.47	15.91	0.66
30	20	10.26	10.04	15.67	15.89	0.61

Table 7-4 provides the hole accuracy measurement results obtained from the hole identification algorithm. The average error of the hole diameter measured at different angles is 0.58 mm, which proves that this algorithm is capable of differentiating two holes with 1 mm size variation.

Table 7-5 illustrates the translation accuracy and Table 7-6 indicates the rotational accuracy obtained from the hole identification algorithm. The average translational error of the holes at differently angled surfaces is 0.53 mm. Similarly, the average error in determining the rotation of the hole plane is 0.7°. This clearly indicates that the novel hole feature identification algorithm is robust and sufficiently accurate to detect hole features on random 3D surfaces.

Table 7-5 : Translation accuracy measurement

Tilt angle	Trials	Hole size	Distance measured (mm)			Average error (±) (mm)
			M10_2	M14_1	M14_2	
0	20	M10_1 M10_2 M14_1	50.00 0 R	38.52 79.91 0	80.81 39.15 99.0	0.24
10	20	M10_1 M10_2 M14_1	49.76 0 R	37.76 79.49 0	79.89 38.37 98.51	0.76
20	20	M10_1 M10_2 M14_1	50.01 0 R	38.49 79.60 0	80.74 38.98 98.51	0.37
30	20	M10_1 M10_2 M14_1	50.04 0 R	37.97 80.26 0	79.20 38.61 97.76	0.75
R - Repeated measurement						

Table 7-6 : Rotation accuracy measurement

Tilt angle	Trials	Plane pose (degree)		Rotation obtained (degree)								Average error (±) (degree)
		θ_x	θ_y	M10_1		M10_2		M14_1		M14_2		
				θ_x	θ_y	θ_x	θ_y	θ_x	θ_y	θ_x	θ_y	
0	20	0.3	0.2	1.1	0.7	1.3	0.5	0.8	0.2	1.2	0.6	0.6
10	20	0.4	9.5	2.1	9.8	1.2	9.7	0.2	8.7	0.8	8.6	0.7
20	20	0.7	19.4	1.7	19.6	1.6	18.8	0.7	18.8	1.1	20.1	0.5
30	20	0.6	29.7	2.6	28.2	1.4	27.8	0.2	29.3	0.3	29.9	0.9

All the errors reported in the results are cumulative errors which include error in the robot manipulation, the laser scanner data acquisition, the determination of tool point (TCP) for the robot arm, the 3D calibration and the algorithms developed for object and feature identification.

7.8 Results

The assembly of bolts located in clutter into their corresponding size of threaded holes on the fastening plate which is also placed at random locations was successfully carried out. The assembly method developed in C# programming language was able to identify and segment bolts based on their size by using prior knowledge (i.e. bolt shape, pitch and thread length) as a reference. It was also able to identify and locate different sizes of threaded holes with chamfer on the fastening plate. The correct size bolt was picked up from the clutter and fastened into the corresponding size hole using the tightening spindle without any cross threading or misalignment.

The experiment result shows that the developed 3D fastener assembly is 96% successful for a profile distance of 0.5 mm, bolts lying in clutter and threaded holes with chamfered edges kept in a random location. The assembly process can be improved by scanning the region with 0.25 mm profile distance and at better assembly conditions. The hole identification algorithm was able to determine a 3D hole with a sub-millimetre accuracy, proven by the successful assembly and also has a 0.62 mm accuracy in determining the diameter of the hole. In addition, the bolt identification algorithm was also successful, as it was able to detect the M10 bolts successfully for all the trials carried out. The developed identification algorithms were able to identify the bolt in an average of 1.1 seconds and the hole in an average of 0.93 seconds.

Evaluation showed that the translation and rotation accuracy of the hole feature identification algorithm in detecting chamfer-less hole at different 3D position is 0.53 mm and 0.7° respectively. Similarly, the repeatability of the bolt detection algorithm is ± 0.09 mm and ± 0.2˚ in translation and rotation respectively. The performance and the accuracy of these algorithms indicate that the fastener assembly method is robust and flexible, thereby applicable to industrial scenarios.

CHAPTER 8 - CONCLUSIONS

A detailed review on the existing assembly technologies was conducted and it was concluded that the available research and commercial methods are not sufficiently fast or accurate to perform the majority of the non-structured industrial assembly applications. To address this issue, a systematic investigation was carried out for developing a fastener assembly system to assemble a range of bolts into their corresponding size holes on the mating component, and to analyse its applicability in a non-structured industrial environment. Initially, the most suitable system hardware and devices required for performing the fastener assembly were realised and identified. An experimental demonstrator was also developed using the selected hardware and devices comprising of a dual-arm robot, a gripper, a tightening tool and vision sensors.

The second stage of this research involves investigation of the use of 2D vision to assemble fasteners. Thus, an automated fastening method was developed to assemble fasteners in a single plane using a 2D vision sensor. The 2D fastening was performed in two different lighting conditions i.e. controlled and variable lighting conditions. The results of these experiments showed that the 2D vision based assembly system is prone to variation in lighting conditions and object surface finish. Hence, the 2D vision is very unreliable and only suitable for limited industrial applications where the environment is structured to favour assembly.

The inability of 2D assembly system to cope with variation in lighting, surface finish and the requirement for identifying objects placed in unknown locations necessitated the need for 3D imaging technology. Thus, the third stage involves carrying out an extensive evaluation of the existing 3D technologies and sensors in different lighting conditions and objects with different surface finishing. As a result of the evaluation carried, it was found that the laser triangulation technology provides a better visual perception in a non-structured environment. This technology also has a high accuracy and minimal effect to external lighting and surface finishes.

In many industrial assembly scenarios, the bolts and the threaded holes could be located in a random workspace - requiring 3D identification and localisation to perform assembly. Hence, the final stage was to develop an automated fastening method, to assemble fasteners in random 3D workspaces. The bolts located in clutter are identified, segmented and localised using an existing object identification method with an enhancement to the input reference CAD model. On the other hand, at present there is no method available to identify the threaded holes located at random 3D workspace. Thus, a novel hole feature identification method was developed as a part of this research. The experiment results proved that the automated fastening method developed for this research was robust, as it was able to assemble fasteners with high accuracy and repeatability.

An extensive evaluation was also carried out on the bolt identification and the hole feature identification algorithms by introducing random variation in the location of objects within the workspace. The results showed that both methods have sub-millimetre accuracy in determining the location and also require less processing time (i.e. approximately 1 second); therefore proving its suitability for many industrial applications.

The key deliverables achieved as a part of this research are explained as follows:

Automated Freeform Fastening System

An automated freeform assembly system was successfully developed, which is capable of fastening a range of bolts into their corresponding size holes in a non-structured environment.

- ✧ The fastener assembly system was able to replicate the human fastening action using a tightening tool and a gripper with two fingers.
- ✧ The system was developed by integrating existing commercial systems and technology coupled with novel algorithms to perform robust fastener assembly.

- ✧ A 3D calibration method was developed to transform the pose obtained with respect to the laser scanner into the pose with respect to the robot tool.
- ✧ The experiments results proved a 100% success rate for the developed bolt and threaded hole feature identification algorithms and only 96% success in performing the fastener assembly. The failures are understood to be caused by errors in the 3D pose of the threaded hole. These errors were identified to be cumulative and include errors due to the feature identification algorithm, the 3D calibration, the robot inaccuracies and the laser scanner inaccuracies.

Automated Bolt Pick Up Method

An automated method was developed to pick up bolts placed in random clutter.

- ✧ A bolt identification algorithm was developed as a part of this method to identify different size bolts placed randomly within the workspace. The algorithm has an average identification time of 1.1 second.
- ✧ The developed method is also able to locate various size bolts located at a random 3D workspace with a repeatability of ± 0.09 mm in translation and ± 0.2˚ in rotation, thus the method is proved to be highly robust.

Automated Threaded Hole Identification Method

An automated identification method was developed to find threaded hole features on the fastening plate (represents a target component) located in a random workspace.

- ✧ An edge detection algorithm based on difference in gradient method was developed as a part of the hole identification method to identify any sharp edge features present in the target component.
- ✧ This method is able to identify and classify the circular outer edges of different size threaded holes (including chamfer features in industrial components) with an average processing time of 0.9 seconds with an average translation and rotation accuracy of 0.53 mm and 0.7° respectively.

Automated Bolt Alignment and Fastening Method

An automated method was developed to align the bolt with their corresponding size threaded hole and carry out torque controlled fastening.

- ✧ This method identifies the axis perpendicular to the hole plane in order to guide the bolt into the hole for fastening.
- ✧ The fastening method includes pre-programmed torque control modules embedded into the tightening tool controller for fastening different size bolts.
- ✧ The method is able to monitor the torque in near real time and prevent cross-threading by stopping the fastening process. Furthermore through this program, cross-threading can be distinguished from the final tightening torque by monitoring the location of the bolt relative to the threaded hole.

Table 8-1, summarises the research achievements in comparison with the research objectives outlined in section 1.5 . This table indicates that the objectives are fully or partially achieved with recommendations for further work.

Table 8-1 : Summary of research achievements

Research Objectives	Achieved	To be achieved
Bolt pick up method	A bolt identification method was developed with high accuracy and repeatability. Bolts are identified and located from random 3D clutter. Bolts are picked up from clutter using a two-finger gripper.	Extending the method to pick up bolts from a bin (i.e. avoiding collision with other objects)
Hole identification method	Hole feature identification method was developed with high accuracy and less processing time. Threaded holes are identified and localised in 3D.	Extending the method to identify other primitive shape features such as semi-circles, planes, ellipse and non-primitive shapes.
Bolt alignment with the hole method	A strategy was developed to identify the hole plane and the assembling axis to align the bolt	
Fastening process	A pre-defined program was developed in the tightening tool to control and monitor the	Correction mechanism to adapt to the misalignment errors

	torque applied during fastening Cross-threading was prevented by stopping the fastening process if the torque exceeds the threshold limit.	
Selecting suitable hardware and devices	Hardware and devices are identified and evaluated for fastener assembly	Identifying or developing a tightening tool with advanced external feedback control
Establishing communication and control for the selected hardware and devices	Communication setup was established to integrate the devices to one master control	
Evaluating different imaging devices	Micro-Epsilon laser scanner was selected based on the evaluation	Extending the field of view of the 3D vision system
Removing fixtures and robot programming	No dedicated fixtures were used and minimal robot programming is involved.	

8.1 Contributions to knowledge

This research made two major contributions to knowledge. The details are explained below:

1) An automated freeform fastener assembly system - This research has led to the development of an automated assembly system capable of performing fastening in non-structured industrial conditions. The flexibility and adaptability achieved by this system help to accommodate variation in product locations and also to assemble different components or parts without much modification. In addition, this system requires minimal or no robot programming and also does not require jigs or component specific fixtures.
2) A novel hole feature identification algorithm - A novel hole feature identification algorithm was developed as a part of this research. Following a comprehensive review of the literature, to the best of author's knowledge, the developed method is at present the only method that can identify and localise chamfered and threaded holes located at random environment.

Furthermore, there are three minor contributions, as explained below:

1) Analysing 2D vision for assembly in different lighting conditions - Identifying objects using a 2D vision is a well-established research area. In this research, the 2D vision assembly system was developed to analyse its suitability to identify and assemble objects in different lighting conditions. It was concluded that the 2D vision is highly recommended only if the objects are in a single plane located on a controlled lighting environment.
2) Enhanced 3D bolt identification method - The 3D object identification method used in this research was an existing method, enhanced for detecting bolts. The enhancement made in presenting the input reference CAD model has resulted in increasing the performance (i.e. by reducing the processing time to about one third when compared to using the CAD model without modification).
3) Identifying suitable 3D imaging technology - Prior to this research, there were no methods available for the evaluation of different 3D imaging technologies. Thus an evaluation method based on different lighting conditions and object surface qualities was developed. The results obtained show that the laser triangulation technology is less prone to different lighting conditions and object surface finishes; therefore proving more suitable for fastener assembly in random industrial conditions.

8.2 Research Limitations

The research is focused on the fastener assembly, which is a widely used method in industrial sectors. Some of the assumptions made in this research have led to limitations in relation to the application requirements as explained in Table 8-2.

Table 8-2 : Limitations of this research

Application requirements	Constraints applied
Assembling different types of fasteners	The research focus was limited to fasteners with hexagon head drive bolts. The developed method may need modifications for other types

	of fasteners or components. Bolt size, head drive, pitch, tolerance, tightening torque and material are defined to limit the scope of this research
Presenting the assembly components	The bolts and the target component has to be within the robot's workspace but can be placed randomly inside the workspace.
Assembling environment	The experiments are conducted at ambient lighting conditions with no vibration.
Equipment limitation	The workspace dimension is limited to the working volume of the Micro-Epsilon laser scanner.
Fastening process monitoring and correction mechanism to prevent cross threading	Torque applied during fastening process is monitored using prior knowledge of tightening torque. Cross threading is prevented by stopping the fastening process and no correction mechanism was implemented to counter it. Despite the fact that this was not a part of this research objective, it limits the application of the proposed method and should be researched further.
Robustness	The developed algorithms were evaluated to quantify the accuracy and repeatability achieved only for a trial run of 25 times. Only two different sizes of bolts and four different size holes were used for robustness evaluation. Sub-millimetre accuracy was considered as the target in this research. This is based on the target industries requirement i.e. automotive and aerospace assembly. However, the range of sizes and the accuracy considered should be extended to validate the obtained robustness values.

8.3 Recommendations for future work

This research successfully demonstrated the freeform automated assembly of threaded fasteners in a non-structured environment, which is an important step to achieve completely freeform automation. Further development of this project is recommended in the following areas

- ✧ Extending the assembly workspace for providing greater flexibility to the automated assembly system by using a combination of 2D and 3D vision sensors.
- ✧ Integrating force-torque sensor to infer and control misalignment errors occurring during the fastening process and thereby adding a cognitive decision making capability.
- ✧ Extending the 3D object identification method to pick up bolts from a bin (i.e. avoiding collision with other objects)
- ✧ Improving the 3D object identification method for better segmentation of objects (i.e. separating different size objects that are occluded) and to improve the accuracy and reduce the processing time.
- ✧ Extending the 3D hole identification method further to identify other primitive shape features such as semi-circles, planes, ellipse and non-primitive shapes.
- ✧ Improving the hole feature detection method for making it immune to large noises and extending it to identify different feature shapes.
- ✧ Identifying or developing a tightening tool with advanced external feedback control.
- ✧ Exploring the advantages of collaborative assembly using multiple robots for achieving completely freeform automated assembly.
- ✧ Developing the automated fastener assembly system further to assemble a family of real industrial products to achieve greater flexibility in the reconfiguration of the assembly systems.

REFERENCES

[1] N. Herakovic, “Robot Vision in Industrial Assembly and Quality Control Processes,” *Robot Vision*, pp. 501–535, 2010.

[2] R. Bogue, “Europe fights back with advanced manufacturing and assembly technologies,” *Assembly Automation*, 2012.

[3] “What is Automation,” *Automation Federation*, 2012. [Online]. Available: http://www.automationfederation.org/Content/NavigationMenu/General_Information/Alliances_and_Associations/The_Automation_Federation/About1/What_is_Automation_/What_is_Automation_.htm. [Accessed: 10-Jun-2012].

[4] G. Michalos, S. Makris, N. Papakostas, D. Mourtzis, and G. Chryssolouris, “Automotive assembly technologies review: challenges and outlook for a flexible and adaptive approach,” *CIRP Journal of Manufacturing Science and Technology*, vol. 2, no. 2, pp. 81–91, 2010.

[5] G. Michalos, S. Makris, N. Papakostas, D. Mourtzis, and G. Chryssolouris, “Automotive assembly technologies review: challenges and outlook for a flexible and adaptive approach,” *CIRP Journal of Manufacturing Science and Technology*, vol. 2, no. 2, pp. 81–91, Jan. 2010.

[6] G. M. Bone and D. Capson, “Vision-guided fixtureless assembly of automotive components,” *Robotics and Computer-Integrated Manufacturing*, vol. 19, no. 1–2, pp. 79–87, Feb. 2003.

[7] M. Klingajay and P. Toncharoen, “The Intelligence Automated Thread-Fastening Assembly using the Newton Raphson,” *World Academy of Science, Engnieering and Technology*, pp. 127–131, 2008.

[8] “Fastening & Assembly,” *Society of Manufacturing Engineers*, 2012. [Online]. Available: http://manufacturing.stanford.edu/processes/Fastening&Assembly.pdf. [Accessed: 10-Jun-2012].

[9] M. Klingajay, “Parameter estimation during automated screw insertions,” *IEEE International Conference on Industrial Technology*, 2002.

[10] M. Holzer, “Aircraft Fasteners,” *AVIATIONPROS.COM*, 2011. [Online]. Available: http://www.aviationpros.com/article/10370291/aircraft-fasteners. [Accessed: 25-Jul-2012].

[11] J. Hwang, D. Jung, and Y. Roh, “Low-cost automatic screw machine using a commercial electric screwdriver,” *… and Systems (ICCAS …*, pp. 1055–1060, 2012.

[12] M. T. Hoske, “415 Parts Seen: Machine Vision Guides Robot,” *Control Engineering*, 2009. [Online]. Available: http://www.controleng.com/index.php?id=483&tx_ttnews[tt_news]=8180&cHash=062910.

[13] P. Waurzyniak, “Aerospace Automation Picks Up the Pace,” *Automation in Aerospace*, 2013.

[14] a. Hernansanz, a. Casals, and J. Amat, “A multi-robot cooperation strategy for dexterous task oriented teleoperation,” *Robotics and Autonomous Systems*, vol. 68, pp. 156–172, 2015.

[15] B. Esakki, R. B. Bhat, and C. Y. Su, “Robust control of collaborative manipulators - Flexible object system,” *International Journal of Advanced Robotic Systems*, vol. 10, 2013.

[16] P. Tsarouchi, S. Makris, G. Michalos, M. Stefos, K. Fourtakas, K. Kaltsoukalas, D. Kontrovrakis, and G. Chryssolouris, “Robotized Assembly Process Using Dual Arm Robot,” *Procedia CIRP*, vol. 23, pp. 47–52, 2014.

[17] J. Krüger, G. Schreck, and D. Surdilovic, “Dual arm robot for flexible and cooperative assembly,” *CIRP Annals - Manufacturing Technology*, vol. 60, no. 1, pp. 5–8, 2011.

[18] S. Kock, T. Vittor, B. Matthias, H. Jerregard, M. Källman, I. Lundberg, R. Mellander, and M. Hedelind, “Robot concept for scalable, flexible assembly automation: A technology study on a harmless dual-armed robot,” *Proceedings - 2011 IEEE International Symposium on Assembly and Manufacturing, ISAM 2011*, no. 230902, 2011.

[19] H. Ding, M. Schipper, and B. Matthias, “Collaborative behavior design of industrial robots for multiple human-robot collaboration,” *2013 44th International Symposium on Robotics, ISR 2013*, vol. 49, no. 0, 2013.

[20] N. Nguyen-Duc-Thanh and D. Stonier, “A new approach for human-robot interaction using human body language,” *Convergence and Hybrid Information Technology*, pp. 762–769, 2011.

[21] P. Gröndahl and M. Onori, “Standardised flexible automatic assembly – evaluating the Mark IV approach,” *Assembly Automation*, vol. 20, pp. 217–224, 2000.

[22] G. Rosati, M. Faccio, A. Carli, and A. Rossi, “Fully flexible assembly systems (F-FAS): a new concept in flexible automation,” *Assembly Automation*, vol. 33, no. 1, pp. 8–21, 2013.

[23] C. Finetto, M. Faccio, G. Rosati, and a. Rossi, “Mixed-model sequencing optimization for an automated single-station fully flexible assembly

system (F-FAS)," *International Journal of Advanced Manufacturing Technology*, vol. 70, no. 5–8, pp. 797–812, 2014.

[24] C. Finetto, G. Rosati, M. Faccio, and A. Rossi, "Implementation framework for a fully flexible assembly system (F-FAS)," *Assembly Automation*, 2015.

[25] B. Lara, K. Althoefer, and L. D. Seneviratne, "Automated robot-based screw insertion system," *IECON '98. Proceedings of the 24th Annual Conference of the IEEE Industrial Electronics Society (Cat. No.98CH36200)*, vol. 4, pp. 2440–2445, 1998.

[26] N. Fei, F. Zhuang, L. Renqiang, C. Qixin, and Z. Yanzheng, "An image processing approach for jigsaw puzzle assembly," *Assembly Automation*, vol. 27, no. 1, pp. 25–30, 2007.

[27] B. Jerbic, M. Hrman, and B. Vranjes, "Intelligent Robotic Assembly by active vision system integrated with CAD," in *7th International Reserach/Expert Confernece "Trends in the Development of Machinery and associated Technology,"* 2003.

[28] B. Jerbić, B. Vranješ, M. Hrman, and Z. Kunica, "Intelligent Robotic Assembly Using Machine Vision and CAD Integration," *Transactions of Faculty of Mechanical Engineering and Naval Architecture (FAMENA)*, vol. 29, no. 1, pp. 17–30, 2005.

[29] P. Webb, S. Eastwood, N. Jayaweera, and Y. Chen, "Automated aerostructure assembly," *Industrial Robot: An International Journal*, vol. 32, no. 5, pp. 383–387, 2005.

[30] N. Jayaweera and P. Webb, "Automated assembly of fuselage skin panels," *Assembly Automation*, vol. 27, no. 4, pp. 343–355, 2007.

[31] N. Jayaweera and P. Webb, "Adaptive robotic assembly of compliant aero-structure components," *Robotics and Computer-Integrated Manufacturing*, vol. 23, no. 2, pp. 180–194, Apr. 2007.

[32] N. Jayaweera and P. Webb, "Metrology-assisted robotic processing of aerospace applications," *International Journal of Computer Integrated Manufacturing*, vol. 23, no. 3, pp. 283–296, Mar. 2010.

[33] J. Su, H. Qiao, C. Liu, and Z. Ou, "A new insertion strategy for a peg in an unfixed hole of the piston rod assembly," *The International Journal of Advanced Manufacturing Technology*, vol. 59, no. 9–12, pp. 1211–1225, Aug. 2011.

[34] J. Su, H. Qiao, Z. Ou, and Y. Zhang, "Sensor-less insertion strategy for an eccentric peg in a hole of the crankshaft and bearing assembly," *Assembly Automation*, vol. 32, no. 1, pp. 86–99, 2012.

[35] H. Chen, G. Zhang, H. Zhang, and T. a. Fuhlbrigge, “Integrated robotic system for high precision assembly in a semi-structured environment,” *Assembly Automation*, vol. 27, no. 3, pp. 247–252, 2007.

[36] H. Chen, J. Wang, G. Zhang, T. Fuhlbrigge, and S. Kock, “High-precision assembly automation based on robot compliance,” *The International Journal of Advanced Manufacturing Technology*, vol. 45, no. 9–10, pp. 999–1006, May 2009.

[37] S.-J. Huang and J.-P. Tsai, “Robotic automatic assembly system for random operating condition,” *The International Journal of Advanced Manufacturing Technology*, vol. 27, no. 3–4, pp. 334–344, Mar. 2005.

[38] I. Lopez-Juarez and M. Howarth, “Knowledge acquisition and learning in unstructured robotic assembly environments,” *Information Sciences*, vol. 145, no. 1–2, pp. 89–111, Aug. 2002.

[39] I. Lopez juarez, J. Corona castuera, M. Pena cabrera, and K. Ordaz hernandez, “On the design of intelligent robotic agents for assembly,” *Information Sciences*, vol. 171, no. 4, pp. 377–402, May 2004.

[40] M. P.-C. Corona-Castuera, J, Reyes Rios-Cabrera, Ismael Lopez-Juarez, “An approach for intelligent fixtureless assembly: Issues and experiments,” *MICAI 2005*, pp. 1052–1061, 2004.

[41] M. Peña-Cabrera, I. Lopez-Juarez, R. Rios-Cabrera, and J. Corona-Castuera, “Machine vision approach for robotic assembly,” *Assembly Automation*, vol. 25, no. 3, pp. 204–216, 2005.

[42] J. Fleischer, G. Lanza, M. Otter, and J. Elser, “Spatial alignment of joining partners without fixtures, based on component-inherent markings,” *Journal of Manufacturing Systems*, vol. 32, no. 3, pp. 489–497, 2013.

[43] L. Wang, A. Mohammed, and M. Onori, “Remote robotic assembly guided by 3D models linking to a real robot,” *CIRP Annals - Manufacturing Technology*, vol. 63, no. 1, pp. 1–4, 2014.

[44] L. Tingelstad and O. Egeland, “Robotic Assembly of Aircraft Engine Components Using a Closed-loop Alignment Process,” in *5th Conference on Assembly Technologies and Systems (CATS)*, 2014, vol. 23, pp. 110–115.

[45] N. Jayaweera, P. Webb, and C. Johnson, “Measurement assisted robotic assembly of fabricated aero-engine components,” *Assembly Automation*, vol. 30, no. 1, pp. 56–65, 2010.

[46] Z. Zhang, H. Li, Q. Han, and H. Gao, “Visual sensor-guided robotic adaptive assembly of aero aluminum alloy tube,” *The International Journal of Advanced Manufacturing Technology*, vol. 78, no. 9–12, pp. 2057–2068, 2015.

[47] V. S. Vyawahare and N. V. Afzulpurkar, “Uncalibrated Eye in Hand Visual Servoing for Fixtureless Assembly Automation,” *2006 IEEE International Conference on Industrial Technology*, pp. 2244–2249, 2006.

[48] U. Khan, I. Jan, N. Iqbal, and J. Dai, “Uncalibrated eye-in-hand visual servoing: an LMI approach,” *Industrial Robot: An International Journal*, vol. 38, no. 2, pp. 130–138, 2011.

[49] F. S. C. F. S. Cheng and a. D. a. Denman, “A study of using 2D vision system for enhanced industrial robot intelligence,” *IEEE International Conference Mechatronics and Automation, 2005*, vol. 3, no. July, pp. 1185–1189, 2005.

[50] A. Agrawal, Yu Sun, J. Barnwell, and R. Raskar, “Vision-guided Robot System for Picking Objects by Casting Shadows,” *The International Journal of Robotics Research*, vol. 29, no. 2–3, pp. 155–173, 2010.

[51] I. Lopez-Juarez, R. Rios-Cabrera, M. Pena Cabrera, and R. Osorio-Comparan, “Learning and fast object recognition in robot skill acquisition: a new method,” *Mexican Conference on Pattern Recognition (MCPR)*, pp. 40–49, 2010.

[52] I. López-juárez, R. Rios-cabrera, and M. Peña-cabrera, “Fast Object Recognition for Grasping Tasks using Industrial Robots,” *Computación y Sistemas*, vol. 16, no. 4, pp. 421–432, 2012.

[53] S. Lee, J. Kim, M. Lee, K. Yoo, L. G. Barajas, and R. Menassa, “3D visual perception system for bin picking in automotive sub-assembly automation,” *IEEE International Conference on Automation Science and Engineering*, pp. 706–713, 2012.

[54] D. Holz, M. Nieuwenhuisen, and D. Droeschel, “Active Recognition and Manipulation for Mobile Robot Bin Picking,” *Gearing Up and Accelerating Cross-fertilization between Academic and Industrial Robotics Research in Europe: Springer Tracts in Advanced Robotics*, vol. 94, pp. 133–153, 2014.

[55] K. Böhnke and A. Gottscheber, “Fast Object Registration and Robotic Bin Picking,” *Research and Education in Robotics - EUROBOT*, vol. 82, pp. 23–37, 2010.

[56] D. Buchholz, S. Winkelbach, and F. M. Wahl, “RANSAM for Industrial Bin-Picking,” *41st International Symposium on Robotics*, vol. ISR, pp. 1–6, 2010.

[57] M.-Y. Liu, O. Tuzel, a. Veeraraghavan, Y. Taguchi, T. K. Marks, and R. Chellappa, “Fast object localization and pose estimation in heavy clutter for robotic bin picking,” *The International Journal of Robotics Research*, vol. 31, pp. 951–973, 2012.

[58] J.-K. Oh, S. Lee, and C.-H. Lee, “Stereo vision based automation for a bin-picking solution,” *International Journal of Control, Automation and Systems*, vol. 10, no. 2, pp. 362–373, Apr. 2012.

[59] G. Sansoni, P. Bellandi, F. Leoni, and F. Docchio, “Optoranger: A 3D pattern matching method for bin picking applications,” *Optics and Lasers in Engineering*, vol. 54, pp. 222–231, 2014.

[60] K. Ono, T. Ogawa, Y. Maeda, S. Nakatani, G. Nagayasu, R. Shimizu, and N. Ouchi, “Detection , Localization and Picking Up of Coil Springs from a Pile,” *2014 IEEE International Conference on Robotics and Automation*, pp. 3477–3482, 2014.

[61] N. Dhayagude, Z. Gao, and F. Mrad, “Fuzzy logic control of automated screw fastening,” *Robotics and Computer-Integrated Manufacturingntegrated Manufacturing*, vol. 12, no. 3, pp. 235–242, 1996.

[62] C. Deters, E. L. Secco, H. a. Wuerdemann, H. K. Lam, L. D. Seneviratne, and K. Althoefer, “Model-free fuzzy tightening control for bolt/nut joint connections of wind turbine hubs,” *2013 IEEE International Conference on Robotics and Automation*, pp. 270–276, May 2013.

[63] C. Deters, H. Lam, E. L. Secco, H. A. Würdemann, L. D. Seneviratne, and K. Althoefer, “Accurate Bolt Tightening Using Model Free Fuzzy Control for Wind Turbine Hub Bearing Assembly,” *IEEE Transactions on Control Systems Technology*, pp. 1–12, 2014.

[64] M. Klingajay and N. Giannoccaro, “The automated threaded fastening based on on-line identification,” *International Journal of Advanced Robotic Systems*, vol. 1, no. 4, pp. 263–272, 2004.

[65] Y. Fan, C. Guo, and W. Meng, “Study of distributed multiaxial intelligent tightening machine based on fieldbus control system,” *2010 International Conference on Intelligent Control and Information Processing*, pp. 415–419, Aug. 2010.

[66] S. Wiedmann and B. Sturges, “A Full Kinematic Model of Thread-Starting for Assembly Automation Analysis,” *Journal of Mechanical Design*, vol. 128, no. 1, p. 128, 2006.

[67] S. Wiedmann and B. Sturges, “Spatial Kinematic Analysis of Threaded Fastener Assembly,” *Journal of Mechanical Design*, vol. 128, no. 1, p. 116, 2006.

[68] M. a. Diftler and I. D. Walker, “Experiments in aligning threaded parts using a robot hand,” *IEEE Transactions on Robotics and Automation*, vol. 15, no. 5, pp. 858–868, 1999.

[69] S. Pitipong, P. Pornjit, and P. Watcharin, “An automated four-DOF robot screw fastening using visual servo,” *2010 IEEE/SICE International Symposium on System Integration*, pp. 379–383, Dec. 2010.

[70] K. Althoefer, B. Lara, and L. D. Seneviratne, “Monitoring of Self-Tapping Screw Fastenings Using Artificial Neural Networks,” *Journal of Manufacturing Science and Engineering*, vol. 127, no. 1, p. 236, 2005.

[71] N. Giannoccaro and M. Klingajay, “Identification of threaded fastening parameters based on least square method,” *SICE 2004 Annual Conference*, pp. 2592–2597, 2004.

[72] R. Chumakov, “An artificial neural network for fault detection in the assembly of thread-forming screws,” *Journal of Intelligent Manufacturing*, vol. 19, no. 3, pp. 327–333, Apr. 2008.

[73] C. Saygin, D. Mohan, and J. Sarangapani, “Real-time detection of grip length during fastening of bolted joints: a Mahalanobis-Taguchi system (MTS) based approach,” *Journal of Intelligent Manufacturing*, vol. 21, no. 4, pp. 377–392, Nov. 2008.

[74] L. Rusli and A. Luscher, “Fastener identification and assembly verification via IR tracking,” *Assembly Automation*, vol. 32, no. 3, pp. 262–275, 2012.

[75] S.-H. P. Won, F. Golnaraghi, and W. W. Melek, “A fastening tool tracking system using an IMU and a position sensor with Kalman filters and a fuzzy expert system,” *IEEE TRANSACTIONS ON INDUSTRIAL ELECTRONICS*, vol. 56, no. 5, pp. 1782–1792, 2009.

[76] B. Drost, M. Ulrich, N. Navab, and S. Ilic, “Model Globally, Match Locally: Efficient and Robust 3D Object Recognition,” in *Computer Vision and Pattern Recognition (CVPR)*, 2010, pp. 998–1005.

[77] E. Wahl, U. Hillenbrand, and G. Hirzinger, “Surflet-pair-relation histograms: a statistical 3D-shape representation for rapid classification,” *Fourth International Conference on 3-D Digital Imaging and Modeling, 2003. 3DIM 2003. Proceedings.*, 2003.

[78] K. Khoshelham, “Extending generalized hough transform to detect 3d objects in laser range data,” *ISPRS Workshop on Laser Scanning, Proceedings, LS …*, pp. 206–210, 2007.

[79] H. Chen and B. Bhanu, “3D free-form object recognition in range images using local surface patches,” *Pattern Recognition, 2004. ICPR 2004. Proceedings of the 17th International Conference on*, vol. 3, pp. 136–139 Vol.3, 2004.

[80] A. Aldoma, M. Vincze, N. Blodow, D. Gossow, S. Gedikli, R. B. Rusu, and G. Bradski, “CAD-model recognition and 6DOF pose estimation using 3D

cues," *Proceedings of the IEEE International Conference on Computer Vision*, pp. 585–592, 2011.

[81] Y. Wang, R. Liu, F. Li, and S. Endo, "An effective hole detection method for 3D models," *20th European Signal Processing Conference (EUSIPCO 2012)*, no. Eusipco, pp. 1940–1944, 2012.

[82] G. H. Bendels and R. Klein, "Detecting Holes in Point Set Surfaces," *The Journal of WSCG*, vol. 14, no. ISSN 1213–6972, p. 8, 2006.

[83] C. Papazov and D. Burschka, "An efficient RANSAC for 3D object recognition in noisy and occluded scenes," *Lecture Notes in Computer Science (including subseries Lecture Notes in Artificial Intelligence and Lecture Notes in Bioinformatics)*, vol. 6492 LNCS, no. iii, pp. 135–148, 2011.

[84] D. Borrmann, J. Elseberg, K. Lingemann, and A. Nüchter, "The 3D Hough Transform for plane detection in point clouds: A review and a new accumulator design," *3D Research*, vol. 02003, 2011.

[85] "Assembly in Action: Nutrunners Decrease Cycle Times," *Assembly Magazine*, 2006. [Online]. Available: http://www.assemblymag.com/articles/84441-assembly-in-action-nutrunners-decrease-cycle-times.

[86] "Assembly in Action: Fastener Handling System Saves Time," *Assembly Magazine*, 2002. [Online]. Available: http://www.assemblymag.com/articles/83302-assembly-in-action-fastener-handling-system-saves-time.

[87] J. Lewis, "Vision-guided robots automate oil tool assembly," *Control Engineering*, 2012. [Online]. Available: http://www.controleng.com/single-article/vision-guided-robots-automate-oil-tool-assembly/dd55c77a0fbe3e98be6346ad981e475d.html.

[88] Yasakawa Motoman, "Motoman Dual Arm SDA20D Robot - SDA20D," 2012. [Online]. Available: http://www.motoman.com/datasheets/SDA20D.pdf. [Accessed: 03-Aug-2012].

[89] Schunk, "Schunk PGN-Plus 80," 2014. [Online]. Available: http://www.schunk.com/schunk_files/attachments/PGN-plus_80_En.pdf. [Accessed: 20-Jun-2014].

[90] "Tightening Spindle," 2013. [Online]. Available: http://www.boschrexroth.com/dcc/Vornavigation/Vornavi.cfm?Language=EN&VHist=g97568,g96077,g96768,g153567&PageID=p331596. [Accessed: 21-Jan-2013].

[91] Basler, “Basler Industrial Cameras - ace Series - acA1600-20gm,” 2013. [Online]. Available: http://www.baslerweb.com/products/ace.html?model=168. [Accessed: 03-Jul-2013].

[92] Micro-Epsilon UK, “Micro-Epsilon scanControl 2900-25 Laser Profile Scanner,” 2014. [Online]. Available: http://www.micro-epsilon.co.uk/laser-scanner/scanCONTROL/Laser-scanner-selection_dynam/index.html. [Accessed: 05-Jan-2014].

[93] ODVA, “Technology Overview,” 2013. [Online]. Available: http://www.odva.org/Home/ODVATECHNOLOGIES/DeviceNet/DeviceNetTechnologyOverview.aspx. [Accessed: 12-Mar-2014].

[94] HMS Anybus, “Anybus X-gateway - DeviceNet Scanner/Master,” 2013. [Online]. Available: http://www.hms.se/products/products.asp?PID=117&ProdType=Anybus X-gateway. [Accessed: 12-May-2013].

[95] Yasakawa Motoman, “DX100 INSTRUCTIONS FOR ETHERNET SERVER FUNCTION.” pp. 1–56, 2012.

[96] HMS Anybus, “DeviceNet Serial Gateway - Anybus Communicator,” 2013. [Online]. Available: http://www.hms.se/products/products.asp?PID=105&ProductType=Anybus Communicator. [Accessed: 12-May-2013].

[97] CCS INC., “Ring Light Units [Direct Lighting] - LED Light Units - LDR2-120BL,” 2013. [Online]. Available: http://www.ccs-grp.com/s2_ps/src/pro_item/1/1/1/1/37/e.html. [Accessed: 03-Jul-2013].

[98] Halcon, “HALCON Image Processing Libraries,” 2014. [Online]. Available: http://www.halcon.com/. [Accessed: 14-Mar-2014].

[99] J. Canny, “A computational approach to edge detection.,” *IEEE transactions on pattern analysis and machine intelligence*, vol. 8, no. 6, pp. 679–98, Jun. 1986.

[100] Imaging Development Systems (IDS), “Ensenso N10 stereo 3D cameras with CMOS sensors,” 2014. [Online]. Available: http://en.ids-imaging.com/store/produkte/kameras/ensenso-3d.html. [Accessed: 05-Jan-2014].

[101] PrimeSense, “3D sensor Carmine 1.09 (Short range),” 2014. [Online]. Available: http://www.openni.org/rd1-09-specifications/. [Accessed: 05-Jan-2014].

[102] Vision Components, “VC nano 3D: Vision Components GmbH,” 2014. [Online]. Available: http://www.vision-

components.com/en/products/smart-cameras/vc-nano-3d/. [Accessed: 17-Feb-2014].

[103] Chemetall, “Chemetall Group - Ardrox® 9D1B,” 2013. [Online]. Available: http://www.chemetall.com/che/en/products/trademark/ardrox/ardrox.jsp. [Accessed: 19-Oct-2013].

[104] Optical Gaging Products (OPG), “SmartScope Flash 200,” 2014. [Online]. Available: http://www.ogpnet.com/ogpVidFlash200.jsp. [Accessed: 08-Oct-2014].

APPENDIX A - TECHNICAL DATA AND SPECIFICATIONS OF SYSTEM HARDWARE AND DEVICES

A1. Motoman SDA20D

The Motoman is a dual-arm robot with human-like flexibility and fast acceleration. The robot specifications are shown in Figure A 1.

SDA20D SPECIFICATIONS		
Structure		Articulated
Mounting		Floor
Controlled Axes		15 (7 axes per arm plus base rotation)
Payload		20 kg (44.1 lbs)/arm
Horizontal Reach per Arm		910 mm (35.8")
Horizontal Reach (P-point to P-point)		2,590 mm (102")
Vertical Reach		1,820 mm (71.7")
Repeatability		±0.1 mm (±0.004")
Maximum Motion Range	Rotation-Axis (Waist) S-Axis (Lifting) L-Axis (Lower Arm) E-Axis (Elbow) U-Axis (Upper Arm) R-Axis (Upper Arm Twist) B-Axis (Wrist Pitch/Yaw) T-Axis (Wrist Twist)	±180° ±180° ±110° ±170° ±130° ±180° ±110° ±180°
Maximum Speed	Rotation-Axis S-Axis L-Axis E-Axis U-Axis R-Axis B-Axis T-Axis	125°/s 130°/s 130°/s 170°/s 170°/s 200°/s 200°/s 400°/s
Approximate Mass		380 kg (837.9 lbs)
Power Consumption		4.4 kVA
Allowable Moment	R-Axis B-Axis T-Axis	58.8 N • m 58.8 N • m 29.4 N • m
Allowable Moment of Inertia	R-Axis B-Axis T-Axis	4 kg • m^2 4 kg • m^2 2 kg • m^2

Figure A 1 : Motoman SDA20D Robot Specifications

The controller version used for this robot model is DX100 and its specifications are provided in Figure A 2.

DX100 CONTROLLER SPECIFICATIONS**	
Dimensions (mm)	1,200 (w) x 1,000 (h) x 650 (d) 47.2" x 39.4" x 25.6")
Approximate Mass	250 kg max. (551.3 lbs)
Cooling System	Indirect cooling
Ambient Temperature	During operation: 0° to 45° C (32° to 113° F) During transit and storage: -10° to 60° C (14° to 140° F)
Relative Humidity	90% max. non-condensing
Primary Power Requirements	3-phase, 240/480/575 VAC at 50/60 Hz
Digital I/O NPN-Standard PNP-Optional	Standard I/O: 40 inputs/40 outputs consisting of 16 system inputs/ 16 system outputs, 24 user inputs/24 user outputs 32 Transistor Outputs; 8 Relay Outputs Max. I/O (optional): 2,048 inputs and 2,048 outputs
Position Feedback	By absolute encoder
Program Memory	JOB: 200,000 steps, 10,000 instructions CIO Ladder Standard: 15,000 steps Expanded: 20,000 steps
Pendant Dim. (mm)	169 (w) x 314.5 (h) x 50 (d) (6.7" x 12.4" x 2")
Pendant Weight	.998 kg (2.2 lbs)
Interface	One Compact Flash slot; One USB Port (1.1)
Pendant Playback Buttons	Teach/Play/Remote Keyswitch selector Servo On, Start, Hold, and Emergency Stop Buttons
Programming Language	INFORM III, menu-driven programming
Maintenance Functions	Displays troubleshooting for alarms, predicts reducer wear
Number of Robots/Axes	Up to 8 robots, 72 axes
Multi Tasking	Up to 16 concurrent jobs, 4 system jobs
Fieldbus	DeviceNet Master/Slave, AB RIO, Profibus, Interbus-S, M-Net, CC Link, EtherNet IP/Slave
Ethernet	10 Base T/100 Base TX
Safety	Dual-channel Emergency Stop Pushbuttons, 3-position Enable Switch, Manual Brake Release Meets ANSI/RIA R15.06-1999, ANSI/RIA/ISO 10218-1-2007 and CSA Z434-03

Figure A 2 : DX100 Robot Controller Specifications

A2. Schunk PGN-plus 80-1

The PGN-plus 80-1 is a universal 2-finger parallel gripper with large gripping force and high repeatability. The technical specifications are illustrated in Figure A 3.

Technical data

Description		PGN-plus 80-1
ID		0371101
Stroke per finger	[mm]	8
Closing force	[N]	415
Opening force	[N]	465
Min. spring force	[N]	
Weight	[kg]	0.5
Recommended workpiece weight	[kg]	2.1
Air consumption per double stroke	[cm³]	21
Min./max. operating pressure	[bar]	2.5/8
Nominal operating pressure	[bar]	6
Closing/opening time	[s]	0.04/0.04
Max. permitted finger length	[mm]	110
Max. permitted weight per finger	[kg]	0.6
IP class		40
Min./max. ambient temperature	[°C]	-10/90
Repeat accuracy	[mm]	0.01
Cleanroom class ISO-classification 14644-1		5

Figure A 3 : Schunk PGN-plus technical data

A3. Bosch Rexroth tightening spindle (Size 4 – 150 Nm)

1) Torque measurement accuracy

Cut-off value **- 128 Nm**

No of Trials **- 50**

Measurement Conditions - Not provided (temperature, humidity and friction)

	Mean(Nm)	SD(Nm)
Reference data	128.72	0.38
Measured data	128.36	0.30

2) Angle measurement accuracy

The Angle accuracy test details are **not provided** by manufacturer.

A4. Basler Ace 1600-20gm Camera

The Basler is a 2D monochrome camera and it specifications are provided in Figure A 4.

Resolution (H x V pixels)	1626 px x 1236 px
Pixel Size horizontal/vertical	4.4 µm x 4.4 µm
Frame Rate	20 fps
Mono/Color	Mono
Interface	GigE
Video Output Format	Mono 8, Mono 12, Mono 12 Packed, YUV 4:2:2 Packed, YUV 4:2:2 (YUYV) Packed
Pixel Bit Depth	12 bits
Synchronization	▪ external trigger ▪ free-run ▪ Ethernet connection
Exposure Control	▪ programmable via the camera API ▪ external trigger signal
Housing	box
Housing Size (L x W x H) in mm	42.0 x 29.0 x 29.0
Housing Temperature	0 °C - 50 °C
Lens Mount	▪ C-mount ▪ CS-mount
Digital Input	1
Digital Output	1
Power Requirements	PoE or 12 VDC
Power Consumption (typical)	2.9 W
Power Consumption PoE	3.4 W
Weight (typical)	90 g
Sensor Vendor	Sony
Sensor Name	ICX274
Shutter	global shutter
Max. Image Circle	1/1.8 inch
Sensor Type	CCD
Sensor Size (mm)	7.16 mm x 5.44 mm
Order Number	104847

Figure A 4 : Basler Ace 1600-20gm Specifications

A5. Micro-Epsilon scanControl 2900-50

The technical data of Micro-Epsilon 3D laser scanner is given in Figure A 5.

Technical Data

Model	scanCONTROL		
	29xx-25	29xx-50	29xx-100
Measuring range Z-axis	25 mm	50 mm	100 mm
Start of measuring range	53.5 mm	70 mm	190 mm
End of measuring range	78.5 mm	120 mm	290 mm
Start of measuring range, extended, approx.	53 mm	65 mm	125 mm
End of measuring range, extended, approx.	79 mm	125 mm	390 mm
Line length midrange (X-axis)	25 mm	50 mm	100 mm
Linearity [1]	± 0.16 % FSO (3 σ)		
Resolution X-axis	1280 points/profile		
Profile frequency (depending on sensor model)	200 - 2000 Hz		
Light source laser	Semiconductor laser, approx. 658 nm, 20 °... 25 ° aperture angle, laser class 2M: capacity 8 mW, reduced 2 mW		
Protection class (DIN EN 60529)	IP 65		
Operating temperature	0 °C ... +45 °C (+32 ... +113 °F)		
Storage temperature	-20 °C ... 70 °C (-4 ... +158 °F)		
Outputs/inputs	Ethernet, Laser on/off (optional), 1x RS422 programmable (Half-duplex), 3 switching inputs programmable HTL/TTL, all inputs and outputs galvanically isolated		
Supply	11 ... 30 VDC, 500 mA IEEE 802.3af Power over Ethernet, class 2		
Displays	1x state / 1x laser on		
Electromagnetic compatibility (EMC)	according to: EN 61326-1: 2006-10 DIN EN 55011: 2007-11 (group 1, class B) EN 61000-6-2: 2006-03		

FSO = Full Scale Output | MMR = Midrange

Figure A 5 : Micro-scanControl 2900-50 specifications

A6. Fastening plate

The fastening plate is a test component that is created to represent an industrial component with threaded holes located at different 3D surfaces. The dimensions of the fastening plate are provided in the Figure A 6.

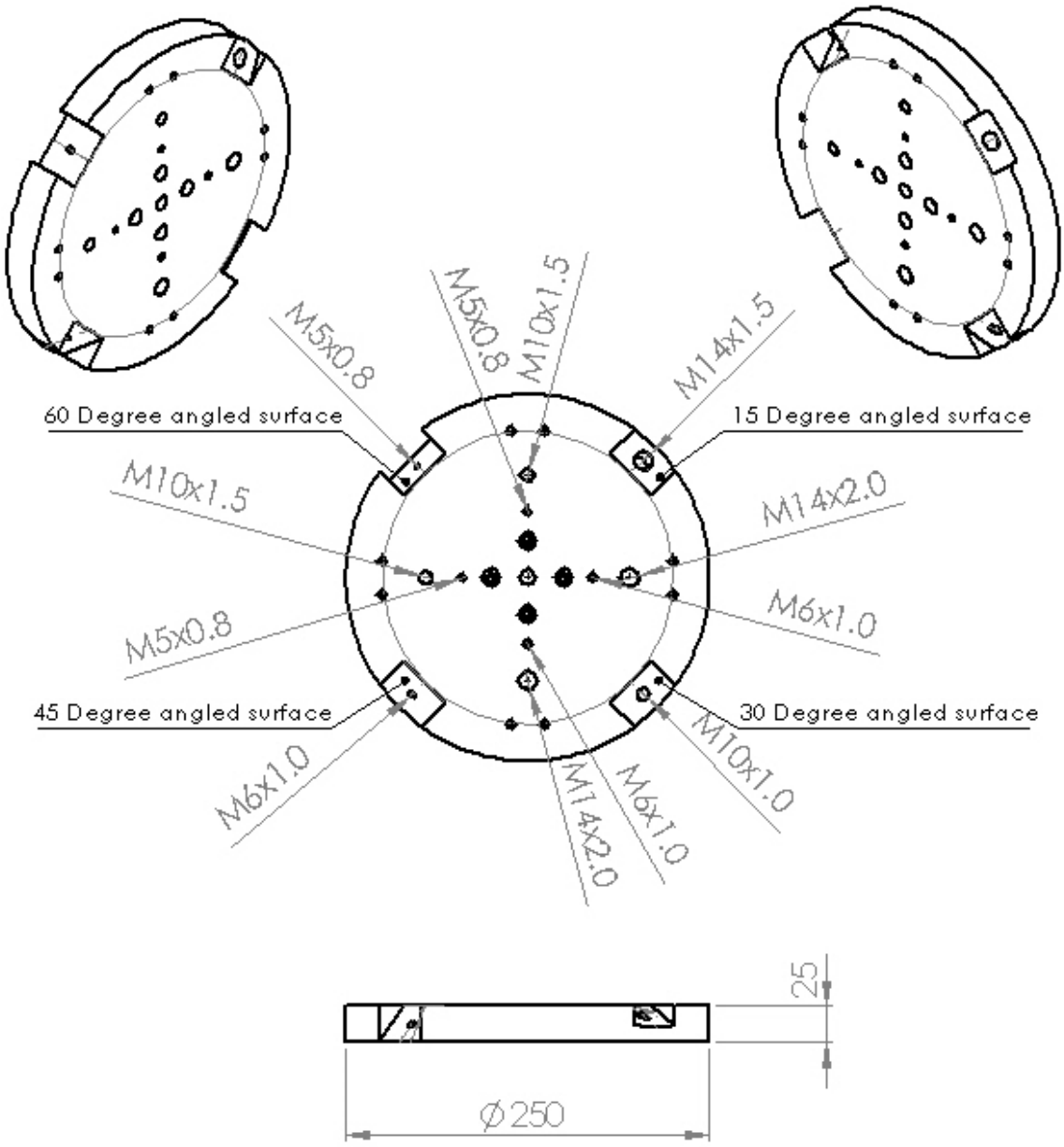

Dimensions are in 'mm'

Figure A 6 : Fastening plate dimensions

A7. HMS Anybus Communicator

Anybus Communicator is a device used to enable communication between any serial device and a DeviceNet network. The specifications of this device are illustrated in Figure A 7.

TECHNICAL SPECIFICATIONS	
Size:	120 mm x 75 mm x 27 mm
Power Supply:	24 VDC
Temperature:	0 to +55°C
Current Consump:	Max 300 mA
Baud Rate:	125, 250, 500 kbit/s
Sub Baud Rate:	1.2, 2.4, 4.8, 9.6, 19.2, 35.7, 38.4, 57,6 kbit/s
I/O Input:	512 byte
I/O Output:	512 byte
Mech Rating:	IP20
Supp Features:	I/O Slave messaging: Bit strobe, Polling, Cyclic, COS, Explicit Messaging
Config Method:	Anybus Configuration Manager for Windows (TM)
Appl Interface:	RS232, RS422, RS485
Included accessories:	Cd with software and User Manuals, Configuration Cable RS232, Dsub with screw terminals for Sub-Network, Installation Leaflet
Galvanic isolation:	Standard for both bus side and serial side
Order Code:	**AB7001**

Figure A 7 : HMS Anybus Communicator Specifications

A8. OGP SmartScope Flash 200

The SmartScope Flash 200, shown in Figure A 8 with specifications, is an automatic measurement system. It uses vision with magnified lens to measure object features.

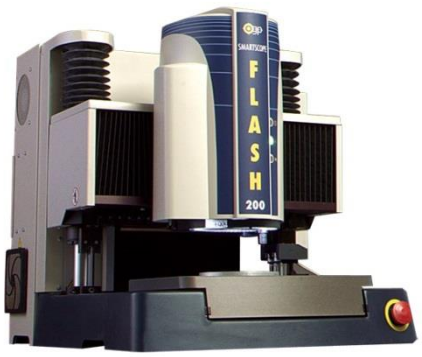

XYZ Stage Travel: 200 x 200 x 150 mm
Area Accuracy: (2.0 + 6L/1000) µm
Z Accuracy: up to (1.4 + 6L/1000) µm

Figure A 8 : OGP SmartScope Falsh 200 and its specifications

APPENDIX B - TIGHTENING PROGRAMS, 2D IMAGE PROCESSING ALGORITHMS AND 2D CALIBRATION

B1. Tightening programs

The programs for fastening are pre-programmed using the Tightening Software Interface (shown in Figure B 1) provided by the manufacturer (Bosch Rexroth).

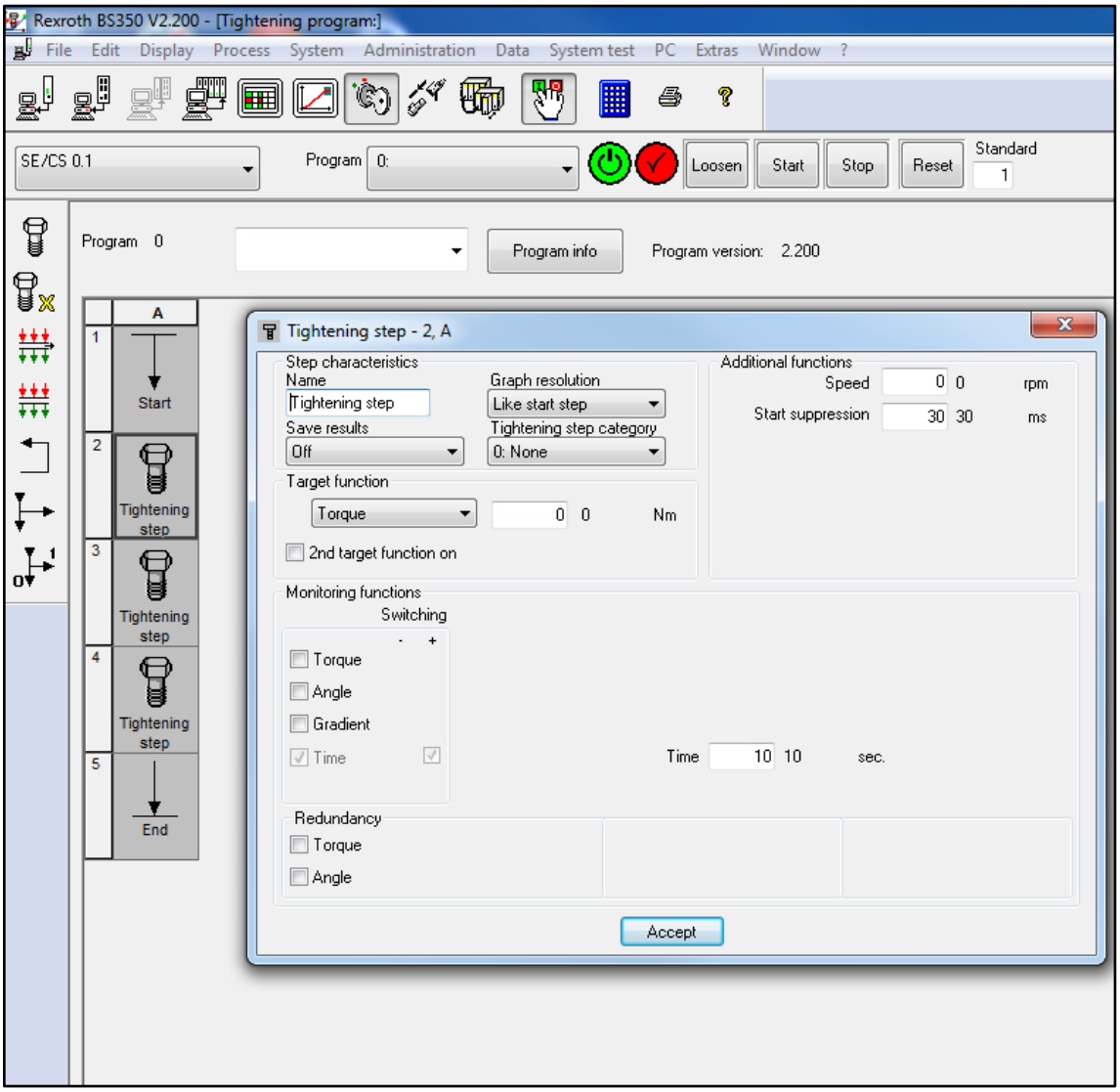

Figure B 1 : Tightening software interface

a) Tightening Program – Slow Rotation

This program is a single step tightening operation as shown in Figure B 2. This program is used for picking up the bolt from bolt holder during 2D fastener assembly.

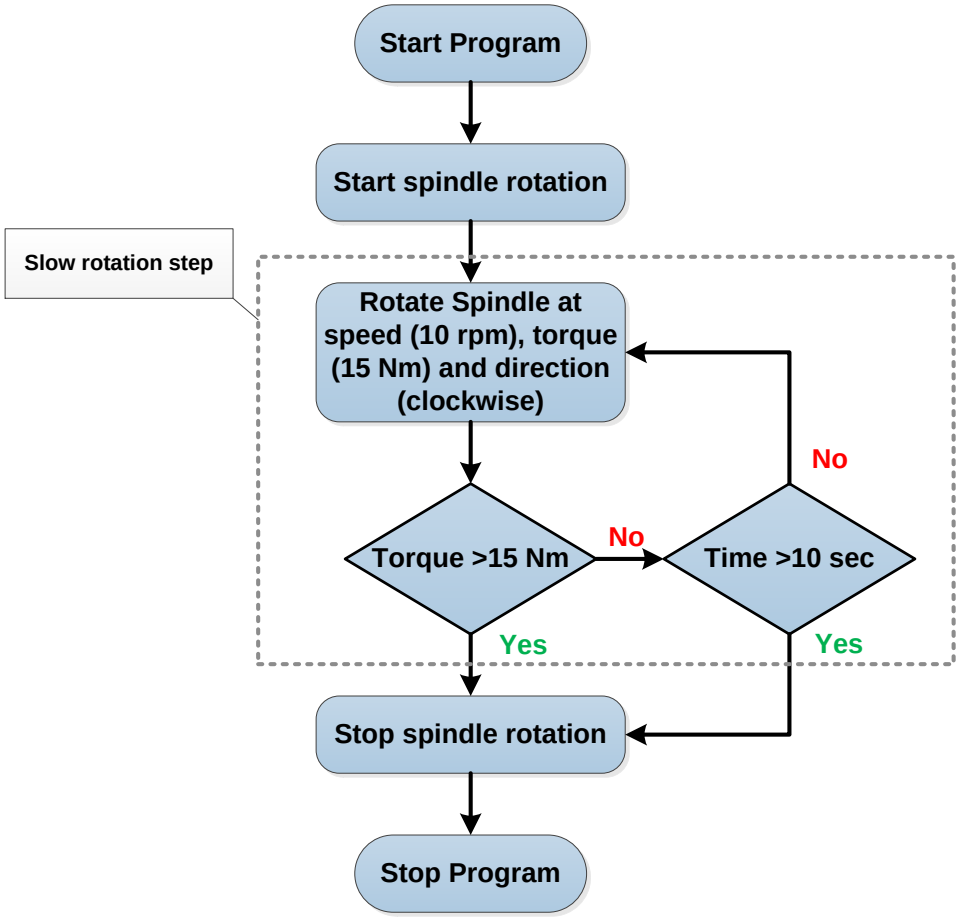

**Time is a secondary constraint used to stop the program and 10 seconds is more than the time required to fasten a bolt into a hole (user defined)*

Figure B 2 : Slow rotation - tightening module

b) Tightening Program – Bolt fastening

This is a three step program used to fasten a M10 bolt into its corresponding size threaded hole as illustrated in Figure B 3.

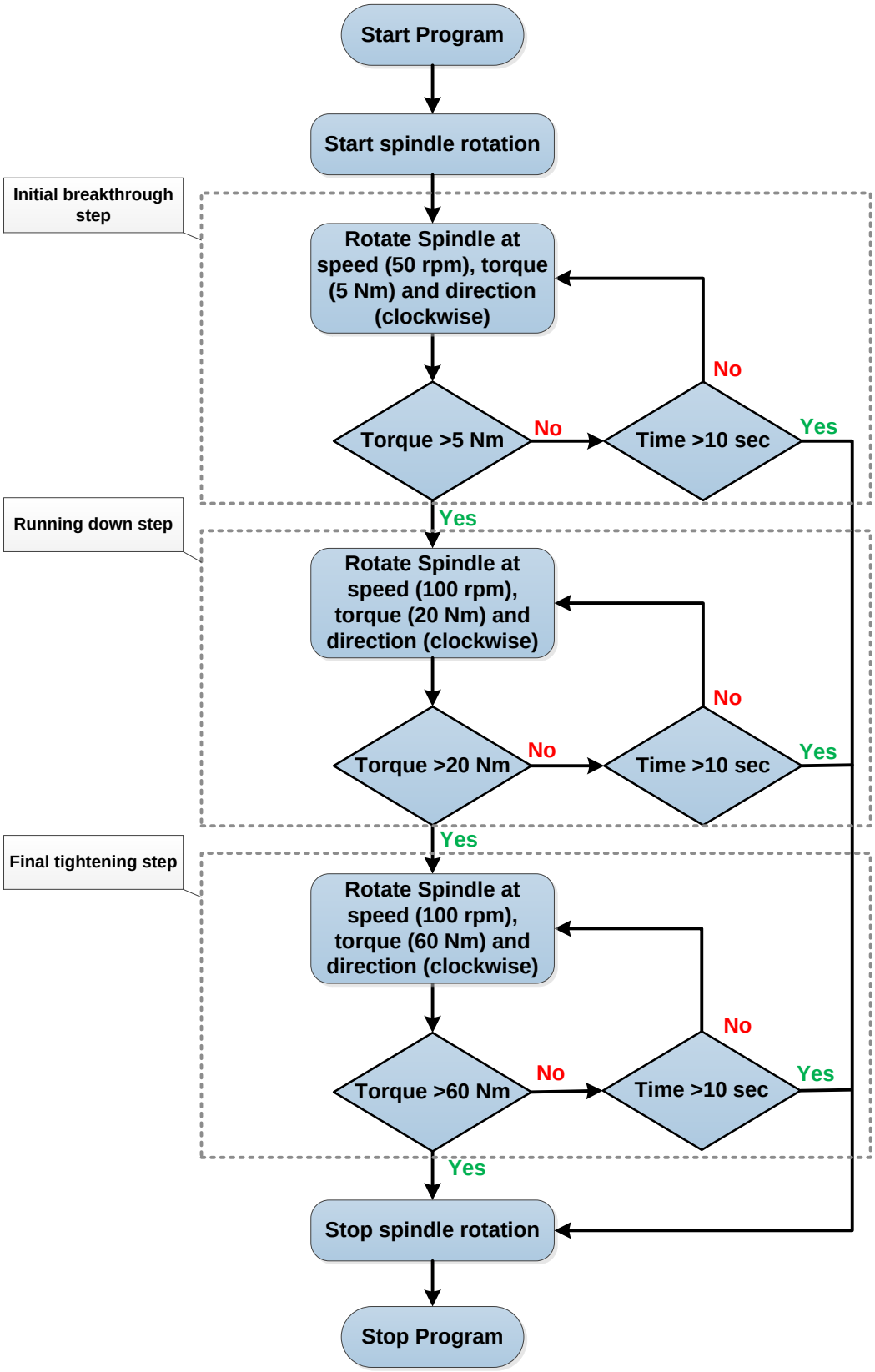

Time is a secondary constraint used to stop the program and 10 seconds is more than the time required to fasten a bolt into a hole (user defined)

Figure B 3 : Bolt fastening – tightening module

B2. 2D Image processing algorithms

This section describes various 2D image processing algorithms used in this research (i.e. in 2D fastener assembly method to detect bolts and holes).

a) Sharpening (Emphasize)

This process enhances the contrast of the image, thereby emphasizing the corners and edges of the image. This process involves two steps

1) Linear smoothing of Gray values of the image with a low pass filter (size Mask Height and Mask Width specified by the user). The resulting Gray values is the mean value.
2) The output image Gray Values (output) is given by the equation

Output = round ((original – mean) * Factor) + original

The 'Factor' is used as a parameter to control contrast of the image. The 'original' represents the original Gray values of the input image.

b) Edge Detection

There are different types of edge detection techniques developed to identify sharp edge features from a 2D image. After conducting a study of different edge detection techniques, the three major techniques as shown in Figure B 4 were selected for evaluation.

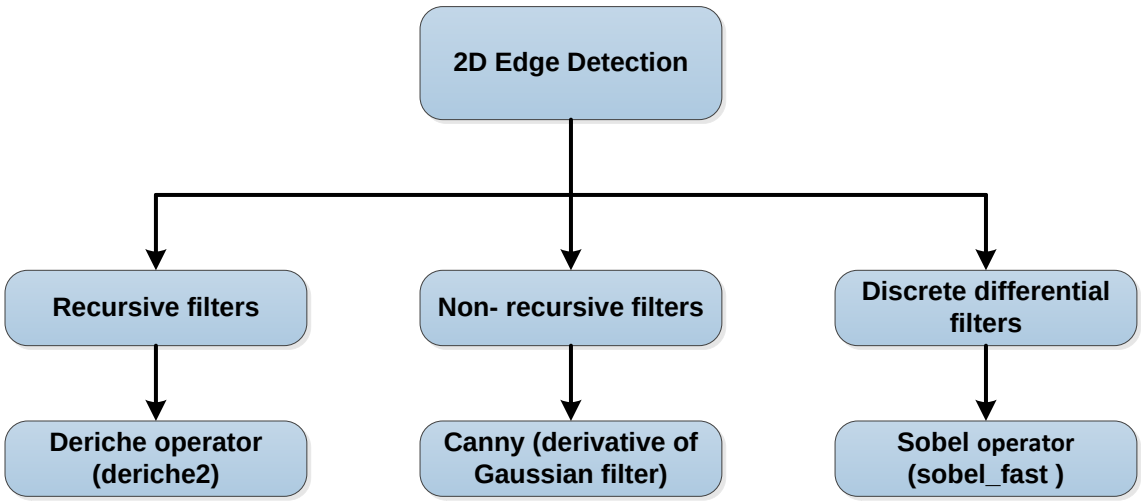

Figure B 4 : Edge detection techniques

This evaluation is carried out to select the most suitable edge detection technique for implementing in this research. An image of the fastening plate is used as the input image and the different edge detection operators are implied on the image to identify the most suitable operator. The input image is sharpened to emphasize the edges and corners in the image before applying the edge detection operators. The parameters such as alpha and threshold values of the operators are varied and the results are provided in Figure B 5.

	Hysteresis Threshold (*Low = 20 and High = 40)*	
Alpha = 2.5	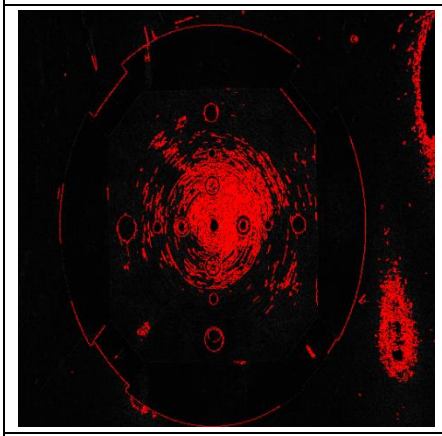	Deriche Operator
	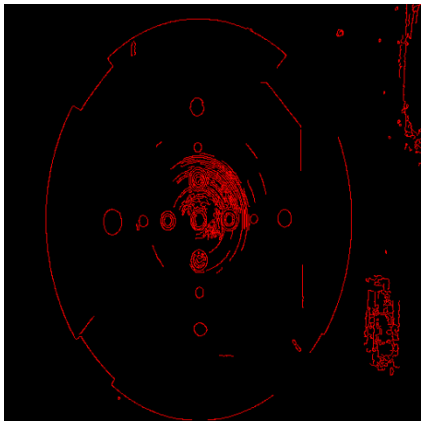	Canny Operator
	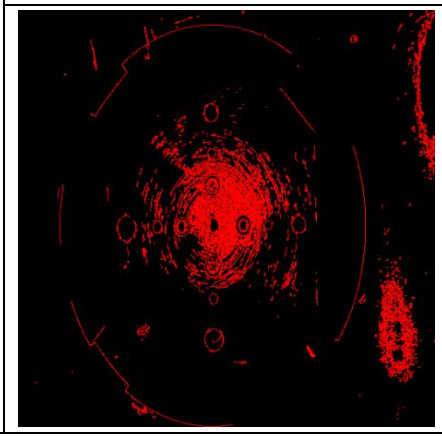	Sobel_Fast Operator

Figure B 5 : Comparision of different techniques

c) Connected regions

This process determines the edge regions that are connected in the image (obtained after edge detection with hysteresis threshold). An 8 cell neighbourhood operator is used to determine the edge pixels connection and continuity. The pixels which are continuous are grouped together to form a connected region.

d) Area

Area of a connected region represents the number of pixels in the region.

e) Roundness

The roundness factor determines the mean deviation between the contour and the centre of the area. The roundness is a factor of mean distance from the centre (d_{mean}) and standard deviation of the distance (sigma).

$$d_{mean} = \frac{1}{Area} \sum |p_{centre} - p_i|$$

$$sigma^2 = \frac{1}{Area} \sum (|p_{centre} - p_i| - d_{mean})^2$$

$$roundness = 1 - \frac{sigma}{d_{mean}}$$

Where 'p_{centre}' denotes centre pixel of the region and 'p_i' denotes the pixels

f) Number of sides

The number of sides in a polygon (a region) is determined using the following equation.

$$number\ of\ sides = 1.4111 \left(\frac{d_{mean}}{sigma}\right)^{0.4724}$$

g) Diameter and centre point

Diameter - the maximal distance between two boundary points of a region

Centre point - mean value of the column coordinates of all the pixels in a region.

B3. 2D Calibration

The calibration is a process used to obtain metric information from an image (i.e. pixels). The intrinsic and extrinsic parameters of a 2D camera can be determined by performing a calibration, which is then used for converting the pixel information into real world measurements.

A calibration object is a flat plate with a multi-dot pattern sheet on its top as shown in Figure B 6. The multi-dot pattern sheet consists of black dots arranged in a matrix (size - 21 rows and 21 columns) on a white sheet. The calibration process involves presenting the calibration plate to the camera at a minimum of 15 different poses and taking an image each time. Each image is then processed to identify the shape, the position and the centre of all the dots in the calibration plate. This information along with the known parameters such as calibration plate dimensions and camera specifications, are used to determine the intrinsic and extrinsic parameters of the camera.

Calibration inputs

Calibration Plate Dimensions	
Dot pattern matrix size	21 x 21
Dot diameter	6 mm
Distance between dots	10 mm
Thickness of the plate	4 mm

Camera Specifications	
Cell width	4.4 µm
Cell height	4.4 µm
Focal length	8
Model	Area Scan

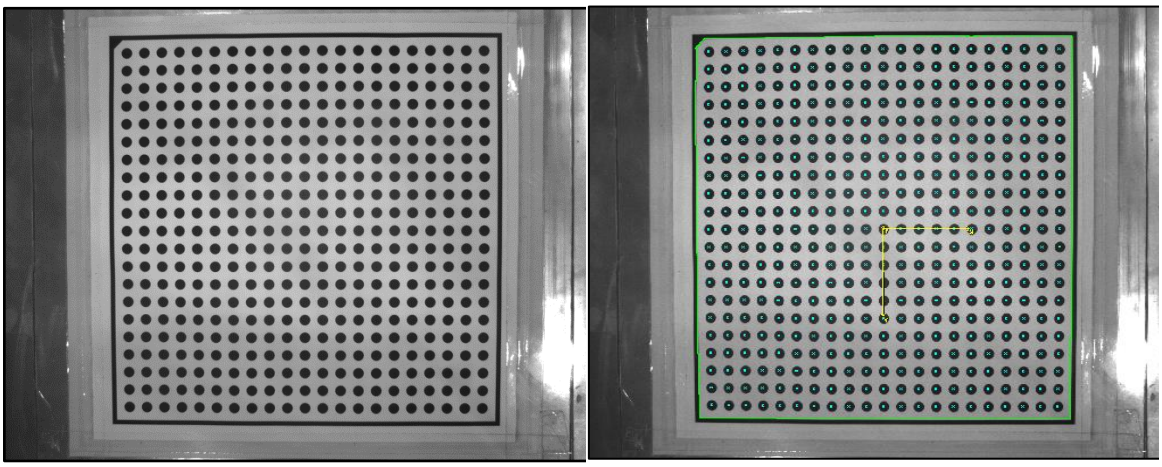

Figure B 6 : Calibration plate and the image of the dot pattern identified for registering pixels into real world measurements (i.e. mm)

Calibration outputs

The outputs of the calibration include the intrinsic and extrinsic camera parameters.

Intrinsic camera parameters	
Cell width	4.4003 µm
Cell height	4.4000 µm
Focal length	8.2303
Kappa	-1259.07
Centre column	823.744
Centre row	615.253
Image width	1626 pixels
Image height	1236 pixels
Pixel error	0.1465

Extrinsic camera parameters (Camera pose)	
X	1.636 mm
Y	0.011 mm
Z	389.525 mm
X_θ	0.372°
Y_θ	359.774°
Z_θ	0

Software used

The calibration is performed using the image processing libraries and the calibration assistant interface provided by HALCON software.

APPENDIX C - POINT CLOUD PROCESSING ALGORITHMS AND 3D CALIBRATION

Halcon Image processing library is used in this research for processing the point cloud data.

C1. Clarification on acquiring point cloud data from laser scanners

Point cloud data of a cylindrical object located in a flat surface obtained from a laser scanner can only provide the top surface of the cylindrical object (a curve in the laser scanner output as shown in Figure C 1). The scanner is limited to view the top surface, as the remaining part of the object is hidden beneath the top surface.

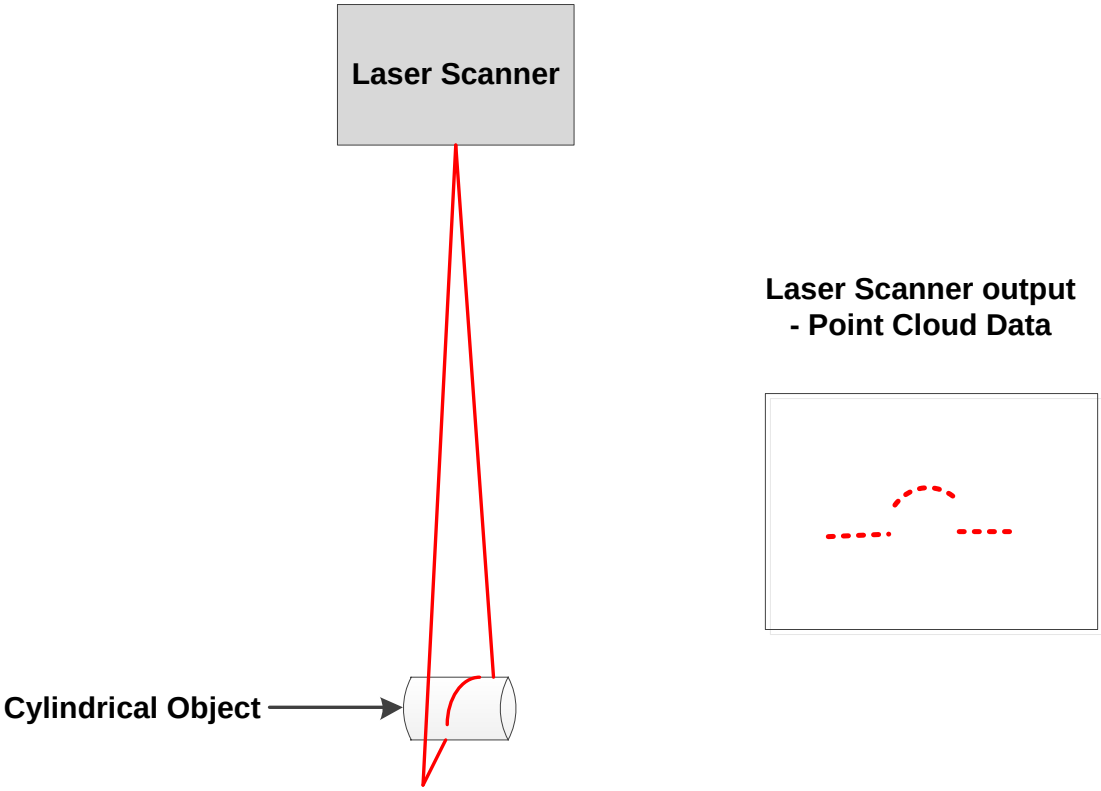

Figure C 1 : Clarification on Point Cloud Data acquisition

C2. Point Cloud Processing Algorithms

a) Resampling

The process of sampling a point cloud data (PCD) is called as resampling. The voxel grid filter is the method used for sampling. The resampled data contains points that are equidistant from each other and the distance between the points is the sampling distance (defined by the user).

b) Surface normal estimation

This process calculates the surface normal of each and every point of a 3D object model. The method used for surface normal estimation is 'Moving Least Squares (MLS)'.

For each point (p), the method fits a planar or higher order polynomial surface to its nearest neighbours (the number of nearest neighbours to be considered is defined by the user). Using the weighted least squares the parameter of the planar or polynomial surface is estimated. The closest neighbours will have a higher contribution in the surface estimation than other points by controlling the weight function (w (p')).

$$w(p') = \exp\left(-\frac{\|p' - p\|^2}{a^2}\right)$$

Where p' – closest neighbours of point (p), 'a'– control factor of the weight function

The projection of this point with respect to the surface estimated using the weight function will provide the normal of that point. This step is repeated for all points to determine the surface normal.

c) Removing outliers or noise points

An isolated noise point represents either a false point or a small dent in the surface of the object as illustrated in Figure C 2.

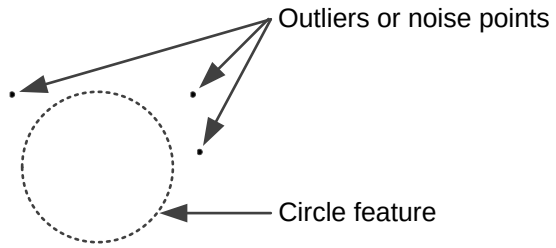

Figure C 2 : Outliers or noise points in a feature

This process involves determining the average maximum distance between all pair of points and if any pair of points has a distance greater than the approximate diameter of a hole are considered as outliers and are removed.

The 3D distance is calculated using the equation

$$d = \sqrt{(x2 - x1)^2 + (y2 - y1)^2 + (z2 - z1)^2}$$

Where‘d’ – distance between points

d) Identifying circular features

After edge detection, the sharp features are of different shapes such as lines, curves and circles. To identify the circular features and remove all other shapes, the features are subject to the general equation of a circle in 3D.

If a point in a circle is represented by (*Xp*, *Yp* and *Zp*) and its circle centre by (*Xc*, *Yc* and *Zc*), then the general equation of a circle with radius ‘r’ is given by

$$(Xc - Xp)^2 + (Yc - Yp)^2 + (Zc - Zp)^2 = r^2$$

Any feature that satisfies this equation is considered as a circular feature.

e) Diameter and Centre point

Diameter - mean of largest distance between the pair of points in a feature

Centre point - weighted mean of centre of all the point pairs in a feature.

C3. 3D Calibration

a) Reference object dimension

The reference object is a known object used as a common reference to transform the data obtained using a 3D sensor into a robot co-ordinate system. The dimensions of the reference object are provided in Figure C 3.

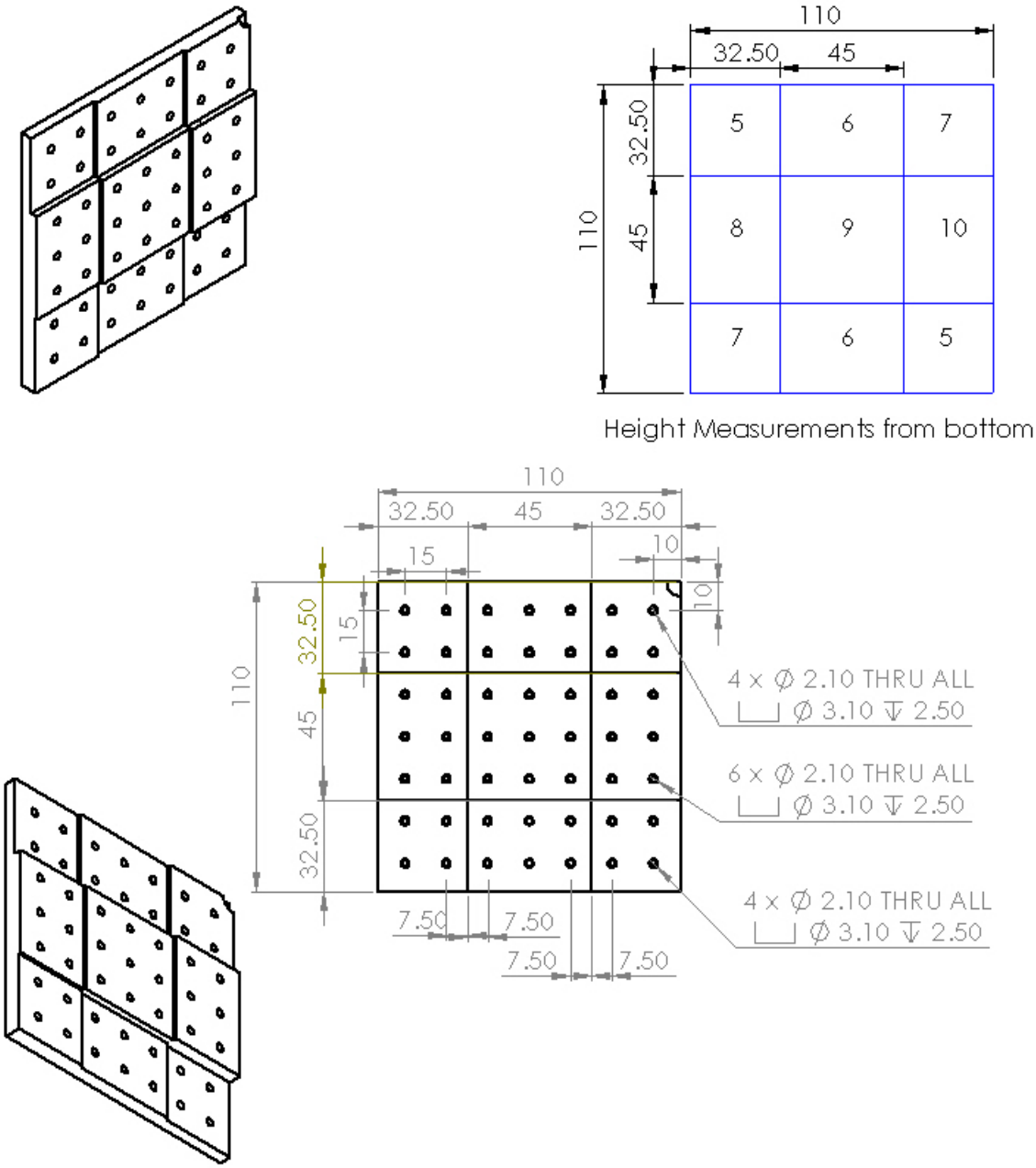

Dimensions are in 'mm'

Figure C 3 : 3D Claibration reference object

b) Laser line alignment with styli

The alignment of laser line with the styli is guided manually (human vision) by moving the Micro-Epsilon scanner until the line is projected on the centre of ruby sphere on top of the styli as shown in Figure C 4.

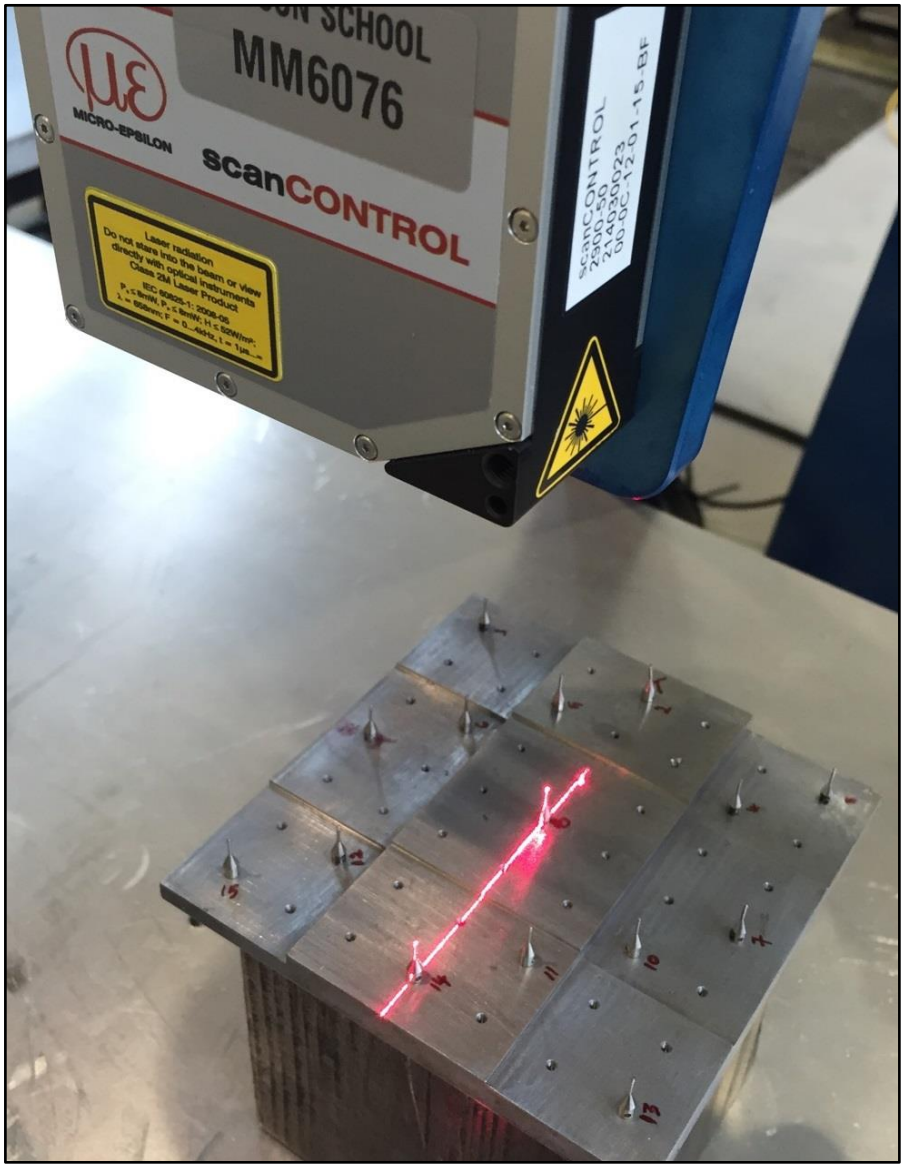

Figure C 4 : Laser line alignment with the styli

At the same time, the interface provided by Micro-Epsilon is used to check the alignment by looking for the points representing the ruby sphere on top of the styli as illustrated in Figure C 5.

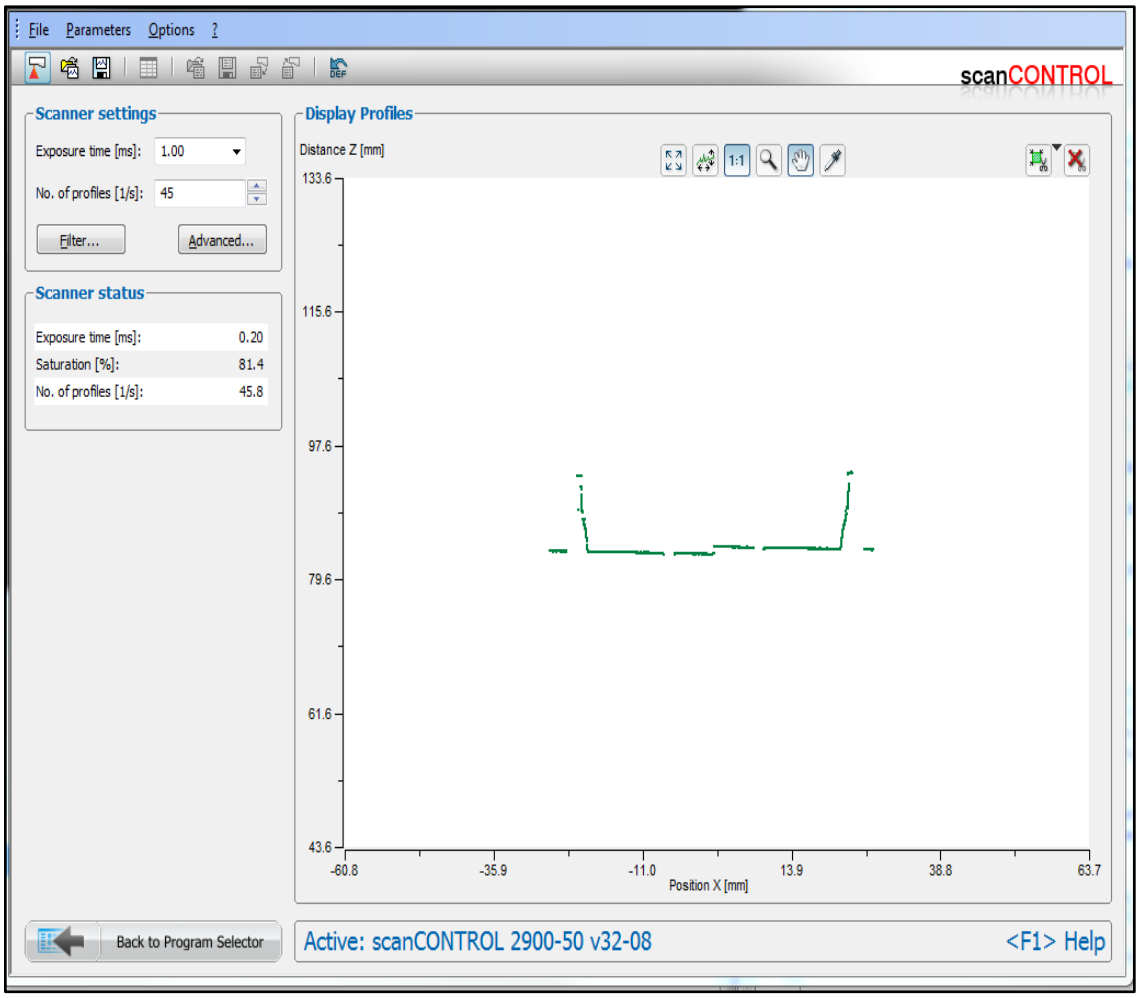

Figure C 5 : Laser line profile on two styli obtained using the Micro-Epsilon interface software

c) Calibration output

The calibration output provides the transformation matrix and the pose of the camera with respect to the work area co-ordinate system. This work area co-ordinate system is a user defined co-ordinate system for the robot.

$$Camera\ In\ Work\ Area = \begin{bmatrix} 0.9888 & 0.0051 & 0.0588 & 16.121 \\ 0 & 1 & 0 & 0 \\ -0.0027 & 0.0192 & 0.9804 & -93.372 \end{bmatrix}$$

$$Pose = [16.121, 0, -93.372, 0, 3.403, 359.7045, 0]$$

APPENDIX D – DISSEMINATION OF RESEARCH

Dissemination of research

This research work has been presented at a conference and submitted to international journals. These include:

- This research work has been presented at the 'Manufacturing the Future' conference held at Glasgow, UK in 2014.
- Two research papers were submitted to an international journal, 'Robotics and computer-integrated manufacturing' for peer review.

JOURNAL 1

Free-form Robotic assembly of threaded fasteners in random environment

Karthick Dharmaraj[1], Radmehr P Monfared[2], Philips S Ogun[3], Michael R Jackson[4]

[1, 2, 3 & 4]EPSRC Centre for Innovative Manufacturing in Intelligent Automation, Holywell Park, Loughborough University- LE11 3TU

[1]K.Dharmaraj@lboro.ac.uk, [2]R.P.Monfared@lboro.ac.uk, [3]P.S.Ogun@lboro.ac.uk, [4]M.R.Jackson@lboro.ac.uk

ABSTRACT

Over the past two decades, a major part of the manufacturing and assembly market has been driven by the increasing demand for customised products. This creates the need for smaller batch sizes, shorter production times, lower costs, and the flexibility to produce families of products - or to assemble different parts - with the same sets of equipment. Consequently, manufacturing companies have deployed various automation systems and production strategies to improve their resource efficiency and move towards right-first-time production. Threaded fastening operations are widely used in assembly and are typically time consuming and costly. In high-volume production, fastening operations are commonly automated using jigs, fixtures, and semi-automated tools. However, in low-volume, high-value manufacturing, fastening operations are carried out manually by skilled workers. The existing approaches are found to be less flexible and robust for performing assembly in an industrial environment. This motivated the development of a flexible solution, which does not require fixtures and is adaptable to variation in part locations and lighting conditions. A number of algorithms have been developed to identify and localise the assembly components located in a random environment. An automated bolt fastening demonstrator was also developed to test and validate the proposed solution. Experimental results show that the solution is robust enough to be implemented in real industrial environments.

Keywords: *Free-form assembly, Flexible automation, Machine vision, Fastener assembly, 3D hole feature detection, 3D object detection*

JOURNAL 2

Flexible robotic assembly of clearance fit components using 3D machine vision

Philips S. Ogun, Karthick Dharmaraj, Zahid Usman, Michael R. Jackson
EPSRC Centre for Innovative Manufacturing in Intelligent Automation, Wolfson School of Mechanical and Manufacturing Engineering, Loughborough University, Loughborough, UK
*****Corresponding author. Email: p.s.ogun@lboro.ac.uk Telephone: +44(0)150 922 6579

ABSTRACT

The use of robots in assembly operations requires that the geometries and the poses of the components to be assembled be known within a given workspace. These requirements have been met either through predefined poses of components using fixtures or by determining the poses through various machine vision techniques. Vision-guided assembly robots can handle subtle variations in geometries and poses of components. Therefore, they provide greater flexibility than fixtures that hold the components in fixed poses. The current vision-guided assembly systems use 2D vision, which is limited to three degrees of freedom. The work reported in this paper is focused on flexible automated assembly of clearance fit components using 3D vision. The recognition and pose estimation of the assembly components are achieved by matching their CAD models with the acquired point cloud data of the scene. A robotic assembly of rings on a shaft is used to show that the approach enables robots to operate in a more intelligent and adaptable manner, thereby introducing a greater level of flexibility.

Keywords: 3D vision, robotics, automated assembly, object recognition